INFLUENCE OF TIME DEPENDENT PROPERTIES AND TEMPERATURE EFFECTS ON THE PERFORMANCE OF COMPOSITE BRIDGE GIRDERS

By

HEMA JAYASEELAN

Bachelor of Engineering in Civil Engineering
Government College of Technology
Coimbatore, Tamil Nadu, India
2000

Master of Science in Civil Engineering
Oklahoma State University
Stillwater, Oklahoma
2007

Submitted to the Faculty of the
Graduate College of the
Oklahoma State University
in partial fulfillment of
the requirements for
the Degree of
DOCTOR OF PHILOSOPHY
December, 2019

INFLUENCE OF TIME DEPENDENT PROPERTIES

AND TEMPERATURE EFFECTS ON THE

PERFORMANCE OF COMPOSITE BRIDGE GIRDERS

Dissertation Approved:

Dr. Bruce W. Russell

Dissertation Adviser

Dr. Tyler Ley

Dr. Mohamed Soliman

Dr. Ning Wang

ACKNOWLEDGEMENTS

First and foremost, I would like to thank God for this opportunity to further my studies. Next, I would like to thank my advisor Dr. Russell for his guidance and support throughout my Ph.D. program. His expertise and knowledge have inspired me to excel both in academics and in the development of my personal character. It has been an honor and a blessing to be his student. I am thankful to my fellow graduate students Allana Webb, Dillon Cochran and Alla Acheli for all their time and hard work in this research program. I also want to thank the team of undergraduate research assistants who contributed to my research. I want to thank all my family members especially my husband Jayaseelan Pushparaj for his continued support and encouragement.

I am thankful for all my professors for their support and guidance. Most importantly I would like to thank Dr. Kerry Havner for his gracious financial support through scholarships during my Ph.D. program. I gratefully acknowledge the sponsors of this research, Oklahoma Department Of Transportation (ODOT) and W&W Steel/AFCO Steel Co.

.

Name: HEMA JAYASEELAN

Date of Degree: DECEMBER, 2019

Title of Study: INFLUENCE OF TIME DEPENDENT PROPERTIES AND TEMPERATURE EFFECTS ON THE PERFORMANCE OF COMPOSITE BRIDGE GIRDERS

Major Field: CIVIL ENGINEERING

Abstract: **This dissertation seeks to understand the mechanical properties of concrete, and its interaction with steel bridge girders with the purposes of deepening our understanding of the behavior of steel girder bridges made composite with concrete slabs.** This research program identifies and documents several causes for undesirable elevation profiles and recommends design and construction practices to help mitigate problems associated with unwanted deformations and extend the life span of bridges. Forensic investigations were performed on field bridges provided evidence that poor elevation control and improper construction practices resulted in unevenness in bridge deck elevations and thin bridge decks. Additionally, laboratory testing on overhang brackets confirmed that the commercially available brackets used for bridge rehabilitations are insufficient to support the deck cantilevers outside the exterior girders. Accordingly, these brackets are unable to provide the elevations control resulting in poor elevation controls and thin bridge decks.

A full-scale prototype bridge was built and instrumented at the Bert Cooper Engineering Laboratory at Oklahoma State University in Stillwater, OK USA. The concrete strains associated with volume change, including both temperature-related strains and shrinkage strains, were found large enough to be considered as one possible cause for adverse ride quality and unwanted deformations in steel girder bridge. Real-time thermal loading was applied to the bridge deck of the laboratory prototype bridge. The temperature gradients developed in the bridge deck produced internal thermal strains and stresses that directly resulted in bridge deformations. A large array of electronic gauges and sensors were employed to measure and monitor concrete and steel strains, concrete and steel temperatures, overall bridge deflections and inclinations. Synthesis of data collected from the sensors along with analytical computational models that were developed using the measured constitutive properties of concrete validated the methods for structural monitoring. This dissertation provides a practical means of monitoring bridge performance and offers a good experience for implementation and structural monitoring for both laboratory and field bridges. **The dissertation demonstrates that the cumulative effect due to volumetric changes in concrete, temperature effects and poor bracing system can adversely affect the ride quality, cause deck cracking and excessive deflections, decrease durability and reduce long-term performance of steel girder bridges.**

TABLE OF CONTENTS

Chapter Page

Chapter Page

Chapter Page

LIST OF TABLES

Table Page

LIST OF FIGURES

Figure Page

Figure Page

Figure Page

Figure Page

CHAPTER I

INTRODUCTION

Within the State of Oklahoma, the Oklahoma Department Of Transportation (ODOT) maintains 3,727 span bridges (Russell August 2017). Of those, 1617 bridges are made with steel girder superstructures with an average construction year of 1963. In 2010, about 706 bridges in the state of Oklahoma were classified as structurally deficient (ODOT 2017). Of those listed as structurally deficient, approximately 270 were bridges supported by steel superstructures.

Steel bridges throughout Oklahoma are being newly reconstructed or rehabilitated with new concrete decks on top of existing steel girders. New decks are typically thicker, or wider than existing decks. Several of these newly rehabilitated bridges have exhibited poor ride quality and generally displayed “dips” in roadway elevations. These “dips” generally occur nearer the mid-spans of the bridges, or at least in locations that are not near the supports provided by bridge piers. In some bridges, roadway elevations dipped more than 1 in. at midspan compared to elevations at the pier supports, and in many cases, within spans less than 60 ft in length.

Forensic investigations were performed on three newly rehabilitated bridges in Oklahoma. The investigations provided evidence that poor elevation controls were caused by poor design details for formwork and bracing or by construction practices that did not properly control elevations during construction. The combination of factors resulted in unevenness in bridge deck elevations and thin bridge decks in two of the three cases studied. Additional laboratory testing on overhang brackets confirmed that the commercially available brackets used for bridge rehabilitations to

support the cantilever portions of the concrete bridge decks are insufficient to provide the elevations control resulting in undesired deflections.

Bridges built composite with concrete decks generally undergo downward deflections caused by self-weight of the concrete (before setting), upward deflections caused by heating of the hydrating concrete deck immediately after initial set, which, in turn is followed by downward deflections due to cooling of the hardened concrete plus the effects of initial shrinkage. The downward deflection of the bridge beams that results from self-weight of the cast-in-place concrete deck slabs is considered in design. However, following volume changes in the concrete are not considered. Instead volume changes in concrete bridge decks are considered small and are therefore not considered for design; however, concrete begins to change volume immediately after taking initial set.

A full-scale prototype bridge was built and instrumented at the Bert Cooper Engineering Laboratory on the campus of Oklahoma State University in Stillwater, OK USA. A full-scale model of the bridge allows to capture the absolute values of the original time dependent properties of concrete deck that cannot be completely captured using a small-scale model. Early age deflections of the bridge were measured, as were concrete temperatures, concrete strains, steel girder strains and inclinations of the steel girders at ends. Data were analyzed and their relationship to time dependent concrete properties are established. The results indicated that the concrete strains associated with volume change, including both temperature-related strains and shrinkage strains, are large enough to be considered as one possible cause for adverse ride quality and unwanted deformations in steel girder bridge. Analytical computational models were developed to predict the thermal and shrinkage indices strains, stresses and deformations due to volume changes in the slab at early ages.

Concrete bridge decks are also subject to repeated temperature changes that cause temperature gradients through the depth of the slab and through the depth of the cross section. These temperature gradients produce internal thermal strains and stresses that directly result in bridge deformations.

Generally, restraint from the composite girders cause compression in the slabs during heating and tension in the slabs during cooling. Thermal loading was applied to the prototype bridge deck after 56 days of curing. Uniform heating of the deck caused a temperature gradient within the bridge deck resulting in differential strains and stresses at various location of the bridge deck. The results from the real time thermal loading on the prototype bridge decks showed that the temperature gradients produced internal thermal strains and stresses that directly resulted in bridge deformations. Computational analytical models were developed to predict and validate the stresses and strains developed in the composite cross-section of the prototype bridge. The models found good correlation with the measured overall bridge deflections.

This research seeks to understand the mechanical properties of concrete, and its interaction with steel bridge girders with the purposes of deepening our understanding of the behavior of steel girder bridges made composite with concrete bridge decks. The research demonstrates that the cumulative effect due to volumetric changes in concrete, temperature effects and poor bracing system can diversely affect the ride quality, cause deck cracking and excessive deflections, decrease durability and reduce long-term performance of steel girder bridges made composite with concrete deck slabs. The over-riding objectives are to provide recommendations for ODOT on improving the construction methods and concrete materials employed in practice, with the hope of extending the lifespan of bridges and improving their overall performance in service.

The structural monitoring system used in this research program combines sensors from diverse technologies into a seamless system using a single database and user interface system allowing for real time data acquisition and analysis. The instrumentation system was programmed to monitor both early age and long-term performance of the laboratory prototype bridge. Synthesis of data collected from the sensors along with analytical computational models that were developed using the measured constitutive properties of concrete validated the methods for structural monitoring. Concrete strains and temperatures measured from the VWSGs and thermocouples in the early ages during and

immediately after bridge deck cast provided a good understanding of the early age strains developed in the concrete deck. The research principally used the measured concrete temperatures from thermocouples during heat load testing to predict and validate the thermal strains, stresses and deflections in bridge decks. This dissertation provides a practical means of monitoring bridge performance and offers a good experience for implementation and structural monitoring for both laboratory and field bridges.

Summary of Research Methodology

The following generally describe the research methodology, and provide an outline for this dissertation:

Chapter II: This chapter includes a thorough literature review of the effects of time dependent properties on steel girders made composite with concrete slabs. Review of previous research investigating the effects of creep of concrete both in tension and compression and effects of early age shrinkage of concrete in composite bridge girders is presented. Previous research on the effects due to cracking of bridge decks due to shrinkage and creep of concrete are also discussed. Detailed literature review on bridge deck overhang systems that pertains to experimental testing performed on bridge overhang brackets is presented. A thorough literature review on the temperature gradient in bride decks, influence of thermal stresses and strains and effects due to the coefficient of thermal expansion of the concrete are discussed.

Chapter III: This chapter includes a thorough literature review of bridge instrumentation, types of sensors and datalogger systems used in the monitoring of bridge structures. This chapter describes in detail the instrumentation of a full-size prototype bridge and the structural monitoring of the bridge for short-term and long-term bridge performance. This chapter also includes descriptions of the instrumentation that is chosen for use, the reasons for specific instrumentation choices, and how the instrumentation is deployed for both short-term and long-term structural monitoring of bridges. A

detailed description of the scope, installation and performance of each sensor used in this research are discussed. The advantages and limitations are presented for each type of sensor used. The planning and implementation of structural monitoring of a field bridge are presented.

Chapter IV. This chapter focuses on excessive and undesired deformations that occur during construction of newly rehabilitated steel bridges. The chapter highlights the problems with elevation control and subsequent ride quality problems exhibited in newly constructed or newly rehabilitated steel girder bridges made composite with concrete decks cast atop steel girders. This chapter reports the findings from forensic investigations that were performed on three newly rehabilitated bridges in Oklahoma. Evidence due to poor elevation control and poor design details, unevenness in bridge deck elevations were reported. In addition, laboratory experimental investigations on overhang bracket systems and its influence on poor elevation control and unexpected deflection in overhang portions of the bridge deck is also reported.

Chapter V: This chapter focuses on deflections and deformations that occur at early ages in newly rehabilitated bridges made from steel girders and composite concrete deck slabs. This chapter describes the construction of the full-sized bridge at the Bert Cooper Engineering Laboratory. The chapter highlights how the early age deflections of the bridge, concrete temperatures, concrete strains, steel girder strains and inclinations of the steel girders at ends were measured. The chapter shows how the collected data were analyzed and correlated to the time dependent concrete properties. This chapter also shows that simple analytical computational models can be developed to predict the thermal and shrinkage indices strains, stresses and deformations due to volume changes in the slab at early ages.

Chapter VI: This chapter focuses on determining the impact of thermal loading on durability and serviceability of steel girder bridges made composite with concrete slabs. This chapter illustrates the application of thermal loading to the bridge deck of a full-size prototype bridge built in laboratory

conditions. This chapter displays that how the uniform heating of the deck can cause a temperature gradient within the bridge deck resulting in differential strains and stresses at various location of the bridge deck. The chapter demonstrations the development of a detailed computational analytical models that can predict and validate the stresses and strains developed in the composite cross-section of the prototype bridge.

Chapters in this dissertation are generally written as "stand-alone" manuscripts so there may be some redundancies in reading from chapter to chapter. Because of this organization each of the Chapters III through VI will contain relevant background Information. Additionally, each chapter contains a separate and distinct list of research objectives and a separate and distinct discussion and conclusions. Chapter VII of this dissertation intends to be a summary and conclusions chapter that incorporates and includes the summaries and conclusions of all the individual chapters.

Research Objectives:

Chapter III:

1. To build a full-sized laboratory bridge with composite concrete deck that will experience the similar mechanisms of bridges built in field.

2. To install a structural monitoring system that can capture both the short term and long-term performance of bridges built both in the lab and in field.

3. To identify the specific type of instrumentation and sensors that are effective for the monitoring of bridges in field.

4. To determine the explicit type of data acquisition system required to monitor and acquire data on the performance of bridges.

Chapter IV:

1. To identify the causes for undesirable elevation profiles and excessive deformations in newly constructed or newly rehabilitated composite bridges built in field.

2. To develop design and construction methods and recommendations to help mitigate problems with ride quality and unexpected deflections in ODOT bridges.

3. To evaluate the performance of C-49 overhang brackets when used in combination with shallow girders and larger overhangs.

Chapter V:

1. To determine the factors that influence the early age deformations in steel girder bridges built composite with concrete slabs.

2. To build a full-sized bridge with composite concrete deck that will experience the similar early age mechanisms in the concrete decks of the bridges built in field.

3. Improve understanding on early age volume changes in concrete due to thermal and shrinkage and its effects on bridge deformations.

Chapter VI:

1. Measure and quantify the effects of thermal gradient and resulting thermal stresses on the performance of steel-concrete bridges.

2. To compare and correlate the measured and AASHTO positive vertical temperature gradient developed in steel-concrete composite bridge girders.

3. To validate the deformations and thermal stresses and strains developed in the composite section with the use of analytical computational models.

CHAPTER II

BACKGROUND

A bridge that is structurally deficient has significant deterioration or defects of the bridge deck, superstructure, or substructure. The U.S. Federal Highway Administration (FHWA) lists 614,387 bridges within the US National Bridge Inventory (NBI). These are bridges positioned on highways identified as the National Highway System (NHS), and consist of principally of Interstate Highways and other major U.S. Highways. Of those bridges, almost 40 percent are 50 years or older. Moreover, in 2016 about 9.1% (56,007) of the NBI were rated structurally deficient (ASCE 2017). As the average age of America's bridges keeps increasing, many of the nation's bridges are approaching the end of their design life. Therefore, an increasing number of nation's bridges require major rehabilitation to extend the lifespan of these bridges.

Within the State of Oklahoma, the Oklahoma Department Of Transportation (ODOT) maintains 3,727 span bridges (Russell August 2017). Of those, 1617 bridges are made with steel girder superstructures with an average construction year of 1963. In 2010, about 706 bridges in the state of Oklahoma were classified as structurally deficient (ODOT 2017). Of those listed as structurally deficient, approximately 270 were bridges supported by steel superstructures. In recent years, the ODOT has been actively rehabilitating steel girder bridges by casting new concrete decks on top of existing steel girders.

This method of rehabilitation is chosen as cost effective means of repairing bridges that are structurally deficient, functionally obsolete, or both. In the process, the life span of a single bridge can be lengthened dramatically while helping to ensure the safety of the traveling public. The Oklahoma Department of Transportation (ODOT) is committed to reducing the number of structurally deficient bridges in the state and the current eight-year plan includes improvements on all the known structurally deficient bridges.

During the rehabilitation process, new bridge decks are often made both wider and thicker. In many of these bridges, concrete slab depths increased from the original construction of 152 mm to 203 mm, and the roadways were widened to allow modern lane widths with shoulders. Often, the structural designs of the newly rehabilitated bridges "worked" as shear studs are added to ensure composite behavior and increase shear capacity to account for heavier design loads in more recently adopted rating and design codes. In addition, the increased deck thickness also worked to help increase live load capacities, which offset the increasing dead loads.

As the State undertook an aggressive policy of rehabilitating these steel girder bridges, many newly reconstructed steel girder bridges exhibited poor ride quality and generally displayed "dips" in roadway elevations. These "dips" generally occur nearer the mid-spans of the bridges, or at least in locations that are not near the supports provided by bridge piers. In some bridges, roadway elevations dipped more than 1 in. at midspan compared to elevations at the pier supports, and in many cases, within spans less than 60 ft in length.

In 2012, as an early part of the research program, forensic investigations (Russell October 2014) were performed on three recently rehabilitated bridges. Two of these bridges were identified with poor ride quality. The forensic investigation found that ride quality problems resulted directly from inadequate bracing and poorly supported by formwork that supported outside edges (or cantilevered sections) of the bridge deck. In those bridges, the screed rails used to establish

roadway elevations were supported formwork that was supported by cantilevered bracing extending outside the steel girder centerlines by as much as 4 ft. In the third bridge where ride quality was rated as "good," screed rails set to establish roadway elevations were supported directly on top of existing steel girders, and cantilevered portions were finished by hand. Recommendations to remediate this problem through construction and project quality controls have been made to the ODOT. In addition, the research undertook the goal of measuring and assessing the volume changes within a newly constructed concrete deck to determine whether time dependent temperatures changes, shrinkage and other volume changes could affect the ride quality of rehabilitated bridges.

Composite action

Composite action in structures can be defined as the interaction of different structural elements in which the materials act as a single unit under superimposed loads. Bridges consisting of a cast-in-place reinforced concrete slab on a steel beam are one of the most common composite structures. Steel studs are the most common method for providing composite action between the concrete deck and steel girders. In the design of composite steel and concrete structures, the engineer should understand the bond between the components.

Oehlers and Bradford (2013) state that there are several reasons for combining steel and concrete elements to form composite members. When the steel and concrete are bonded together, the steel will be subjected to tension and the concrete will resist the compressive forces. This can double the flexural strength and stiffness of the beam leading to reductions in span to depth ratios and overall cost savings.

The composite action occurs in a steel girder bridge when the strains at the bottom of the concrete slab equal the strain at the top of the steel flange. As the concrete deck undergoes hydration, takes initial set and hardens, a partial interaction phase exists between the concrete and steel before

achieving the fully composite action. During this phase a compressive force develops at the bottom fiber of the concrete slab while an equal and opposite tension reaction is imposed on the top fiber of the steel beam. As a result of these forces, the neutral axis of the slab is shifted downward while that of the beam is shifted up.

Once the bridge becomes composite, the shrinkage of the concrete slab is restrained by the steel beam. Tensile stresses develop in the concrete and cracking occurs when these stresses exceed the tensile strength of the concrete. Laboratory testing and research conducted by Abdelmeguid (2016) concluded that shrinkage in concrete could be a possible cause for adverse deflection in composite steel girders. Therefore, an accurate prediction of when the composite action happens between the concrete and steel is important. This will allow the engineers to make necessary changes to construction practices to limit excessive deflections and prevent early age cracking in bridge decks.

The early age composite action was evaluated by Bao, Hoehler et al. (2017). A long span steel-concrete composite beam was constructed in the National Fire Research Laboratory (NFRL) at the National Institute of Standards and Technology (NIST). The beam was instrumented with fully distributed fiber optic sensors to monitor the early age temperature and strain distributions in the concrete. The results were used to understand the effects of composite action on the evolution of strains in concrete. Composite floor beams, 12.8 m long were constructed in the NFRL at NIST. Light weight concrete slab measuring 12.8m x 1.83 m was cast on top of fluted galvanized metal decking and supported by a single W 18 x35 steel girder welded on the top flange with 19mm diameter shear studs spaced at 305mm . The concrete was reinforced with 6x6 W1.4/W1.4 welded wire mesh and thickness of concrete varied from 84mm to 160mm. A plastic-fiber reinforced lightweight concrete with a w/cm ratio of 0.46 was mixed at a commercial batching plant and transported to NIST for placement. The distributed fiber optic sensor was embedded in the concrete deck and along the length of the steel girder. The temperature and strain distributions

in concrete decking were measured during the first two days of curing. From the recorded data it was found that the concrete temperature readings increased due to hydration of cement and was relatively uniform along the length of the composite beam. In comparison, the recorded strain readings were non-uniform and decreased over time. The paper concluded that the non-uniform strain readings might be due to development of cracks in concrete. The paper recommended further studies to understand the effects of early age composite action between the steel beam and concrete deck.

Overhang Bracing Systems

A bridge overhang is the portion of the concrete deck that extends from the centerline of the external girder to the edge of the deck. A temporary formwork system that comprises of timber joists and plywood sheathing supported by steel overhang brackets are generally used for supporting and shaping the overhang concrete deck. The proper design of bridge overhang bracket systems is critical to hold the dead weight of the fresh concrete, finishing screed and other construction loads during the time of deck pour.

Experimental investigation was conducted on three main types of commercially available overhang bracket forming systems. Among them was the Dayton Superior C-49 overhang bracket which is widely used in both prestressed concrete girders and in composite steel girders. The overhang bracket system was load tested and the results showed excessive deflection of the bracket system that was mainly contributed due to buckling of bracket, excessive rotation at the connection to the steel hanger via coil rod and hanger (Clifton 2008).

(Clifton 2008) Experimental investigation was conducted on three main types of commercially available overhang bracket systems to determine their feasibility with TxDOT pretensioned concrete I-girders. The test program, funded by Texas department of Transportation was conducted by University of Texas Austin, at the Phil M.Ferguson Structural Engineering

Laboratory. Thirteen different types of load tests were performed to understand the behavior of the current overhang bracket systems which were attached to the new TxDOT I-girders.

Four types of fully pretensioned concrete I-girders, 30 ft long were fabricated, instrumented and tested in the Ferguson Structural Engineering laboratory. Three main types of commercially available overhang bracket forming systems along with their accompanying accessories were attached to the girders and tested for performance. Among the three was the Dayton Superior C-24 45° Pres-Steel Precast Half Hanger Type 4-APR used along with the C-49 Bridge overhang bracket. The C-24 Type 4-APR was the standard steel overhang hanger used in precast applications and placed in the top flange of the girders during prestressed concrete beam fabrication. The C-49 overhang bracket is widely use in both prestressed concrete girders and in steel girders composite with concrete deck slabs. The bracket is typically made of light gage steel pipe and channel sections. The loading criteria and bracket spacing were reviewed according to manufactures specifications. A stable self reacting frame was implemented at the Ferguson laboratory, where both sides of the girder were loaded simultaneously. Two brackets on both sides of the girder were loaded simultaneously. A hydraulic ram was used to load the brackets and Interface load cells of 100 kip were used to capture the load. Linear potentiometers were placed capture the deflection of the top flange and the end of overhang brackets. Strain gages were installed on the mild steel reinforcing bars located at the top flange of the concrete girder.

Various types of failure mechanisms including punching shear at the hanger tip, combined punching shear/tensile failure at the embedded face of the top flange and excessive deflection of the bracket system were identified. Results showed that the excessive deflection of the bracket system was mainly contributed due to excessive damage, rotation, buckling of bracket, coil rod or hanger. The experimental results showed that the top flange of the girder cracked at 6500 lbs and the bracket system failed under an applied vertical load of 7000lbs with the buckling of the top chord of the C-49 overhang bracket. Inelastic damage was observed in all four brackets and the

significant rotations were observed on some of the C-24 hangers. Based on these results recommendations were made to the Texas DOT on allowable construction loads on the overhang bracket systems.

The overhang bracket systems that are attached to the external steel girders with embedded hangers and threaded coil rods are likely to impose unbalanced eccentric and torsional loads on the girders. Yang (2009) investigated the instability of a twin steel girder system with combined flexure and torsion due to unbalanced overhang loads. Their study concluded that unbalanced eccentric overhang loads leads to a significant amount of lateral displacement and twist of twin girder systems particularly in bridge widening applications. Experimental studies conducted by Patil (2009) at Oklahoma State University have proven that precast bridge deck overhang systems can provide an effective construction technique that can be implemented on both rehabilitated and new bridge construction.

Effects of time dependent properties on composite steel beams

Time dependent deformations in concrete structures have become of great importance in recent decades. Creep and shrinkage of concrete are interdepended and cause time depended deformations due to the gradual changes in stresses and strains over time. These stresses and strains sometime become too excessive affecting the durability of the concrete resulting in cracking of bridge decks and unexpected deformations in bridge girders.

Shrinkage of concrete

There are two primary types of shrinkage in concrete – drying shrinkage and autogenous shrinkage. Drying shrinkage is the result of water loss in hardened concrete. As the water evaporates from the concrete, the volume of concrete reduces. Autogenous shrinkage is the concrete shrinkage without loss of water. This shrinkage occurs when there is a low w/cm ratio and increases with the use of silica fume, high range water reducing admixtures (HWRAs) and

finer cement Hadidi, Saadeghvaziri et al. (2003). The majority of shrinkage occurs during the hydration process. Concrete is prone to volumetric changes due to thermal and moisture related shrinkage at early ages. When concrete is restrained and prevented from shrinking freely, tensile stresses develop in the restrained concrete. Research performed by Khan, Murray et al. (2015) found that these tensile stresses induced by shrinkage are relaxed by creep. This makes it important to quantify the early-age tensile creep and shrinkage of concrete.

Shrinkage in composite bridges is important for serviceability as it affects both stress limitations and deflection. Alexander (2003) studied the effects of concrete shrinkage on composite steel beams. His article explains the theory behind shrinkage of concrete and calculates its effects on serviceability which includes stress limitations and deflections in composite beams. His analytical model assumes that a contraction force is applied to the steel beam as an external force. The beam stresses, curvature and deflections were calculated using simple beam mechanics. Two potential sources of contraction forces that includes 1) Early age thermal loading due to hydration effects and 2) Early age shrinkage of concrete were used in his model. Early age thermal loading was ignored here since the slab deflects upwards during the period of hydration due to the heat of hydration and deflects back downwards at the end of hydration period. The author also states that although shrinkage occurs continuously, it is also relieved by some amount of creep in the concrete. Atypical shrinkage limit of 400 micro strains for internal conditions can be adopted. Eurocode 4 states that the calculation of stresses and defamations at the serviceability limit shall take into account the effects of creep and shrinkage of concrete, and further that the effect of curvature due to shrinkage of concrete should be included when the ratio of span to overall depth of the beam exceeds 20 and the predicted free shrinkage strain of the concrete exceeds 400×10^6. The author highlights the significance of deflection due to shrinkage by including it as a part of the long-term deflection. A simple rule was to assume a limit for shrinkage deflection, which would be equivalent to span/750 unless estimated by a more accurate calculation.

Research by Li and Glisic (2017) developed a practical method for evaluating initial strains and stresses due to early age shrinkage in steel-concrete composite structures that can be used universally in the structural health monitoring of composite beam like structures. Experimental tests on scale-model test structure was performed and the initial strain state due to early age shrinking was measured through elastic strain measurements. Analytical methods were employed to determine the reasonable range of early age shrinkage and deflections due to that. In addition, finite element modelling was also performed to simulate and quantify the magnitude of shrinkage in the concrete slab of the composite structure. The scale model structure consisted of a three W 16x57 steel girder line beams, 30 feet span with 8-inch-thick and 12 feet wide concrete deck on top. The strains and temperature for both steel and concrete was measured using fiber optics and temperature sensors attached to the steel girder and embedded in concrete prior to deck cast. The structure was placed on level ground after formwork removal and then the scale model structure was subjected to two types of static loading events seven days after slab cast. For the first static loading the structure was lifted at two intermediate jacking locations and for the second the structure was simply supported between two wooden supports. The strain data were recorded before and during these loading events. A 3D finite element model was created to analyze the two static load cases. Both the measured and simulated results exhibited liner strain profile across the full depth that strongly supported the composite beam theory. The modelled and measured strain measurements correlated well with each other. Early age strain distribution across the depth of the girder was measured and compared with the estimated values arrived from finite element analysis. Using compatibility equations and simplified analysis the authors claim to predict the effective curvature and the resulting deflection induced due by early age shrinkage due to the double-cantilever effect. The paper concluded that the early age shrinkage in composite steel-concrete beam like structures could lead to partial activation of the beam's self-weight, that would create a non-zero initial strain conditions in the overall composite structure. From experimental testing and study, it was found that the magnitude of early age shrinkage strains

constituted to about 27% of the magnitude of the maximum bending strain due to self-weight of the structure. Further research on steel-concrete structures was recommended to improve further understanding of the behavior of composite beam like structures in the presence of early-age shrinkage of concrete components in general.

The early age behavior of concrete due to temperature and shrinkage was evaluated by Bao, Hoehler et al. (2017). A long span steel-concrete composite beam was constructed in the National Fire Research Laboratory (NFRL) at the National Institute of Standards and Technology (NIST). The beam was instrumented with fully distributed fiber optic sensors to monitor the early age temperature and strain distributions in the concrete. The results were used to understand the effects of composite action on the evolution of strains in concrete. Composite floor beams, 12.8 m long were constructed in the NFRL at NIST. Light weight concrete slab measuring 12.8m x 1.83 m was cast on top of fluted galvanized metal decking and supported by a single W 18 x35 steel girder welded on the top flange with 19mm diameter shear studs spaced at 305 mm. The concrete was reinforced with 6x6 W1.4/W1.4 welded wire mesh and thickness of concrete varied from 84mm to 160mm. A plastic-fiber reinforced lightweight concrete with a w/cm ratio of 0.46 was mixed at a commercial batching plant and transported to NIST for placement. The distributed fiber optic sensor was embedded in the concrete deck and along the length of the steel girder. The temperature and strain distributions in concrete decking was measured during the first two days of curing. From the recorded data it was found that the concrete temperature readings increased due to hydration of cement and was relatively uniform along the length of the composite beam. In comparison, the recorded strain readings were non-uniform and decreased over time. The paper concluded that the non-uniform strain readings might be due to development of cracks in concrete. The paper recommended further studies to understand the effects of early age composite action between the steel beam and concrete deck.

Experimental field investigation was performed on a 3-span continuous steel girder bridge composite with concrete deck on top located in Evansville, Vest Virginia (William, Shoukry et al. 2008). The bridge deck was extensively instrumented to monitor the strains and temperature in the concrete deck and strains in the reinforcing bars. The main objective of this paper was to identify the contribution of concrete shrinkage to the premature transverse cracking of concrete bridge decks and provide recommendations to reduce or eliminate the frequency of occurrence. The paper also highlights the importance of shrinkage and thermal stresses induced in bridge decks and recommends its inclusion in the current practice and standards along with the design of the bridge to sustain traffic loadings.

The Evansville Bridge was a typically three span continuous steel girder bridge with a skewed angle of 55º. The bridge carries WV Route 92 across Little Sandy Creek in Preston County, West Virginia. The bridge is supported by two piers and two integral abutments. The bridge featured a seven-girder line, with an edge span of 14.78m and central span of 15.24m long. The bridge supports a concrete deck of thickness of 200mm between the girders and 225mm over the girders. The bridge structure was designed in accordance to 1999-AASHTO LRFD bridge design specifications for a HL-93 live load model. The bridge was constructed in two stages and was instrumented with about 232 sensors during the first stage of construction. Two types of strain gages including the vibrating wire strain gages and wire resistance strain gages were placed at strategic locations on three girders to measure the long-term strains due to static loading and environmental effects and short-term dynamic loads due to traffic loading. Geokon vibrating wire sensors specifically captured the long-term triaxial state of strain caused by environmental variations and concrete temperature with embedded thermistors within the sensors. In addition to strain measurements other sensors were also used to record temperature gradient through the deck thickness, strains in the reinforcing bar, crack with opening, girder inclinations, expansion joint openings and local weather conditions. The sensors were connected to multiplexors and the data

was recorded and monitored using CR10 Campbell Scientific datalogger systems. The dataloggers were powered by marine batteries which were charged using solar panels. The dataloggers were equipped with a phone modem to retrieve data for any location in the USA via a phone line.

The deck was composed of a monolithic Class K concrete deck approved by West Virginia Division of Highways. The deck was placed on June 2003 and wet cured for seven days with burlap sacks and covered with plastic sheets to prevent the escape of moisture. Standard concrete cylinders were prepared and cured on site and transported to the lab to measure the mechanical properties. In addition, three concrete cylinders with embedded vibrating wire strain gages were subjected to uniaxial compressive loading to measure the axial and radial strains. From recorded early age thermal strains, it was shown that the thermal strains were much higher in magnitude than the flexural strains induced due to the self-weight of the deck. The magnitude of tensile stresses developed due to drying shrinkage was observed to be higher than the modulus of rupture of concrete for 1-day strength. This was concluded to be the primary cause for the early age cracks in the bridge deck. The effect of volumetric changes due to drying shrinkage was found to be higher than the effect due to temperature variations. The results indicated that the magnitude of tensile stresses induced in the concrete deck slab due to both drying shrinkage and temperature variations during curing were relatively high compared to those induced due to traffic loading. The paper also concluded shrinkage induced tensile stresses and early age cracking in the concrete can be reduced by using low shrinkage concrete and increased modulus of rupture.

Research on the effects of shrinkage on shrinkage induced deformations in composite steel and concrete bridges was also performed by Abdelmeguid (2016). In this research prototype beams were cast and monitored for temperature, strains and deflections. The laboratory testing indicated that the strains associated with volume change, including both temperature and drying shrinkage were large enough to be one possible cause for adverse deflections in steel girder bridges.

Furthermore, analytical models were developed and compared with the results from the prototypes. The results from the research affirmed that the volume changes in concrete can cause bridges to deflect downward. The results further show steel strains to be consistent with the change in temperature and concluded that shrinkage in concrete slabs do not contribute to the strains that occur in steel girders.

Creep in Concrete

Concrete creep is the increase in deformation under a constant or sustained load. This phenomenon is better understood in compression and not so much in tension. Experimental tests have proven that the actual tensile creep is not equal to compressive creep Forth (2015). Creep in tension is significantly more important than the creep in compression especially in early age concrete (Rossi, Tailhan et al. 2013). Tensile creep in early age concrete delayed cracking induced due to shrinkage in concrete Khan, Murray et al. (2015). From the restrained shrinkage tests they found that, the increasing degree of restrain in concrete induced more tensile stresses and hence reducing the time to cracking. Deflection in concrete structures are influenced by the tension stiffening capacity of the composite section. Hence tensile creep in concrete is more important for accessing early-age cracking risk and evaluating the long-term deformation of bridge structures.

Concrete Compressive Strength

Compressive strength is defined as the measure of maximum resistance of concrete specimen to axial compressive loading (Association 2002). Cracking in bridge decks is often correlated to high concrete compressive strength. High strength concrete with higher rate tensile strength has much lower creep and a high cracking potential than regular concrete(Peyton, Sanders et al. 2012). Concrete Bridge deck slabs built on composite steel girders when loaded develop inherent strength due to restraint in the lateral direction hence developing a compressive membrane action.

This mechanism enhances the ultimate strength of deck slabs in composite steel girder bridges. Experimental testing by Zheng, Taylor et al. (2010) indicated that the compressive membrane action is highly influenced by the concrete compressive strength and lateral restraint stiffness of the concrete deck slabs.

Modulus of Elasticity of Concrete

Elastic modulus is the property of concrete that can be characterized as the relationship between the stresses and strains in the concrete material. Gradual changes in stress during the service life of a structure produces additional instantaneous and creep strains. These additional strains are superimposed on the creep strains due to the initial stresses and to all previous stress changes. Due to concrete aging these additional strains are much less than those which would arise if the same stress changes occurred right after the instant of first loading. This effect is accounted for by the use of age adjusted effective modulus, originated by Trost (209R-92 1992). The effective modulus of elasticity of concrete is reduced due to creep effects; it combines the effect due to elastic strain and creep of concrete as an elastic deformation on concrete section. Therefore, the right understanding of the time dependent properties of concrete will not only enable to control deflections in concrete members but also decrease the extra transfer of stress to other concrete elements which can cause the concrete to crack or fail prematurely Liu (2007).

Early age cracking in Bridge decks

Early age bridge deck cracking in newly constructed or rehabilitated steel composite bridge girders has been a common problem in Oklahoma state department of transportation. This causes severe durability and ride quality problems and can adversely affect the strength and serviceability of bridges. Bridge deck cracking is caused due to a combined mechanism of restrained shrinkage, creep, development of concrete strength over time, heat of hydration and differential temperature gradient between the concrete and steel girders. A full understanding of

the above mechanical properties is an integral part of predicting the cracking potential of a bridge deck (Pesek, Riding et al. 2017). The failure to account for cracking due to unanticipated shrinkage restraint, temperature gradient and construction loads on lightly loaded reinforced concrete members can result in significant underestimation of deflection (Gilbert 2012).

The amount of thermal restraint on bridge decks arrives from the thermal gradient and in coefficient of thermal expansion between the concrete deck and steel girders. When the temperature of concrete increases due to heat of hydration, the concrete will expand in proportion to its coefficient of thermal expansion and temperature. As the steel girders restrain the expansion of concrete deck, the thermal strains are effectively converted into compressive thermal stresses. The eventual decrease in temperature results in stress relaxation and reduces the compressive stress in concrete. A further decrease in concrete temperature causes tensile stresses in concrete to increase.

The authors (Riding, Poole et al. 2009) researched how materials and construction methods can influence the thermal stresses in bridge decks that lead to early age cracking in bridge decks. This research used rigid cracking frames to examine the concrete early age stress development by capturing the full effects of creep and modulus development in concrete from casting through setting and hardening. This method was developed to evaluate the effects of placement time and concrete coefficient of thermal expansion, which was used along with rigid cracking frames to calculate the cracking tendency of different concrete placement scenarios. In addition, field bridge located in Austin, TX was instrumented and monitored for bridge deck temperature development for varying concrete placement times. The temperature sensors were installed both in horizontal and vertical direction of the bridge deck. Coefficient of thermal expansion of hardened concrete was measured according to AASHTO Provisional Standard TP60-00. The experimental testing showed that the early age thermal stresses in newly poured bridge decks were reduced up to 50% by using coarse aggregate with lower coefficient of thermal expansion

and placing concrete at night. The time of placement and coefficient of thermal expansion of concrete are significant parameters contributing to thermal cracking in bridge decks.

Subramaniam, Kunin et al. (2010) investigated the thermal movements and stresses in the concrete deck and steel girders due to changes in temperature introduced by heat of hydration release that occurred during the first few hours after casting the concrete deck. When majority of the researchers had given considerable attention to the cracking of concrete decks due to restrained shrinkage, his paper focused on the correlation between the temperature changes and cracking in bridge decks. The paper concluded that at the end of the heat of hydration period the concrete deck gains sufficient stiffness and restrains the movement of the top flange of the girder. Concrete begins to set at the end of the heating period and has lower tensile strength. A large temperature gradient in the steel girder at the end of the heating period induces larger tensile stresses in the concrete which may increase the likelihood for concrete to crack. It was also found that larger difference in temperature between the concrete deck and the top flange of the steel girder at the end of the cooling period could contribute to larger magnitude of tensile stresses in the concrete deck.

Temperature gradients in composite bridges

Bridges are subjected to repeated cycles of heating and cooling from solar radiation and the surrounding air. For concrete-steel composite bridges, this exposure produces thermal movements and stresses in bridges due to external restraints and dissimilar material properties. These temperature-induced stresses depend on the end conditions of the bridge structure and the temperature distribution. The temperature variations caused by thermal loads in the bridge superstructure are referred to as the temperature gradient. Current AASHTO specifications (American Association of State and Transportation 2014) provide probable temperature ranges to account for the overall expansion and contraction due to the presence of thermal changes through

the depth of the structure. For the design temperature gradients, a map of the United States is divided in to four regions. For each region, a temperature T_1 and T_2 value is provided which defines the design positive temperature gradient. Oklahoma falls under zone 2 where the reference temperatures T_1 and T_2 are given to be 46 ºF and 12 ºF respectively.

Research by Rojas (2014) investigated the effects of temperature changes in two bridges in California and Utah over a period of more than two years. The research study analyzed the data from thermocouples that was used to determine the average bridge temperatures over time and compare it to the 2010 LRFD Bridge design specifications of the American Association of State Highway and Transportation Officials (American Association of State and Transportation 2010). The research found that the maximum measured average bridge temperature gradients for both of the bridges monitored exceeded the service limit state established in the 2010 AASHTO LRFD Bridge Design Specifications. The temperature gradients were measured, and flexural stresses were calculated. The stresses and temperature gradients were found to exceed the service state established in the 2010 AASHTO LRFD Bridge Design Specifications in the case of the California Bridge. The average maximum and minimum bridge temperatures were predicted for both the bridges using the Kuppa Method (1998) and the Black and Emerson Method (1976) and compared to the measured temperatures in field. This research formulated a better predictive method called the ERL (stands for Edyson Rojas Lopez) to quantify the average bridge temperatures.

The California bridge, constructed in 1975, was a continuous span bridge with two equal span lengths of 39.32 m (129 ft.). The bridge was supported at the ends with reinforced concrete open-ended hinged diaphragms and reinforced concrete columns at the mid span. The bridge had a concrete deck thickness of 0.20 m (8 in.). The bridge had a clear roadway width of 12.20 m (40 ft.) with 0.30 m (1 ft.) overhand on each side. The superstructure of the bridge consisted of post-tensioned cast-in-place concrete box girders with four cells. A total of 71 sensors including foil

strain gauges, velocity transducers, vibrating wire strain gauges, thermocouples and tiltmeters were installed on the super structure of the bridge to monitor the structural health of the bridge. A total of 44 thermocouples were installed to monitor the changes in temperature throughout the box girders. A temperature gradient profile was developed using the thermocouple readings and the tiltmeters measured the changes in rotation due to temperature effects.

The Utah Bridge, constructed in 1976, was a single span bridge of length 24.90 m (81 ft 8 in.). The bridge was supported with reinforced concrete integral abutments at the ends. This bridge also had the same deck thickness of 8in. as the California bridge. The superstructure of the bridge consisted of five AASHTO type IV, prestressed concrete girders. The Utah bridge also had the same instrumentation setup very similar to the California bridge accounting to a total of 46 sensors recording and monitoring the structural health of the bridge. A total of 31 thermocouples were installed on the Utah Bridge to monitor the changes in temperature and record the temperature gradient throughout the depth of the bridge girder. The maximum positive and negative temperature gradients were measured for both the bridges and the values were compared to the temperature gradient recommended by the AASHTO LRFD Bridge Design Specification (2010) and the Priestley method (1978). The flexural temperature induced stresses were also measured using the other sensors and compared to the tension limit established in the AASHTO LRFD Specifications (2010).

The maximum measured average bridge temperature for the California bridge exceeded the recommended AASHTO Bridge specifications by 0.49°F (0.28°C) and the Utah bridge exceed by 1.5°F (0.83°C). The maximum and minimum average bridge temperatures for the both the bridges were predicted using the ERL, Kuppa (1991) and the Black and Emerson (1976) methods respectively. The research paper concluded that the ERL Method more accurately predicted the maximum and minimum average temperatures for both the bridges in comparison to the other methods. The maximum temperature induced tensile stresses in the California bridge due to the

temperature gradient only and exceeded the recommended limit by 39%. It was noted that the temperature induced tensile stresses in the Utah bridge did not exceed the recommended limit but was very close to cracking stresses without taking into account dead, live and other loads.

Jeffrey Johnson (2005) investigated and studied the response of three Saco Bridge decks subjected to environmental loads. The three bridge decks were located within a mile of each other and they specifically differed in their reinforcement steel and the type of concrete mix used for them. The change in the behavior of the three bridges due to the above factors was observed. The first bridge deck was designed in accordance to Montana department of Transportation practices and was referred to as the Conventional Deck. The second one was designed using the AASHTO Empirical Deck Design procedure. This resulted in considerably less reinforcement in the bridge deck than the conventional design. The third deck was constructed using High performance concrete combined with traditional reinforcement.

The three bridges were instrumented with vibrating wire strain gages (model VCE-4200) by Geokon. These gages were embedded directly in the concrete deck and were typically used to monitor long- term strain and temperature in structures. The vibrating wire strain ages were suspended in the concrete between the reinforcing bars. Strain and temperature measurements were monitored and recorded at an hourly rate as soon as the decks were poured. The results showed that the thermally induced strains on the filed bridges were of the same magnitude as the tensile cracking strains exhibited in plain concrete. It was also found that the thermal strains measured were much larger than the maximum static strains measured during live load testing of the Saco bridges.

Bridge structures are exposed to thermal loads daily, due to variations caused by solar radiations, ambient air temperature, humidity and wind. When these thermal loads are restrained the temperature, variations cause thermal stresses leading to deflections in bridge structures. In

addition, other factors including the orientation of the bridge structure, material of the deck surface, structural dimensions and the cross-section geometry are also found to affect the thermal response of the bridge.

Researchers (Krkoska and Moravcik 2017) performed long term monitoring of the temperature load on a chosen concrete bridge in Europe. A concrete box girder bridge located in Zilina, Slovakia was instrumented with concrete embedded strain gages to measure strains and temperature. In addition, thermocouples were also used to measure concrete surface temperature and thermometers to measure air temperature. The results showed that the variations in the air temperature can affect the overall temperature distribution of the cross section causing large temperature gradient across the depth of the bridge section. The vertical temperature gradient can sometimes exceed the allowable value in bridge design standard. Underestimation of the vertical temperature gradients in bridge cross sections can cause significant stress distribution in bridge decks resulting in cracking.

Fu, Ng et al. (1990) investigated the transient temperature and thermal stress distributions in various composite bridge structures. The effects of solar radiation and ambient temperature, material properties, and geometry on the distribution of temperature in a composite bridge were studied. From this research, it was found that the most influential variable on the temperature distribution was the slab overhang to depth ratio. This variable controls the area of the steel that is exposed to direct solar radiation. Additionally, Fu concluded that the convection constant substantially affected the temperature distribution. Possibly the most pertinent conclusion to his paper, however, is that the daily air temperature extremes had a remarkable influence on the thermal behavior of a composite bridge.

Giussani (2009) investigated the effects of non-linear distributions of thermal variations on composite steel-concrete elements. The author states that non-linear thermal stresses are

developed due to temperature gradient along the vertical axis of the composite section. This causes the development of self-equilibrated thermal stresses within the cross-section composite beams. The author recommends that these thermal stresses must be added to the stresses due to shrinkage of concrete slab and stresses due to dead and live loads for the design of composite steel-concrete beams.

Pavelchak and Williams (2013) performed a case study on the assessment of safe load capacity of an existing bridge structure constructed in 1968 that provided a sole means of access to a large privately held facility subjected to a 400-million-dollar expansion and renovation. The bridge consisted of AASHTO Type I beams with a composite cast-in-place concrete deck slab. The bridge spanned over five equal spans of 44 ft and the substructure was driven on precast concrete piles with cast-in-place bents. The available drawings indicated a design live load of H20-S-16-44 as per AASHTO 1965 design code. It was anticipated that the construction loads would significantly exceed the designed live loads of the bridge which created a need to inspect and assess the performance of the bridge. The bridge was first inspected to identify the current condition of the bridge for rating purposes and to document the condition of the bridge prior to initiation of heavy construction vehicle traffic over the bridge. The inspection report identified numerous maintenance issues to be addressed but generally the spans were found to be in good condition. The temperature of the structure was also monitored to understand the behavior of the structure. The recorded data showed that the differential heating and cooling of the bridge deck during the course of the day caused cyclic sweeping deflection changes due to differential thermal expansion and contraction. Higher temperatures during the day produced upward deflections, while cooler night time temperature produced downward deflections in the bridge.

Coefficient of Thermal Expansion of Concrete CTE

Coefficient of Thermal Expansion (CTE) is an empirical parameter which is defined as the measure of strain in a material due to changes in temperature. Concrete expands when subjected to higher temperatures due to heat of hydration or environmental temperature changes that causes internal thermal strains. CTE of concrete varies with paste, aggregate type, w/cm, concrete age and relative humidity of concrete mix (Johnson 2005). However, the CTE of concrete is highly influence by the aggregate type which approximately makes up to 60% of the total volume of the concrete mix. CTE of concrete is an important parameter when investigating thermal effects on bridge decks due to environmental temperature changes. Ebisch (2013) investigated the thermal effects in concrete pavements. The study investigated the coefficient of thermal expansion of concrete made with aggregates from various sources within Oklahoma. The study developed a new testing method, modified from the AASHTO T 336 standard method for the evaluation the coefficient of thermal expansion of concrete materials with a goal to provide accurate results with real time data. The research utilized the Auburn University's method of temperature isolation practice, that measured the deflection change in real time.

AASHTO T336-09 (T336) "Standard Test Method for the Coefficient of Thermal Expansion of Hydraulic Cement Concrete" is the most widely used method for determining the CTE of concrete. The T336 method, approved as a standard test method in 2009 and used by all state DOTs was based on AASHTO TP 60-00, "Provisional Test Method for the Coefficient of Thermal Expansion of Hydraulic Cement Concrete" (Tanesi, Crawford et al. 2012). In T 336 -09 method, CTE of concrete was determined subjecting the concrete specimen to varying temperature cycles and the change in length of the specimen was measured. The test setup consisted of mounting a saturated concrete specimen in a metal frame, submerged in a water bath subjected a temperature change from 10 to 50 ºC (50 to 122ºF). A spring loaded LVDT was installed in the metal frame and placed in contact with the top surface of the concrete specimen to

measure the change in length of the specimen. The deformation of the frame was accounted for by measuring the change in length of a steel specimen of known CTE value. Researchers from Auburn University (Sakyi-Bekoe 2008) further modified the T 336 method to minimize the temperature change of the LVDT during the time of testing. Three specific modification that included the provision of a machined ceramic collar to isolate the LVDT from the cross bar, machine ceramic spacer to isolate the tip of the LVDT from the water and a machined invar cylinder to isolate the ceramic spacer from the concrete specimen and water were provided (Byard 2010). Researchers from Auburn University further modified the T 336 method to minimize the temperature change of the LVDT during the time of testing. Researchers at OSU made slight modifications to the Auburn University's T 336 method and created a setup to continuously measure the change length of the concrete specimens during the CTE testing.

Researchers at OSU (Ebisch 2013) made additional slight modifications to the AASHTO T 336 method and used Auburn University's temperature isolation practice and created a setup that can continuously measure the change length of the concrete specimen real time during the CTE testing. The apparatus consisted of a rigid steel frame built in accordance with ASHTO T 336. A machined ceramic collar to isolate the LVDT from the cross bar, machine ceramic spacer to isolate the tip of the LVDT from the water and a machined invar cylinder to isolate the ceramic spacer from the concrete specimen and water were provided. The water bath consisted of a VWR signature heated/refrigerated water circulator, used for maintaining the desired water temperature within the holding tank. In addition, an external holding tank was used to evaluate two samples at the same time. A mass concrete vibration damper was used to reduce vibrations in the water from the circulator before they reach the holding tank. GCD-121-125 Schaevitz gage head DC LVDTs that were widely used by the FHWA, Auburn University and the University of Texas was employed in this test method. A National Instruments NI USB 9162 series datalogger was used to monitor and collect data from the LVDT sensors.

The 4 x 8 concrete cylinders were cut to a length of 7.0+-0,1"and prepared from standard ODOT mix for pavement design. About 11 different coarse aggregate types were used to evaluate the CTE for each mix. All the concrete samples were saturated in a lime water bath for 48 hours in accordance to AASHTO T 336. The concrete samples were then measured and mounted on to the metal frame. The data recording is initiated as soon as the samples are placed in the water bath. The water bath temperature is set to 50º F to start with and them ramped to 122º F over a period of 24 hours. The LVDT recorded the length measurements every 150 second over a period of 24 hours, which was found to be sufficient time for the samples to reach initial equilibrium. The data collected using the LAB view software were then filtered fir any noise interference. The results from this research confirmed that the modified version of the CTE test method developed at Auburn exhibited consistent and repeatable results. Further to this the modifications made by OSU researchers to isolate the LVDT from varying temperatures was efficient and was recommended to be incorporated for future CTE testing methods.

Jeffrey Johnson (2005) performed laboratory testing on the three types of concrete mixes used in the three field bridges to determine the CTE of concrete. Three concrete specimens from each bridge were used for this CTE investigation. The size of the specimens was 406.4 x 101.5 x 76.2 mm and were cast during the time the deck was poured for each of these bridges. Strain gages type N2A-06-40CBY-350 from Micro Measurements and Type T thermocouples form Omega were installed on the specimens to measure the thermal strain and temperature in each specimen respectively. The specimens were placed in a 2 x 2 x 2 m environmental chamber and subjected cyclic temperatures ranging from -40 deg C to +40 deg C. The CTE was calculated as the first derivative of strain with respect to temperature. The results showed that there were significant variations in the CTE of concrete with respect to temperature changes. It was understood that this variation was due to the change in the moisture content in the concrete specimens. It was also found that the CTE values of the traditional and the high-performance concrete were the same but

at temperatures below 0deg C the HPC had notably much lower CTE values. This was related to the microstructure and pore size of the high-performance concrete.

The CTE values of the field data were found to be higher than those measured in the laboratory. This difference was justified due to the composite action of the steel and concrete in the field samples. The results contradicted AASHTO statement for the difference in the CTE values between concrete and steel. A second factor that also contributed to the increase in the CTE values was the difference in the relative humidity experience between the laboratory and field concrete. The presence of physical water in the cement paste was found to have a noticeable effect on the concrete CTE values.

Researchers, Naik, Kraus et al. (2011) also investigated the CTE and variation splitting tensile strength for 15 different types of concrete mixtures made with 6 different types of coarse aggregates obtained from different sources to support the implementation of AASHTO's Mechanistic Empirical Pavement Design Guide (AASHTO 2008) in Wisconsin. The CTE of the concrete specimens were measured using AASHTO TP 60 method (AASHTO 2000). The testing concluded that the types of coarse aggregate influenced the CTE of concrete, experimentally determined value of CTE of a concrete mixture avoids variation in CTE owing to a change in aggregate types.

CHAPTER III

BRIDGE INSTRUMENTATION AND STRUCTURAL MONITORING

Introduction

The structural monitoring system used in this research program combines sensors from diverse technologies into a seamless system using a single database and user interface system allowing for real time data acquisition and analysis. A full-scale prototype bridge was built and instrumented at the Bert Cooper Engineering Laboratory on the campus of Oklahoma State University in Stillwater, OK USA. The bridge was constructed to replicate the Eagle Chief Creek Bridge "A" on SH 14 in Woods Co., Oklahoma. A full-scale model of the bridge allows to capture the absolute values of the original time dependent properties of concrete deck that cannot be completely captured using a small-scale model.

An array of sensors were employed to measure and monitor concrete and steel strains, concrete and steel temperatures, overall bridge deflections at several locations, and inclination of the steel girders. The sensors that were selected to perform these measurements include: Electrical Resistance bonded foil Strain Gauges (ERSG), Thermocouples, Vibrating Wire Strain Gauges (VWSG), Linear Variable Differential Transducers (LVDT) and Inclinometers. Synthesis of data collected from the sensors along with analytical computational models that were developed using the measured constitutive properties of concrete validated the methods for structural monitoring.

The main purpose of this chapter is to build a full- sized bridge in the laboratory and install a structural monitoring system that can capture both the short term and long-term performance of bridges built both in the lab and in field. This chapter aims to identify specific type of sensors and data acquisition system that are effective to monitor the performance of bridges in field. This chapter provides a practical means of monitoring bridge performance and offers a good experience for implementation and structural monitoring for both laboratory and field bridges.

The following are the primary objectives for this chapter

1. To build a full-sized laboratory bridge with composite concrete deck that will experience the similar mechanisms of bridges built in field.

2. To install a structural monitoring system that can capture both the short term and long-term performance of bridges built both in the lab and in field.

3. To identify the specific type of instrumentation and sensors that are effective for the monitoring of bridges in field.

4. To determine the explicit type of data acquisition system required to monitor and acquire data on the performance of bridges.

Background

"*Structural Monitoring (SM) is defined as a technology driven automated solution where sensing devices are installed in a structure with an intention to capture structural data continuously over a period of time, with a sole purpose of objectively and accurately assess the structural performance of the structure*" (TRB April 2019). In recent years SM has emerged as the cost-effective method to monitor bridge performance and provide real time damage detection. Over the past decade there has been significant technological advancements in sensors and bridge instrumentation (Pavelchak and Williams 2013).

According to Farrar and Worden (2007) structural monitoring is a strategy employed to identify infrastructure damages in civil, mechanical and aerospace engineering fields. The majority of the monitoring technologies include highly effective non-destructive tools. The use of structural monitoring tools for monitoring infrastructure including bridges and buildings has increased rapidly in recent years. Bridges all over the world are subjected to continuous environmental and physical destructive effects due to thermal radiation, low temperatures, deicers, pollutants, material aging, increasing traffic volume and overloading. This leads to structural deterioration and reduced life span of the bridges. According to the Federal Highway Administration (FHWA), of the 614,387 bridges in the US National Bridge Inventory, about almost four in 10 are 50 years old or older. Moreover, as of 2016 about 9.1% (56,007) of the nation's bridges were rated structurally deficient (ASCE 2017). As the average age of America's bridges keeps increasing, many of the nation's bridge are approaching the end of their design life. Therefore, an increasing number of nation's bridges will require major rehabilitation to extend the lifespan of these bridges. In 2010, 706 bridges in Oklahoma were classified as structurally deficient. Through a targeted strategy with significant budget allocations, the number of structurally deficient bridges in in Oklahoma had been reduced to 185 in the year 2017, a 74% reduction between 2010 and 2017 ODOT (2017). Whether a bridge is newer, older, in good repair or poor condition, structural monitoring is a means to regularly provide information regarding condition assessment. Accordingly, these data may be useful in allocating future resources and in planning for a programmatic asset management system.

Farhey (2005) discussed presently accepted bridge management approaches, diagnostic procedures for condition assessment and performance evaluation methods, testing methods, structural monitoring, data acquisition systems, instrumentation and sensors. Based on the above information and experience, an attempt was made to identify and explore more dependable and reliable approaches suitable for practical bridge diagnostics and management. Farhey's research

states that the reliability of structural monitoring is strongly determined by the dependable performance of all the sensors and the data acquisition systems. His research draws the following conclusions.

1) Common misconceptions persist in the installation of the systems due to technical and technological limitations of the sensors. These include measurement range and length of sensors, method of attachment, self-stiffness, malfunction, recalibrations, embedment and attachment procedures.
2) Long-term performance of sensors subjected to environmental conditions need to be evaluated. Sensors that perform well under laboratory conditions may not be suitable for field applications. Therefore, it is required to exclude sensors requiring additional specialized sensing hardware for taking readings, fragile parts, delicate handling specifications, exceptional attachment requirements or additional procedures when subjected to harsh field conditions.
3) Prior to choosing the sensors it is necessary to determine the required measurement range based on loading conditions and expected deformations. In addition, care should be taken in choosing the sensors with self-stiffness matching with the material to be tested on. Highly sensitive sensors that are traditionally compatible for laboratory-based application may not be suitable for field applications.
4) Embedded sensors are preferred for measuring long term monitoring of reinforced concrete structures. Consideration should be made for a certain percentage of malfunctions in the sensor and the data-acquisition system although the latter is considered a major issue requiring technical service beyond the capability of structural engineers. Typically, it is necessary to install redundant sensors to accommodate for malfunction as well as to average measured phenomenon and correlate consistency.

5) Sensors requiring periodic recalibration must be avoided for field monitoring systems due to their high total cost, operational discontinuity to the monitoring process and inconvenience. It is also important to investigate the capability of sensor and the specific technology used for long-term performance bridge monitoring.
6) Modern bridge management necessitates the development of integrated administrative and engineering solutions that are not only financially and technically feasible but also practical and rapid.

Robertson et al. (2005) investigated and reviewed the performance of various sensors and instruments installed on North Halawa Valley Viaduct (NHVV) over a 10-year monitoring program. The NHVV was a 1.5 km box-girder viaduct with span lengths up to 110m. Four spans of the inbound via duct were selected for instrumentation and all instruments were installed by personnel from the University of Hawaii and Construction Technology Laboratories (CTL). Over 200 electrical strain gauge, displacement, temperature and load sensors were installed during the construction of the girder and were monitored continuously since installation. A variety of sensors including vibrating wire strain gages, electrical resistance strain gauges, thermocouples, extensometers, tendon load cells, base-line deflection systems, tiltmeters and automated datalogger recording systems were used to measure concrete strains, concrete temperatures, concrete creep and shrinkage strains, span shortening, tendon forces, span deflections and support rotations respectively.

Electrical Strain gages (bonded to the reinforcing steel) and vibrating wire (VW) strain gauges were embedded in the concrete to measure and monitor longitudinal concrete strains. Ten VW strain gages were installed around the box girder cross-section at each end span and eight at the mid-span cross-section. Extensometers coupled with LVDTs were instrumented to monitor the overall span longitudinal deflections of the box-girder. The vertical deflections were monitored by installing taut-wire base line system in each of the four instrumented spans of the box-girder.

The embedded vibrating wire strain gage contained a thermistor that measured the temperature in concrete. In addition, Copper-constantan Type T thermocouples were located to measure ambient temperature and relative humidity inside and outside the box girder.

Through analysis and comparison of the recorded results it was found that the vibrating wire strain gages provided accurate and reliable results for both short term and long-term monitoring of concrete strains in the prestressed box girder. Electrical resistance strain gauges were effective for short term monitoring but not as much reliable for long term strain monitoring due to changes in the lead wire and data logger connections resulting in loss of reading continuity. The simple taut-wire base line system proved to be very effective for the measurement of short-term and long-term vertical deflections while both thermistors and thermocouples were effective in monitoring internal concrete temperatures.

An analytical study was performed on the two fiber reinforced polymer composite bridges in Kansas (Adams et al. 2005). Based on background studies a procedure for selecting and installing appropriate systems for non-destructive evaluation of the bridges was discussed. The main objective of this paper was to address long-term performance problems of the fiber-reinforced polymer composite decks installed on two existing bridges. Non-destructive testing and a finite element analysis of the bridge were performed to accomplish the objectives. The two-lane bridge consisted of fourteen W12 x 68 steel girders and spans approximately 13.7m over a river bed in southern Kansas.

Two types of structural monitoring techniques, Non-destructive evaluation (NDE) and Structural health monitoring (SHM) were implemented on the FRP composite bridge. Both techniques were used to detect damage and serviceability on the FRP composite bridge. They both incorporated a number of different sensors to acquire desirable measurements and used similar data acquisition systems. Unlike NDE the SHM system continuously monitored, inspected and detected damage

of structures with least amount of labor possible. The various types of sensors and how they apply to the KDOT bridge were discussed. They included the following; fiber optics sensors that can measure strains, piezoelectric transducers that measured deformations, strain gages bonded to the structure to measure strains, acoustic emissions to measure the structural integrity of the FRP composite deck, accelerometers to measure the change in physical properties of the bridge and linear variable displacement transducers that can be used to measure displacement in the bridge.

Multitudes of different sensors have applications for several different industries. Sensors are either used alone or in a series of network. It is vital to choose the right sensor based on the parameter that needs to be measured. The paper concluded that a complete understanding of the structural system was necessary to select the appropriate monitoring technique. The critical location positions for sensors have to be identified so that the implementation of the sensor and monitoring technique adopted can together yield good results. The way the sensors are installed also plays an important role in how accurate the measurements are.

Smolenski (2004) investigated three new bridges near Saco, Montana for alternative bridge deck designs to minimize cracking and subsequent steel corrosion. The research program was performed by the Western Transportation Institute at Montana State University and funded by Montana Department of Transportation. All three bridges were built in the summer 2003 and had the same global dimensions (44.5 m long x 9.1m wide). The primary difference between them was the composition of the reinforced concrete deck. The main objective of this project was to identify any differences in structural behavior and durability that may exist due to the varying deck designs.

Strain gauges and temperature sensors were installed to observe both long term and short-term live load deck responses. The strain in concrete and in reinforcing bars were monitored separately and the instrumentation was developed to be durable, reliable, adaptable and redundant. A three-

dimensional analytical model of the bridges was created using the Visual Analysis finite element package to aid in selecting critical locations for sensors. The location extreme fiber stresses generated from the finite element modeling was identified that served as location points for the installation of the instruments on the bridge deck. Based on this a formal instrumentation plan was generated that detailed the gauge type, location and expected level of response.

Each of the bridge decks were instrumented with 35 bonded-foil resistance strain gauges bonded directly to the reinforcement, 9 concrete embedded strain gauges and 20 vibrating wire strain gauges. The bonded foil strain gages were fabricated by Micro-Measurements Group, Inc., type CEA-06-250UN-350. They measured the local strains in the steel reinforcement and were bonded directly to the top and bottom surfaces of the reinforcement with a special epoxy. The concrete embedded strain gauges were also fabricated by Micro-Measurements group, Inc. They were specially designed to measure strains inside the concrete. Geokon Model VCE-4200 vibrating wire strain gauges were installed in bridge decks for monitoring long-term concrete strains and temperatures. Each vibrating wire gauge was equipped with a thermistor that measures temperature at the gauge.

Four intelliducer sensors, pre-manufactured by Bridge Diagnostics, Inc. (BDI) were mounted to the bottom of the bridge girders. They measured the strain at the surface of structural elements. Three independent data acquisition systems were installed to store and transfer data for each bridge site. Each system consisted of a single data acquisition unit (CR5000), two multiplexers (AM16/32), supporting circuitry, a 12 volt-battery connected to a 60-Watt solar panel through a regulator and RF400 spread spectrum radio unit connected to an antenna. Campbell Scientific, Inc. manufactured all the instruments whereas the solar panels, batteries, regulators and the radio antennas were purchased from other sources. Since the dataloggers were only able to accommodate 20 differential inputs, multiplexers were used to expand the number of sensors monitored by the dataloggers.

The Campbell Scientific CR5000 was a rugged, high performance data acquisition system. It was chosen for its durability, wide range of temperature operation, internal computing and storage capabilities. The collected data from the control system was transferred on command to MSU using an Internet connection via RF400 radios. The instrumentation was temporarily reorganized during the live load testing to accommodate a large number of sensors operating at high acquisition speeds. A different program was used to monitor bonded-foil and embedded strain gages at a high rate of speed (~50 Hz) during each live load testing.

Kim et al. (2015) investigated the application of high-early strength self-consolidating concrete (SCC) for precast, prestressed bridge girders. A full-scale experimental testing was performed on Texas DOT (TXDOT) girders to evaluate their flexural response and bond performance. The girders featured 40 feet span with 8in thick and 64-inch-wide cast in place deck. The girders were designed in accordance with AASHTO LRFD specifications and the TXDOT Bridge Design manual. A total of 10 LVDTs were installed to measure longitudinal deformation, strain profiles and crack widths in the constant moment region. A total of 24 strain gages were installed to the bottom flange of the girder (at the centroid of strands), girder web, top flange of the girder, and mid depth of the bridge deck. These strain gages provided the strain distribution over the girder depth and the corresponding curvature was calculated. From the principle of mechanics, the deflection of the girder was determined at three sections, 38in from each end support and at the mid-span. String potentiometers were also installed to measure girder deflections at the mid-span and supports. The data acquisition system recorded data at 5 second intervals during the load test testing of the girders. A load cell was used to measure the force applied by the hydraulic ram. The loading increment was selected based on the estimated load to first cracking and the strain of the top concrete fiber on the deck at mid-span.

Pavelchak and Williams (2013) presented a case study of the successful use of Structural Health Monitoring (SHM) techniques as a part of a cost-effective risk-based approach for pseudo real

time monitoring of bridge performance subjected to large construction loads. The bridge was constructed in 1968 and provided the sole means of access to a large privately held facility that was being subject to a $400 M expansion and renovation. The multi-year expansion and renovation of the facility positioned the bridge to be subjected to heavy construction loads to progress with the expansion on schedule and in the most efficient manner. Due to limited information available on the reinforcement and design capacity of the bridge, a multifaceted bridge inspection, evaluation and instrumentation program was implemented to not only monitor bridge performance but also to maintain the project's construction on schedule.

The bridge consisted of AASHTO Type I beams with a composite cast-in-place concrete deck slab. The bridge spanned over five equal spans of 44 ft and the substructure was driven on precast concrete piles with cast-in-place bents. The available drawings indicated a design live load of H20-S-16-44 as per AASHTO 1965 design code. It was anticipated that the construction loads would significantly exceed the designed live loads of the bridge which created a need to inspect and assess the performance of the bridge. The bridge was first inspected to identify the current condition of the bridge for rating purposes and to document the condition of the bridge prior to initiation of heavy construction vehicle traffic over the bridge. The inspection report identified numerous maintenance issues to be addressed but generally the spans were found to be in good condition.

This paper was a substantial evidence that an economical means of monitoring bridge performance can easily be achievable by utilizing commercially available sensors. In situations where limited information is provided, structural analysis may not be the best solution, but implementation of structural health monitoring may be the key for real time solutions.

Monitoring Methods for Full-Sized Prototype Bridge

A full-sized prototype bridge was built at the Bert Cooper Engineering Laboratory (BCEL). The bridge was constructed to replicate the Eagle Chief Creek Bridge "A" on SH 14 in Woods Co., Oklahoma. The prototype bridge spans 38 ft -10in. from center-to-center (c/c) of bearings with an 8 in. concrete deck supported by W24x94 Gr. 50 steel girders. The steel girders were spaced at 6 ft. apart, matching the spacing for the Woods Co. bridge, and constructed with C12x20.7 steel diaphragms at the ends and mid-span locations. The bridge deck is 14 ft- 0 in. wide supported by two girders. With this geometry, the deck possesses four feet wide cantilevered overhangs.

Altogether 100 electronic gages and sensors were employed to measure and monitor concrete and steel strains, concrete and steel temperatures, overall bridge deflections at several locations, and inclination of the steel girders. Figure 1 shows the schematic instrumentation and data acquisition for the laboratory bridge. Instrumentation was installed prior to casting the concrete deck. The instrumentation included the following:

(1) Electrical resistance bonded foil strain gages (ERSGs) to measured strains in the steel girders;

(2) ERSGs to measure strains on the surfaces of hardened concrete;

(3) Vibrating wire strain gauges (VWSG) embedded within the concrete deck prior to casting to measure the concrete strains and concrete temperatures within the hardening deck;

(4) Thermocouples to measure the temperature within the concrete and ambient temperatures near the bridge deck;

(5) Linear Variable Differential Transducers (LVDTs) to measured deflections of the bridge girders at various locations; and,

(6) Inclinometers to measure angle of inclination at the ends of girders.

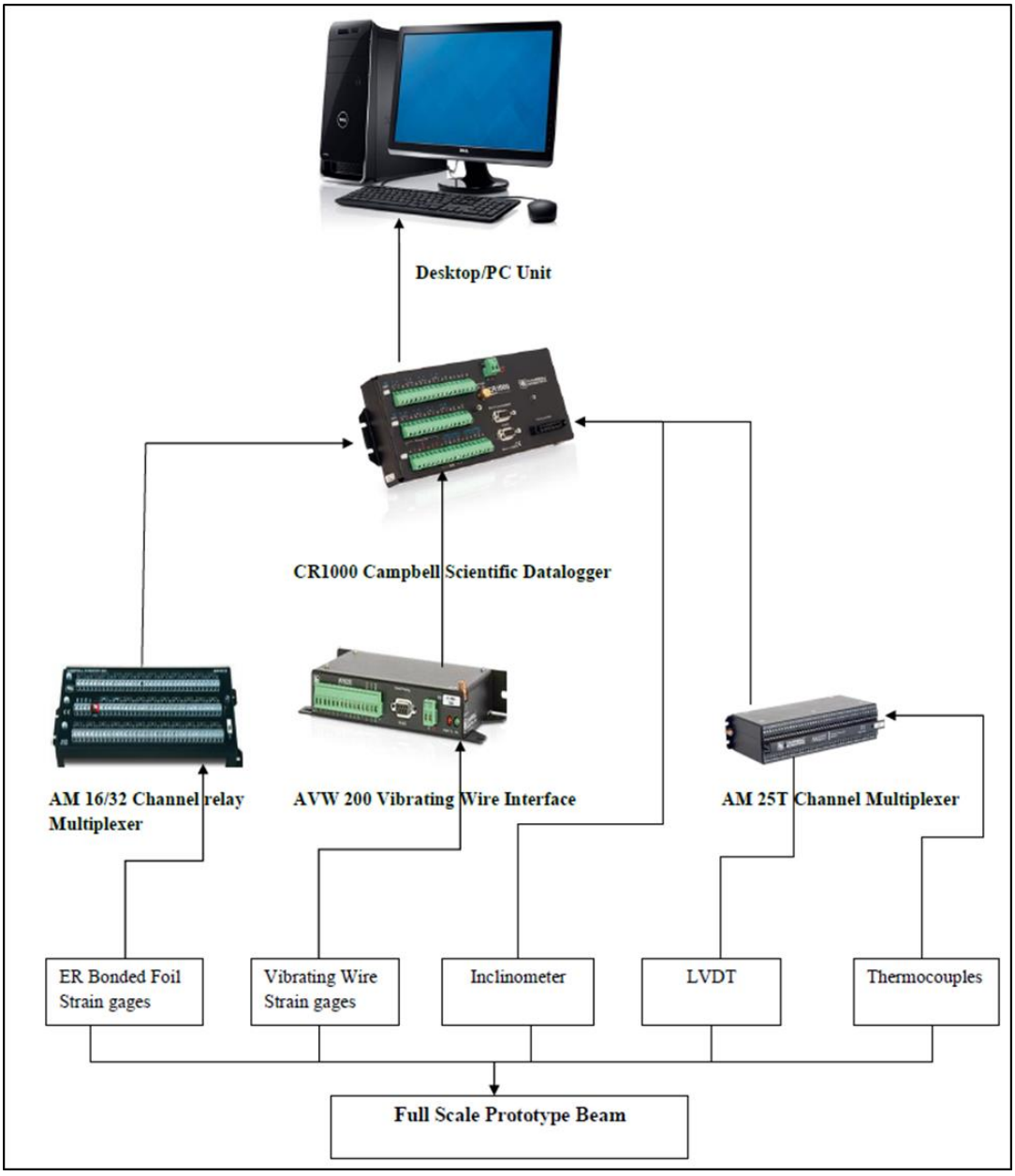

Figure 1. Laboratory prototype bridge instrumentation setup

Sensor locations and placement is an integral part of Structural Monitoring. Structure evaluation and performance solely rely on the data acquired form the sensors. Strategic sensor locations were chosen on the prototype bridge to maximize data with an aim to encompass the structural response and short term and long-term behavior of the structure. Generally, with increased

number of sensors more data can be obtained for real time analysis of the structure. However, the number of sensors installed on the prototype bridge was limited by cost associated with the data acquisition systems, processing and frequency of data collection. The sensors were installed at the mid-span, quarter span and some closer to the supports of both the north and south girders respectively. A symmetrical arrangement of sensors was implemented on the bridge deck to compare data and maximize data points both in the longitudinal and transverse directions of the bridge deck. Primarily the sensors were installed at mid span locations where the maximum strains and deformations are expected to occur. The sensors were chosen in such a way to record and monitor both global and local response of the bridge structure. Sensors that included the inclinometers and LVDTs measured the global deflection of the bridge girders whereas the sensors such as ERSGs, thermocouples and VWSGs monitored the local response at various locations on the prototype bridge.

Electrical Resistance Bonded Foil Strain Gauges

Strain is defined as the relative change in length due to an applied stress. A strain gauge is a sensor whose resistance varies with an applied stress. The strain gauge converts the change in length into a measurable change in electrical resistance. Bonded foil strain gauges have been used to measure strains for over 70 years (Walter 2009).

The strain gage consists of a grid of very fine metallic wire, foil, or semiconductor material bonded to the strained surface. The gage is electrically insulated from the base material by a thin layer of epoxy. The foil acts as the electrical resistor. When the applied surface is strained, the change in length causes a change in electrical resistance of the gauge. This variation in the electrical resistance is measured as using a special arrangement called Wheatstone bridge which gives the indication of the strain of the applied material. Figure 2 shows a typical electrical resistance bonded foil gauge that is commonly used for strain measurements. Two types of

bonded foil strain gauges from Micro-Measurements Group, Inc, were used in this research. The type CEA-06-500UW-350 were used to measure strains in the steel and type C2A-06-20CLW-350 measured strains on concrete surfaces. Figure 3 shows the layout and locations of these strain gages on the full-size prototype bridge.

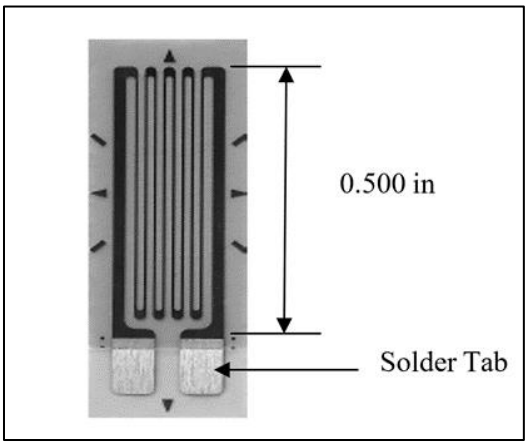

Figure 2. Electrical Resistance bonded foil Strain Gage

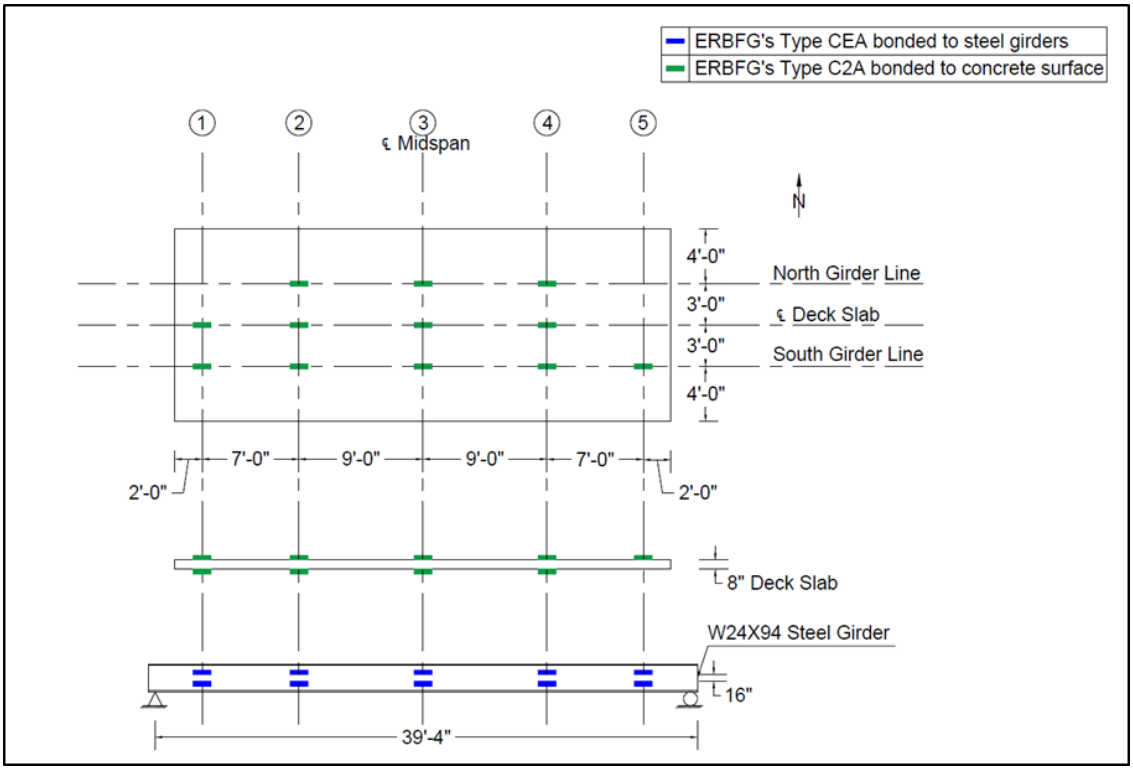

Figure 3. Layout of Electrical Resistance Bonded foil Strain Gages on the laboratory bridge deck and steel girders.

The type CEA gages series are the most widely accepted as general purposes gages commonly employed in general purpose stress analysis applications in the world today (micro-measurements.com) . These gages are made of constantan (copper-nickel alloy) and fully encapsulated in polyamide with exposed copper-coated tabs. The lead wires are directly soldered to the exposed copper tabs. The active gage length of the CEA-06-500UW-350 gages used in this research was 0.50 in. and their resistance were 350 Ω. The temperature range over these gages is -100°F to +350°F. The maximum strain limit of these gages is approximately ±5000με with a fatigue life of 10^5 cycles at ±1500με. About 16 no. quarter bridge CEA type bonded foil strain gauges were installed on the surface of the steel girders. Figure 4 shows the picture of the quarter bridge strain gauges bonded to the webs of the steel girders at one location. At each location, two gages were bonded to the web of the steel girders, each at four inches from the top and bottom of the flanges to measure the strain gradient through the depth of the girder during testing.

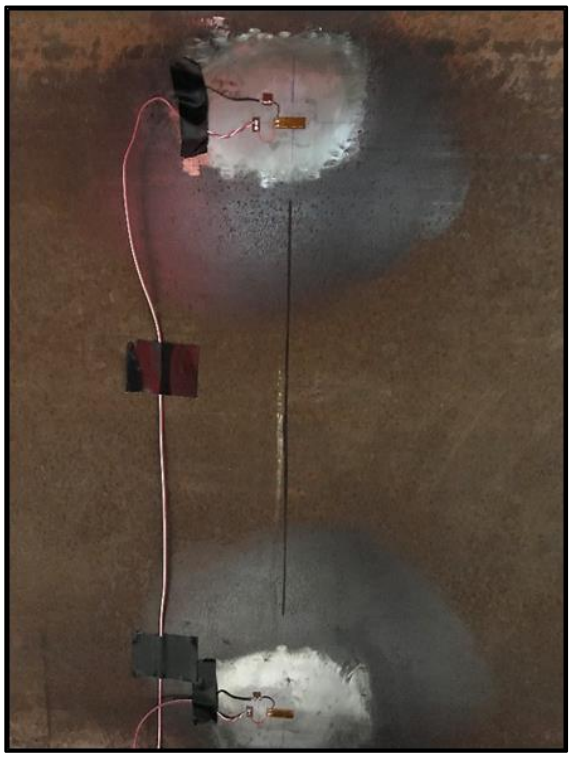

Figure 4. Electrical Resistance Strain Gauges bonded to the web of the steel girder

Bonded Foil ERSGs were bonded to the webs of the steel girders to monitor and record the strain in the steel girders. During the time of deck cast the bridge is subjected to fresh weight of the concrete, screed rail loads if any and other construction loads. The gages were located close to the extreme fibers of the section to record and monitor the maximum strain response in the steel girders. The strain data recorded from the steel girders was used to calculate the curvature induced in steel girders and hence the bridge deformations was computed, which was then compared with the measured deflections from the LVDTS to validate the results. Although these gages are stated to be self-temperature corrected, some minor variations in strains were found to exist during heat load testing of the prototype bridge.

Strain gauges can be bonded to almost any solid material surface if the surface of the material is properly prepared. Micro-Measurements recommends a thorough cleaning and surface preparation process to achieve strong stable bonds between the strain gauge and the surface material. The recommended five steps for surface cleaning and surface preparation include 1) Solvent Degreasing, 2) Dry and Wet abrading, 3) Application of gage layout lines, 4) Conditioning and 5) Neutralizing. Individual suppliers of strain gages will also provide recommendations for the proper surface preparation and installation of the strain gages (vishaypg.com).

Concrete being a nonhomogeneous material with a combination fine and coarse aggregate, proper selection of gauge length is necessary to ensure that the strains of the composite material is measured accurately. Strain gauges with length less than ¾ in. may only measure the strains in the coarse aggregate rather than the whole concrete. The type C2A gauges were specifically chosen for measuring strains on concrete surface and save time in gage installation. They are fully encapsulated constantan alloy gages with pre-attached 3-conductor instrument cables. The active gage length was 2.0 in. with a resistance of 350Ω with strain limits of approximately ±3%. Figure 5 shows the type C2A gauges along with the dummy gauge bonded to the concrete surface.

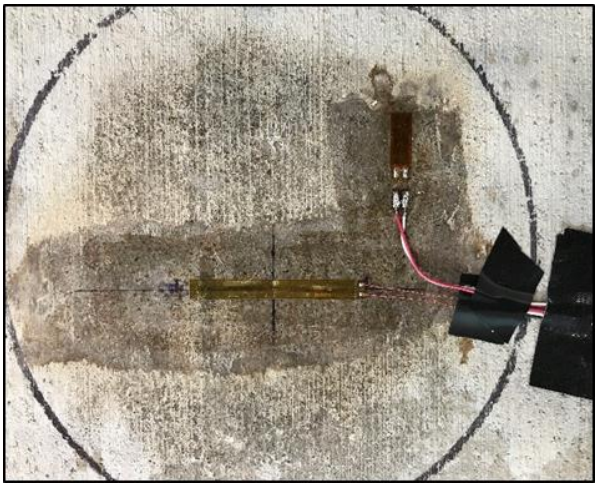

Figure 5. Electrical Resistance Strain Gauge with dummy gauge bonded to the surface of the concrete deck.

In order to achieve satisfactory bonding to the surface of the concrete proper surface preparation is required. The surface of the concrete is first cleaned with a stiff-bristled brush and degreased with a mild detergent to remove any loose soil and grease. A generous amount of M-Prep Conditioner, a mildly acidic solution is applied to the surfaces around the gaging area and scrubbed in with a stiff-bristled brush. The gaging area is rinsed thoroughly with clean water and the surface acidity is reduced by scrubbing in with M-Prep Neutralizer. The surface is then allowed to dry thoroughly before the application of the adhesive.

A suitable gauge-bonding surface is achieved by applying a 100% solid adhesive to the gauging area. M-Bond AE-10 adhesive is recommended for temperatures up to +200 ºF. The adhesive is worked into any voids and levelled to form a smooth surface. After the adhesive is cured, the surface is abraded with 320-grit abrasive paper until the base material is exposed. Layout lines for the gauge is drawn with a ballpoint pen or a round pointed metal rod and scrubbed with conditioner and neutralizer. The gauge is then bonded to the concrete surface with a slow curing adhesive like M-Bond AE-10 that will allow time for realigning of the gauge if necessary. (www.micromeasurements.com)

About 16 quarter bridge C2A gauges were bonded to the top and bottom surfaces of the cured concrete deck to record concrete surface strains during the heat load testing. The resistance of the strain gages often changes with increase in temperatures which may result in false apparent strain readings. This is corrected by installing a dummy gauge on the same base material. A gauge that is not subjected to any load induced stress and acts as the resistive element of the Wheatstone bridge arm opposite to the active gauge is referred to as a dummy gauge. During the heat load test, with the two opposing gauges experiencing the same temperature conditions, the temperature offset effects on the active gauge is nullified by the equivalent temperature effects on the dummy gauge. The change in resistance of the lead wires due to temperature effects was minimized by using three wire circuit for all the strain gages used in this research.

All the bonded foil gauges were wired into the datalogger via AM16/32 interface. Strain gauges with a full bridge configuration are more sensitive than the quarter bridge, however a full bridge requires three more strain gages than the quarter bridge to complete the wheat stone bridge. A single full bridge completion resister called the 4WFB 350-ohm resistance Terminal Input Module (TIM) was wired to the datalogger to complete the full bridge for all the quarter bridge strain gages wired to a single AM 16/32 multiplexer. The Wheatstone bridge circuit converts small changes in resistance to an output voltage that the CR1000 datalogger can measure. The quarter bridge strain gages measure either axial or bending strains, however slight variations in resistance may occur due to temperature changes. To eliminate the variations in the lead wire resistance due to temperature, three wire configurations was adopted for the quarter bridge gauges.

Advantages

Bonded foil gages are generally very stable and uses a well know technology in wide use. The gauges are typically small, less expensive and can be custom manufactured to desired configurations. They have good repeatability and linearity over a wide range of strains.

Limitations

The gauges require a tedious surface preparation procedure in order to achieve a good bond to the surface where the strains are measured. They are highly sensitive and the wear of adhesive over time reduces the accuracy of the gages. The gauges require periodic zero calibration and temperature compensation for operation under high temperature loads.

Static Vibrating Wire Strain Gages

The vibrating wire strain gauges are designed primarily for long-term monitoring of strains in mass concrete. They can be directly embedded into the concrete deck to measure the concrete strains and temperatures. The vibrating wire sensor measures the change in length using a wire that vibrates at a high frequency. When stress occurs in the base material, the tension in the vibrating wire changes which in turn changes the frequency in which the wire vibrates. The change in frequency is measured. The sensor sends a voltage signal that is calibrated to vary with the change in length of the sensor. The sensor is composed of a steel tube with flanges at either ends. Inside the body of the sensor is a steel wire that is stretched and held in tension between the two flanges. As the concrete surrounding the sensor contracts or expands, the tension in the wire is changed by the movement of flanges relative to one another. This causes changes in the resonant frequency of the vibrating wire. The vibrating wire is excited with a range of frequencies by plucking it with an electromagnetic coil. The electromagnetic coil detects the resonant frequency of the vibrating wire. The detected frequencies are converted to a DC voltage and recorded by the datalogger as strain values. Each vibrating wire strain gauge is equipped with a

thermistor that measures the temperature (20°C to +80°C) in the surrounding concrete at the gauge level. These measurements can be applied as temperature corrections to the measured raw strains. These temperature corrections are applied due to the change in coefficient if thermal expansion between the steel and concrete. The sensor has a gage length of 152mm, capped with end plates of diameter 19mm. The gauge has an operatable range of 3000 microstrain (με), with a resolution of ±0.1 με. The sensor has long term stability, maximum resistance to the effects of water and a frequency output suitable for transmission over very long cables. The components of the gauge are made from stainless steel for corrosion protection and they are fully waterproof. VWSGS when coupled with Campbell Scientific vibrating wire analyzers allows them to make both static and dynamic measurements at sampling frequencies as high as 333Hz.

The act of clamping the gauge shortens the vibrating wire slightly, causing it to over register the strain. This is compensated by applying a gauge factor supplied for each gauge type. For the Geokon 4200 gauge used in the laboratory prototype bridge, a gauge factor of 3.304 was used. Therefore, the apparent change in output strain is given as

$$\mu\varepsilon_{apparent} = (R_1 - R_0)B \qquad \text{Eq (1)}$$

where,

R_0 = initial reading

R_1 = current output reading taken in a position

B = batch factor supplied with each gauge

When (R_1-R_0) is positive, the strain is tensile.

The concrete temperatures are always measured alongside strain measurements. This is done to take into account the temperature variations especially during concrete curing. These temperature

variations also affect the strain gage. The increase in concrete temperatures cause the vibrating wire inside the gage to elongate and thus go slack, indicating what would appear to be compressive strains in concrete. In addition, the coefficient of expansion of steel is different from the coefficient of expansion of concrete. This is corrected by the use of a temperature correction. Therefore, the load related strain in concrete caused due to both external loads and temperature effects corrected for temperature is given by,

$$\mu\varepsilon_{actual} = (R_1 - R_0)B + (T_1 - T_0)(C_1 - C_2) \quad \text{Eq (2)}$$

T_0 = initial temperature

T_1 = current output temperature reading taken in a position

C_1 = coefficient of expansion of steel, taken as 12.2 microstrains/ºC

C_2 = coefficient of expansion of concrete, measured from experimental testing

C_2 = coefficient of expansion of concrete, measured from experimental testing

A total of six Geokon model vibrating wire strain gages were embedded at various locations in the laboratory prototype bridge deck as shown in Figure 6 At the mid-span location of the bridge deck, three vibrating wire sensors were installed vertically at 2 in. c/c spacing along the centerline of the deck, to capture the strain gradient throughout the depth of the concrete slab. At other locations the vibrating wire sensors were embedded at mid-height of the concrete slab. The gauges were suspended in concrete by tying them to two short pieces of rebar with nylon tie-wraps which were then tied to the existing rebar. This method was adopted to avoid problems with resonance.

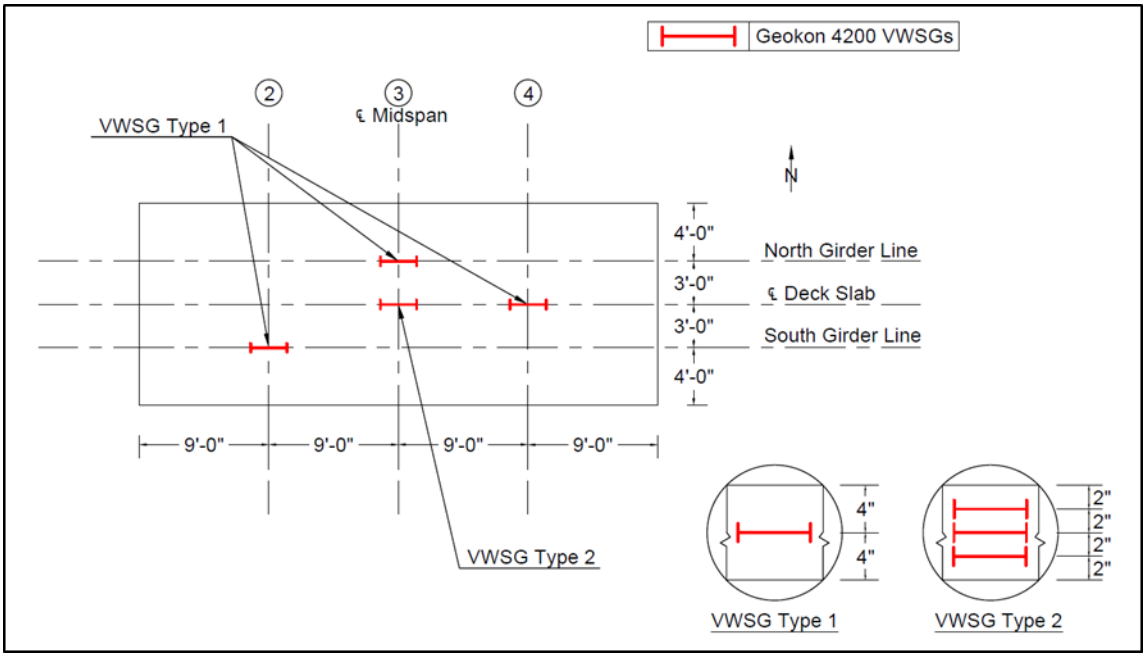

Figure 6. Layout of Geokon VWSG on the prototype bridge

All the VWSGs were installed in the longitudinal direction of the deck to capture the maximum concrete strains during deck cast, curing and heat load testing. The gages were placed above the girders at midspan location where maximum response was expected. Additional VWSGs were installed on the centerline of the deck slab to capture the variations in strains between the two locations caused due to shear lag effects.

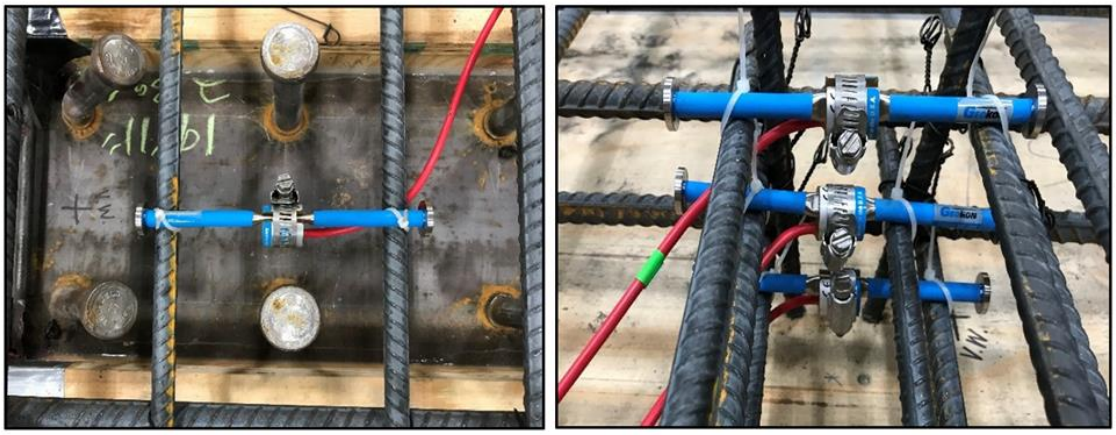

Figure 7. Installation of the VWSG on the bridge deck. VWSG Type 1 (left); VWSG Type 2 (right)

Figure 7 shows the installation of the VWSGs on the prototype bridge deck. The VWSGs measured the concrete strains from the time of pour and during curing. The strains in concrete were also measured during the time of heat load testing after 56 days of curing.

Advantages

The VWSG has long term stability and maximum resistance to the effects of water. They are easy to install, and frequency output is suitable for transmissions over long cable lengths. The gages are fully water proof and corrosion resistant. The gauge is immune to electrical noises, very rugged and designed to withstand rigors of concrete placement. VWSGs can successfully monitor both static and dynamic responses of structures at one time which makes them the utmost sensors for bridge monitoring systems.

Limitations

The vibrating wire strain gauges are more expensive than the commercially available bonded foil strain gages. Temperature correction for the gauges embedded in concrete is required to compensate for the slack due to elongation of the vibrating wire when subjected to high concrete curing temperatures.

Thermocouples

A thermocouple is a sensor that is used to measure temperature. It comprises of two wires or two wire “legs”, separated electrically by insulation, and made from dissimilar metals. The wire legs are joined together at a measurement junction to form a circuit and the temperature is measured at this junction as shown in Figure 8. A voltage potential is generated when the junction experiences a difference in temperature. The thermocouples are often enclosed in a protective sheath to isolate it from the local atmosphere. This protective sheath reduces the effect of corrosion of the thermocouple wires.

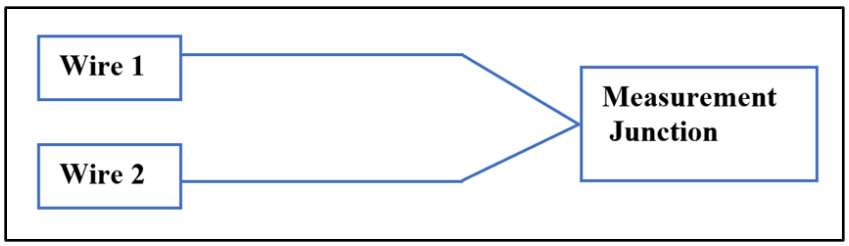

Figure 8. Temperature measurement principle of a Thermocouple

Type T thermocouples (Copper/Constantan) extension grade wire was installed on the laboratory prototype bridge deck to measure the concrete temperatures. This is the most common type of thermocouple used in the industry. It is also inexpensive, accurate and reliable and has a temperature range of 32°F to 392°F. It has an accuracy of +/- 0.75%. A total of 25 thermocouples were installed at five different locations of the bridge deck slab. Figure 9 Shows the layout of thermocouples on the prototype bridge. At each location, five individual thermocouples were aligned vertically at 2 inches apart to capture the temperature gradient in the concrete slab. Figure 10 Shows the installation of the thermocouple wires on the bridge deck. Concrete temperatures were recorded from the time of pour, during curing and heat load testing.

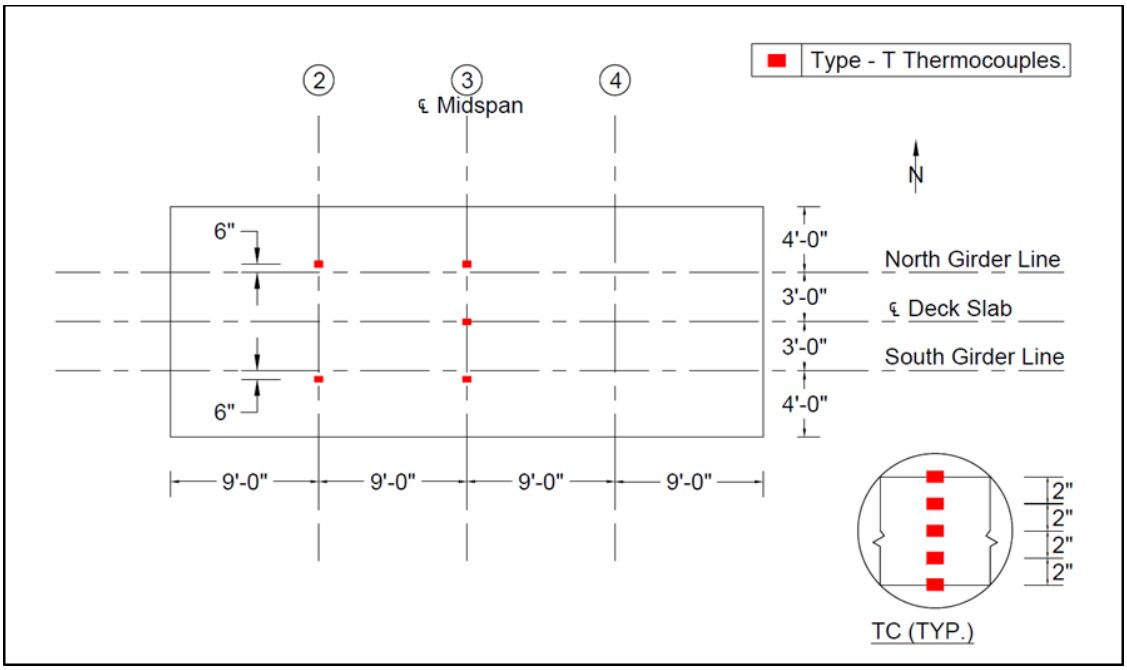

Figure 9. Layout of thermocouple sensors on the prototype bridge deck.

Figure 10. Installation of thermocouples on the bridge deck.

Advantages

Thermocouple sensors are inexpensive, durable and provide highly accurate results. These sensors do not require excitation and are self- powered. They are robust and can measure over a wide temperature range.

Limitations

Thermocouples are hard to calibrate and can only measure the temperature difference at a location. They are subjected to corrosion when exposed to high humid environment in the long-term.

Linear Variable Displacement Transducer

This is a type of electrical transducer that is used for measuring linear displacement. It converts a position or linear displacement from a mechanical reference to a proportional electrical signal. The LVDT operation solely relies on electromagnetic coupling and does not require an electrical contact between the moving part and the coil assembly. As shown in Figure 11, the LVDT has three solenoidal coils that are placed end to end around a tube. The center coil A is the primary coil and the outer two coils named B are the secondary coils. A cylindrical ferromagnetic tube slides along the axis of the tube. This ferromagnetic tube is attached to the surface whose position is to be measured. When a current is driven through the primary coil A, it causes an induction current to be generated through the secondary coils at B. As the core moves the primary coil's linkage to the secondary coils changes and causes the induced voltage to change.

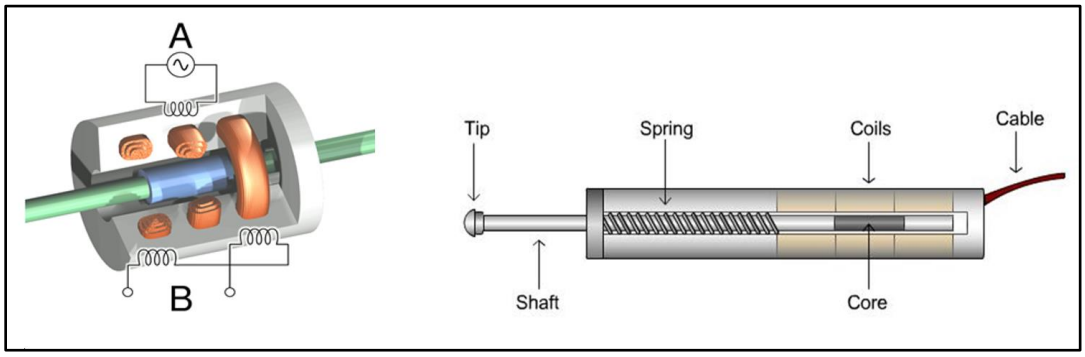

Figure 11. Working principle of Linear Variable Displacement Transducer

The LD620 DC output displacement transducers by OMEGA engineering were used in this research work. The sensors have a ±5 Vdc output with less than 0.2% linearity. The LVDTs have improved IP 67- rated sealing, coupled with new polymer guides with rigid carriers. They are accurate and reliable and highly corrosion resistant. They have unusually large bore-to-core clearance which makes it easier to install and helps prevent misalignment on attached surfaces. A total of 7 LVDT sensors were installed at strategic locations of the laboratory prototype bridge to monitor deflections of the steel girders and overhang portions of the bridge deck. Deflection were

recorded from the time of pour, during curing and heat load testing. Figure 12 shows the layout of the LVDT sensors and inclinometers on the prototype bridge and Fig 13 shows the installation of the LVDT sensors on the bridge. The LVDTs are mainly concentrated at the mid-span location of the bridge girders where the maximum deflections were expected.

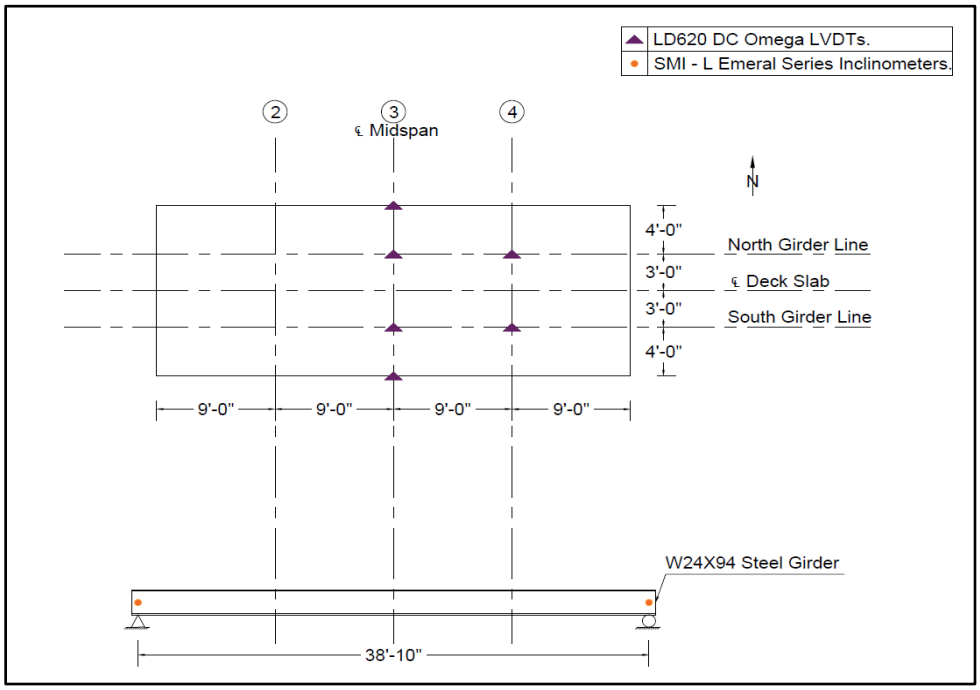

Figure 12. Layout of LVDTs and inclinometers on the prototype bridge

Figure 13. Installation of LVDT sensors on the laboratory prototype bridge

Advantages

LVDTs provide direct measurements of relative linear displacement and are highly accurate and precise. They are stable and easy to align and mount.

Limitations

The sensors require a fixed reference point to be mounted from which poses practical problems in measuring deflection is bridges with very high clearance.

Inclinometers

Inclinometer sensors were invented to overcome the shortcomings of direct measurement methods used by the LVDT sensor technology. Researchers (Hou et al. 2005) found a promising bridge deflection method using inclinometers that offered simple, practical, inexpensive method of measuring static and dynamic deflections of bridges than span over traverse great heights. Inclinometers or tiltmeters are the type of instrumentation that is used to measure the angles of slope or tilt, elevation or depression of a member with respect to gravity. They can measure both positive and negative slopes using three different units of measure such as degrees, percent and topo. The sensor technology that has been implemented in the inclinometers is very similar to the ones used in aircraft flight controls, cameras, automobile security systems etc.

The type of inclinometer used in this research is an Emerald Series Model SMI-L which belongs to a forced balanced sensor. This sensor has a very high precision, rugged and is a single axis inclinometer. The sensor has a torque motor present in the main part of the servo sensor. This torque is intentionally unbalanced in its plane of allowable angular motion. The sensors are typically mounted on the end support of the bridge beams where the inclination is the maximum. When there is a tilt to the member that it is attached to the sensor then a torque that is proportional to the tilt is applied on the torque motor. This torque causes an angular motion that is

detected by a position sensor. A total of four Emerald series inclinometers were mounted to the end supports of each steel girder to monitor the change in inclination during slab cast, curing and heat load testing. Figure 14 shows the photograph of the Emerald Series inclinometer installed on the end support of the steel girder of the prototype bridge. The sensor has a 4-20mA output wired to the datalogger via a CRUS100(100-ohm Current Terminal Input Mode) which converts the current signal to voltage signal.

Figure 14. Installation of Jewell inclinometer on the steel girders

The angular values collected from the inclinometer readings were evaluated to calculate the girder midspan deflections. Figure 15 shows the North and South girder deflections measured using both the inclinometers and the LVDT sensors for a time period of 28 days. The inclinometers have variations in output due to AC voltage signals whereas the LVDT output is rather smooth due to DC output signals. The inclinometer readings correlate well for the first 12 days of curing time after deck cast. The removal of formwork was initiated after 12 days of the deck cast. The high variation in the inclinometer deflections reflect that these sensors may be disturbed during the process of formwork removal. Also due to the sensitive nature of these

sensors the movement of the supports may also contribute to a lot of noise in the recorded readings. Therefore, it is highly recommended to install additional inclinometers along the span of the bridge at regular spacings to evaluate the angular measurements and arrive at accurate prediction of bridge deflections. In addition, a housing is required to protect these sensors from damage and disturbance during construction process and formwork removal.

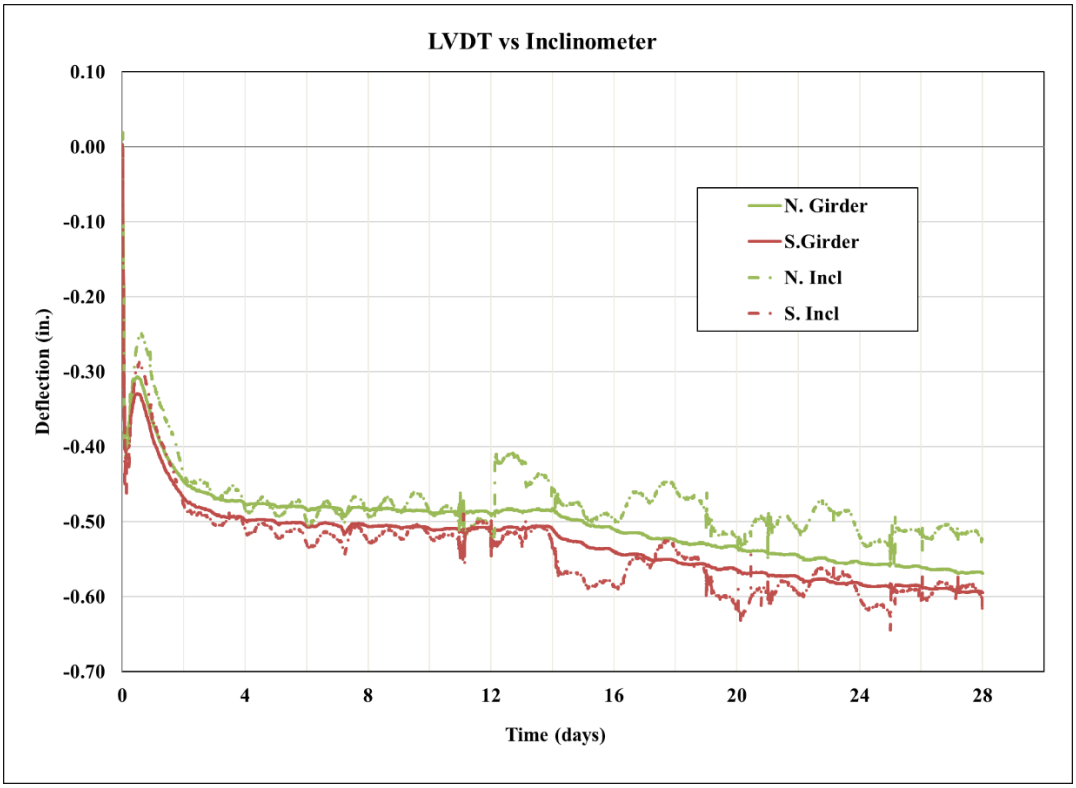

Figure 15. LVDT vs Inclinometer deflection comparisons

Advantages

This sensors technology does not require a fixed observation position unlike the LVDT sensors. This makes the inclinometers are well suited for measuring high bridges traversing over rivers, highways, canyons and sea. They are relatively inexpensive, and the data is easy to capture and analyze. Inclinometers provides an opportunity to measure angles of rotation along any three

orthogonal axes at a time which makes the sensor superior to other commercially available deflection measurement technologies.

Limitations

Inclinometers are highly sensitive. When using AC output sensors the signals may require to be filtered to convert to an unregulated DC voltage signal.

Data Acquisition and Interface Systems

The different components of a data acquisition system include the dataloggers, interfaces systems, sensors, reliable data retrieval system and monitoring system. The dataloggers are designed to read electrical signals and are programmed to convert them to engineering units. The CR1000 datalogger which has a broad range of measurement and control functions was used for this research program to measure and monitor the laboratory prototype bridge. The CR1000 has been built on the foundation of Campbell Scientific's CR10x datalogger and has been already used all over the world. With increased memory and more measurement channels, it is a powerful core component for data-acquisition system.

The main objective of a data acquisition system is to take measurements and store data files on a PC. The data is mainly copied, not moved from the datalogger to the PC. This was achieved using Campbell Scientifics' own datalogger support software package "Loggernet". The loggernet software supports programming, communication and data retrieval between dataloggers and a PC. It consists of several applications integrated into a single product.

The CR1000 has a total of 4 Megabytes of Static Random Access Memory (SRAM) out of which approximately 3.7 MB of memory is available for data table storage and the remaining is used for programs and communications. The availability of the above memory storage depends on the frequency at which the data is stored. The datalogger can auto allocate its data tables, so the

newest data begins to overwrite the oldest data at approximately the same time. Therefore, it is important to program the datalogger retrieve the data on a day to day regular basis. SRAM is generally battery packed; so, the data and programs remain in the memory of the CR1000 when it is powered down. The CR1000 was programmed to store data periodically or conditionally in the form of tables. All the sensors were wired into a datalogger through various multiplexers required for each type of sensor. Figure 16 shows a photograph of the brain box that contains the datalogger and the interface systems used in this research.

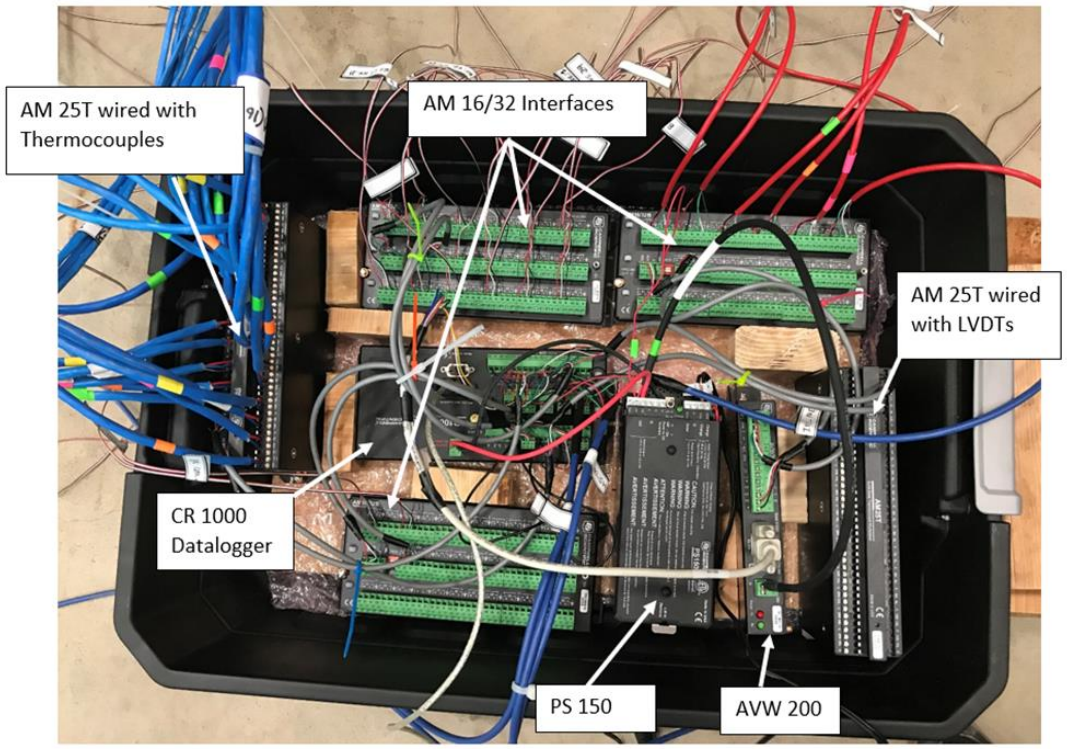

Figure 16. Brain Box with datalogger and interface systems

As shown in the schematic set up Fig 1, a total of 32 no bonded quarter bridge ERSGs were wired programmed into the datalogger system through two AM 16/32 multiplexers. The main role of the AM 16/ 32B multiplexer is to significantly increase the number of sensors that can be measured using a Campbell Scientific Datalogger. It interfaces with the datalogger and adds more

terminals so that sensors of any type can be wired to the datalogger. Here each of the AM16/32 multiplexes up to16 sensors each.

A total of 6no. concrete embedded Geokon model 4000 VWSGs were wired to the datalogger system through a combination of an AM16/32 and an AVW200 multiplexer. The AVW200 multiplexer is called a vibrating-wire analyzer module. This interface uses vibrating-wire spectral analysis technology (VSPECT^{TM}). The VSPECT observes the incoming sensor signal, performs a Fourier Transform and a spectral analysis, which transforms the time series into individual sinusoidal components in the frequency spectrum, and determines the sensor frequency by identifying the largest signal in the acceptable range while filtering out environmental and electrical noise. The AVW200 provides better measurements by significantly reducing incorrect readings generally caused by noise sources.

AM25T, a 25- channel solid state multiplexer, was used to interface with the datalogger to sequentially connect a total of 25 thermocouples installed in the prototype bridge deck. The AM 25T has a platinum resistive thermometer is attached to its grounding bar providing a temperature reference for the thermocouple measurements. The heat capacity of the grounding bar and an insulated aluminum cover reduce thermal gradients along the length of the multiplexer there by allowing for more accurate temperature measurements.

The datalogger was powered by an external battery to maintain constant power during data collection and also as a backup power during times of power shut down. PS150 battery was used to power the datalogger and sensors used in the laboratory prototype bridge. It provides a 12 Vdc power supply along with a rechargeable 7 Ah valve regulated lead-acid battery and charging regulator. The PS150 is equipped with several safety features that is intended to protect the charging source, battery, charger and load devices. It provides protection against high amperage

and high voltage damage to power supply. The PS150 includes battery protection reversal and surge protection on all of its inputs and outputs.

The datalogger network was configured using a walkthrough set up called EZsetup. It uses a point–and-click format for setting up communications between and CR1000 and the PC. This is the very first step in using the logggernet with the datalogger. The program was written using Campbell Scientific's very own program generator called Short Cut. The Short Cut is a simple "Program Generator" software application that creates datalogger programs based on sensors and selected output intervals. The Shortcut also generates a wiring diagram for connecting the sensors to the datalogger. The program was created by the Shortcut can then be edited in the CRBasic editor. The datalogger was programmed to scan data at a rate of every minute and the data tables were programed to recorded data at 5-minute time interval during the time of deck pour and thermal load testing. For long-term monitoring a lower frequency sampling rate of 1 data point for every 30 minutes was chosen for better data management.

The Loggernet® is a comprehensive datalogger support software package that supports simple and complex programming, communications, data processing, viewing and retrieval between the Campbell Scientific dataloggers and a PC. The Connect Screen in the loggernet was used as a real-time communication with a datalogger during the time of deck casting and throughout the testing program. Real time data was viewed both in numerical and graphical displays throughout the testing regime.

Long-term Structural Monitoring

Long-term structural monitoring is mainly intended to develop structural behavior and response of bridges structures to traffic loads, wind loads, heat loads and other environmental effects. The response of the structure is monitored continuously and typically utilizes data collected at low frequency sampling rates. Successful condition assessment and damage detection can be achieved

with long term structural monitoring of bridges. Long-term structural monitoring can help to predict failure mechanisms of bridges depending on the intensity of instrumentation installed on the bridge structure itself. In addition, it helps to study the actual behavior of bridges and aid to direct bridge management for future designs and maintenance procedures (Farhey 2005).

Temperature monitoring

A continuous monitoring of temperature variations is essential to understand and evaluate the performance of bridges long-term. Concrete deck temperatures of the laboratory prototype were continuously monitored by Type T thermocouples embedded at various locations in the deck slab. Low cost, simplicity of fabrication and ease of installation make the Copper-constantan Type T thermocouples ideal sensors both short-term and long-term monitoring. Figure 17 shows the concrete deck and ambient temperatures recorded on the laboratory prototype bridge for 1 year.

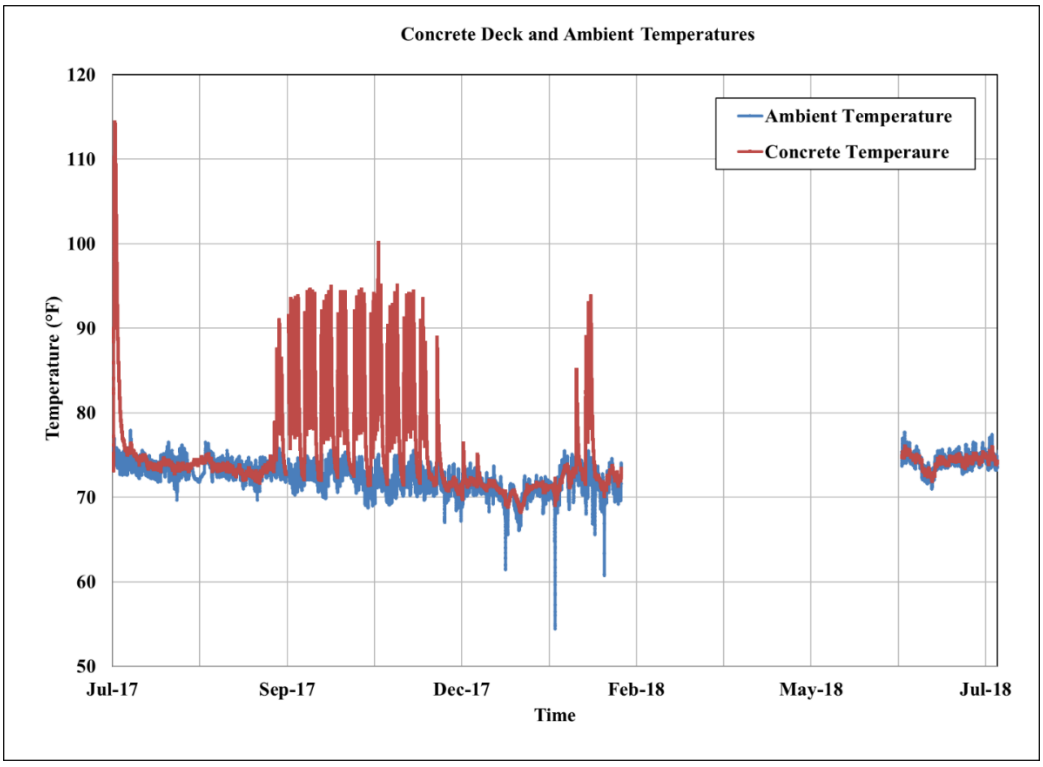

Figure 17. Long-term monitoring of concrete deck and ambient temperatures on the prototype bridge

The trend shows the heating and cooling of concrete temperatures at early ages during curing of the concrete deck. At the end of the cooling cycle the concrete deck temperatures very much resemble the laboratory ambient temperatures. The graph also shows the heating and cooling cycles of the heat load testing performed on the prototype bridge after 56 days of curing. At the end of the heat load testing it can be noted that the concrete deck temperatures revert to replicate the ambient temperatures. Although the laboratory ambient temperatures were maintained at about 73 ºF throughout the year, we can see a sharp drop in temperatures during some days of the winter months. This may be due to the fact that the bay doors of the BCEL could be kept open that could have led to lowering the lab temperature significantly for a short period of time. It can be noted that there is a break in data collection for about 4 months. This was due to power supply failure to the datalogger and the interface systems. This shows that an uninterrupted supply of AC power is imperative to continuously monitor bridges both at the lab and in field.

Concrete Strain monitoring

In order to monitor the long-term strain effects in concrete it is generally preferred to use concrete embedded strain gauges. VWSGs have a stable zero over time with less digital drift unlike the electrical resistance strain gauges making them an ideal sensor for monitoring long term strains in concrete. Figure 18 shows the long-term strains measured using the VWSG Type 1 located at the midspan on top of N. Girder of the prototype bridge.

At early ages the initial peak in concrete strains represent the early age thermal strains during hydration period, followed by the decrease in strains at the end of the cooling cycle. The bridge deck was wet cured for 14 days prior to the removal of formwork. It is interesting to note that the concrete strains continue to increase in compression over time beyond the curing period. The concrete slab continues to shrink over time in-spite of being restrained by the steel girders and are

found to become stable after January 2018, about 6 months after deck cast. The increase in concrete strains in compression is mainly contributed due to shrinkage of concrete.

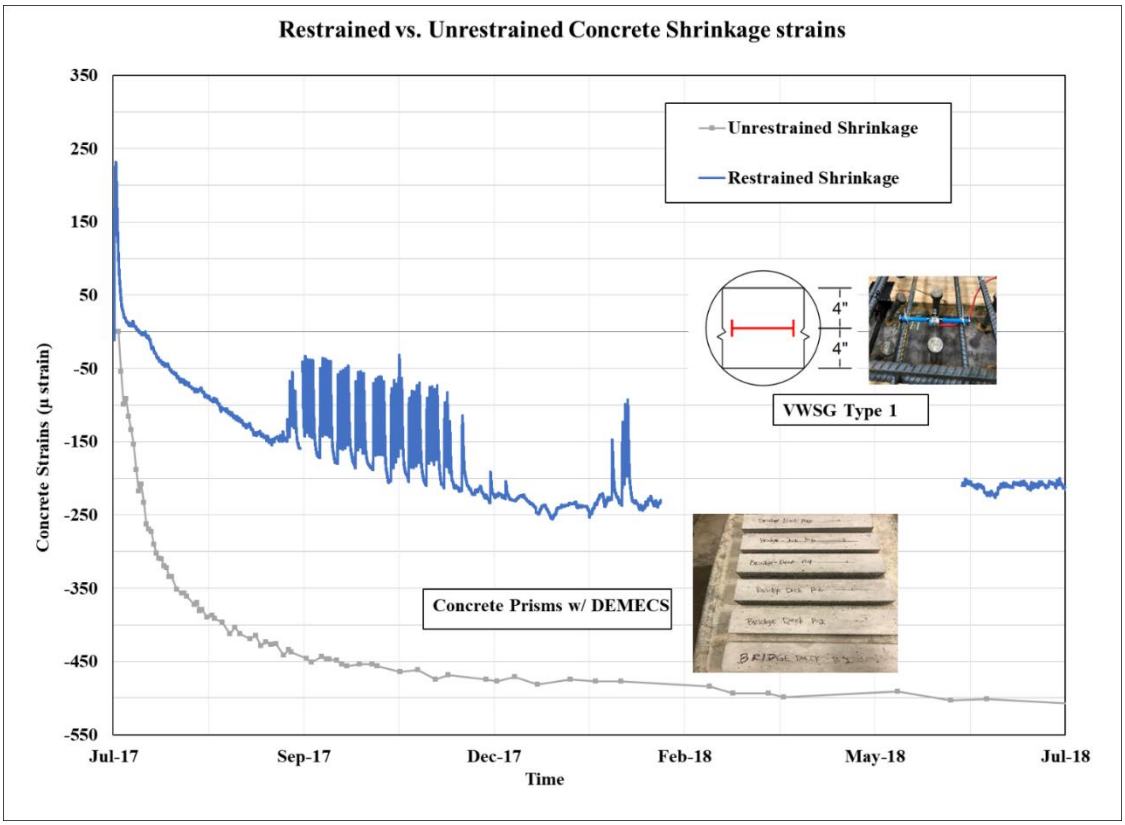

Figure 18. Long-term monitoring of restrained and unrestrained strains in concrete

About 2 months after the bridge deck cast, the peaks and troughs in the graph are represented by the cyclic heating and cooling of the bridge deck during heat load testing. This variation in shrinkage strains causes the development of tensile strain gradient within the concrete deck resulting in non-zero stress levels. In some cases where the thermal shrinkage is greater, the strain gradient within the deck could be sufficient to cause bridge deck cracking. From this one can see that large temperature swings during the heating and cooling cycle could contribute directly to larger strain profiles through the depth of the cross section, which in turn could lead to cracking. However, no cracking has been reported on the laboratory bridge deck.

Also plotted in the same graph are the average unrestrained shrinkage strains measured from the shrinkage prisms prepared at the time of the bridge deck cast. Fig 18 shows that the VWSG recorded a strain of about 200 $\boldsymbol{\mu\varepsilon}$ in the middle of the deck compared to an unrestrained shrinkage strain of 500 $\mu\varepsilon$ (10^{-6} in/in), at 365 days. A difference of about 300 $\mu\varepsilon$ (10^{-6} in/in) can be observed between the restrained and unrestrained shrinkage strains. The difference is accounted for in that concrete shrinkage with the composite deck is restrained by the steel girders whereas the measured shrinkage in the prisms are unrestrained.

Deflection monitoring

The long-term vertical deflections at the midspan location of the North and South steel girders are shown in Figure 19. The defections are shown to correlate well with the long-term temperature graph as shown in Fig 17. The initial data shows that over the course of 24 hours after the slab cast the bridge experienced upward deflections due to heating of the deck and downward deflections as the concrete temperatures cooled down to ambient temperatures at the end of the hydration period. It can be noted that after 14 days of wet curing the bridge deck continued to deflect downward even after the concrete temperatures returned to ambient temperatures. This deflection data correlates well with the increase in restrained concrete strains towards compression as shown in Fig 18.

The long-term average downward girder deflections at the end of one year is reported to be 0.753 in. The average initial deflections in the steel girders right after slab cast was about 0.4 in. Therefore, the long-term bridge deflections due to shrinkage alone is about 0.33 in. This supports the proposition that the shrinkage of concrete causes additional downward deflection in bridge girders after concrete hardening. The graph also shows the cyclic sweeping deflection changes from the heat load testing performed on the prototype bridge after 56 days of curing. The graph again correlates well with the change in concrete deck temperatures and concrete strains as shown

in Figs 17 and 18. These changes were a result of differential heating and cooling of the bridge deck causing differential thermal expansion and contraction during the heat load testing. The higher temperatures produced upward defections and the lower temperatures resulted in downward deflections in the bridge girders.

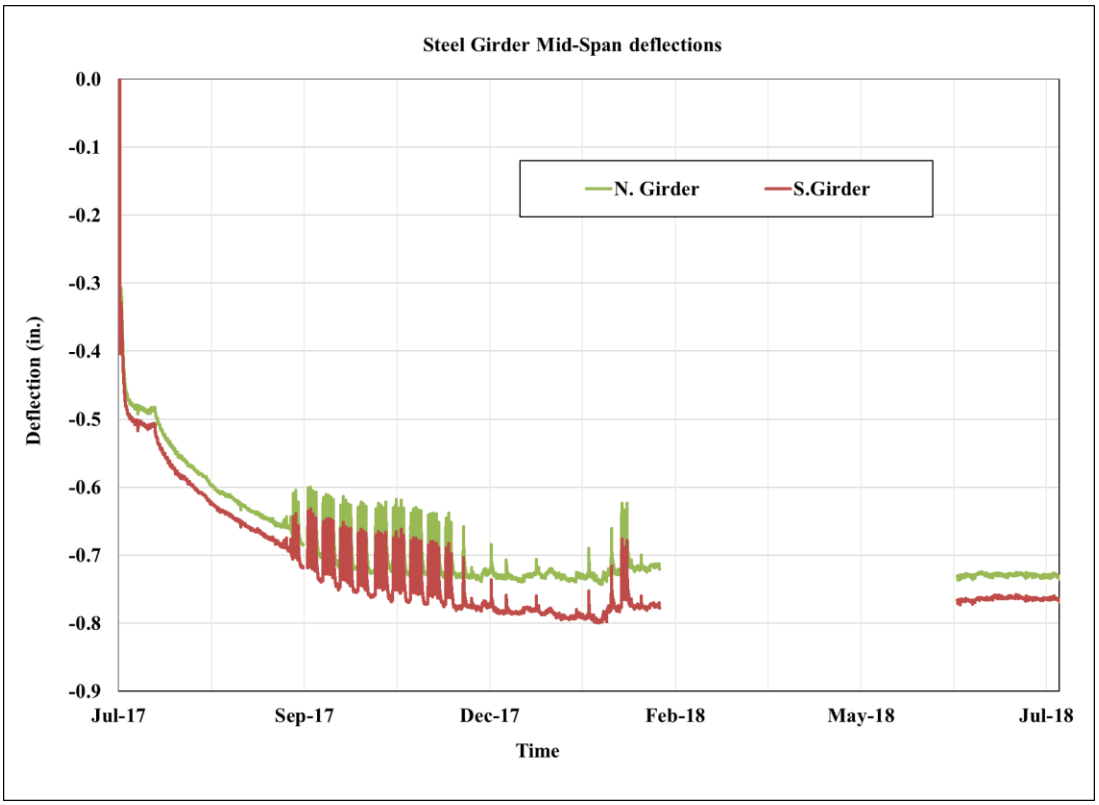

Figure 19. Long-term defections in the steel girders of the laboratory prototype bridge

Field Bridge Instrumentation

Through the experience gained from installation and monitoring of the laboratory prototype bridge, a structural monitoring system was set up and installed for a field bridge. With aid from the ODOT field division, SH-14 Bridge "A" located in Kay County Oklahoma was identified as a potential bridge candidate for field instrumentation. The bridge was built over Chikaskia river and overflow located about 60 miles North of Stillwater near the Kansas State line. The bridge consists of four 100 ft. continuous spans built with a skew of about 30 degrees. The bridge is built

with 6 girder lines of 54 in. deep x 3/8 in thick steel plate girders supported on steel bearings, some of which act as pins and some which are constructed to act as rollers. The bridge is scheduled to be rehabilitated in August 2019, by casting a new 8 in. thick slab atop the existing steel plate girders.

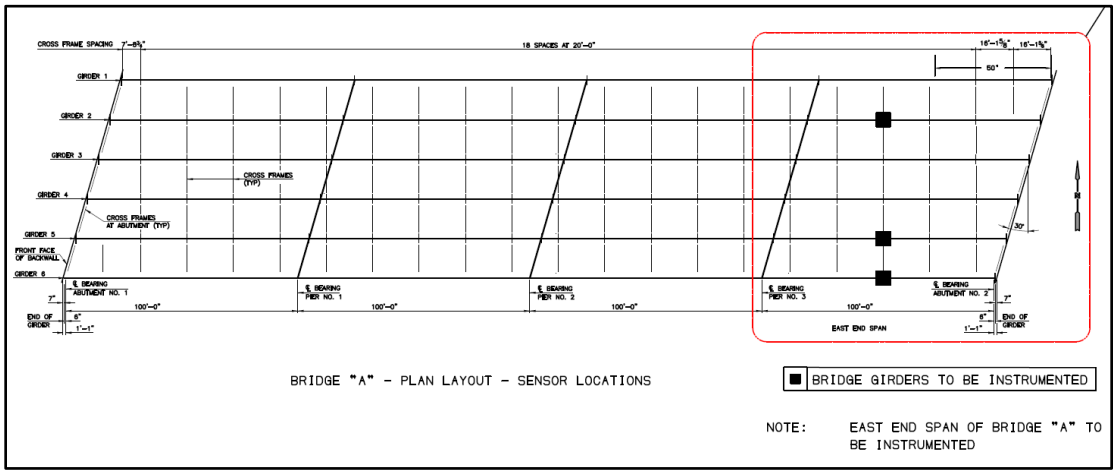

Figure 20. Bridge “A” Plan Layout identified with Girders to be Instrumented

Figure 20 shows the plan drawing of S-14 Bridge “A” marked with the bridge girders to be instrumented. From figure the east most span of girders 2,5&6 were identified to be instrumented for this research program. The natural ground elevation on the east most span of the bridge provided a fairly level working platform underneath the bridge to access the steel plate girders and the construction site. The location of the various type of sensors and data acquisition box is shown in Figure 21.

About 50 sensors are set to be employed to measure and monitor concrete and steel strains, concrete and steel temperatures, and inclination of the steel girders. Figure 22 shows the section detail drawing with the location of each sensor along the depth of the girders to be instrumented. The type of sensors to be installed on the girders included the following:

(1) Vibrating wire strain gauges (VWSG) attached to the steel girders to measure the steel strains prior to and after the deck casting;

(2) Vibrating wire strain gauges (VWSG) embedded within the concrete deck prior to casting to measure the concrete strains and concrete temperatures within the hardening deck;

(3) Thermocouples to measure the temperature within the concrete and ambient temperatures near the bridge deck;

(4) Inclinometers to measure angle of inclination at the ends of girders.

The instrumentation system was programmed to monitor both early age and long-term performance of the field bridge.

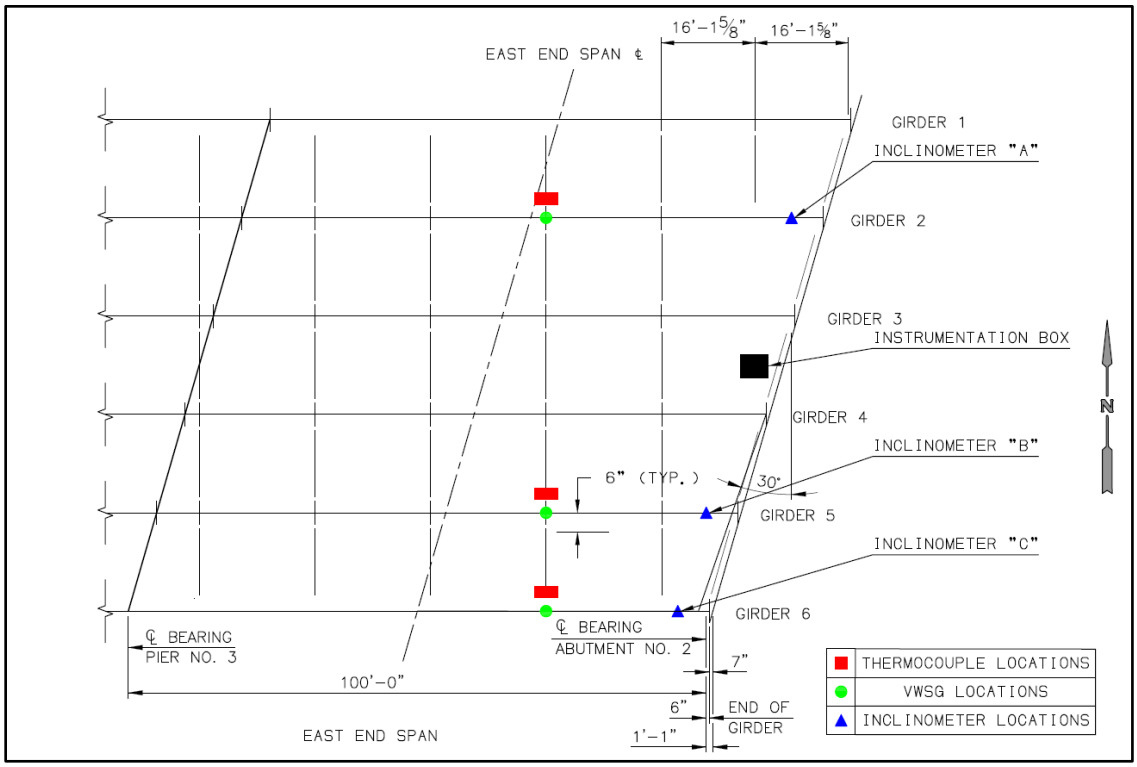

Figure 21. Sensor locations on East-end span of Bridge "A"

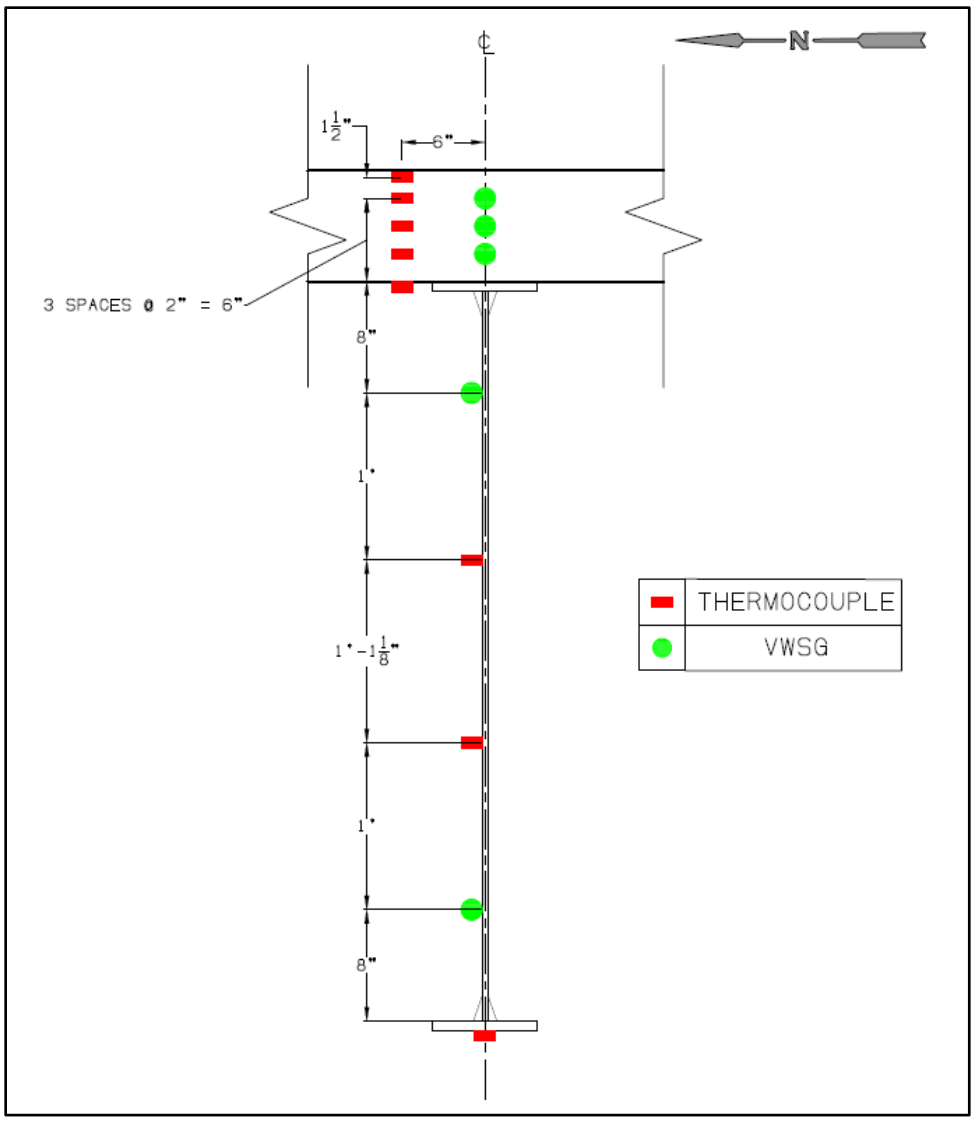

Figure 22. Typical cross section detail drawing with sensor locations

Data acquisition, Interface Systems, Communication and Power Supply

A CR1000X datalogger was used for the field bridge monitoring. The CR1000X was chosen over the CR1000 datalogger due to its reliability for long-term data collection and high accuracy for analog sensors. The CR1000X is built in with both digital and analog ports that can accommodate a varied selection of sensors. The reliability and ruggedness of the CR1000X makes it an excellent choice for remote environmental applications. The AV200 and AM16/32 combination interface was used to accommodate both the concrete embedded and steel girder bonded VWSGs.

The AM25T- 25 channel interface was used to connect the thermocouples and the inclinometers were directly wired into the CR1000X panels. The sensors were programmed to collect data for every 2 min intervals. Figure 23 shows the schematic plan of the field bridge instrumentation

The datalogger, interface systems and the remote cell modem were simultaneously were powered by a rechargeable 12Vdc, 24 Ah battery pack BP24. The BP24 battery provides all the features supplied by the PS150 battery and is typically intended for high current drain systems. The remote location of the bridge candidate and inaccessibility to AC power supply required for a photovoltaic solar panel. A 20-watt solar panel, SP20 was used in this research due to high power requirements. It easily connects to the Campbell Scientific datalogger and BP24 battery base to recharge the battery for a continuous and uninterrupted power supply. Continuous monitoring of the bridge was possible through a local network and remote cell modem. RV50, an industrial 4G LTE cellular gateway provided internet connectivity to the Campbell Scientific dataloggers and the interfaces. It works with Verizon network sim card and data plan that is programmed in the device.

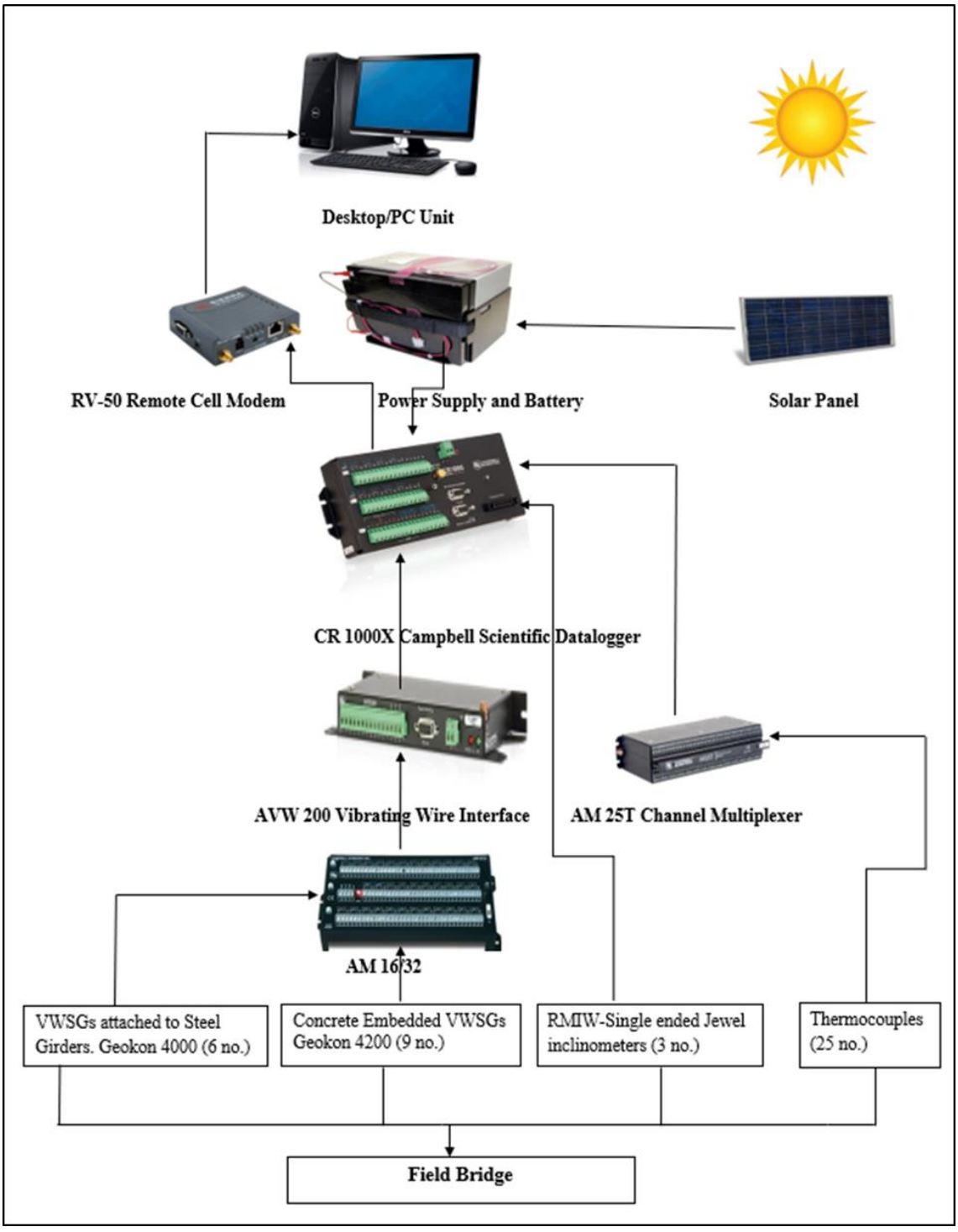

Figure 23. Field bridge monitoring and instrumentation schematic plan

Strain Monitoring

VWSGs were located at specific areas of the bridge deck and steel girders to record and monitor both short-term and long-term strains. As shown in Fig 22 a total of 5 VWSGs will be installed along the cross section of each bridge girder set to be instrumented. 3 no. Geokon 4200 type VWSGs are to be embedded in the 8 in. thick concrete bridge deck. The sensors will be installed in the longitudinal direction of the bridge deck and spaced vertically at 2 in. c/c along the centerline of the girders. The gauges are to be suspended in concrete by tying them to two short pieces of rebar with nylon tie-wraps which were then tied to the existing rebar. 2 no. Geokon 4000 model VWSGs are to be installed on the steel girders and are spaced at 8 in from the top and bottom of the girders along the same guidelines as the Geokon 4200 sensors to capture the strain gradient throughout the depth of the cross-section. The Geokon 4000 and 4200 series work on the same principle. Geokon model 4000 consists of a length of steel wire tensioned between two mounting blocks. The blocks are welded to the surface of the steel member. Under loading the deformation of the member causes relative movement between the mounting blocks which in turn changes the tension in the wire and a corresponding change in its frequency of vibration.

Geokon 4000 model VWSGs sensors are typically specified to be arc welded or spot welded to the structural steel. To prevent concentration of stresses on the plate girders, another common alternative attachment method that uses adhesive such as superglue or epoxy was used in this research. Based on laboratory study conducted by some researchers (James and Yarnold 2017), selective adhesives were identified and used for easy installation and rapid set times when bonded to the steel plate girders on field. A combination of Loctite superglue with Loctite 5-minute Epoxy was used to bond the Geokon 4000 VWSGs to the steel girders. Laboratory testing was performed on the laboratory prototype bridge to evaluate the performance of the welded and the glued VWSGs. One gauge was attached close to the bottom flange of the steel girder by welding the end mounting blocks and clamping the VWSG to the blocks. The second gauge was installed

on the opposite face of the steel beam by bonding the end mounting blocks to the face of the steel beam and then clamping the VWSG to it. A bead of epoxy was then applied along the sides and back of each end mounting blocks for durability purposes. Figure 23shows photographs of Geokon 4000 VWSGs welded and bonded to the webs of the steel girder.

Figure 24. Geokon model 4000 VWSGs welded and glued to the steel beam of the prototype bridge

After the strain gauges had been installed for about 24 hours, loading tests were performed on the prototype bridge to evaluate the performance and compare the strains in both the welded and bonded strain gauges. An unsymmetrical load test was conducted on the prototype bridge and the strains were recorded and monitored using a CR1000X Campbell Scientific datalogger along with an AVW200 and AM16/32 interface systems. Figure 25 plots the strains over time that was recorded from both the VWSGs. The graph clearly shows that the strains recorded form both the welded and bonded VWSGs correlate well with each other. It can also be noted that at the end of the loading cycle, after the removal of the load both the strains returned to zero.

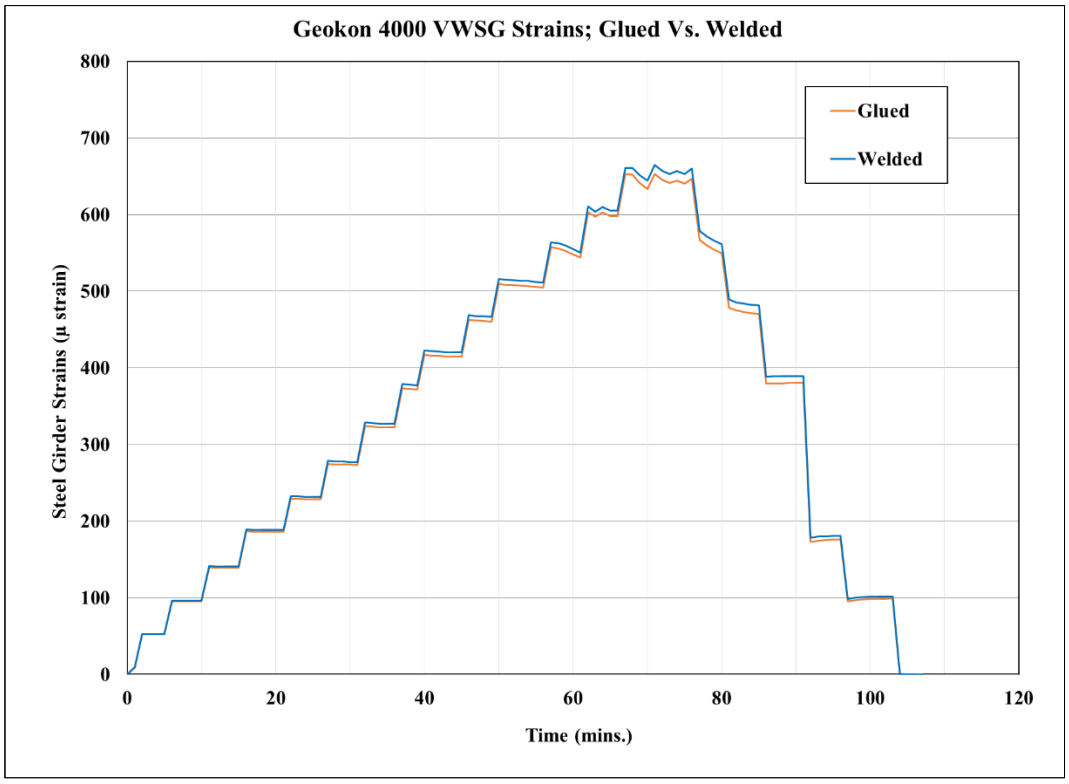

Figure 25. Performance of Glued vs. Welded Geokon 4000 VWSGs

Temperature monitoring

Thermocouple sensors were set to be installed at specific locations on the girder 5 and 6 and in the concrete slab above them to measure the temperature gradient throughout the depth of the cross section. As shown in Fig 22, 5 thermocouples were installed vertically at 2 in. c/c spacing along the centerline of the girders. The bottom 4 thermocouples were spaced at 2 in. c/c vertically while the top thermocouple was placed at ½ in. below the surface to avoid damages during concrete pour and surface finishing. Thermocouples were also attached to the bottom flange and in between the VWSGs. in order to record temperature gradient along the depth of the steel girder.

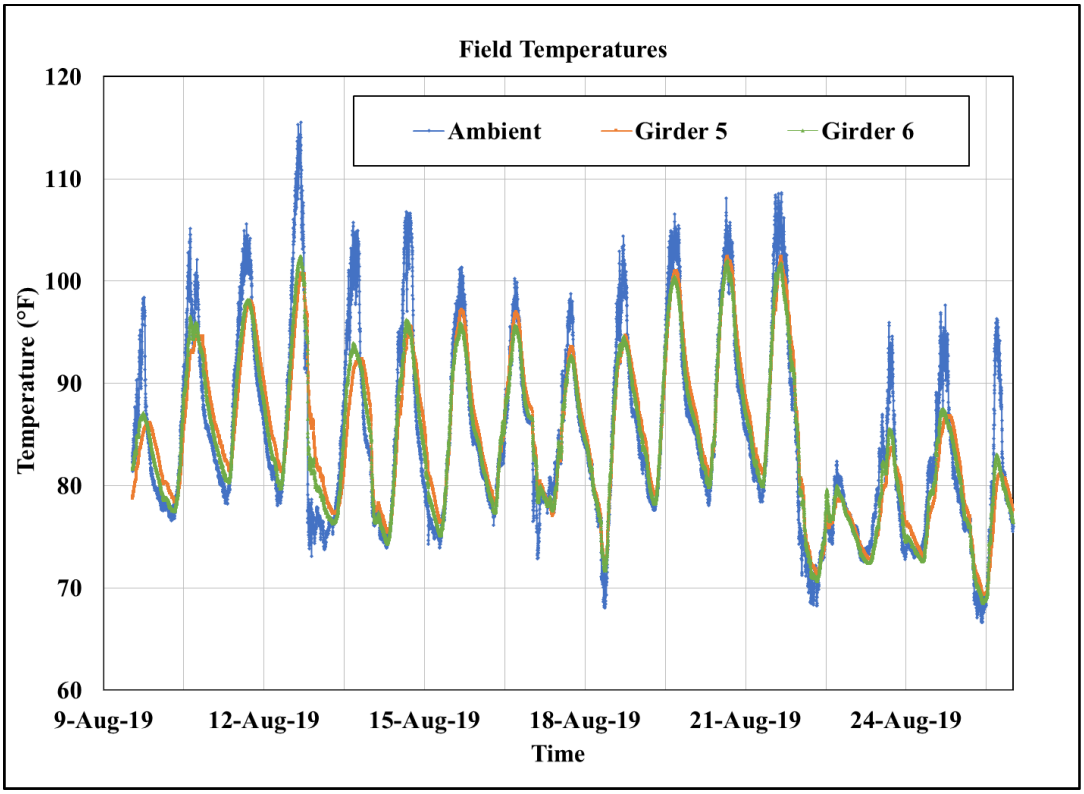

Figure 26. Trend Plot of girder temperatures measured on SH-11 Bridge "A"

Trend plots graphed with time in x-axis form the backbone of structural evaluation. These plots established for varying temperatures, strains and deflections over time. Figure 26 shows the trend plot for temperatures measured in girders 5 and 6. The girder temperature shown in this graph were measured form thermocouples installed at about 20 in. from the top flange as shown in Fig 22. An additional thermocouple was installed to measure and record ambient temperatures at the job site. The recorded ambient temperature is true representation of Oklahoma summer days with temperatures reaching as high as 115 ºF during the day and low as 68 ºF at night time. The data shows that the bridge experiences cyclic heating and cooling cycles as a result of differential heating and cooling of the bridge during the course of the day. Both the girder temperatures correlate well with the increase and decrease in the ambient temperatures. It is noted that the exterior girder 6 recorded slightly higher temperatures than the interior girder 5.

Summary and Conclusions

The structural monitoring system implemented in this research program combines sensors from diverse technologies into a seamless system using a single database and user interface system allowing for real time data acquisition and analysis. A full-scale prototype bridge was built at the Bert Cooper Engineering Laboratory. The bridge was built with a composite concrete deck that experiences the similar mechanisms of a field bridge. A full-scale model of the bridge allows to capture the absolute values of the original time dependent properties of concrete deck that cannot be completely captured using a small-scale model. The prototype bridge was instrumented and installed with an array of sensors to monitor both the short term and long-term performance of the bridge. Synthesis of data collected from the sensors along with analytical computational models that were developed using the measured constitutive properties of concrete validated the methods for structural monitoring. The structural monitoring of a field bridge was successfully implemented through the experience from the laboratory prototype bridge.

1. VWSGs are highly recommended for measuring strains within concrete due to their ease of installation, long term stability and maximum resistance to moisture.

2. VWSGS embedded in the concrete are efficient in capturing the early age concrete strains and temperatures in the concrete deck due to heating of the deck during hydration and subsequent cooling and shrinkage of concrete.

3. VWSGs can successfully monitor both static and dynamic responses of structures at one time which makes them the utmost sensors for bridge monitoring systems.

4. The durability and accuracy of thermocouples make them ideal and economic sensors to measure temperatures in both concrete and in steel girders.

5. Thermocouple sensors embedded in the concrete and attached to the steel girders are efficient in capturing the thermal gradient developed across the composite cross section of the prototype bridge. Measured thermal gradient from the thermocouples can be used to predict the thermal strains, stresses and deflections in the prototype bridge.

6. The ease of installation of LVDT sensors makes it ideal for laboratory experimentation where they require a fixed reference point to be mounted from.

7. Inclinometers serve as ideal surrogates for LVDT sensors to measure bridge deformations in field conditions where a fixed reference point is not required.

8. Inclinometers provides an opportunity to measure angles of rotation along any three orthogonal axes at a time which makes the sensor superior to other commercially available deflection measurement technologies.

9. The datalogger and interface systems used in this research are proven to provide reliable data retrieval and monitoring systems for both short term and long-term monitoring of bridges.

10. The reliability and ruggedness of the Campbell Scientific Datalogger along with its capability to accommodate a variety of sensors from different manufacturers makes it an ideal both laboratory and remote applications.

11. Continuous monitoring of remote bridge structures is made possible through interfacing with local network and remote cellular modem.

12. A photovoltaic solar panel was successfully installed in the field bridge to provide a continuous and uninterrupted power supply for the instrumentation systems.

CHAPTER IV

INVESTIGATION OF POOR RIDE QUALITY IN STEEL BRIDGE GIRDERS BUILT COMPOSITE WITH CONCRETE SLABS

This chapter focuses on excessive and undesired deformations that occur during construction of newly rehabilitated steel bridges. The research program responds to problems with elevation control and subsequent ride quality problems exhibited in newly constructed or newly rehabilitated steel girder bridges made composite with cast concrete decks. Forensic investigations were performed on three field bridges. Those investigations discovered strong evidence that cantilevered portions of concrete decks were not supported adequately during construction loadings. In addition, a full-scale laboratory prototype bridge was built where deformations of formwork and bracing were measured. Supported by shallow bracing, the formwork was shown to deform locally due to self-weight of the concrete plus construction loadings. These deflections are significant and can be shown to produce unevenness in bridge deck elevations (or "dips" in the driving lanes) and thin bridge decks. The purpose of the research program is to identify causes for undesirable elevation profiles, and to recommend design and construction practices to help mitigate problems created for the highway users and extend the life span of bridges.

Introduction and Background

The U.S. Federal Highway Administration (FHWA) lists 614,387 bridges within the US National Bridge Inventory (NBI). These are bridges positioned on highways identified as the National Highway System (NHS), and consist of principally of Interstate Highways and other major U.S. Highways. Of those bridges, almost 40 percent are 50 years or older. Moreover, in 2016 about 9.1% (56,007) of the NBI were rated structurally deficient (ASCE 2017). As the average age of America's bridges keeps increasing, many of the nation's bridge are approaching the end of their design life. Therefore, an increasing number of nation's bridges require major rehabilitation to extend the lifespan of these bridges.

Within the State of Oklahoma, the Oklahoma Department Of Transportation (ODOT) maintains 3,727 span bridges (Russell August 2017). Of those, 1617 bridges are made with steel girder superstructures with an average construction year of 1963. In 2010, about 706 bridges in the state of Oklahoma were classified as structurally deficient (ODOT 2017). Of those listed as structurally deficient, approximately 270 were bridges supported by steel superstructures. In recent years, the ODOT has been actively rehabilitating steel girder bridges by casting new concrete decks on top of existing steel girders. This method of rehabilitation is chosen as a cost-effective means of repairing bridges that are structurally deficient, functionally obsolete, or both. In the process, the life span of a single bridge can be lengthened dramatically while helping to ensure the safety of the traveling public.

During the rehabilitation process, new bridge decks are often made both wider and thicker. In many of these bridges, concrete slab depths increased from the original construction of 6 in. to 8 in., and the roadways were widened to allow modern lane widths with shoulders. Often, the structural designs of the newly rehabilitated bridges "worked" as shear studs are added to ensure composite behavior and increase shear capacity to account for heavier design loads in more

recently adopted rating and design codes. In addition, the increased deck thickness also worked to help increase live load capacities, which offset the increasing dead loads.

As the State undertook an aggressive policy of rehabilitating these steel girder bridges, many newly reconstructed steel girder bridges exhibited poor ride quality and generally displayed "dips" in roadway elevations. These "dips" generally occur nearer the mid-spans of the bridges, or at least in locations that are not near the supports provided by bridge piers. In some bridges, roadway elevations dipped more than 1 in. at midspan compared to elevations at the pier supports, and in many cases, within spans less than 60 ft in length.

This chapter focuses on excessive and undesired deformations that occur during construction of newly rehabilitated steel bridges. The chapter highlights the problems with elevation control and subsequent ride quality problems exhibited in newly constructed or newly rehabilitated steel girder bridges made composite with concrete decks cast atop steel girders. This chapter reports the findings from forensic investigations that were performed on three newly rehabilitated bridges in Oklahoma. Evidence due to poor elevation control and poor design details, unevenness in bridge deck elevations were reported. In addition, laboratory experimental investigations on overhang bracket systems and its influence on poor elevation control and unexpected deflection in overhang portions of the bridge deck is also reported.

The following are primary objectives for this chapter

1. To identify the causes for undesirable elevation profiles and excessive deformations in newly constructed or newly rehabilitated composite bridges built in field.

2. To develop design and construction methods and recommendations to help mitigate problems with ride quality and unexpected deflections in ODOT bridges.

3. To evaluate the performance of C-49 overhang brackets when used in combination with shallow girders and larger overhangs.

Forensic Investigation of known Bridges

In 2012, as an early part of the research program, forensic investigations were performed on three recently rehabilitated bridges. The three bridges selected were: 1) SH 86 over Stillwater Creek in Payne Co.; 2) SH 14 over Eagle Chief Creek, Bridge "A" in Woods Co., and 3) US 281 over Mule Creek in Woods Co. Of these bridges, SH 86 and SH 14 were reported to have ride issues relatively soon after construction was completed. The bridges at SH 86 and SH 14 had decks that were cast with screed elevations set at the edge of the concrete deck slabs, at locations cantilevered 3 ft. or more from the C.L. of the outside girder. In contrast, screeds for the deck slabs on the US 281 were set directly atop the outside girders, and elevations outside of the screeds were set by hand float. All three of these bridges were thoroughly inspected.

SH 14 Over Eagle Chief Creek Bridge "A", Woods Co.

A photograph of the Eagle Chief Creek, Bridge "A" in Woods Co. is shown in Fig. 27 looking south along the east side of the bridge. Site investigations were performed on September 18 and September 23 of 2014. The Woods Co. Bridge is 30 ft - 8 in. wide measured out-to-out (o/o) and supported by five girder lines with 3 ft - 4 in. cantilevered overhangs. The two end spans were at 40 ft - 9 in. and the two middle spans were 40 ft - 0 in. from center-to-center (c/c) of bearings. The plans for the retrofit called for an 8 in. concrete deck slab with a super-elevation slope of 1%. Decks are supported by W24x94 Gr. 50 steel girders, and shear studs were installed as part of the rehabilitation. The steel girders are spaced at 6 ft and constructed with steel diaphragms at the ends and mid span locations. Steel girders were supported by steel bearings, some of which act as pins and some which are constructed to act as rollers.

Figure 27. SH 14 Over Eagle Chief Creek, Bridge “A” in Woods Co.

New slabs were cast in 2010 or 2011 atop existing steel girders. At the same time, some rehabilitation or reconstruction of abutments was also done. Immediately upon construction, the bridge was reported to have issues with ride quality. Field investigations were performed as part of this research effort. Inspection found that the concrete deck slabs were uniformly in good condition with minor cracking exhibited both top and bottom of the bridge deck. There was also evidence of repair and new detailing at the abutments. Bridge piers and pier caps, and bearing assemblies were found in good condition. Elevation measurements were taken to assess the elevation changes within the driving lanes, and to also help determine causes for possible adverse beam deflections. In Fig. 27., the girders possess a visible sag, perhaps in place from earlier construction or perhaps developed over the period of long service prior to the retrofit. Elevations at the bottoms of the beams were measured, and these confirmed that the bottoms of the beams have lower elevations at midspan than at supports.

Elevation measurements were made with traditional surveying equipment including an engineering level and leveling rod marked in hundredths of a foot as shown in Fig. 28.

Elevations were measured at the bottoms of steel girders, at the bottom of concrete decks and atop the roadway surface (at the top of the concrete deck). Elevations were referenced to the T.O. of the east edge of the South Bridge Abutment (Abutment #1).

Figure 28. Elevations measurements made with traditional surveying equipment including an engineering level and a leveling rod.

Table 1. reports roadway elevations at the top of the concrete deck. Elevations at the North bound and South bound shoulders were measured immediately outside of the lane stripe. Centerline (CL) elevations at or near the center line striping. CL Elevations vary from 3.51 to 3.58 ft. The "crown height" reported in the table measures the elevation at CL compared to the average elevation of the two shoulders. "DG" indicates locations where diamond grinding was visible in the traffic lanes, so it is possible and even probable that reported problems with ride were corrected somewhat with diamond grinding.

Table 1. Roadway elevations at the top of concrete deck of SH -14 bridge

Elevation Readings (ft) T.O. Roadway Deck						
	Feet from South Joint	ELEV @ N-Bound Shoulder	Crown Height (ft)	ELEV @ CL		ELEV @ S-Bound Shoulder
Span #1	0	3.46	0.08	3.51	DG	3.40
	10	3.42	0.11	3.52	DG	3.40
	20	3.41	0.12	3.54		3.42
	30	3.40	0.12	3.53		3.42
	40	3.47	0.11	3.57		3.45
Span #2	40	3.46	0.10	3.55		3.44
	50	3.38	0.11	3.51		3.41
	60	3.39	0.11	3.51	DG	3.41
	70	3.40	0.13	3.53	DG	3.41
	80	3.47	0.12	3.57	DG	3.44
Span #3	80	3.48	0.11	3.57	DG	3.44
	90	3.47	0.11	3.56	DG	3.43
	100	3.44	0.11	3.55		3.43
	110	3.45	0.11	3.56		3.44
	120	3.49	0.10	3.59		3.48
Span #4	120	3.50	0.09	3.58		3.48
	130	3.46	0.13	3.58		3.45
	140	3.46	0.13	3.58		3.45
	150	3.47	0.12	3.58	DG	3.45
	160	3.52	0.08	3.57	DG	3.45
N. Approach	160	3.52		3.57		3.45
	170	3.43		3.50		3.38
	180	3.32		3.41		3.27

Notes:
1. Elevations measured relative to the Top of Abutment #1 (SE Corner Abutment).
2. N-Bound Shoulder and CL Elevations were measured from Instrument Location SE of the bridge deck. S. Bound Shoulder Elevations were measured from Instrument Location NW of bridge deck.
3. "ELEV @ CL reports the elevations at the roadway centerline.
4. "DG" indicates where diamond grinding was visible. Crown Height is the ELEV @CL minus the average ELEV @ the shoulders.

The values reported in Table 1. are also shown in the chart in Fig. 29. Fig. 29 shows the elevations of the SH 14 bridge at the centerline and at the North and South bound shoulders. The

elevations were graphed from the South end of the bridge to the North end. From Fig 29, we can see that Span #2 (40 ft. to 80 ft.) has the worst elevation “dip”, about 5/8 in. at CL, but with as much as 1.0 in. dip at the South-bound shoulder. Diamond grinding has apparently relieved some of the ride-ability issues since the construction was completed. The elevations shown in both Table 1. and Fig. 29 also indicate a super-elevation consistent with the "1 percent slope" prescribed on the construction drawings. A 1 percent slope in 12 ft. of lane width correlates to a 0.12 ft. elevation change, which is equivalent to 1.5 in.

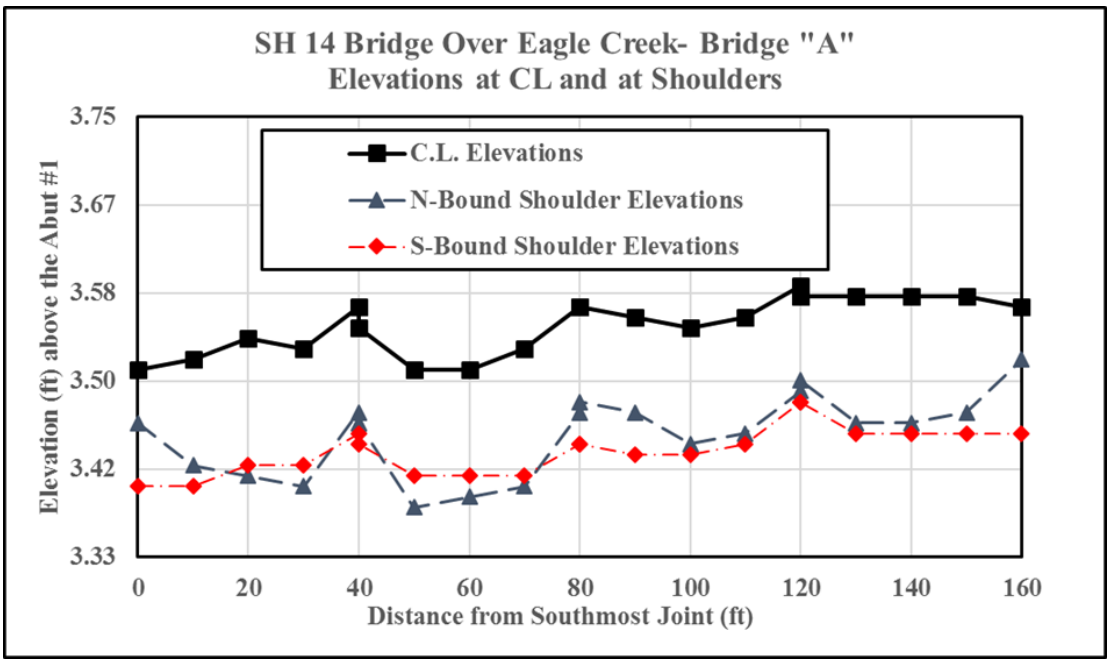

Figure 29. Elevations charted from the South end of the bridge to the North end.

Table 2. reports the roadway elevations recorded at the bottom of the deck slab. The readings were recorded at locations “outside” the girders, and at locations approximately mid-way between the steel girders. Altogether, for each station measured in “Distance from the Joint at Abutment #1,” six direct elevation measurements were made. The reported “Average Elevation at Bridge CL” is computed from the average of the two nearest elevations.

Table 2. Roadway elevations recorded at the Bottom of the Deck Slab for SH-14 Bridge

Elevation Readings (ft) at the B.O. Concrete Slab								
	Distance from the Joint at Abut #1 (ft)	Outside East Girder (#1)	Between #1 and #2 Girders	Between #2 and #3 Girders	Average Elev @ Bridge CL	Between #3 and #4 Girders	Between #4 and #5 Girders	Outside West Girder (#5)
Span #1	2	2.72	2.80	2.85	2.84	2.84	2.79	2.74
	20	2.78	2.78	2.83	2.83	2.82	2.80	2.75
	38	2.79	2.80	2.86	2.86	2.87	2.81	2.80
Span #2	42	2.77	2.80	2.88	2.87	2.87	2.83	2.78
	60	2.79	2.78	2.87	2.86	2.85	2.79	2.74
	78	2.79	2.93	2.93	2.94	2.95	2.91	2.87
Span #3	82	2.80	2.84	2.87	2.87	2.88	2.82	2.80
	100	2.79	2.79	2.84	2.85	2.87	2.82	2.76
	118	2.80	2.82	2.87	2.87	2.88	2.86	2.82
Span #4	122	2.80	2.84	2.87	2.87	2.88	2.82	2.80
	140	2.79	2.79	2.84	2.85	2.87	2.82	2.76
	158	2.80	2.82	2.87	2.87	2.88	2.86	2.82

Notes:
1. Elevations measured relative to the T.O. Abutment #1 (SE corner abutment).
2. Readings recorded approximately mid-way between the steel girders, or immediately outside the exterior girder.

The elevations measured and reported in Tables 1. and 2. are compared to one another in Table 3., where the slab thicknesses are reported. Slab thicknesses are computed from the measured elevations and represent the difference between the elevations at the bottom of the slab to the elevation of the driving surface. Red numbers in Table 3. indicate measurements where the deck slab thickness is less than the required 8 in. Again, "DG" denotes areas where diamond grinding was performed in the traffic lanes. It is also noted and reported that the diamond grinding visibly reduced the depth of the tines that were likely installed with finishing.

Pre-existing core holes were discovered in Span #2 and Span #4 at the center of the northbound driving lane. Photographs of the two core holes and the related thickness measurements are shown in Fig 30. Thicknesses at the core holes were measured at approximately 7.25 in. in Span

#2 and approximately 8.25 in. in Span #4. The measured thicknesses match the slab thicknesses computed in Table 3. These observations confirm that the method for determining slab thickness from measured surface elevations is an accurate means to obtain forensic data. The slab thicknesses measured using the engineering level were consistent with the depth of the slab measured from pre-existing core holes in the deck in Spans #2 and #4. The cores were from unknown origin.

Table 3. Computed slab thicknesses from measured elevations of SH 14 Bridge

Slab Thickness (ft)					
	Feet from South Joint	N-Bound Shoulder	CL		S-Bound Shoulder
pan #1	0	0.74	0.67	DG	0.66
	10	0.67	0.69	DG	0.66
	20	0.63	0.71		0.67
	30	0.61	0.69		0.65
	40	0.68	0.71		0.65
Span #2	40	0.69	0.68		0.66
	50	0.60	0.65		0.65
	60	0.60	0.65	DG	0.67
	70	0.61	0.63	DG	0.61
	80	0.68	0.63	DG	0.58
Span #3	80	0.68	0.70	DG	0.65
	90	0.67	0.70	DG	0.66
	100	0.65	0.70		0.68
	110	0.66	0.70		0.66
	120	0.69	0.72		0.67
Span #4	120	0.70	0.70		0.69
	130	0.66	0.72		0.67
	140	0.67	0.74		0.69
	150	0.68	0.73	DG	0.67
	160	0.72	0.70	DG	0.64

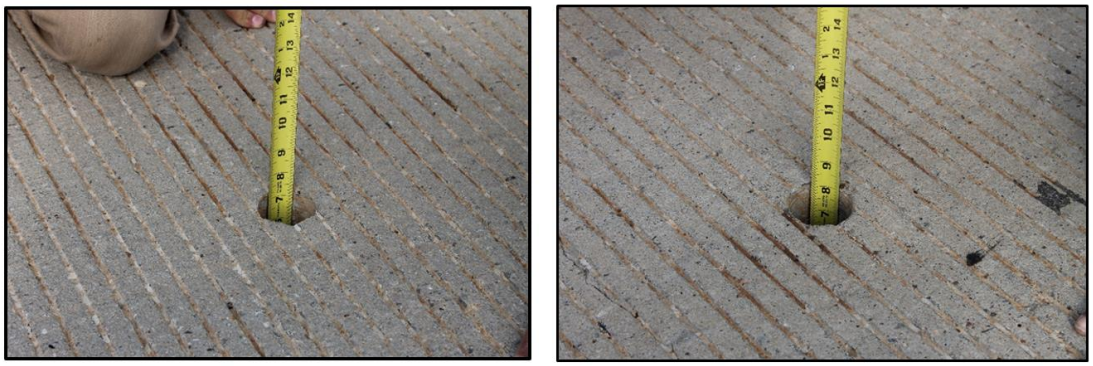

Figure 30. Pre-existing core holes discovered in Span #2 (left) and Span #4 (right)

SH 86 Bridge over Stillwater Creek, Payne Co.

The SH 86 Bridge was reported by witness accounts as having ride-ability issues immediately after construction. Interviews were conducted with both the Contractor's representative and the ODOT Field Engineer. Fig. 31 shows a photograph of the SH 86 Bridge looking southwest and spanning Stillwater Creek.

Figure 31. SH 86 over Stillwater Creek

The bridge is located at the westernmost reaches of Lake Carl Blackwell, which is wholly located on property owned by the Oklahoma A&M University system. This land was part of the original "Land Grant" made in accordance with the Morrill Act that instituted the Land Grant Universities in numerous states. This bridge has three spans, each approximately 60 ft in length. During or about 2011, the bridge was rehabilitated by casting a new concrete deck atop existing steel bridge girders.

Table 4. Measured Elevations of the driving surface -SH 86 Bridge over Stillwater Creek, Payne Co.

Deck Slab (Roadway) Elevations (FT Above T.O. North Abutment)						
Distance measured . from the. Joint at Abut #1 (ft)		East Edge (Against Guardrail)	Just Outside N. Bound Lane Marker	CL	Just Outside S. Bound Lane Marker	West Edge (Against Guardrail)
North Span	0	3.90	3.96	4.05	3.96	3.90
	10	3.83	3.88	3.97	3.89	3.83
	20	3.77	3.85	3.95	3.86	3.82
	30	3.76	3.82	3.92	3.86	3.81
	40	3.78	3.85	3.95	3.89	3.83
	50	3.81	3.88	4.00	3.93	3.83
	60	3.90	3.97	4.00	3.97	3.91
Middle Span	60	3.88	3.96	4.00	3.96	3.88
	70	3.84	3.91	4.01	3.91	3.81
	80	3.79	3.88	3.98	3.88	3.82
	90	3.78	3.86	3.96	3.88	3.81
	100	3.79	3.88	3.98	3.88	3.81
	110	3.81	3.91	4.01	3.93	3.81
	120	3.91	3.97	4.05	3.98	3.92
South Span	120	3.90	3.97	4.05	3.97	3.90
	130	3.82	3.92	4.03	3.93	3.83
	140	3.82	3.89	4.01	3.90	3.83
	150	3.82	3.90	3.99	3.89	3.81
	160	3.83	3.91	4.01	3.91	3.82
	170	3.86	3.93	4.03	3.93	3.88
	180	3.95	3.99	4.10	4.00	3.96
S. Approach	180	3.96	4.00	4.10	4.00	3.96
	190	3.94	3.99	4.08	3.99	3.95
	200	3.89	3.93	4.05	3.96	3.94

Notes:

1. Elev. 0.00 is taken at the East corner of the North Abutment.
2. CL elevations were taken at or near the centerline striping.
3. The outside lane markers are 12 ft from the C.L.
4. The inside dimension from guardrail to the CL is 15'-6.
5. Prescribed super-elevation is 1.0% sloping outward from the C.L.

The forensic investigation was performed in May 2014 and in September 2014. Elevations of the driving surfaces were taken on all three spans relative to the elevation of the north abutment. These elevations are reported in Table 4. Elevations were measured at 10 ft. intervals at the guardrails, at the outside lane marker and at roadway centerlines. Generally, the topside elevations show a clear pattern where the riding surfaces "dip" approximately 0.75 to 1.75 in. near the mid-spans of all three spans. At the centerline, the measured elevations "dip" 1.3 in. in north span, ¾ in. in the center span and 1.02 in. in the south span. Elevation "dips" at the outside lane markers are more severe and vary from 1.00 in. to 1.75 in. Elevations were measured at the outside lane marker for both Northbound and Southbound Lanes. East and West Guardrail elevations were measured just inside the guardrail. All the measurements were taken to the top of the concrete deck slab.

Fig. 32 clearly shows the patterned changes in roadway elevations where the roadways "dip" approximately 0.75 in. to 1.3 in. at midspan. Fig. 32 also shows elevation changes at the outside lane markers and at the guardrails. The figure shows a clear pattern of lower elevations at the mid-regions of the spans and "humps" at the pier supports. These elevation changes are noticeable to drivers operating at highway speeds, and likely cause concerns for safety. Table 5. reports elevations measured to the bottoms of the deck slab. Elevations on the bottom of the bridge deck were taken only on the northern most span as the other two spans were inaccessible due to water from the lake. Measurements between girders were made at mid-distance between beams. Two measurements were made outside of the outside girders. One measurement was made immediately adjacent to the outside girder at approximately 13 ft – 4 in. from C.L. The measurement shown as "East (or West) Deck Edge" was made at the edge of the deck slab, taken approximately 16 ft – 6 in. from the C.L. of the bridge deck.

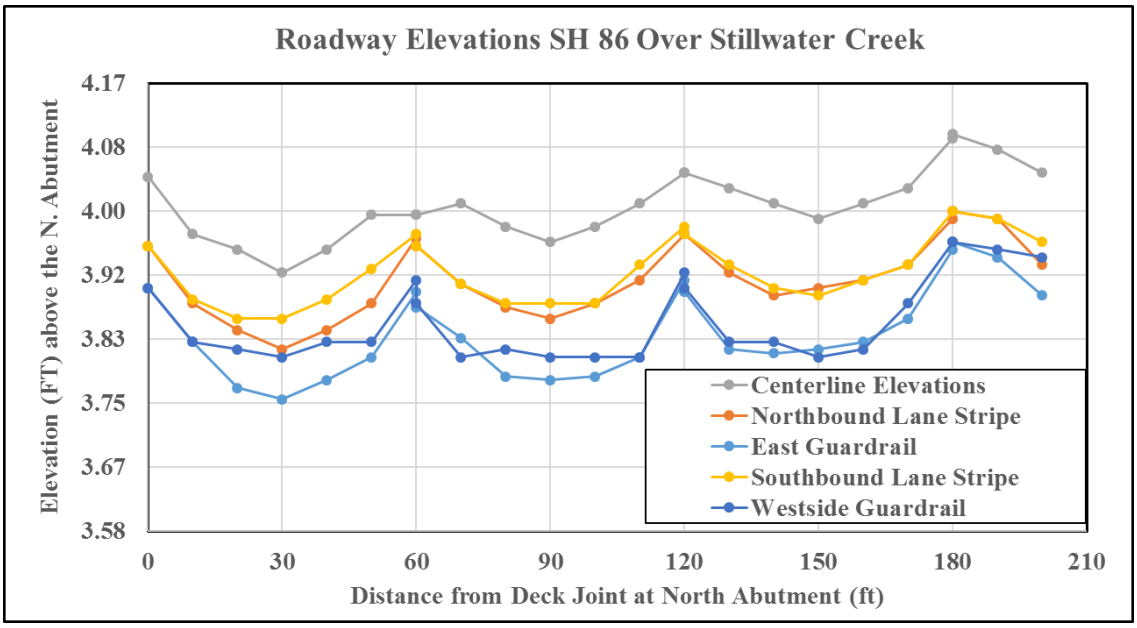

Figure 32. Roadway elevations for SH 86 Bridge over Stillwater Creek, Payne Co. Oklahoma

Stay-in-place forms were used on the SH 86 bridge whereas they were not used on the other two bridges that were inspected. The stay-in-place forms are made from galvanized metal decking. The decking itself is variegated; the depth of the variegation is 1.25 in. Elevations at the bottom of the slab were measured inside the top of the variegation, so elevations were measured at the thinnest part of the slab. Elevations measured outside of the steel girders were made directly to the bottom of concrete, which was exposed and did not feature stay-in-place forms. The concrete decks slab profile in Fig. 33 shows the slab elevations at the midspan of the north span of the bridge. The elevation at the top of the slab is shown as well as the elevations at the bottom of the slab. Elevations of the top of the slab correspond to these values reported in Table 4. at "North Span, 30 ft": East Edge, 3.76; N. Bound Lane Marker, 3.82; C.L., 3.92; S. Bound Lane Marker, 3.86; and West Edge, 3.81. Note that a 1.0 percent slope was required for super-elevation. The actual super elevation slopes are reported in Fig. 33, and it is noted that measured elevations indicate super-elevations of 1.03 percent on the northbound lane and 0.81 percent on the southbound lane.

Table 5. Elevations recorded at the Bottom of the deck slab, North Span. SH 86 Bridge over Stillwater Creek, Payne Co.

		West Deck Edge	O/S West	#7/#6	#6/#5	#5/#4(CL)	#4(CL)/#3	#3/#2	#2/#1	O/S East	Deck Edge East	Dist. Fr. S.
@ Face of North Abutment		3.16	3.23	3.27	3.30	3.34	3.37	3.35	3.26	3.23	3.18	0
@ Dphrm	10'-0	3.13	3.23	3.23	3.30	3.37	3.36	3.32	3.23	3.19	3.11	10
	20'-0	2.85	3.01	3.06	3.11	3.34	3.35	3.29	3.23	3.20	3.08	20
@ Midspan	30'-0	3.06	3.20	3.23	3.29	3.37	3.33	3.30	3.22	3.16	3.03	30
	40'-0	3.10	3.20	3.23	3.30	3.34	3.34	3.31	3.24	3.19	3.04	40
@ Dphrm	50'-0	3.06	3.19	3.25	3.30	3.34	3.33	3.32	3.25	3.22	3.10	50
@ Face of South Pier		3.13	3.24	3.29	3.34	3.37	3.34	3.32	3.28	3.23	3.14	60

Notes:
1. Elev. 0.00 is taken at bottom of bridge deck only on northern most spans.
Measurements (in ft.) made between girders at mid-distances between two beams.

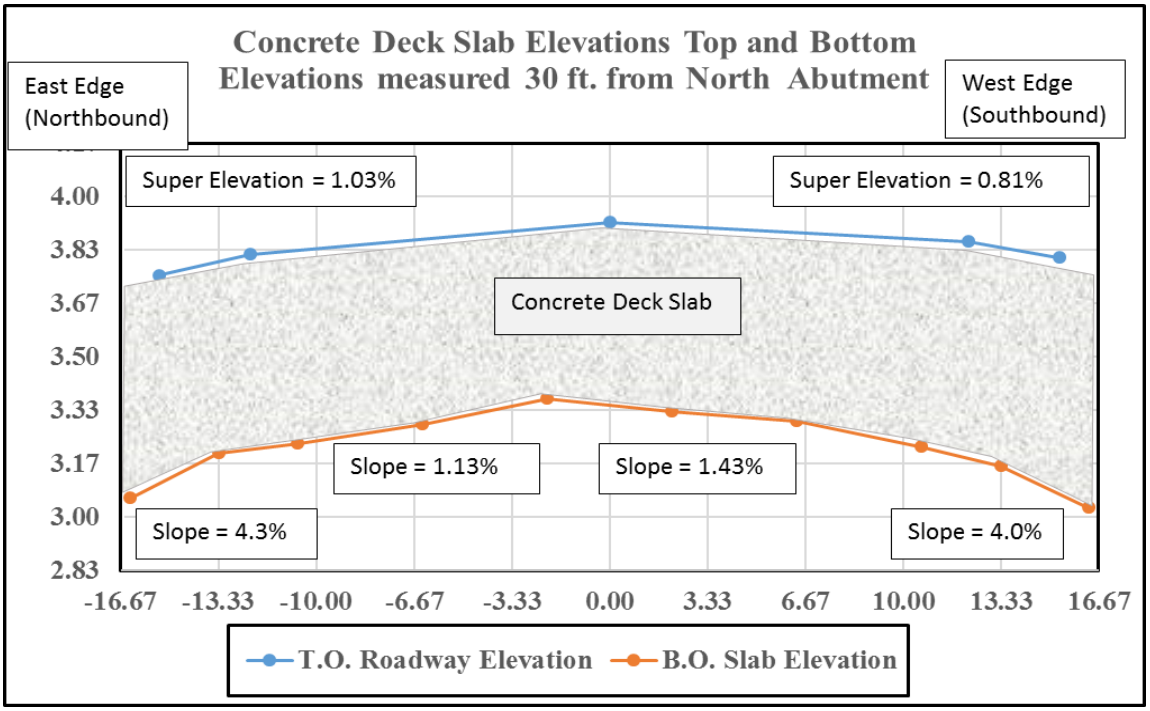

Figure 33. Elevations of the Concrete Deck Slab at Mid-span of the North Span, SH 86 over Stillwater Creek, Payne Co. View looking South.

Fig. 33 also charts the elevations measured at the B.O. of the concrete deck that correspond to values reported in Table 5. at 30 ft – 0 in. from the North Abutment. Those elevations in Table 5. are reported as: 3.06, 3.20, 3.23, 3.29, 3.37, 3.33, 3.30, 3.22, 3.16 and 3.03 feet. The concrete bridge deck resides within the space between the T.O. Deck and the B.O Deck, and the difference between the two sets of elevations provides a direct measure of the bridge deck thickness.

Fig. 33 also shows the slopes on the bottom side of the cast deck slab. Slopes measured from Roadway C.L. to the outside girders are 1.13 percent and 1.43 percent on the Southbound and Northbound sides, respectively. More importantly, Fig. 33 reports larger slopes measured from the outside girder to the outside edge. On the Northbound side the slope is 4.3% and on the Southbound side the slope is 4.0 percent. The slopes at the bottom of the slabs are more severe, or steeper, near the edges of the slab. These regions correspond to portions of the deck slab formwork that cantilevered from the outside girder to the edge of the slab. These intensified slopes indicate unusually large deflections of the bracing and formwork outside of the outside girder. This is significant because the screeds that set elevation controls for the finished elevations of the deck slabs are set directly upon the formwork at the outside edge of the deck slab. The data clearly show that the formwork is inadequately braced, which results in steeper slopes on the bottom of the bridge deck. In turns, these deformations are the direct cause for poor elevation control over the mid-regions of the bridge spans. Not only is poor elevation control the cause for poor ride quality, but it is also the cause for thin bridge decks which will negatively impact service life.

Slab thicknesses on the North Span of the SH 86 Bridge are computed and shown in Table 6. From the tabulation, one can see that bridge deck thickness are significantly less than 8 in. as required by the design, and that some of the thicknesses are less than 7 in. The thinnest measurement for the bridge deck occurs at the C.L. at midspan of the North Span, 0.57 ft, which corresponds to 6-7/8 in. The intent of the Bridge Engineer is that the deck slabs should be 8 in.

thick. The thickness of the slab is required for flexural and shear strength of the deck itself, so clearly the thin decks result in understrength deck slabs. Additionally, the thickness provides cover for reinforcing steel, so thinner decks are likely to adversely affect the durability of these bridges somewhere in the future. Additionally, thin decks reduce the dead load of the bridge superstructure and potentially make the bride more vulnerable to vibration and fatigue from repeated loads. So, the data show that not only are the road way elevations responsible for poor ride quality, the data also show that bridge decks are being cast at significantly thinner depths than required for design.

Table 6. Calculated Slab thicknesses from measured elevation on the North span of the SH 86 Bridge over Stillwater Creek, Payne Co.

Distance from N. Bridge Joint		East Edge (Against Guardrail)	Just Outside N. Bound Lane Marker	CL	Just Outside S. Bound Lane Marker	West Edge (Against Guardrail)
North Span	0	0.72	0.71	0.69	0.71	0.70
	10	0.67	0.65	0.61	0.67	0.70
	20	0.87	0.81	0.61	0.64	0.70
	30	0.65	0.60	0.57	0.67	0.74
	40	0.65	0.63	0.61	0.67	0.74
	50	0.71	0.66	0.66	0.69	0.69
	60	0.73	0.70	0.64	0.71	0.74

Note: Slab Thicknesses in ft.

Altogether the forensic evidence indicates that problems with ride-ability resulted principally from construction related incidences. The evidence strongly suggests that large and localized deflections occurred within formwork that supported the cantilevered portions of the bridge deck slab. Furthermore, these localized deflections also produced larger than expected deflections of the screeds that set elevation controls for the deck slabs, and in turn resulted in finished concrete slabs with elevations at midspan that are lower than the elevations at the piers and abutments. This also caused thin bridge decks as shown in our forensic evidence.

US 281 over Mule Creek, Woods Co.

This bridge features three spans. Each span is approximately 30 ft - 0 in. in length. New concrete bridge decks were cast atop existing steel girders during the rehabilitation of the bridge. The bridge is located approximately 2.5 mi. south of the Oklahoma/Kansas state line, and north of Alva, Oklahoma. Fig. 34 features the photograph of the bridge with a view looking northeast. Summer conditions promote brush and vegetation in this intermittent creek.

Figure 34. A view of the US 281 bridge over Mule Creek in Northern Woods, Co.

Investigation of the concrete deck condition and elevations were performed. Elevations for this bridge were obtained at the top of the concrete deck at centerline, and at the north bound and south bound shoulders. Table 7.and Fig 35 reports the roadway elevations of US 281 Over Mule Creek bridge. The figure illustrates that the centerline elevations vary no more than 1/8 in. for all three spans. Elevations are flat, first of all, but the physical measurement of centerline elevations revealed that the most variation that occurred was 0.01 ft., or 1/8 in. According to a witness account, screed rails for the new concrete decks were set atop the outside steel girders, and that the slab from the rail to the outside edge of the deck was screeded by hand This provides evidence that proper elevation control, through haunch correction and better construction

practices can result in better ride quality in rehabilitated bridges. No diamond grinding has been done to the concrete surface.

Table 7. Roadway Elevations of US 281 Over Mule Creek, Woods Co. OK.

Elevations (ft) T.O. Roadway Deck					
	Dist. from Joint at Abut #1 (ft)	N-Bound Shoulder	Crown	CL	S-Bound Shoulder
S. Approach		3.53	0.18	3.68	3.47
		3.50	0.18	3.67	3.48
		3.51	0.20	3.70	3.49
Span #1	0	3.51	0.19	3.69	3.49
	5	3.47	0.21	3.68	3.47
	10	3.44	0.23	3.68	3.46
	15	3.45	0.23	3.68	3.46
	20	3.48	0.20	3.68	3.48
	25	3.49	0.19	3.69	3.51
	30	3.51	0.18	3.69	3.52
Span #2	30	3.50	0.19	3.69	3.51
	35	3.49	0.20	3.69	3.50
	40	3.49	0.21	3.69	3.47
	45	3.49	0.21	3.69	3.48
	50	3.48	0.21	3.69	3.48
	55	3.48	0.21	3.69	3.49
	60	3.48	0.20	3.68	3.48
Span #3	60	3.49	0.20	3.69	3.49
	65	3.48	0.21	3.70	3.50
	70	3.47	0.21	3.69	3.50
	75	3.47	0.21	3.69	3.50
	80	3.49	0.20	3.69	3.49
	85	3.51	0.19	3.70	3.51
	90	3.55	0.19	3.74	3.54

Note: Instrument Location: S. of Bridge in S. bound lane.

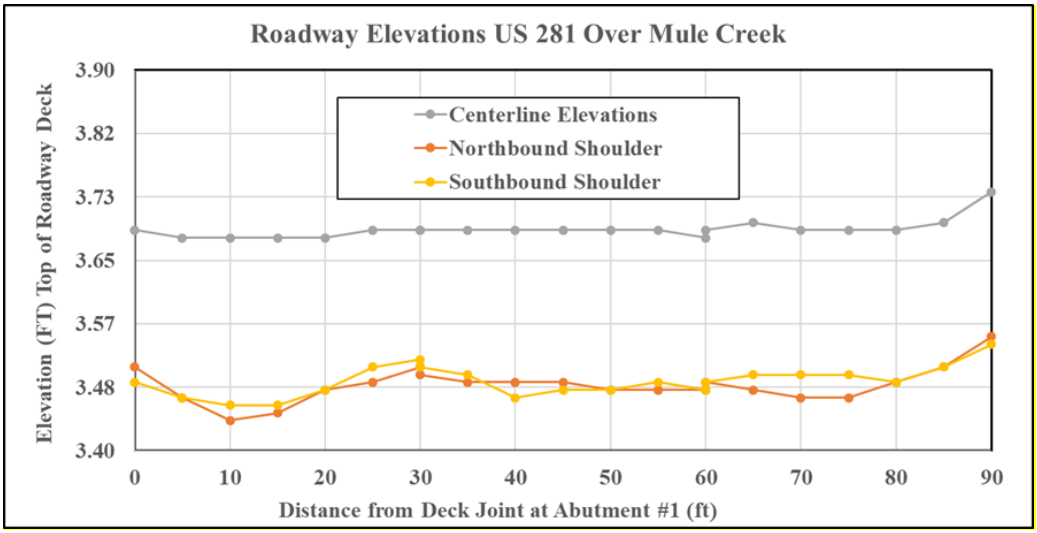

Figure 35. Roadway Elevations of US 281 Over Mule Creek, Woods Co. OK.

Table 8. reports the calculated slab thickness for span #3 of this bridge. It can be noted that the slab thickness is nearly 9 in. throughout span length. Furthermore, this bridge exhibits none of the problems of ride quality or thin construction of bridge decks that are exhibited in the other two bridges.

Table 8. Calculated Slab thicknesses for the US 281 Bridge over Mule Creek.

	Dist. from Joint at Abut #1 (ft)	N-Bound Shoulder	CL	S-Bound Shoulder
Span #3	60	0.73	0.76	0.71
	65	0.72	0.77	0.74
	70	0.72	0.76	0.76
	75	0.73	0.75	0.77
	80	0.76	0.76	0.76
	85	0.78	0.78	0.76
	90	0.82	0.82	0.77

Overhang Bracket System

Bridge decks generally include a cantilevered or overhanging portion that extends from the centerline of the exterior girder to the edge of the bridge deck. The cantilevered sections are normal, as it is logical for the concrete deck to extend beyond the C.L. of the outside girder.

However, in rehabilitation of some bridge decks, the cantilevers are increased beyond original design in order to increase the overall width of the bridge.

The width of the overhang is typically limited to three or perhaps four feet to help balance load distributions between exterior and interior girders. During deck casting, the overhanging portion of the bridge deck is supported using temporary wooden formwork supported by steel brackets that are in turn attached to the exterior girders. Horizontal thrust from the brackets is usually applied against the web of the outside girders. These overhang brackets must be strong and stiff enough to transfer various construction loads to the bridge superstructures. Construction loads include supporting formwork, workers, construction equipment including the screeding machine, the screed rail, and fresh concrete. When large cantilevers are supported by relatively shallow girders, the effects of construction loads are increased by the geometry of the bracing. The proper design of bridge overhang bracket systems is critical to hold the dead weight of the fresh concrete, finishing screed and other construction loads during the time of deck pour.

The C-49 overhang bracket a product of Dayton Superior and one of the most versatile overhang brackets used by DOT bridge contractors (Dayton Superior Bridge Deck Handbook 2017). It is widely use in both prestressed concrete girders and in steel girders composite with concrete deck slabs. The bracket is typically made of light gage steel pipe and channel sections. Steel hangers are placed on top flange of the steel girder and the overhang brackets are held in position via ½" coil rods and steel hook bolts. The bracket typically adjusts from a minimum depth of 30 in to a maximum depth of 50 in. However, the ODOT standard drawings specify that the bottom leg of the braces on the cantilever forming should bear on the girder webs within 6 in. of the bottom flange of the steel girders. The standard drawings also specify that the formwork bracing should continue between the steel girders at intervals of 4 ft. or less where possible through skewed regions at the ends of the deck

Full-sized Prototype Bridge and Testing of Overhang Bracket Systems

A full-sized prototype bridge was built at the Bert Cooper Engineering Laboratory (BCEL). The bridge was constructed to replicate the Eagle Chief Creek Bridge "A" on SH 14 in Woods Co., Oklahoma. The full-sized prototype built with formwork and overhang bracing at the Cooper Lab is shown in Fig. 36

Figure 36. Laboratory Prototype Bridge built with formwork and bracing. View Looking East

The prototype bridge spans 38 ft -10in. from center-to-center (c/c) of bearings with an 8 in. concrete deck supported by W24x94 Gr. 50 steel girders. The prototype bridge is cast with a 14 ft wide deck and supported by two girders at 6 ft spacing and 4 ft cantilevered overhangs. The Woods Co. Bridge has a width of 30ft. and 8 in. measured out-to-out (o/o) and supported by five girder lines with 3 ft- 4 in. cantilevered overhangs. The prototype bridge girders were named North and South girders with respect to their location at the Bert Cooper laboratory. The steel girders were constructed with steel diaphragms at the ends and mid-span locations. Diaphragms matched those provided in the field and consisted of a C12x20.7 with shear tab connections from the channel web to the webs of the W sections. Diaphragms and connections can be seen in Fig. 36.

The temporary formwork for the laboratory prototype bridge was built with 2 x 4 lumber and ¾ in. thick plywood forms, supported with commercially available steel overhang brackets spaced at 4 ft. centers. The steel overhang brackets also match those commonly used by ODOT contractors for on-site construction of similar bridge decks. As with ODOT provided details, the overhang formwork was built to accommodate an additional walkway area on both sides of the girders. The bridge was installed with tension tie rods to connect the two girders at the top and 4 x 4 wooden blocking at the bottom of the webs between the girders in accordance to standard ODOT drawings. Typical standard details prescribed by ODOT for supporting the overhanging formwork are found in Fig. 37.

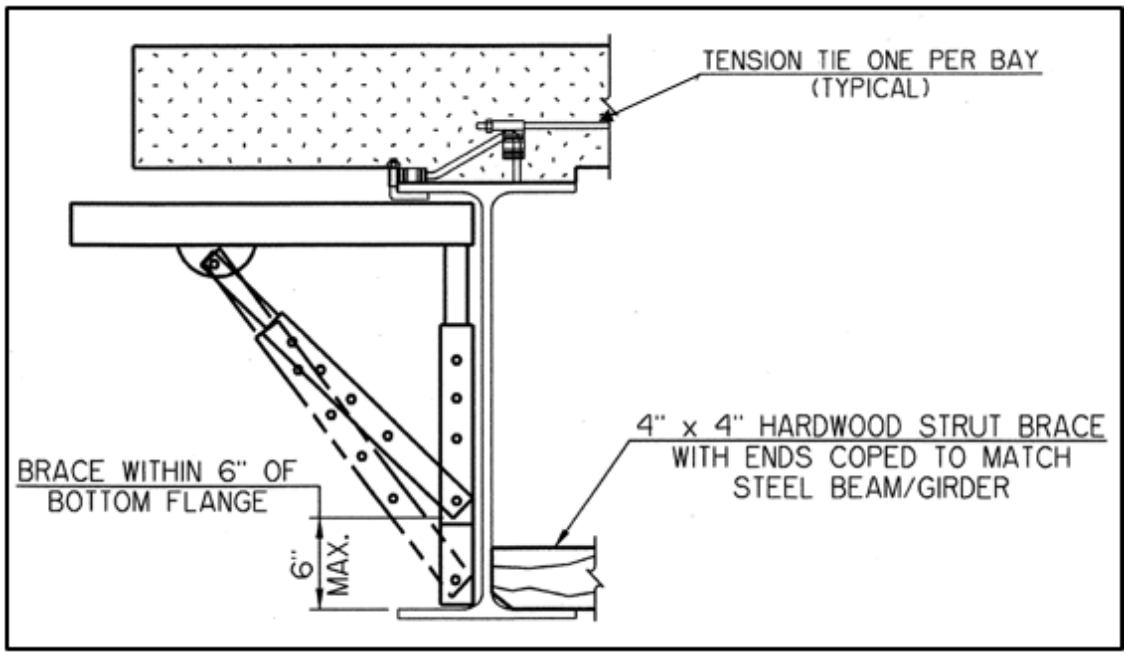

Figure 37. ODOT standard detail drawing for Bridge Deck Overhang Formwork Bracing (Dayton Superior Bridge Deck Handbook 2017)

Load Test on Overhang Bracket System of Prototype Bridge

Prior to the deck cast the overhang formwork was tested for deflections at various locations on the bridge deck overhang and walkway areas. A simple load test was conducted using five 94 lbs

cement bags tallying a total load of 470 lbs. Fig. 38. shows the cement bags load testing performed on mid span bracket located on the South side of Walkway Platform.

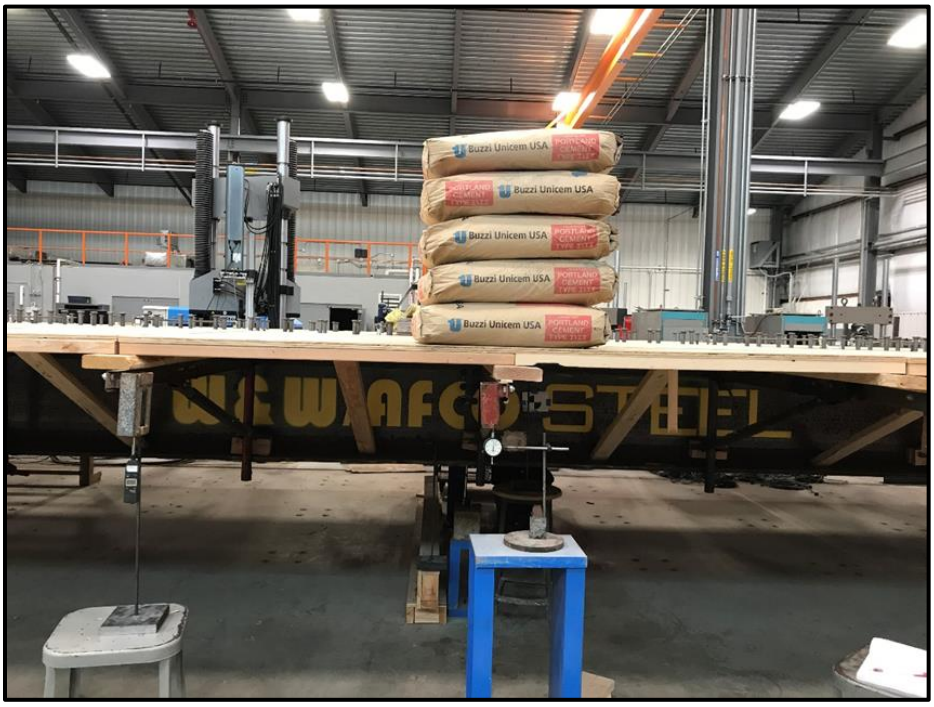

Figure 38. Cement Bag load testing performed on South Girder Walkway Platform

The brackets were loaded on top of the formwork at the bracing locations with increments of one cement bag at the time. Dial gages were installed to monitor the deflections in the overhang formwork and the steel girders. In addition, the lateral deflection of the steel girders due to the overhang loads were also monitored. The test was performed on both the walkway and deck locations for comparative study. For the walkway loading the overhang brackets were loaded at 5 ft. from the centerline of the girder on both sides. Both the North and South areas of the overhang formwork were loaded at mid-span bracket (about 9 ft- 5 in. from the end support), end bracket close to the East and West supports and at one quarter point bracket locations (about 4 ft- 8 in. from end support). The spacing of the overhang brackets was not varied during the time of testing. The continuity between the formwork panels and 2x4 framing was maintained and often extended on either side of formwork panel joints.

Table 9. reports the vertical deflections of the overhang formwork and girders and lateral deflection of the girders for each load positions and various bracket locations along the North and South sides of the formwork. From results it is observed that the deflection of the overhang formwork varies from 0.65 in. to 0.96 in. recorded at the edge of the walkway loading. Note that 1.2 in measured at the West quarter bracket location is an outlier. Further, measured deflections varied significantly depending on the location of the applied loading. It can also be clearly observed that the end brackets deflected the most when loaded close to the East and West end supports of the girders. The tests were repeated with and without the 4 x4 wooden blocking at the bottom of the girders and tension ties that connect the two girders at the top. The results showed no big difference in the deflection of the brackets. In other words, the wooden blocking and the ties made very little if any difference in measured formwork deflections. The steel girders deflected to a maximum of 0.023 in. and continued to rotate and deflect as a result of the deflection of the brackets.

Table 9. Overhang bracing and steel girders deflections without additional wooden bracing

Load Position	Bracket Location	Bracing and Formwork Deflection (inches)	Girder Vertical Deflections recorded at Midspan (inches)		Girder Rotations (radians)
			North	South	
North formwork	East end	0.863	0.002	-0.005	
	East Quarter	0.958	0.011	-0.007	
	Mid span	0.704	0.013	-0.012	0.0017
	West Quarter	0.690	0.014	-0.011	
	West End	1.206	0.003	-0.002	
South formwork	East end	0.764	-0.006	0.001	
	East Quarter	0.685	-0.005	0.014	
	Mid span	0.652	-0.006	0.012	0.0015
	West Quarter	0.721	-0.006	0.011	
	West End	0.750	-0.003	0.001	

Note: Positive values indicate downward deflections and Negative values indicate upward deflections

As reported in Table 9. the steel girders recorded a maximum girder rotation of about 0.0017 radians and 0.0015 radians when loaded at the midspan bracket location of the North and South sides respectively. The results show that the steel girders along with the brackets and the tie beam act as one single system.

Additional wooden bracing was installed in between the existing steel bracing to stiffen up the bracing and formwork. Wooden shims were also provided to gap the holes between the formwork and steel brackets. Deflection tests were repeated by loading the edge of formwork with a single pallet of five cement bags at a time for various load positions. Table 10. reports the vertical deflections of the bracing and the steel girders along with the rotations of the steel girders recorded for each load positions.

Table 10. Overhang bracing and steel girders deflections with additional wooden bracing

Load Position	Bracket Location	Bracing and Formwork Deflection	Girder Vertical Deflections recorded at Midspan (inches)		Girder Rotations (radians)
			North	South	
North formwork	East end	0.149	0.007	-0.003	0.001
	East Quarter	0.111	0.013	-0.004	0.004
	Mid span	0.116	0.016	-0.005	0.001
	West Quarter	0.124	0.013	-0.004	0.003
	West End	0.085	0.007	0.002	0.0004
South formwork	East end	0.090	-0.005	0.005	0.001
	East Quarter	0.129	-0.004	0.016	0.006
	Mid span	0.121	-0.004	0.009	0.001
	West Quarter	0.141	-0.004	0.013	0.005
	West End	0.102	-0.004	0.005	0.001

Note: Positive values indicate downward deflections and Negative values indicate upward deflections

From Table 10., it is observed that the maximum overhang bracket deflections are reduced to about 0.15 inches. This corresponds to about 88% reduction in the deflection of the overhang bracing system when additional support bracing is provided to stiffen the bracing system. The end

bracing is found to deflect more than the others due to the absence of adjacent bracing to share the load. From tabulated results the recorded girder rotations are higher (0.006 radians) at the quarter bracing loading point when compared to the mid-span and the end bracket loading. This is due to the presence of rigid steel diaphragms at the end and mid span locations. Comparing the twisting of the girder at the mid-span location with the diaphragms and the quarter bracing at the end without the diaphragms, the twisting is almost five times more the location with no diaphragms. We can also observe that the twisting due to lateral deflection of the girder due to the loading at the mid and end span bracing is much lesser. This indicates that the presence of the rigid diaphragms prevents the twisting of the girder at the ends and at the midspan.

Overhang and Formwork Deflections on Prototype Bridge during Slab cast

The cantilever portions of the bracing were strengthened by adding wooden bracing to support the construction of the bridge deck on the full-sized prototype bridge beam. The bracing system was further stiffened by adding diagonal wooden struts. In addition, the diagonal struts were shimmed in order to further stiffen the response of the bracing to temporary loads and prevent further deflection of the bracing during deck pour. The prototype bridge was monitored for deflections at various strategic locations during and after deck pour. The concrete deck was cast in July 2017. Concrete placement started at the West support and proceeded to the east and was completed in about two hours.

Steel girder and overhang bracing deflections were measured at the midspan of the bridge during and after the time of deck pour. It was observed that the steel girders deflected downward through slab casting due to temporary construction loading and self-weight of the fresh concrete. The North girder deflected to about 0.38 in. and the South girder to 0.40 in. The estimated deflection of the bridge at mid-span, as computed considering the self-weight of the concrete was 0.405 in. In addition, it was also observed that he North and South cantilevered deck portions deflected to

an additional 0.45 in. beyond that of the steel girders. The results show that the deflections are excessive by any measure, and that the deformations of the formwork are much too large to provide any reasonable assurance that the bracing system will support the formwork, construction equipment and fresh concrete in a manner to prevent excessive deflections of bridge decks. The results provided in this section are consistent with the findings in the forensic investigations; that problems with ride quality are the direct result of improperly supported or inadequately braced formwork.

Assessment of the Overhang brackets for shallow girders with larger overhangs.

A thorough study of the Dayton Superior manufactures guide was done in order to assess the performance of the overhang brackets installed on shallow girders with a larger overhang system. The manual provides guidance to the limitations on the overhang lengths and bracket spacings and load carrying capacity based on varying girder depths and configurations.

Dayton Superior C49 brackets are commonly used for bridge overhang construction. The C49S is a modified version of the C 49 bracket where the vertical adjustment range of the bracket is often adjusted to accommodate for shorter depth girders (D =16 in to 28 in.). The same arrangement was followed for the installation of overhang brackets on the laboratory prototype bridge. Figure 39 shows a typical C49 S bridge overhang bracket arrangement for steel girders taken from the Dayton Superior Bridge Deck Handbook. It can be clearly seen that the manual limits the overall overhang length for these adjusted brackets to a maximum of 3 ft-10 in with a maximum slab overhang length of 2 ft. However, the SH 14 and SH 46 bridges including the laboratory prototype bridge were built with overhang lengths larger than the specified lengths. The overhang lengths of the field bridges and the laboratory bridge built with short depth girders exceed this limit extensively. Moreover, modifying the brackets to accommodate shallow girder

depths reduces their load carrying capacity. This arrangement shows that the brackets simply cannot provide the stability required for this application with their current design.

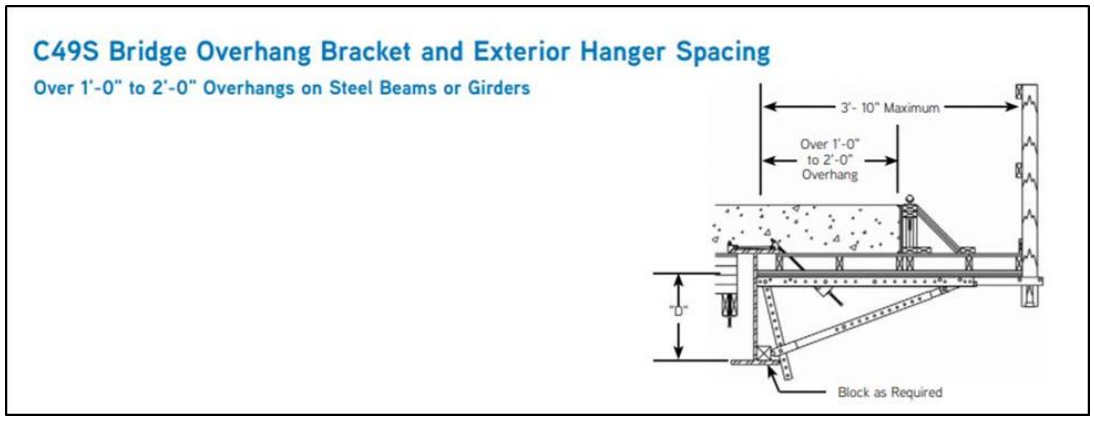

Figure 39. Typical C49S Bridge Overhang Bracket and Exterior Hanger Spacing (Dayton Superior Bridge deck Handbook)

In current practices, although the layout of the overhang brackets is specified in the standard DOT drawings it is often left to the contractor's decision. From the forensic investigations and laboratory testing performed in this research it is obvious that the steel overhang brackets are often re-used for various field works and simply not verified by field engineers if it suits the girder configurations (Yang 2009). Often the limits on the overhang lengths stated for each type of bracket is not strictly followed by contractors. In most cases, brackets that suffered from permanent damage are still being used at job sites.

Fig 40 shows the photographs of C 49 overhang brackets sections with permanent deformations and warped double channel sections that are currently being used in bridge construction. This results in a very flexible bracing systems that can cause excessive deflection locally due to the weight of the fresh concrete and other construction loads imposed on them. This is one of the primary evidences that the formwork was insufficiently braced to firmly establish roadway elevations on the field bridges.

Figure 40. C-49 Overhang brackets with warped and permanently deformed sections

Laboratory Bridge Top of deck Elevation Profile

Figure 41 shows the measured top of deck elevation profile of the Laboratory prototype bridge. The elevations measurements were taken in October 2019, about two years after the deck was placed. Elevations were measured at 6 ft. intervals at the top of the concrete deck at centerline, edge of north overhand and south overhang portions of the bridge deck. The deck surface was finished by hand and no screed rails were used. Note at the time of elevation measurement, two W10x100, 6 ft long beams were placed close to the east end of the bridge deck. From the measured elevations we can see significant variations in elevation profiles along the length of the bridge deck. The mid span region of the bridge deck is fairly flat along the centerline and south overhang of the bridge deck. The top of deck elevations at the west end west start of the same for

all three elevations and as we progress towards the mid span and east end the top of deck elevations significantly dip downward indicating uneven ride surface.

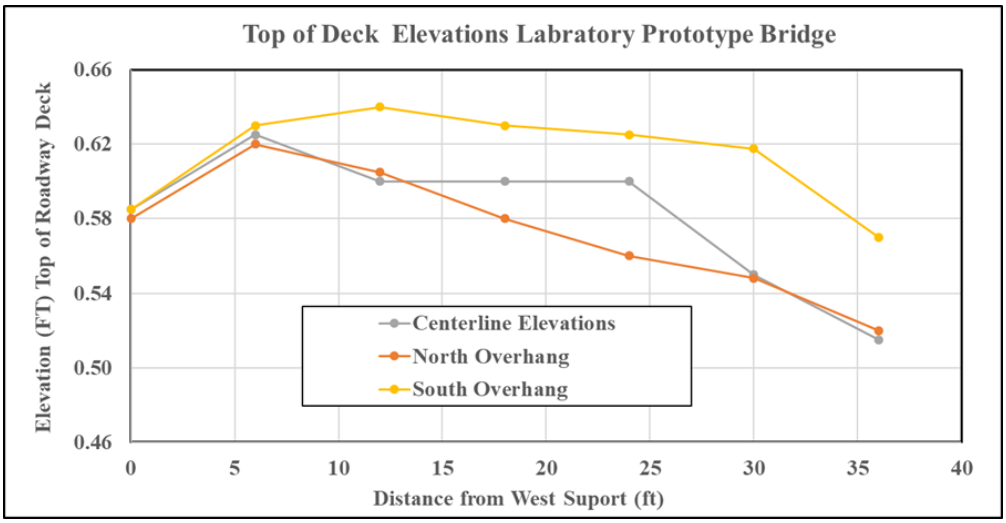

Figure 41. Top of Deck Elevations of Laboratory Prototype Bridge

During the time of deck placement, we noted that both the north and south overhang portion of the bridge deck at mid span locations had deflected to about 0.45 in excesses of the steel girders. From fig 41 we can note that the elevation profiles at the east end of the bridge deck especially along the north edge of the overhang dips to almost 1/16th of an inch in excess to the west and and mid span elevations. This indicates that the west end overhang brackets had further deflected more ½ inches than the steel girders. This provides evidence that the commercially available overhang brackets used for bridge construction are insufficient to provide the necessary elevation controls for the cantilever portions of the bridge deck.

Haunch Detail

The haunch is the area that is typically filled with concrete, between the top of the girders and the deck slab. The haunch generally designed does not extend beyond the flange of the girder. The depth of the haunch may be constant or variable over the length of the bridge. Haunches are generally provided on all types of bridges including steel girders, prestresses concrete beams and

box beams. The purpose of the haunch is to provide a means for final adjustment of the deck slab elevation to match the design roadway elevation profile and slope. It serves to adapt the girder geometry to the profile of the bridge deck.

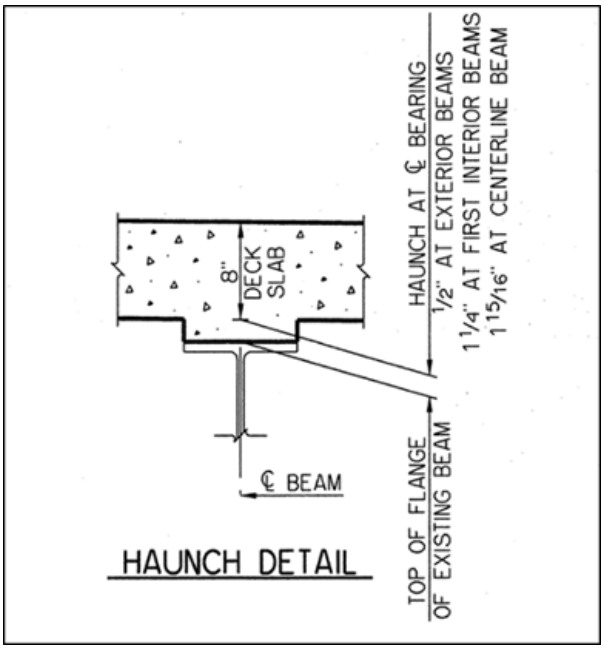

Figure 42. Haunch Detail from ODOT standard Drawings – SH 14 bridge

Figure 42 shows the typical haunch detail of SH 14 bridge as shown on the standard ODOT drawings. Haunches are typically calculated from dead load deflections, that are theoretical beam deflections due to self-weight of the slab, haunch and screed rail loads. Figure 43 shows a typical dead load deflection diagram of the SH 14 bridge as shown in the standard ODOT drawings. These dead load deflections are calculated at every tenth location along the length of the girder and taken into consideration during casting of the deck slab and haunches. The top of haunch elevations is provided along centerline of each girder and are required to maintain the desired road elevation profile. Mis-calculations in haunch thicknesses or poor haunch elevating control during deck slab cast may result in permanent dips in road elevations leading to poor ride quality in bridges.

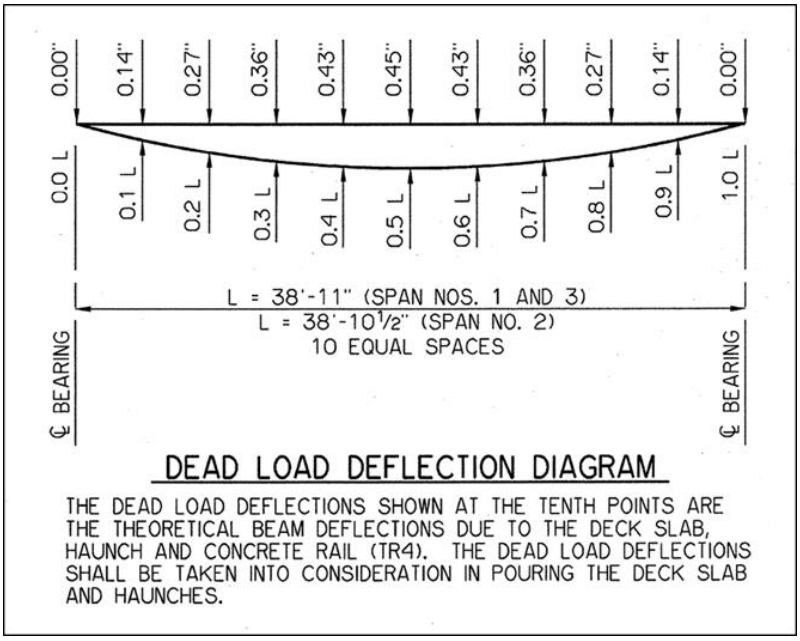

Figure 43. Dead load deflection diagram for Haunch correction – SH 14 Bridge

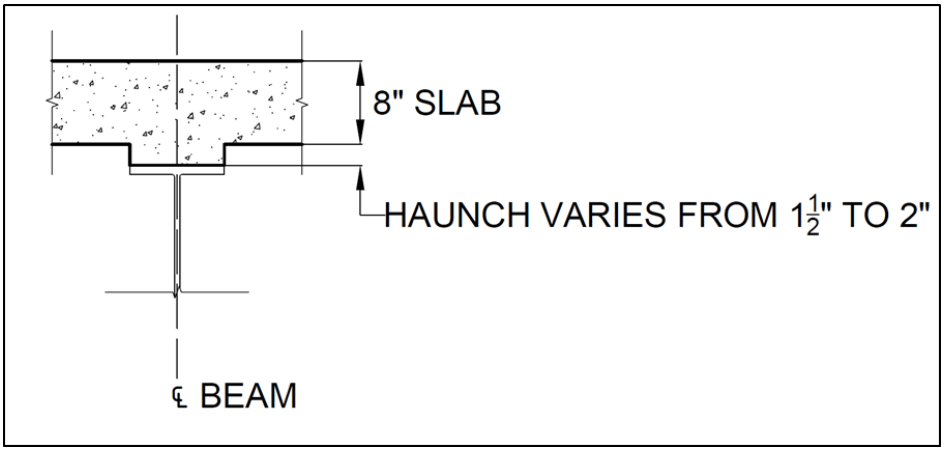

Figure 44 Haunch detail for Laboratory Prototype Bridge

Figure 44 shows the typical haunch detail used on the laboratory prototype bridge. A varying haunch of 1.5 in. at the bearings to 2.0 in. at midspan location of the girder was applied. The haunch was calculated by taking into account the deflection of the girder due to self-weight of the deck slab. The haunch was formed using the wooden formwork and the haunch elevations were

maintained throughout the length of the beam by adjusting the formwork elevations at the corresponding overhang bracket locations. The laboratory prototype girder haunch was included in all dead load calculations by applying a maximum haunch dimension throughout the span of the girder.

Discussion

The results from forensic investigations performed on three field bridges provide strong evidence that unwanted deflections in rehabilitated steel-girder bridges are caused principally by poorly braced or poorly supported formwork. Two of the three bridges had elevation screeds set at the edge of the slabs at the far edges of the cantilevers. One of the three bridges had elevation screeds atop the C.L. of the exterior bridge beam. Measured elevations above and below deck slabs in the SH 86 Bridge show that the out slopes measured on the underside of the deck slabs increased dramatically in the cantilevered portions of the deck slab.

The results from laboratory investigations confirmed the findings of the forensic examinations. Load testing performed on the C-49 brackets clearly indicates that these brackets lack sufficient stiffness to support the overhang lengths of the bridges built with shorter girder depths. Experimental investigation conducted on C-49 brackets (Clifton 2008) at the Phil M.Ferguson Structural Engineering Laboratory at the University of Texas at Austin, also showed that excessive deflection of the overhang bracket support systems lead to differential deformation of the cantilever portion of the bridge decks, thus affecting the ride quality. This provides direct evidence that the bracing and formwork that supported the weight of fresh concrete at the cantilever sections of the overhang, as well as construction activities, was insufficient to resist loading without adverse deflections. As the weight of fresh concrete plus the weight of finishing and screed machines was applied to formwork, the bracing deformed, and the formwork deflected causing permanent downward cast to the concrete surfaces. These loads caused unwanted

deflections of the formwork which resulted in built-in and unwanted variations in ride profile on the bridge deck. Another significant negative side effect of this issue is that the bridge decks were found to be too thin. The bridge deck on SH86 Bridge over Stillwater Creek was less than 7 in. thick and the bridge deck on SH14 in Woods Co. was measured at about 7 ¼ in. However, the issues presented above may be able to be minimized through an innovative precast bridge deck system which removes the need for forming and creates a formless bridge deck (Ley, Browne et al. 2010).

The findings from this research paper indicate that the bracing systems detailed on ODOT's drawings and used by ODOT contractors are wholly insufficient to support the weight of the fresh concrete during slab casting. Moreover, when the weight of the fresh concrete is combined with the live load weights from the screed, other construction equipment, and workers, the deflection of the formwork and bracing can be excessive. An additional consequence is that thin decks were discovered near mid-spans of several structures. These are the most likely causes of adverse ride quality in newly built or rehabilitated bridge. These adverse outcomes are found to be a direct result of errors in both design and construction. Improved construction practices that place responsibility for elevation control on the contractor are highly recommended. ODOT should include performance criteria for the construction contracts that include a pay factor for roadway elevation control.

Summary and Conclusions

Forensic examinations were performed on three bridges. All three bridges were recently rehabilitated with new concrete decks cast atop existing (older) steel girders. As part of the rehabilitation, the new bridge decks are thicker than, and wider than the original designs. As such, dead loads are heavier, and the deck slabs are cantilevered further distances outside of the exterior girder than original designs.

During rehabilitation, concrete deck placement and finished elevations were controlled using a finishing machine. In two of the three bridge decks, the screed rails were supported by the cantilevered formwork, which in turn was supported by bracing supported by the exterior girder. These two bridges were the SH14 Bridge over the Eagle Chief Creek in Woods Co., OK and the SH86 Bridge over Stillwater Creek in Payne Co., OK. The third bridge, US 281 over Mule Creek in Woods Co., OK had the screed rail supported directly atop the exterior girder.

The differences in bridge deck elevation profile, in bridge deck thicknesses and in the cross-section dimensions of the three bridge decks tell a strikingly different stories about the effectiveness of elevation controls for these three bridges.

The following conclusions are drawn from this research

1. Elevation surveys using conventional surveying equipment (i.e., engineering level and leveling rod) are effective in determining bridge deck driving elevations, for determining elevations at the bottom of the bridge decks and for determining bridge deck thickness without destruction testing (Fig. 27).

2. Measured roadway elevations showed measurable and significant “dips” in elevation profiles for two of the three bridges examined. Elevation profiles indicate a pattern where driving surfaces are significantly lower at the mid-spans of recently rehabilitated steel girder bridges. Bridge deck elevations “dipped” about 1.0 in. and as much as 1.75 in. in some bridge profiles. These data are reported, and the conclusions confirmed in Table 1 and Fig. 29 for the S.H. 14, Woods Co. Bridge, and in Table 4 and Fig. 33 for the SH 86, Payne Co. Bridge.

3. Measured roadway elevations confirm that the top surfaces of the bridge decks were screeded and finished in accordance with the 1 percent super-elevation required in construction documents. This is shown in Tables 1,4 and 7 and in Fig. 32.

4. Under-slab elevations reflect the same 1 percent super-elevations measured on the bottom sides of the bridge decks from CL to the exterior girder; however, from the exterior girder outward and including cantilevered formwork, the under-slab elevations indicate a significantly steeper slope on the bottom surfaces of the slab. In the case of the SH 86 bridge, slopes exceeding 4.0 percent were measured on the bottom side of the deck slab. This is shown in Fig. 32 for the SH 86, Stillwater Creek Bridge.

5. Bridge Deck thicknesses reported in Table 3 (SH 14 Woods Co. Bridge) and Table 6 (SH 86 Payne Co. Bridge) are significantly thinner than the 8 in. thickness required by contract documents. On the SH 14 Bridge, deck thickness as little as 7.25 in. was measured by instrument and verified by direct measurements. On the SH 86 Bridge, a slab thickness of 0.57 ft. or 6-7/8 in. was measured at midspan of the northern-most span.

6. In contrast, bridge deck elevations measured on the US 281 Woods Co. Bridge show no elevation dips in the driving surfaces, and thicknesses measured by instrument showed actual concrete deck thicknesses varied from 8-1/8 in. to 8-7/8 in.

7. In the case of SH 14, Eagle Chief Creek Bridge and of SH 86, Stillwater Creek Bridge, the formwork that was cantilevered outside of the exterior girder, and braced against the exterior girder, was not properly supported nor braced during construction activities. This conclusion is supported by the following forensic evidence:

8. Significant “dips” in driving surface elevations measured on both bridge decks,

9. Thin deck sections measured in both bridges.

10. Significantly severe slopes measured on the bottom sides of bridge decks, in areas that were supported by cantilevered formwork, which was in turn supported bracing.

11. For SH86 Bridge, the top side super-elevation from CL to Guardrail was 0.16 ft (2.0 in. on the northbound side, and 0.11 ft (1.375 in. on the southbound side. This compares to the under-slab elevation change from CL to Slab Edge of 0.32 ft. (3.8 in., northbound) and 0.29 ft. (3.5 in., southbound). These elevation differences directly correspond to "dips" in roadway elevations in excess of 1 in. and in thin bridge decks.

12. Laboratory investigations confirm that commercially available bracing used for bridge rehabilitations is insufficient to provide necessary elevation controls for cantilevered portions of the bridge decks.

Recommendations

1. The contract documents should specify that the contractor is responsible for means and methods of supporting bridge decks during construction.

2. The contract documents should specify that the contractor is responsible for maintaining limits on formwork and bracing deflections during construction.

3. The contract documents should specify that the contractor is responsible for roadway elevation profiles and deck slab thicknesses.

4. The Transportation Official's drawings and specifications should remove all references to prescriptive information regarding means and methods for deflection controls.

5. We recommend that the Transportation Official establish a tolerance limit on roadway elevation profiles, and that these elevation profile requirements should be enforced through bonus/penalty contract language.

6. We recommend that the Transportation Official establish tolerance limits and performance criteria for bridge deck thicknesses, and that these bridge deck thickness requirements should be enforced or promoted through bonus/penalty contract language.

7. Bridge overhang lengths should not exceed the limits stated in the overhang bracket manufacture's manual respective to the type and depth of girders used.

8. For shallow girders. the slab overhang length beyond the centerline of the exterior girders should not exceed 2 ft.

9. Field engineers should be assigned to verify that the brackets conform to the girder configurations and any faulty brackets should be replaced.

CHAPTER V

EARLY AGE DEFLECTIONS IN NEWLY REHABILITATE STEEL GIRDER BRIDGES MADE COMPOSITE WITH CONCRETE SLABS

This chapter focuses on deflections and deformations that occur at early ages in newly rehabilitated bridges made from steel girders and composite concrete deck slabs. The research program responds to problems with elevation control and subsequent ride quality problems exhibited in newly constructed or newly rehabilitated steel girder bridges built with composite with concrete decks.

A full-scale prototype bridge was built and instrumented at the Bert Cooper Engineering Laboratory on the campus of Oklahoma State University in Stillwater, OK USA. Early age deflections of the bridge were measured, as were concrete temperatures, concrete strains, steel girder strains and inclinations of the steel girders at ends. Data were analyzed and their relationship to time dependent concrete properties are established. Results indicate that the concrete strains associated with volume change, including both temperature-related strains and shrinkage strains, are large enough to be considered as one possible cause for adverse ride quality and unwanted deformations in steel girder bridge. The purpose of the research program is to identify causes for undesirable elevation profiles, and to recommend design and construction practices to help mitigate problems created for the highway users and extend the life-span of bridges.

Introduction

Concrete bridge decks are typically cast upon steel or precast concrete girders. Freshly placed concrete, upon taking initial set, begins to change volume. Volume changes are caused by temperature variations during curing, drying shrinkage of the hardening concrete, and other time-dependent effects. In the short term, bridges built composite with concrete decks generally undergo downward deflections caused by the self-weight of the concrete (before setting), upward deflections caused by heating of the hydrating concrete deck immediately after initial set, which, in turn is followed by downward deflections due to cooling of the hardened concrete plus the effects of initial shrinkage.

A full-scale prototype bridge was built and instrumented at the Bert Cooper Engineering Laboratory on the campus of Oklahoma State University in Stillwater, OK USA. The bridge was constructed to replicate the Eagle Chief Creek Bridge "A" on SH 14 in Woods Co., Oklahoma. A full-scale model of the bridge allows to capture the absolute values of the original time dependent properties of concrete deck that cannot be completely captured using a small-scale model. In this research, instruments were installed to monitor bridge deformations during and immediately following the casting of the composite concrete deck slab. Overall bridge deflections were measured with Linear Voltage Displacement Transducers (LVDT's) at midspan and at other points along the length of the steel girders. Concrete temperatures were monitored using thermocouples. Concrete strains were measured with vibrating wire strain gages (VWSG's) embedded in the concrete deck. Bridge girder inclinations were measured near the supports. Measurements and monitoring are continued through early ages and test results are reported. The increase in concrete temperature during early ages due to heat of hydration of cement had a significant effect on concrete strains and caused the beam to deflect upward. Concrete shrinkage and measured deflections of the full-size prototype beam indicated that the shrinkage of the concrete contributed to permanent downward deflections in composite bridge girders.

This chapter highlights how the early age deflections of the bridge, concrete temperatures, concrete strains, steel girder strains and inclinations of the steel girders at ends were measured. The chapter shows how the collected data were analyzed and correlated to the time dependent concrete properties. This chapter also shows that simple analytical computational models can be developed to predict the thermal and shrinkage indices strains, stresses and deformations due to volume changes in the slab at early ages.

The following are the primary objectives for this chapter

1. To determine the factors that influence the early age deformations in steel girder bridges built composite with concrete slabs.

2. To build a full-sized bridge with composite concrete deck that will experience the similar early age mechanisms in the concrete decks of the bridges built in field.

3. Improve understanding on early age volume changes in concrete due to thermal and shrinkage and its effects on bridge deformations.

Background

The U.S. Federal Highway Administration (FHWA) lists 614,387 bridges within the US National Bridge Inventory (NBI). These are bridges that are positioned on highways identified as the National Highway System (NHS) and consist of Interstate Highways and other major U.S. Highways. Of those bridges, almost 40 percent are 50 years or older. Moreover, in 2016 about 9.1% (56,007) of the NBI were rated structurally deficient (ASCE 2017). As the average age of America's bridges keeps increasing, many of the nation's bridge are approaching the end of their design life. Therefore, an increasing number of nation's bridges require major rehabilitation to extend the lifespan of these bridges.

Within the State of Oklahoma, the Oklahoma Department of Transportation (ODOT) maintains 3,727 span bridges (Russell August 2017). Of those, 1617 bridges are made with steel girder superstructures with an average construction year of 1963. In 2010, about 706 bridges in the state of Oklahoma were classified as structurally deficient (ODOT 2017). Many of these bridges were originally built with structural steel girders supporting concrete decks. In recent years, the ODOT has been actively rehabilitating these bridges by casting new concrete decks on top of existing steel girders. This method of rehabilitation is chosen as a cost-effective means of repairing bridges that are structurally deficient, functionally obsolete, or both. In the process, the life span of a single bridge can be lengthened dramatically while helping to ensure the safety of the traveling public.

During the rehabilitation process, new bridge decks are often made both wider and thicker. In many of these bridges, concrete slab depths increased from the original construction of 6 to 8 in., and the roadways were widened to allow modern lane widths with shoulders. Often, the structural designs of these bridges "worked" as shear studs are added to ensure composite behavior and increase shear capacity to account for heavier design loads in more recently adopted rating and design codes. In addition, the increased deck thickness increased live load capacities, which offset the increasing dead loads.

As the State undertook an aggressive policy of rehabilitating these steel girder bridges, many newly reconstructed steel girder bridges have exhibited poor ride quality and generally displayed "dips" in roadway elevations. These "dips" generally occur nearer the mid-spans of the bridges, or at least in locations that are not near the supports provided by bridge piers. In some bridges, roadway elevations dipped more than 1 in. at midspan compared to elevations at the pier supports, and in some cases, within spans less than 60 ft in length.

In 2012, as an early part of the research program, forensic investigations (Bruce W. Russell October 2014) were performed on three recently rehabilitated bridges. Two of these bridges were identified with poor ride quality. The forensic investigation found that ride quality problems resulted directly from inadequate bracing and poorly supported formwork that supported outside edges (or cantilevered sections) of the bridge deck. In those bridges, the screed rails used to establish roadway elevations were supported formwork that was supported by cantilevered bracing extending outside the steel girder centerlines by as much as 4 ft. In the third bridge where ride quality was rated as "good," screed rails set to establish roadway elevations were supported directly on top of existing steel girders, and cantilevered portions were finished by hand. Recommendations to remediate this problem through construction and project quality controls have been made to the ODOT and reported separately (Bruce W. Russell October 2014).

In addition, the research undertook the goal of measuring and assessing the volume changes within a newly constructed concrete deck to determine whether time dependent temperatures changes, shrinkage and other volume changes could affect the ride quality of rehabilitated bridges. The primary purpose of this paper is to report experimental findings from a full-sized prototype steel girder bridge with newly constructed concrete deck slabs to determine the mechanisms that affect elevation controls on steel girder bridges. Results of the forensic investigation and subsequent experimental investigations are reported in chapter 4 (Bruce W. Russell October 2014).

Experimental Program

A full-sized prototype bridge was built at the Bert Cooper Engineering Laboratory (BCEL). The bridge was constructed to replicate the Eagle Chief Creek Bridge "A" on SH 14 in Woods Co., Oklahoma. The Woods Co. bridge is shown in Fig. 45, and the full-sized prototype at the Cooper Lab is shown in Fig. 46. Both bridges span 38 ft -10in. from center-to-center (c/c) of bearings

with 8 in. concrete decks supported by W24x94 Gr. 50 steel girders. The Woods Co. Bridge is 30ft. and 8 in. wide measured out-to-out (o/o) and supported by five girder lines with 3 ft- 4 in. cantilevered overhangs. The prototype bridge at the Cooper Lab has a deck 14 ft- 0 in. wide supported by two girders with 4 ft cantilevered overhangs.

Figure 45. Eagle Chief Creek Bridge "A" on SH 14, Woods Co., OK. View looking North.

Figure 46. Full-sized prototype at the Bert Cooper Engineering Laboratory at Oklahoma State University.

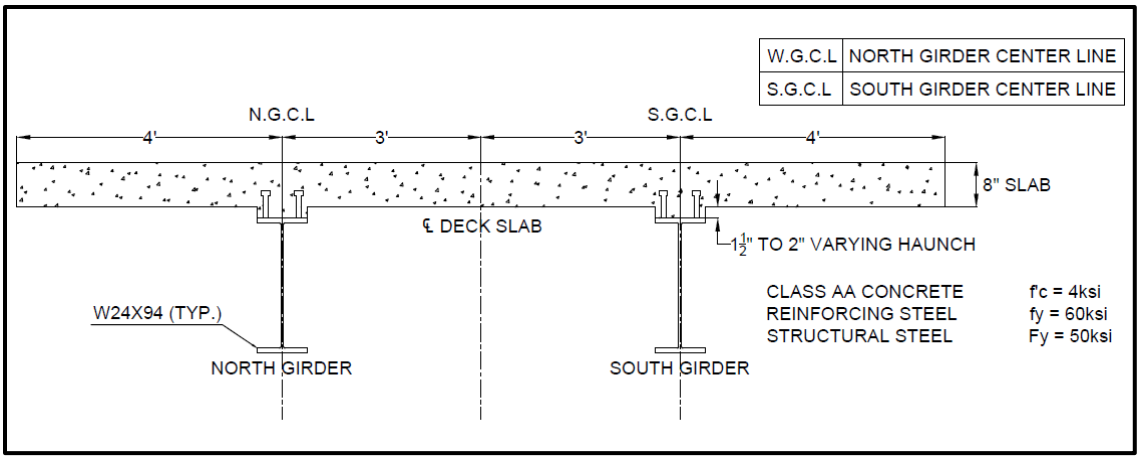

Figure 47. Cross section of composite bridge section from the full-sized prototype.

Figure 47 shows the cross section dimensions for the prototype bridge section. Composite action and shear transfer were affected by pairs of shear studs 7/8 in. diameter x 5 in. long welded to the top flanges at 6 in. The steel girders were spaced at 6 ft. apart and constructed with steel diaphragms at the ends and mid-span locations. Diaphragms matched those provided in the field and consisted of a C12x20.7 tab connections from the channel web to the webs of the W sections. Diaphragms and connections can be seen in Fig. 46. The bridge deck was built with a varying haunch of 1.50 in. at the supports to 2 in. at the midspan. The haunch varies to account for the deflections of the girder during deck casting. The temporary formwork for the laboratory prototype bridge was built with lumber and supported with commercially available steel overhang brackets spaced at 4 ft centers. The steel overhang brackets also match those commonly used by ODOT contractors for on-site construction of similar bridge decks.

Concrete Materials

The concrete mix design conformed to the Class AA specifications contained in the Construction Specifications of the Oklahoma Department of Transportation (ODOT). ODOT concrete mix design proportions are shown in Table 11 Cement conforming to ASTM C150, Type I/II was used for the concrete. Locally available aggregates were used. The coarse aggregate is a crushed

limestone from a quarry near Drumright, Oklahoma that conforms to ASTM C33, #57 gradation. The fine aggregate also conforms to ASTM C33 and is known locally as "Guthrie sand" used in commercial concrete.

Table 11. Class AA ODOT Mix Proportions

Ingredient	**PCY**	**Volume (ft^3)**
Cement	451	2.29
Flyash	113	0.68
Coarse Aggregate	1845	10.56
Fine Aggregate	1362	8.30
Water	238	3.81
WRA (lq. oz.)	22.6	-
HRWRA (lq. oz.)	15.8	-
AEA (lq. oz.)	6.5	-
Air	5%	1.35
TOTAL	**4009**	**27.00**
	Yield (PCF) =	**148.4**

Notes:
Source of Coarse Aggregate is Quapaw # 57 from Drumright, Oklahoma with a Maximum Agggregate Size of ¾ in.
Source of Fine Aggregate is Gutherie, Natural Sand with a Finess Modulus of 1.60

The concrete was batched locally and delivered to the Cooper Lab for placement. The concrete mix targeted 5% air content and was achieved using an air entrainment agent. To ensure workability and ease of placement and finishing, a concrete slump of 7 to 8 in. was specified and achieved using both normal range and high range water reducing agents. The minimum 28-day specified compressive strength (*f'c*) for the ODOT Class AA concrete is 4000psi.

It is noted that the ODOT AA specification for concrete provides a range of proportions for mixture constituents. In our mixture design, 20% of the required cement content was replaced with fly ash. It would be reasonable to expect that ODOT AA concrete mixtures with different mixture proportions and constituents would exhibit different time dependent properties and differing hardened properties.

A total of 14.0 CY was required to cast the prototype bridge deck at the Cooper Lab. Each of two ready-mix trucks delivered 7.0 CY to the Cooper Lab. Fresh concrete properties are reported in Table 12. It is noted that the bridge deck was cast on July 13, and the outdoor air temperature that day was 92 ºF. Ambient temperature inside the Cooper Lab, however, is maintained at 73 ºF. Water was added to the 2nd track at the Cooper Lab in order to attain the 8.25 in. slump that is reported. Additionally, we note that ice was used in place of mixing water at the batch plant; even so, the concrete temperatures exceeded 90 ºF. Hardened Concrete Properties are reported in Table 13.

Table 12. Fresh Concrete properties

Measured Properties	**Truck 1**	**Truck 2**
Slump (inches)	9.5	8.25
Unit Weight (lb/ft^3)	144.2	141.8
Concrete Temperature (º F)	91.5	91.3
Air Content (%)	8	9

Notes:
The fresh cooncrete properties were measured in accordance to following ASTM.
Slump measured in accordance to ASTM C143
Air Content and Unit Weight measured in accordance to ASTM C138

Table 13. Hardened Concrete properties

Age (Days)	**Compressive Strength (psi)**		**Elastic Modulus (ksi)**		**Splitting Tensile Strength (psi)**	
	Truck 1	**Truck 2**	**Truck 1**	**Truck 2**	**Truck 1**	**Truck 2**
1	1485	2095	2404	2620	217	339
3	3440	3870	3059	3355	411	447
7	4195	4465	3378	3774	512	588
28	5245	5605	3843	4027	541	602

Notes:
The hardended concrete properties were measured in accordance to following ASTMs.
ASTM C39 for Concrete Compressive Strength, ASTM C469 for Elastic Modulus and ASTM C496 for Splitting Tensile Strength.

Bridge Instrumentation

Altogether 100 electronic gages and sensors were employed to measure and monitor concrete and steel strains, concrete and steel temperatures, overall bridge deflections at several locations, and inclination of the steel girders. Instrumentation was installed prior to casting the concrete deck. The instrumentation included the following:

1) Thermocouples to measure the temperature within the concrete and ambient temperatures near the bridge deck;
2) Vibrating wire strain gauges (VWSG) embedded within the concrete deck prior to casting to measure the concrete strains and concrete temperatures within the hardening deck;
3) Electrical resistance bonded foil strain gages (ERSGs) to measured strains in the steel girders;
4) ERSGs to measure strains on the surfaces of hardened concrete;
5) Linear Variable Differential Transducers (LVDTs) to measured deflections of the bridge girders at various locations; and,
6) Inclinometers to measure angle of inclination at the ends of girders.

All the sensors were wired into a datalogger through various multiplexers required for each type of sensor. The sensors were programmed to record data continuously through the period of deck casting. The datalogger was programmed to collect data at 5-minute time intervals for the first 28 days after bridge deck cast. Figure 48 shows the sensors locations along the mid-span cross section of the prototype bridge. LVDT sensors were installed at various strategic locations to measure the deflections in the steel girders and bridge overhang. LVDTs' 2 & 3 installed along the girder Center Lines, recorded the deflections of the North and South Girders respectively. LVDTs'1 and 4 recorded the deflections at the edge overhang portions of the deck slab.

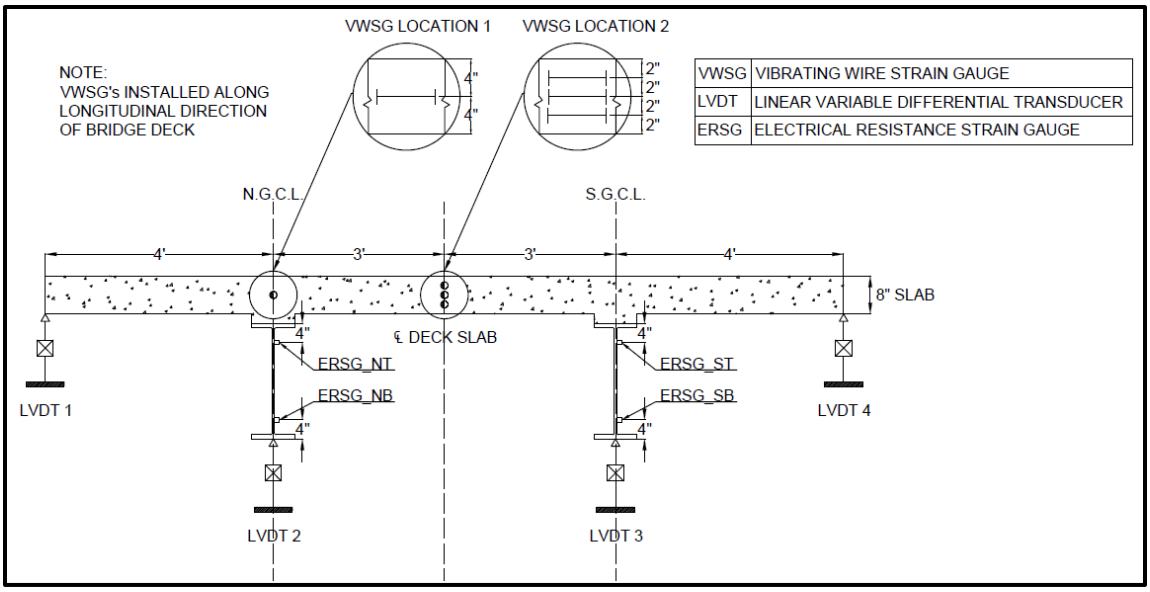

Figure 48. Prototype Bridge Cross Section at Mid-span (View Looking East) showing location of sensors.

Figure 49 shows a photograph of the LVDT 3 installed at mid-span on the underside of the South steel girder and LVDT 4 at mid-span at the south edge of the slab overhang. Geokon 4200 vibrating wire sensors were embedded within the concrete to capture the strains within the concrete deck. As shown in Figure 50a, a single vibrating wire sensor was installed at the mid-height of the concrete slab located along the North Girder's centerline. Figure 50b shows three vibrating wire strain gages that were installed vertically at 2 in. c/c spacing along the centerline of the deck, to capture the strain gradient throughout the depth of the concrete slab. The vibrating wire sensors were placed in the longitudinal direction of the bridge deck and fixed in position by tying two short pieces of rebar to the main reinforcing steel using nylon tie-wraps. Thermocouples were also installed close to the vibrating wire sensor locations to measure the concrete temperatures.

Figure 49. Installation of LVDT sensors at the midspan location of South Girder (LVDT 3) and South edge of slab overhang (LVDT 4)

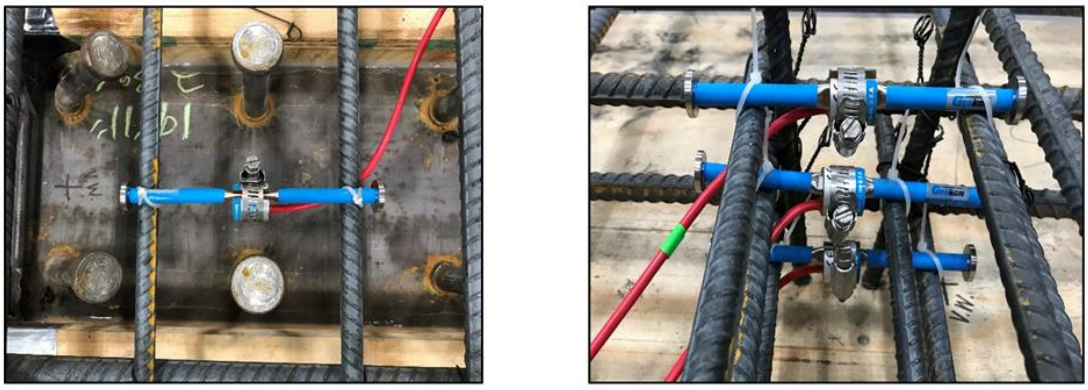

a) VWSG Location 1 Aligned with NGCL

b) VWSG Location 2 at CL of Deck Slab

Figure 50 Installation of Vibrating Wire Strain gages in concrete deck at mid-span

Electrical resistance bonded foil strain gages were attached to the top and bottom of the webs of the North and South girders to capture the steel girder strains. As shown in Fig.51 NT & NB, and ST & SB represents the Electrical Resistance Strain Gages (ERSG) bonded to the top and bottom webs of the North and South girders respectively. The gages were about 16 in. apart and bonded at 4.0 in from the top and bottom of the flanges of the steel girder.

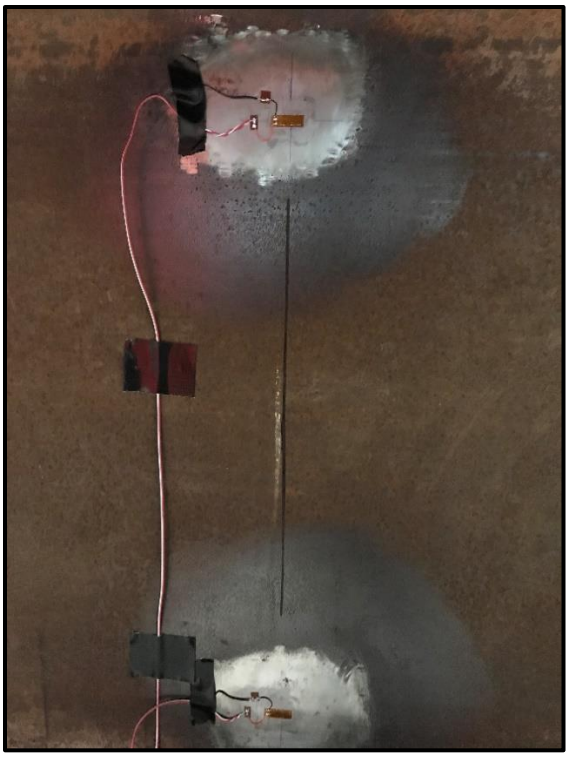

Figure 51. Location of Bonded Foil Electrical resistance strain gages on steel girder (NT/ST and NB/SB)

The structural health-monitoring program implemented in this research combines sensors from diverse technologies into a seamless system using a single database and user interface system. The instrumentation system was programmed to monitor both early age and long-term performance of the prototype bridge. The structural health monitoring of a field bridge was implemented through the experience from the laboratory prototype bridge.

Slab Casting

The concrete deck was cast on July 13, 2017 beginning at 10:55 a.m. The concrete placement was completed in 2.0 hrs. and broom finish was completed at 4.0 hrs. Concrete placement started at the West support and proceeded to the east. Concrete was placed via a ¾ CY bucket supported by the overhead crane at the Cooper Lab. There was no delay in using two trucks for the pour.

Figure 52. shows the concrete deck immediately after casting and prior to finishing. A broom finish was applied to the deck.

Figure 52. Bridge deck after casting and finishing concrete. A broom finish was applied.

Concrete sampling was performed from materials obtained from both trucks. Sampling occurred at times near the beginning of each truck and near the middle of each truck. Table 12 reports the fresh concrete properties measured from the two trucks during the time of pour. A total of 118, 4 in.x8 in. concrete cylinder specimens were prepared in accordance to ASTM C192. The cylinder specimens were demolded after 24 hrs. and cured in accordance with ASTM C 157. Hardened concrete properties were measured from cylinders specimens prepared from concrete materials taken from the two trucks. A total of six 12 in. x 4 in. x 4 in. shrinkage prisms were also prepared during the deck cast using the same concrete that was used in the prototype bridge deck. The prisms were cured in accordance with ASTM C 157. Target points for the Detachable Mechanical Strain Gage (DEMEC) were attached on to the shrinkage prisms after 24 hrs. of curing to measure the unrestrained shrinkage strains.

The ODOT specifies a curing regimen that requires wet curing for 10 days. Figure 53 shows that wet burlap was placed directly on the surface of the concrete. The burlap was subsequently covered with plastic sheeting. Curing was applied at 4.0 hrs. after the beginning of casting. Prior to the application of burlap, the concrete deck surfaces were inspected. No early age cracking was reported. The deck was wet cured for 14 days after casting, and during that time the deck was covered by wet burlap on the top and by formwork on the bottom. Formwork on the underneath of the deck and on the sides of the deck remained in place during curing. Removal of formwork and bracing began after 11 days, but the wet burlap and plastic sheeting remained in place for 14 days. After removal curing materials, the concrete deck was inspected for cracking. No cracks were found.

Figure 53. Wet burlap and 2 mil plastic was applied for 14 days

Results and Discussion

Thermal Effects at Early Age from Concrete Hydration

In its initial stages, the chemistry of Portland cement generally provides a “dormant” period that allows for transportation and placement of the concrete in its fresh state. As the cement hydration continues, initial set of concrete is generally characterized by the onset of rapidly increasing

temperatures. After initial set, increasing temperatures cause volume expansion in the concrete at early ages. However, thermal expansion of the concrete is restrained by the composite steel girders, and thus the increasing hydration temperature induces internal compression stresses within the restrained concrete. Similarly, the newly composite steel-concrete bridge deflects upward as concrete temperatures increase with cement hydration. Our experimental program measured concrete temperatures, concrete strains and overall bridge deformations.

Although considerable amount of attention has been given to cracking of concrete decks due to restrained shrinkage, some researchers (Subramaniam, Kunin et al. 2010) found a significant correlation between early age thermal loading and bridge deck cracking. A large temperature gradient is induced between the concrete deck and the steel girder due to early age thermal loading. The heat of hydration induced in the concrete slab during the early ages of thermal loading causes the bridge deck to deflect upwards and then deflect downwards at the end of hydration period (Alexander 2003). Concrete deck temperatures increase due to hydration of cement. Concrete thermal strains increase with raise in concrete temperatures and decreases over time during the cooling cycle (Bao, Hoehler et al. 2017).

Measured Concrete Temperatures and Strains at Early Ages

Figure 54 shows the concrete temperature and concrete strains measured over time beginning at two hours before slab cast and for the continuing through the first 24 hrs. from slab casting. The concrete temperature and strains were measured by the vibrating wire sensors embedded in the concrete at the mid-height of the slab at the mid-span location along the North Girder (VWSG Location 1). The figure shows that the concrete temperatures elevated to about 114º F reaching peak temperatures at approximately 14 hrs. The measured thermal strains within the concrete correspond well with the concrete temperatures. The measured concrete strains increased with temperature rise and decreased with the fall in concrete temperatures.

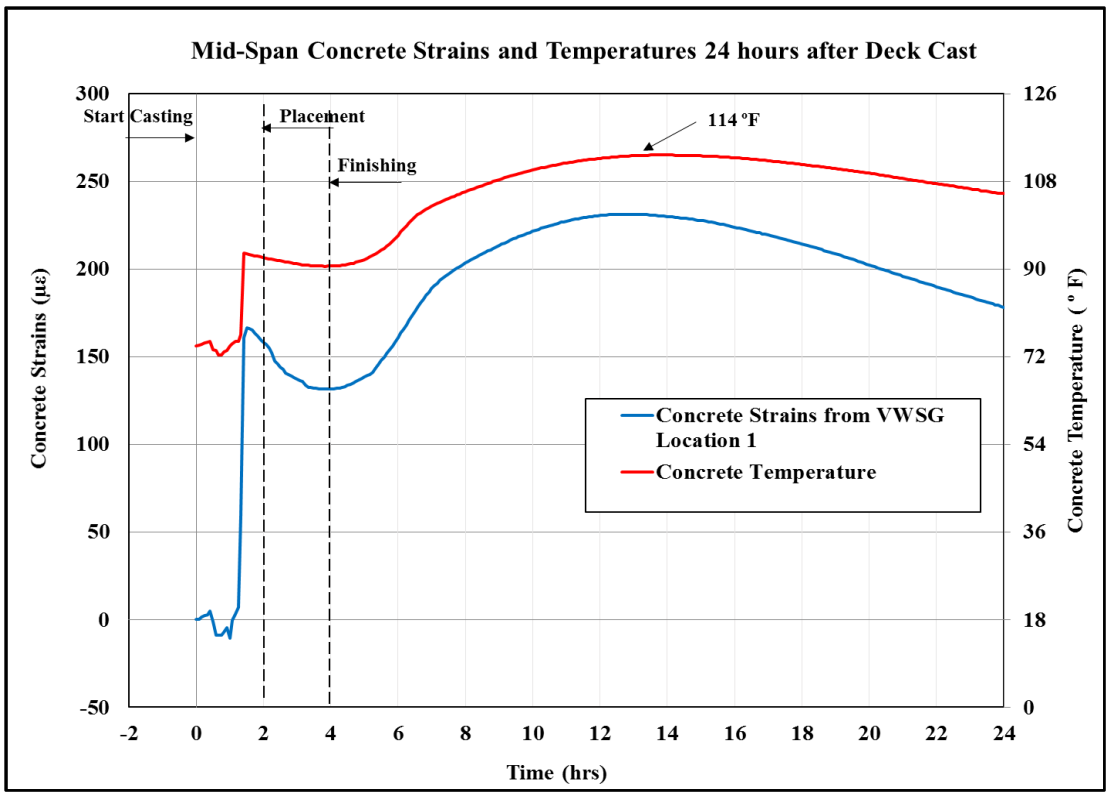

Figure 54. Concrete Temperatures and strains measured at mid-height of deck slab recorded until 24 hours after deck cast

Figure 55 captures the full heating and cooling cycle during concrete hydration along with measured concrete temperatures and strains for the first 96 hrs. after slab cast. The figure highlights that the measured thermal strains within concrete increase with the increase in temperatures and decrease with fall in concrete temperatures. During the process of cement hydration, initial setting of concrete is often defined as occurring with the peak temperature. After initial set, the concrete gains stiffness during the cooling cycle. At the end of the heating cycle, concrete will begin to cool and shrink which is indicated by the decrease in thermal strains and increase in compressive concrete shrinkage strains. This shrinkage can be caused by either or both thermal strains and shrinkage strains. As the steel girders restrain the shrinkage of concrete, tensile stresses within the concrete will begin to develop immediately at the end of the temperature rise. However, no cracking on the surface of concrete deck was reported during this time. Hence it is seems evident that the tensile stresses caused by the restrained shrinkage are not

sufficient to cause bridge deck cracking on the prototype full-sized bridge, at least using these constituent materials subject to these atmospheric conditions.

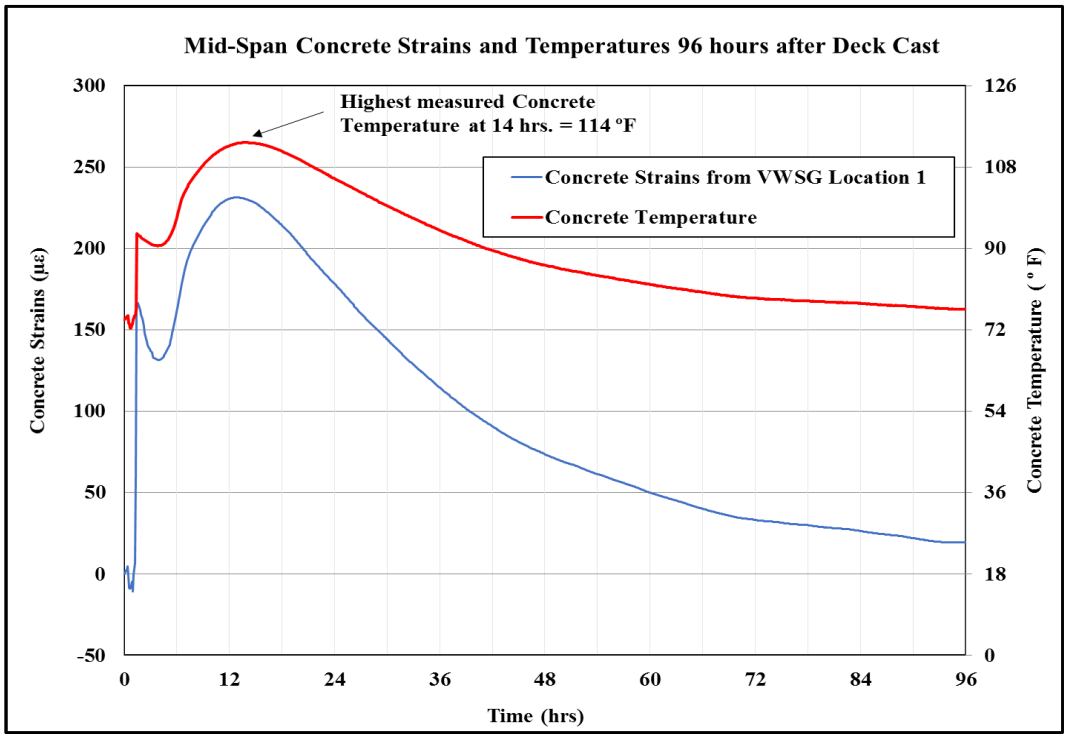

Figure 55. Concrete Temperatures and strains measured at mid-height of deck slab recorded for 96 hours after deck cast.

Early Age Deflections and Concrete Temperatures

Figure 56 shows the bridge deflections and recorded concrete temperatures over time beginning at 2 hrs. before slab casting through the first 24 hrs. after slab cast. Time at 0.0 hrs. corresponds to the start of deck cast. The slab casting was completed in under 2.0 hrs. and the slab was finished in less than 4.0 hrs. Deflections were measured using LVDTs at the mid-span of the bridge; the locations of the LVDT's are shown in Fig. 48.

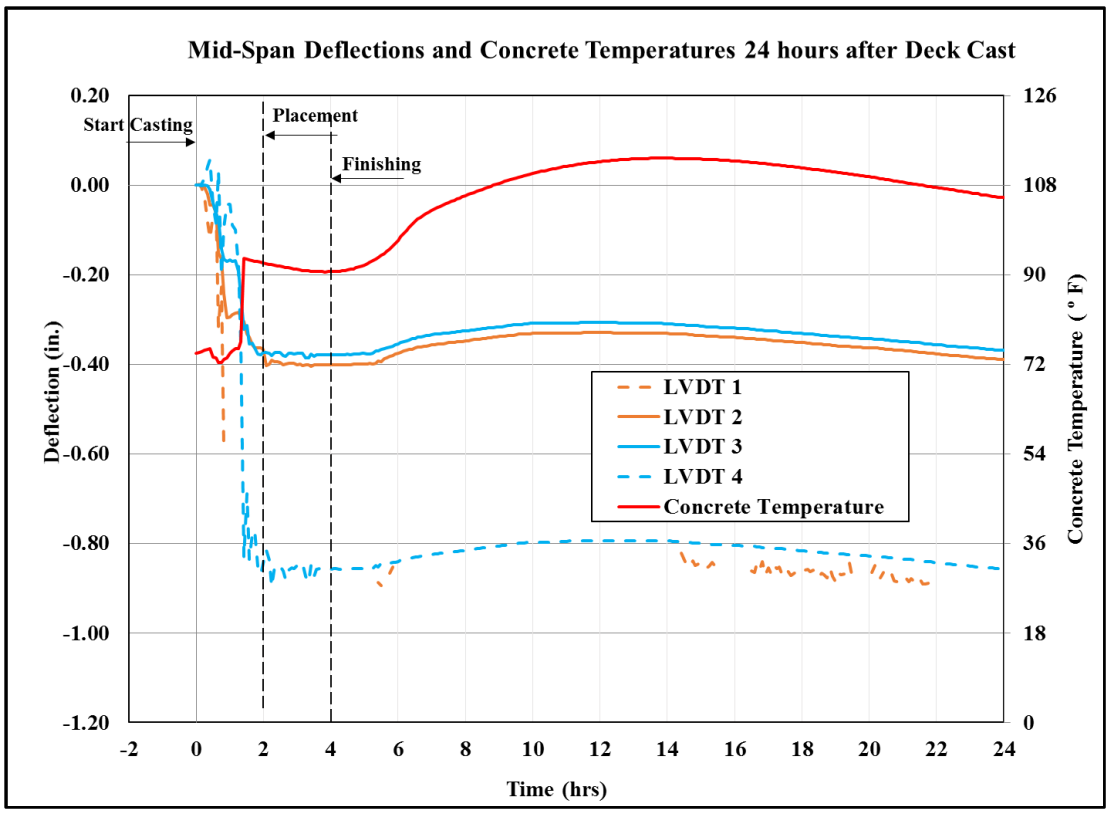

Figure 56. Mid-span deflections of steel girders and overhang deck corresponding to concrete temperatures 24 hours after deck cast

From Fig.56 it is observed that the steel girders deflected downward through slab casting. The North girder deflected to about 0.38 in. and the South Girder to 0.40 in. The estimated deflection of the bridge at mid-span, as computed considering the self-weight of the concrete was 0.405 in. The data also show that the North and South cantilevered deck portions deflected an additional 0.45 in. beyond that of the steel girders. In the field and during actual bridge construction, the deformation of the braced formwork, at the likely location of a screed rail for setting concrete elevations directly results in irregular roadway elevations (“dips” in the bridge) and thinner than expected bridge decks (Bruce W. Russell October 2014).

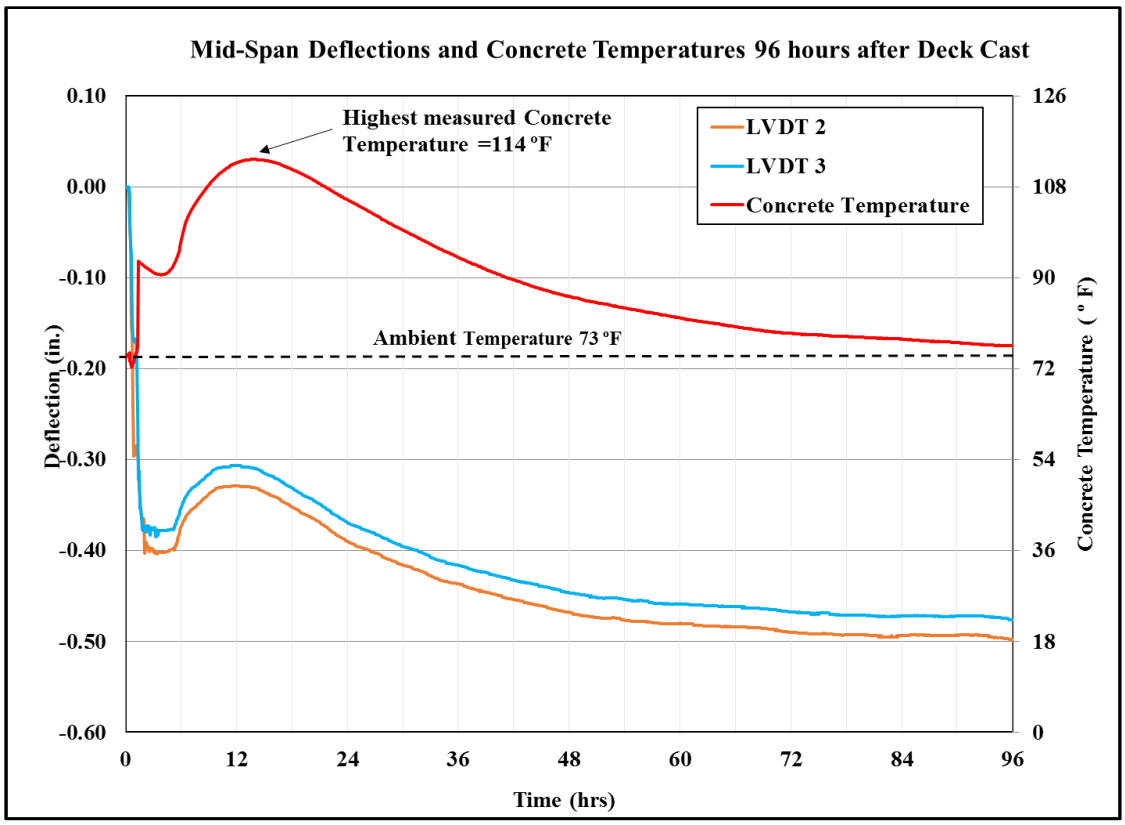

Figure 57. Mid-span deflections of steel girder 96 hours after deck cast

Figure 57 shows the steel girder deflections and corresponding concrete temperatures recorded for 96 hrs. after slab cast. At about 14 hours after slab cast, the concrete temperatures had peaked to about 114 ºF. As the concrete temperatures increase due to cement hydration, upward deflection of the bridge is observed. Figure 57 illustrates that both girder lines deflect upwards to 0.071in. at about 12 hrs. after slab cast. Similarly, as the bridge cools after peak temperature is achieved, the bridge deflects downward. The heating of the concrete had caused the slab to expand and caused the composite steel-concrete girder to camber upwards. It is evident that by this time in concrete hydration, the slab had acquired sufficient stiffness to cause both composite behavior and the observed upward deformation. The recorded data clearly show that the early age temperatures in concrete correlates well with the deflections in the prototype beam. Laboratory temperatures within the Cooper Lab are maintained at approximately 73 ºF. No visible signs of deck cracking were recorded during this time. At about 96 hrs. after the cooling period the slab

temperatures had returned or nearly returned to ambient temperature. At this time, the recorded overall midspan deflections were downward 0.48 in. on the North girder and 0.50 in. on the South girder. The downward deflection is caused by a combination of factors due to self-weight, heating and subsequent cooling of the bridge deck, and concrete shrinkage of the deck slab.

Early age Shrinkage of Concrete

Shrinkage in composite bridges is important for serviceability as it can affect the bridge's elevation profile, and account for the build-up of tensile stresses in the concrete decks. Shrinkage could be one possible cause for adverse deflection in composite steel girders (Abdelmeguid 2015, Belcher 2017). Alexander (2003) highlighted the significance of bridge deflection due to concrete shrinkage by including it as a part of the long-term deflection calculation in the design of composite bridge girders. Russell (1992) indirectly measured the slab shrinkage by directly recording the deflections in composite prestressed concrete bridge girders. The findings showed that the time dependent deformations in composite bridge girders were caused primarily by shrinkage of slab where the composite deck slab was not cracked. Experimental testing and analytical study by Li and Glisic (2017) found that the magnitude of early age shrinkage strains adds about 27% to the magnitude of the maximum bending strain otherwise caused by self-weight of the structure. Other research (William, Shoukry et al. 2008) has shown that the magnitude of tensile stresses induced in the concrete deck slab due to both drying shrinkage and temperature variations during curing can be relatively high compared to those induced due to traffic loading.

Measured Shrinkage Strains in Concrete and Related Bridge Deformations

Figure 58 compares the restrained shrinkage strains recorded by VWSG's within the concrete deck (VWSG Location 1) to the shrinkage strains measured on the unrestrained shrinkage prisms. The unrestrained shrinkage data corresponds to the average data recorded from six prisms in

accordance to ASTM C157. Fig 58 shows that the VWSG recorded a strain of 145 $\mu\varepsilon$ in the middle of the deck compared to an unrestrained shrinkage strain of 333 $\mu\varepsilon$ (10^{-6} in/in), at 28 days. A difference of about 188 $\mu\varepsilon$ (10^{-6} in/in) can be observed between the restrained and unrestrained shrinkage strains. The difference is accounted for in that concrete shrinkage with the composite deck is restrained by the steel girders whereas the measured shrinkage in the prisms are unrestrained.

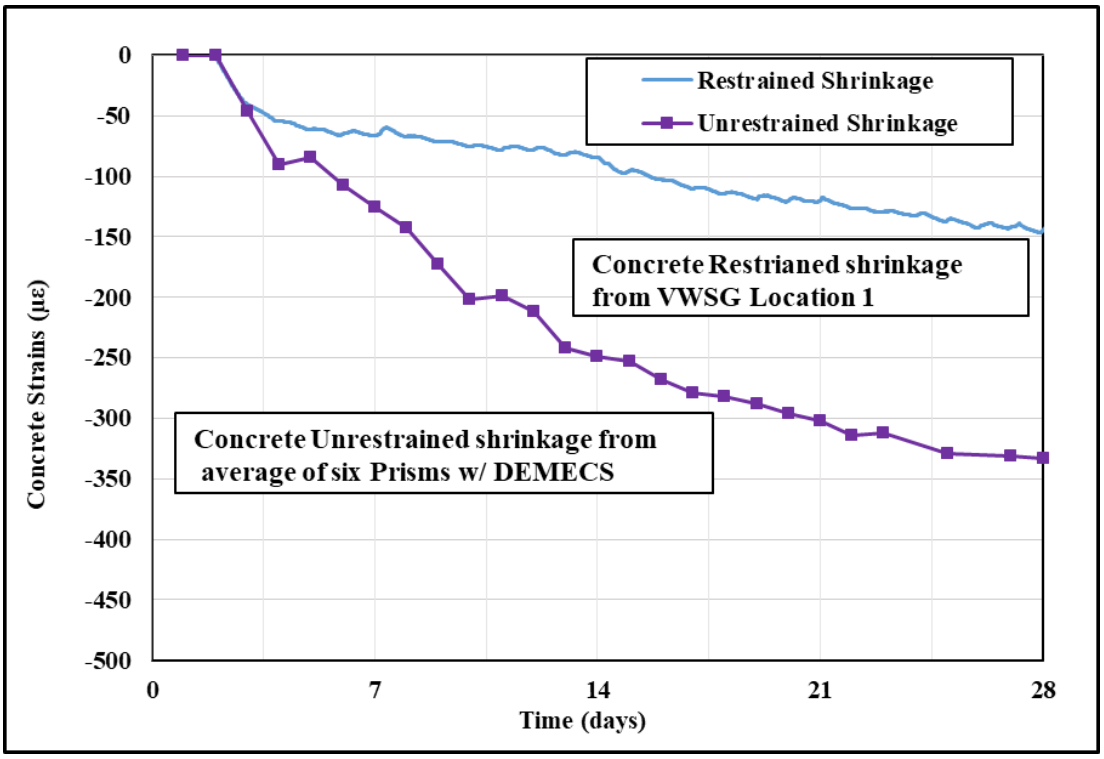

Figure 58. Restrained Shrinkage strains in concrete deck slab in comparison to unrestrained shrinkage strains measured from concrete prisms according to ASTM C 157

Figure 59 plots the strain at mid-depth of the concrete slab (VWSG Location 1) and the deflection of the North Girder (LVDT 2) vs. time. The figure illustrates the relatively large increase in concrete strain and upward deflections at early ages, the downward deflections and diminishing concrete strain that likely results from cooling temperatures. This is followed by decreasing concrete strains and downward deflections that accelerate after wet curing is removed. Additionally, it is observed that downward deflections accelerate after the removal of wet curing.

At 28 days the deflection of the steel girder increased to about 0.19 in. in addition to the dead weight of the deck slab. The results support the proposition that shrinkage of concrete causes additional downward deflection in bridge girders over time and after concrete hardening.

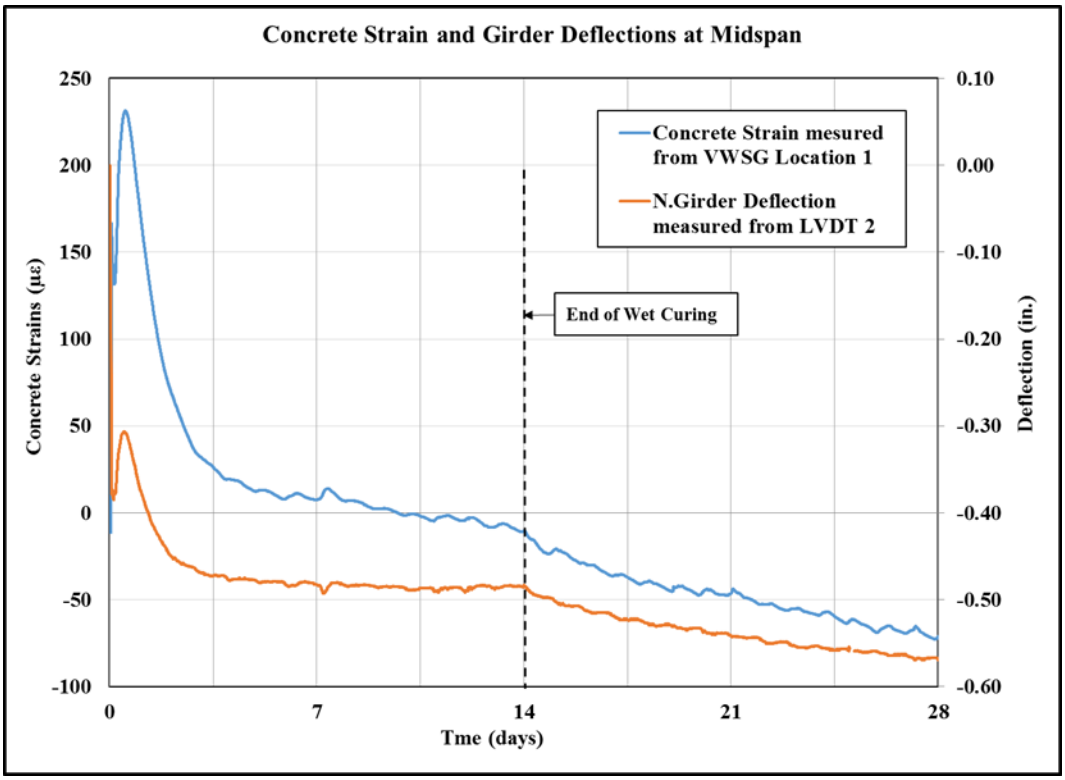

Figure 59. Deflections in North Girder due to restrained shrinkage in concrete deck slab

Figure 60 reports the shrinkage strains measured within concrete at the mid-span location of the slab using three vibrating wires aligned vertically at 2 in. apart from each other recorded at “VW Location 2”. The top vibrating wire measured concrete strains at 2.0 in. from the top of the slab, the second at 4.0 in. and the third at 6.0 in. from the top of the deck respectively. This arrangement of the vibrating wires captures the strain gradient developed in the concrete slab due to the shrinkage of the concrete. The deck was wet cured for 14 days prior to the removal of formwork and then allowed to cure up to 56 days.

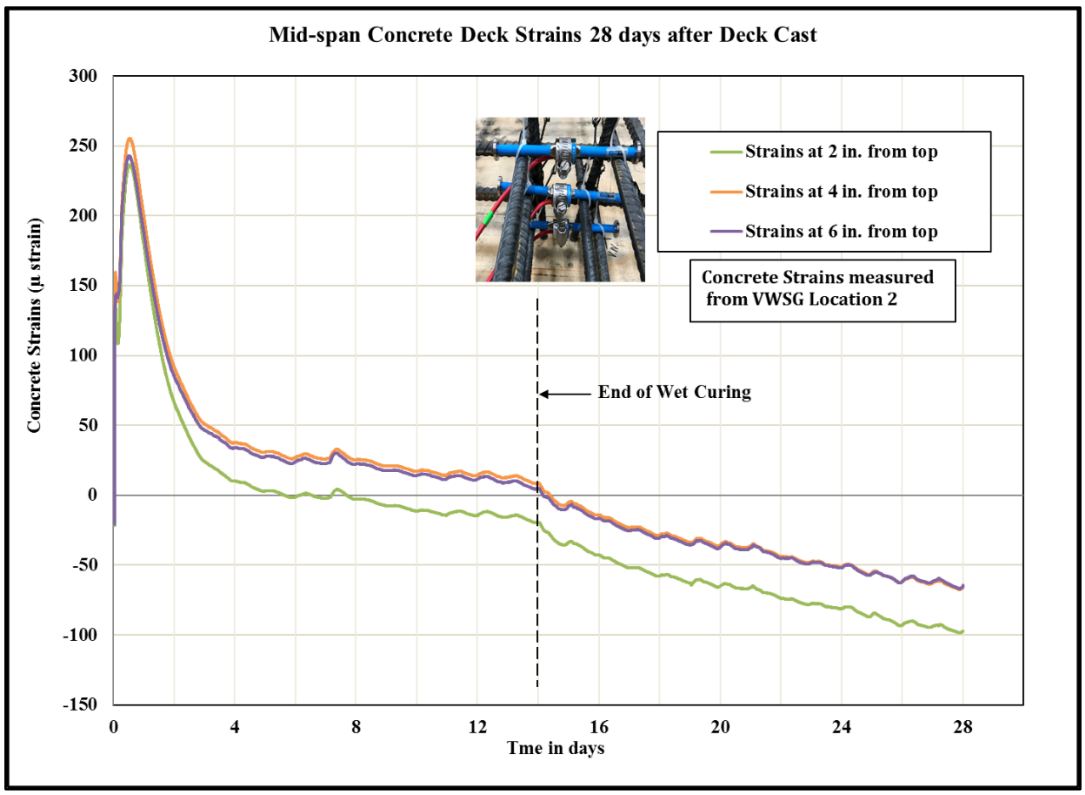

Figure 60. Concrete strains at mid-span location of bridge deck recorded from vibrating wire strain gages

The graph demonstrates that the shrinkage strains within concrete continued to increase during the curing period. The vibrating wire located close to the top of the deck recorded higher strains than the other strain gages. The indication of higher strains recorded close to the surface of the deck is potentially due relatively larger shrinkage strains attributable to more sensitivity to temperature changes (at early ages) and more sensitivity (and more shrinkage) due to the loss of moisture from the concrete into the atmosphere. This variation in shrinkage strains causes the development of tensile strain gradient within the concrete deck resulting in non-zero stress levels. In some cases where temperature variations are larger, or where shrinkage is greater, the strain gradient within the deck could be sufficient to cause bridge deck cracking. The fact that these strains move in parallel after just a few days also indicate that a "permanent" differential strain between layers of concrete is "locked into" the deck slab. From this one can see that large

temperature swings during the curing cycle could contribute directly to larger strain profiles through the concrete deck, which in turn could lead to cracking (Subramaniam, Kunin et al. 2010)

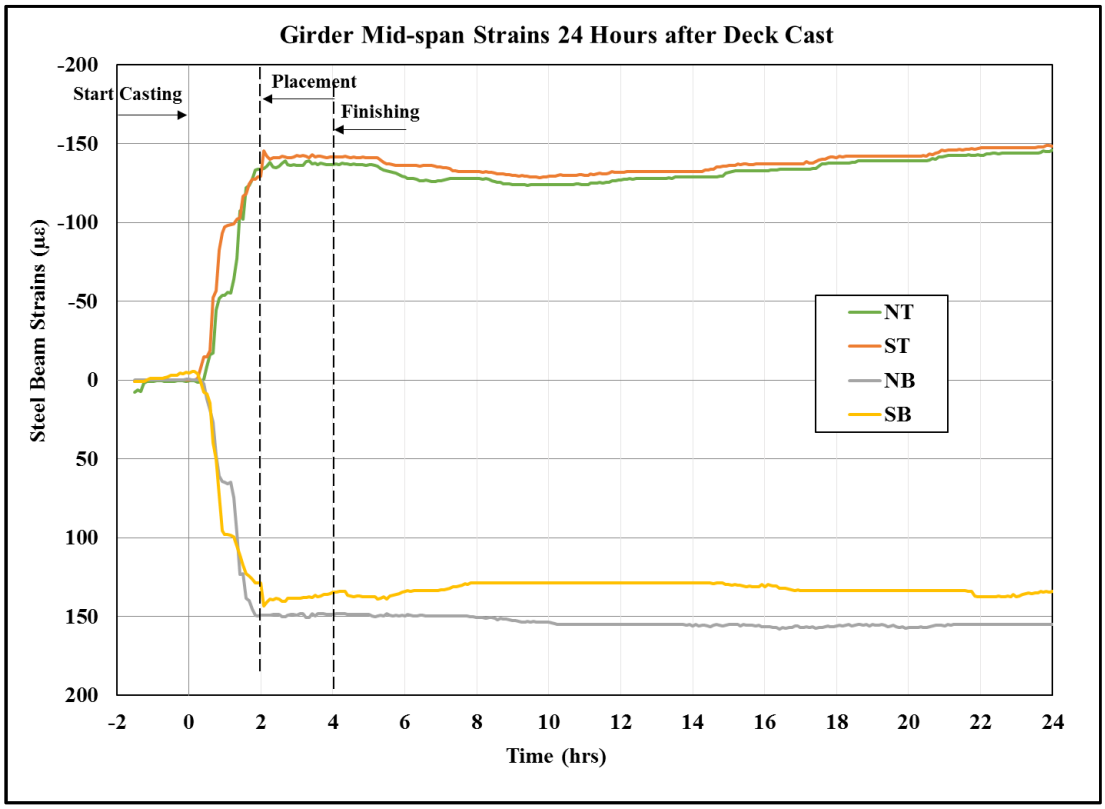

Figure 61. Steel Girder strains at mid span recorded until 24 hours after deck cast

Figure 61 illustrates the early age flexural strains recorded in the steel girders at midspan location, 2 hrs. before the time of cast through 24 hrs. after deck casting. The strains were captured by the bonded foil strain gages (NT & NB and ST & SB) attached on the webs of the steel girders. Both the girders exhibit consistent increase in flexural strains due to the weight of slab during the time of cast. Please note that increasing negative strains (compressive strains) are shown in the top half of the chart whereas positive (tensile) strains are shown in the bottom of the chart. Also, note that casting was completed at 2.0 hrs. after placement began, that the broom finish was applied at 4.0 hrs. after casting followed immediately by the beginning of wet curing.

Table 14 presents the steel girder strains, deflections, concrete strains and temperature that were measured at specific time intervals. Note that the Table reports measured values of selected instrumentation at selected time steps. Our instrumentation systems recorded data at 5 min. intervals from the time of slab placement from -2.0 hrs. through the first 96 hours after placement began. From recorded data, at 4 hrs. after slab cast it is observed that the self-weight of the slab caused a deflection of 0.38 in. in the North girder, which corresponds to measured steel strains of -137 $\mu\varepsilon$ (10^{-6} in/in) at a location 4 in. below the top flange and +149 $\mu\varepsilon$ (10^{-6} in/in) at 4 in. above the bottom flange. The two strain readings discussed above are separated by 16 in. of depth in the steel girder. The strain measurements convert directly to a curvature of 0.704 rad/mm (17.8 E-6 rad/in.) as shown in Eqn. (3).

$$Curvature\ \emptyset = \frac{\in_{top} - \in_{bottom}}{d} = \frac{-137\mu\varepsilon - 149\mu\varepsilon}{16\ in.} = -\ 0.704\ \times 10^{-6} rad/in \qquad \text{Eq (3)}$$

In turn, this curvature predicts a midspan deflection of 0.416 in., which very nearly matches the measured deflection. Also note that the strains correspond to stresses of 3.97 ksi compression near the top 4.32 ksi tension near the bottom.

At about 6 hrs. after slab cast, we can see that the concrete temperature has increased to 96.9 ºF which indicates the heating caused by the hydration of cement. The temperatures continue to increase to about 114 ºF at 14 hrs. This is followed by an increase of concrete thermal strains from 161 $\mu\varepsilon$ (10^{-6} in/in) to 230 $\mu\varepsilon$ (10^{-6} in/in). In addition to this we can notice that the compressive strains recorded near the top web of the steel girder has decreased by 13 $\mu\varepsilon$ (10^{-6} in/in) whereas the tensile strains near the bottom of the web have only decreased by 6 $\mu\varepsilon$ (10^{-6} in/in). This demonstrates that about 5 to 6 hrs. after slab cast the concrete slab had gained stiffness sufficient to cause composite action so that steels strains near the top flange are responding to temperatures in the concrete. At the end of the heating cycle as the concrete starts

to shrink it is restrained by the top flange of the girder and results in increase in compressive strains near to the top flange of the steel girder.

Table 14. Steel girder strains and deflections, concrete temperature and strains recorded at mid-span location of the North Girder.

Time (hours)	Girder Deflection, LVDT 1 (in.)	Concrete Temperature (°F)	Concrete Strains, VWSG Location 1 (μ ε)	N. Girder Steel Strains (μ ε)	
				Top of Web, NT	Bottom of Web, NB
0.0	0.00	74.3	0	1	-1
1.0	-0.17	74.2	-11	-54	65
2.0	-0.37	92.4	158	-134	149
4.0	-0.38	90.6	132	-137	149
5.0	-0.38	92.0	138	-137	149
6.0	-0.35	96.9	161	-129	150
7.0	-0.33	103.0	189	-126	150
8.0	-0.33	105.9	203	-128	151
9.0	-0.32	108.4	213	-124	153
10.0	-0.31	110.3	222	-124	153
11.0	-0.31	111.8	227	-124	155
12.0	-0.31	112.7	231	-127	155
13.0	-0.31	113.3	231	-128	155
14.0	-0.31	113.9	230	-129	156
24.0	-0.37	105.5	178	-146	155
48.0	-0.45	86.3	74	-161	147
72.0	-0.47	79.0	33	-168	141
96.0	-0.48	76.6	19	-171	140

Computational Analysis of Shrinkage Strains

Computational analysis was performed for both full size prototype laboratory bridge and SH 14 field bridge with five girder lines. An ultimate design shrinkage strain of 350 micro strain that was measured at 28 days after slab cast was used for computation purposes. Figure 62 shows the theoretical method used to analyze the shrinkage stresses in the laboratory bridge and Figure 63 represents the SH 14 bridge in field. The early deflection due to dead weight of concrete for both the bridge girders was calculated from the slab weight. The prototype bridge deck slab was 36 ft. long x 14 ft. wide and the field bridge deck slab was 38ft. 8in. long x 30ft. 8in. wide. Both the bridge decks had 8in. thick slab with a 2in. varying haunch. The laboratory prototype bridge shows a mid-span deflection of about 0.44in. which was close to the actual measured deflection of 0.4 in. (fig.56) during the time of pour.

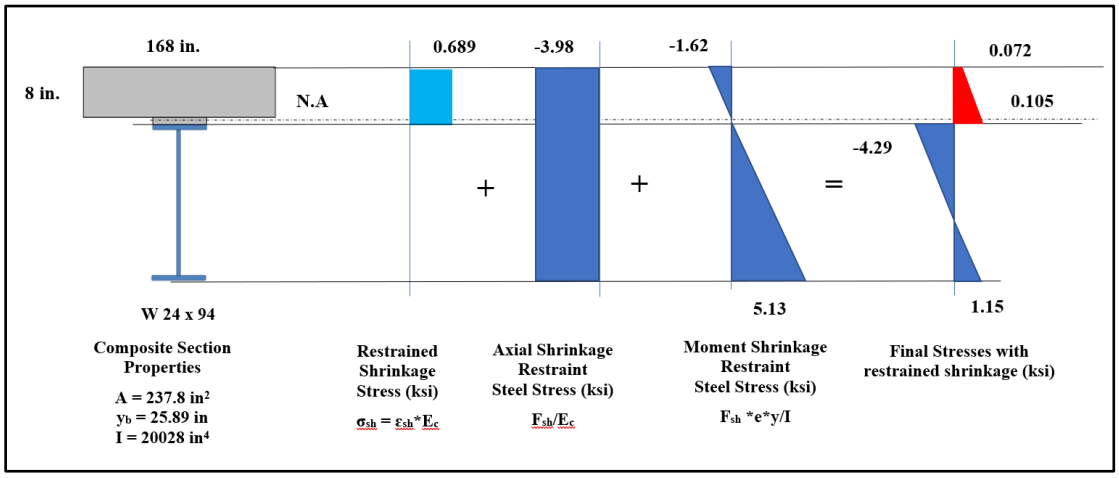

Figure 62. Computational Analysis of Shrinkage strains in laboratory prototype bridge deck at 28 days after deck cast.

The shrinkage of the slab imposes net compressive strains and stresses into the composite cross section as illustrated in fig 62. The eccentric shrinkage forces induce a curvature into the cross section leading to downward deflection of the slab. As the slab shrinkage is restrained by the girder, the slab experiences tensile stresses. The maximum tensile stresses in the concrete deck of

the laboratory prototype beam due to restrained shrinkage was 105 psi and the calculated deflection due to shrinkage stresses was about 0.185 in. This is comparable to the measured deflection of steel girders to 0.19in. (fig. 59) at 28 days after deck cast.

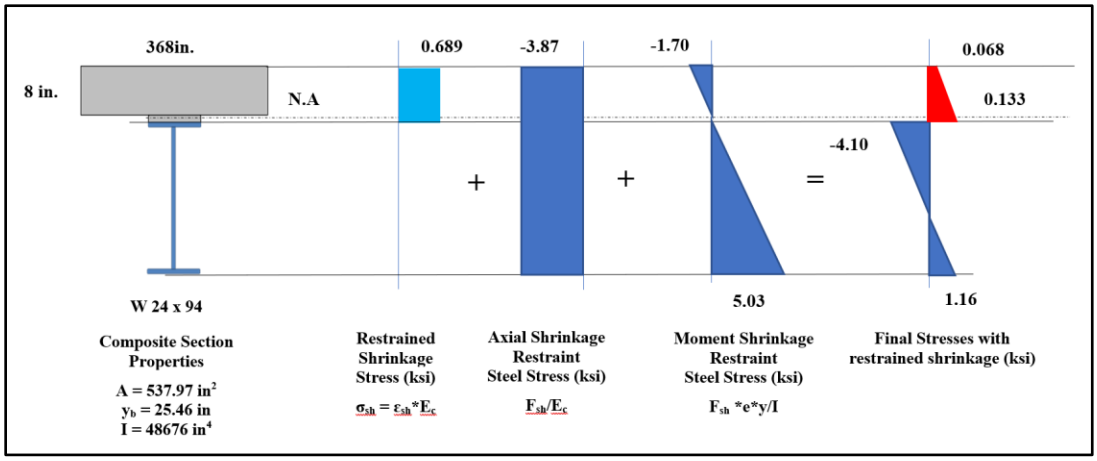

Figure 63. Computational Analysis of Shrinkage strains in SH 14 bridge deck

Figure 63 illustrates theoretical calculations of stresses and deflections in the SH-14 field bridge. The mid-span deflection of the field bridge with five girder lines was calculated to be 0.41in. due to dead weight of the fresh concrete alone. The maximum tensile stresses in the deck slab for the SH 14 field bridge was 133 psi given the same assumptions as the laboratory prototype bridge. However, the deflection due to shrinkage stresses were computed to be the same for both the bridges. This shows that simple computational analysis approach can be effective for the calculation of stresses, strains, curvature and deflections in composite bridge girders.

Early Age Cracking in Bridge Decks

Early age bridge deck cracking in newly constructed or rehabilitated steel composite bridge girders has been a common problem in Oklahoma's bridges. Cracking contributes to durability problems and can adversely affect the strength and serviceability of bridges. Russell (2017) noted that 70 percent of the state's structurally deficient bridges were bridges with steel superstructures, and further that of those 90 percent were rated as structural deficient because of

severe problems in concrete bridge decks. According to William et al. (2005) bridge deck cracking in early ages is mainly caused due to a combined mechanism of increased thermal strains due to heat of hydration and restrained drying shrinkage during the first few days after concrete placement. In addition, other factors that include 1) variation in material properties; 2) non- uniform curing of the concrete deck; 3) vibrations due to adjacent traffic; 4) changes in ambient temperatures are also responsible for crack initiation in new bridge decks. In order to understand and study early age cracking of bridge decks, it is essential to have an effective structural monitoring system to monitor both short term and long-term performance of bridge structures. This research program implements a structural monitoring system that was programmed to monitor both early age and long-term performance of bridges.

Early age Thermal and Shrinkage strains in concrete

Concrete bridge decks can experience significant temperature variations within the first 24 hrs. after concrete placement. Through initial set and after initial set, concrete temperatures increase considerably due to the exothermic reaction of cement hydration. Additionally, some researchers have shown that concrete temperatures during early ages are influenced substantially by fluctuations in ambient temperatures, particularly increases in ambient temperatures that correspond with concrete deck hydration. The temperature variations in the bridge deck and the surrounding ambient conditions has been a significant contributor to early-age cracking (Bao et al. 2017; Riding et al. 2009). Subramaniam et al. (2010) investigated the thermal movements and stresses in the concrete deck and steel girders due to changes in temperature introduced by heat of hydration release that occurred during the first few hours after casting the concrete deck. Whereas the majority of other researchers had given considerable attention to the cracking of concrete decks due to restrained shrinkage, his paper focused on the correlation between the temperature changes and cracking in bridge decks. The paper concluded that at the end of the heat of hydration period the concrete deck had gained sufficient stiffness, which coupled with sufficient

restraint created by the composite steel girders resisting movement of the concrete deck slab. Concrete begins to set at the end of the heating period and has lower tensile strength. A large temperature gradient in the steel girder at the end of the heating period induces larger tensile stresses in the concrete which may increase the likelihood for concrete to crack. It was also found that larger difference in temperature between the concrete deck and the top flange of the steel girder at the end of the cooling period could contribute to larger magnitude of tensile stresses in the concrete deck.

Shrinkage is defined as the time dependent change in the volume of concrete due to the physical and chemical changes that occur in the cement paste. Drying shrinkage is caused by the evaporation of free moisture from concrete (Portland Cement Association 2016). Shrinkage in composite bridges is important for serviceability as it can affect the bridge's elevation profile, and account for the build-up of tensile stresses in the concrete decks. Bridge decks are generally subjected to restraint from the steel girders. During the early ages of curing the concrete decks change in volume and are restrained by the girders. This induces tensile stresses in concrete and when these tensile stresses exceed the tensile strength of concrete cracks develop in concrete. Some researchers (William et al. 2008) have shown that the magnitude of tensile stresses induced in the concrete deck slab due to both drying shrinkage and temperature variations during curing can be relatively high compared to those induced due to traffic loading.

Effects due to early age thermal strains

Figure 55 captures the full heating and cooling cycle during concrete hydration along with measured concrete temperatures and strains for the first 96 hrs. after slab cast. The figure highlights that the measured thermal strains within concrete increase with the increase in temperatures and decrease with fall in concrete temperatures. During the process of cement hydration, the initial set of concrete is generally characterized by the onset of rapidly increasing

temperatures. After initial set, increasing temperatures cause volume expansion in the concrete at early ages. However, thermal expansion of the concrete is restrained by the composite steel girders, and thus the increasing hydration temperature induces internal compression stresses within the restrained concrete.

Computational analysis was performed on the full size protype beam to predict the stresses in concrete due to early age peak hydration temperatures. Figure 64 illustrates theoretical calculations of stresses imposed in the full-size prototype bridge at 14 hrs. after deck cast. The data shows that the concrete temperatures elevated to about 114º F reaching peak temperatures at approximately 14 hrs. The heating of the deck causes a temperature gradient within the slab resulting in restrained thermal strains. The corresponding concrete thermal stresses σ, are determined from Eq (4)

$$\sigma = \alpha(\Delta T)\, E_c \qquad \text{Eq (4)}$$

where,

α = coefficient of thermal expansion of concrete,

ΔT = change in temperature

E_c = Modulus of elasticity of concrete

The restrained thermal stresses are converted to an equivalent restraining force that is applied on the composite cross-section. The compressive restraining force acts at the centroid of the concrete slab which is equilibrated by an eccentric tensile force applied on the cross section. This eccentric restraining force induces an axial stress and bending stress onto the composite cross section. The final stress distribution on the composite cross section are calculated by superimposing both the axial and bending stresses. The theoretical method uses a reduced modulus of elasticity of E_c = 1250 ksi and a lower coefficient of expansion of concrete of about 3.88 x 10^{-6}/ºF (7 x 10^{-6}/ºC) as

early age estimated values for computation purposes. At the peak of heat of hydration concrete las low CTE and high thermal strains. These result in compressive stresses in concrete. The expansion of the slab imposes net tensile thermal strains into the composite cross section. As the slab expansion is restrained by the girder, the slab experiences compression stresses. The maximum compressive stresses induced in the concrete deck of the laboratory prototype beam was calculated to be about 76 psi.

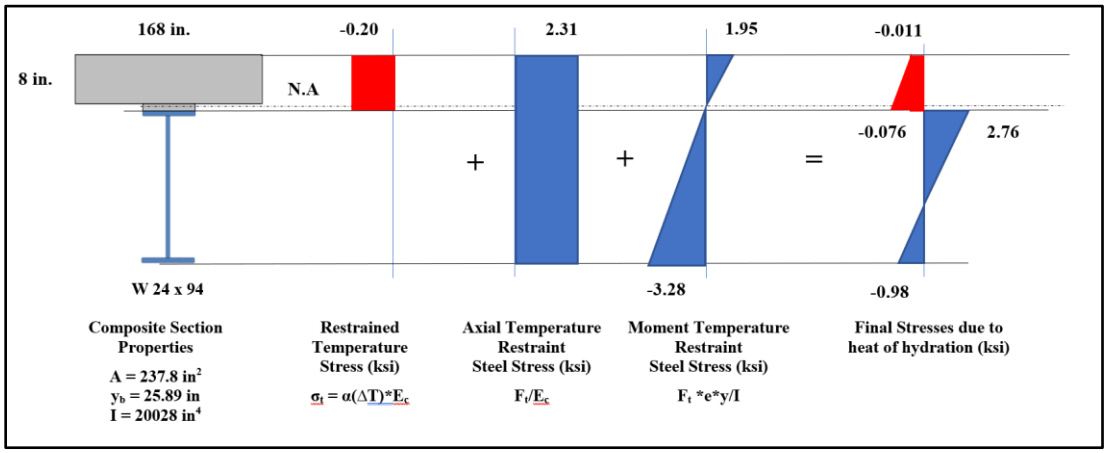

Figure 64. Computational Analysis of thermal strains in prototype bridge deck at 14 hrs. after deck cast

Figure 65 shows the graph of concrete deck peak temperatures measured at mid-height by VWSGs installed at various locations on the prototype bridge deck. The locations of the VWSGs are as shown in Figure 6 in Chapter 3. It is evident that at any instance of time, the peak hydration temperature distribution is non-uniform throughout the deck. Fig 65 shows that VWSG located along the north girder line at midspan (N. Girder mid-span) recorded a maximum temperature of 106 ºF, whereas the one located along the centerline of deck slab on the east side of the bridge recorded 117.5 ºF. The two locations are approximately 9.5 ft apart. The bridge deck was cast in two pours over a time span of two hours. The first pour extended from the west side of the bridge to the centerline of midspan, and the second pour covered the east side of the bridge deck. The fresh and hardened properties of the two pours, represented as trucks 1 and 2 are shown in Tables

12 and 13. The laboratory ambient temperatures were maintained at 73 ºF, during the entire time of bridge deck casting. Despite the fact that the deck was cast within a period of two hours a temperature difference of about 12 ºF is observed between the maximum temperatures recorded at different locations of the slab.

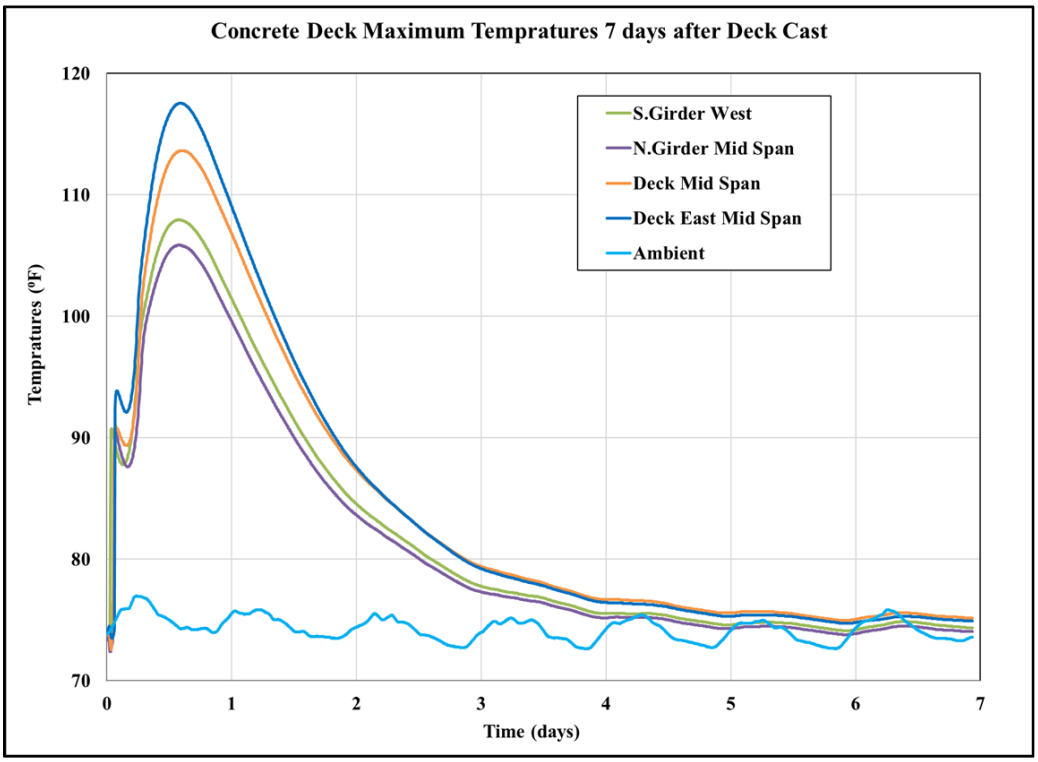

Figure 65. Variation in concrete temperatures at different locations on the prototype bridge during hydration.

This variation in thermal properties along the span of the bridge deck can be attributed to the variation in the concrete mix design between the two trucks. The limited capacity of the concrete mix trucks made the bridge deck to be cast in stages. This results in variation of concrete material properties between the two locations. Because of this the heat of hydrations temperatures also vary between the two locations along the bridge deck. This variation in in-plane temperature difference is reflected in variation of thermal strains at the same locations as shown in Figure 66. The recorded data show that a maximum temperature difference of 12 ºF at two different location on the bridge deck resulted in difference of strain up to 70 µstrain although the difference in

compressive strengths between the two mixes was within 5%. The difference in thermal strains would generate additional stresses in the deck that may lead to premature cracking of the deck (William et al. 2005).

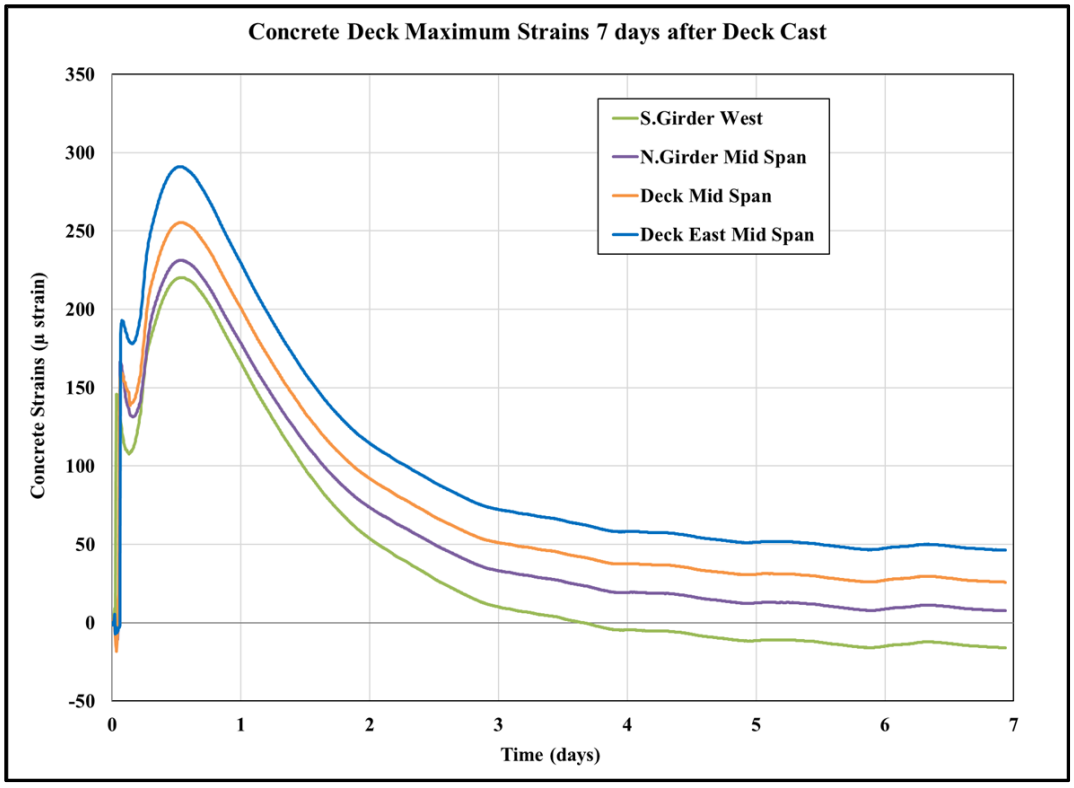

Figure 66. Variation in concrete thermal strains during hydration

In this research the bridge was constructed inside a laboratory where the ambient temperatures were maintained at 73 ºF. In reality, the bridges constructed on field are subjected to higher temperatures, especially when the concrete decks are poured during hot summer days. In addition to this variation in material properties that include changes in flyash content in the concrete mix can also influence the peak concrete temperatures during the process of hydration. The addition of flyash to concrete mix is found to reduce concrete temperatures during hydration thereby causing the reduction in shrinkage strains in concrete. Figure 67 shows the combined effects due to variations in flyash content and field conditions that were are predicted using ConcreteWorks®

software developed at the Concrete Durability enter at the University of Texas as a part pf research funded by the Texas Department of Transportation (TxDOT).

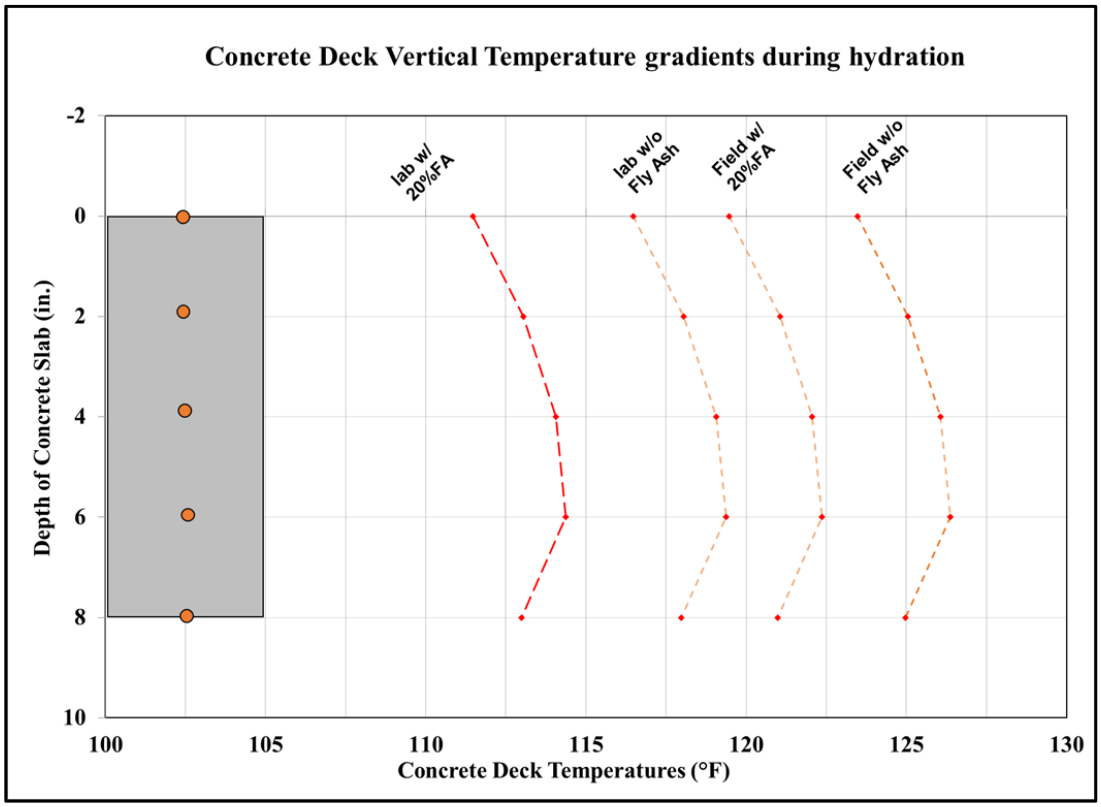

Figure 67. Variation in vertical temperature gradient in concrete decks due to variations in flyash content and field ambient conditions

The graph uses the standard ODOT mix used for the laboratory prototype bridge as the control mix and temperature variations due to variations in flyash and field conditions were estimated. Fig 67 shows that the maximum peak hydration temperatures increase by about 4 ºF for a mix without flyash used under laboratory ambient conditions. The same mix predicts a temperature increase by about 11 ºF when used in field conditions. This increase in concrete temperatures leads to higher thermal strains during the hydration process. As the concrete cools higher thermal strains transform to higher shrinkage strains leading to higher tensile stresses in concrete resulting in early age cracking in bridge decks. To prevent large thermal strains during early age hydration,

it is recommended to cast concrete decks to 10 to 20 ºF cooler than the ambient or outdoor air temperatures (Krauss and Rogalla 1996).

Effects due to early age shrinkage strains

At the end of the heating cycle, concrete will begin to cool and shrink which is indicated by the decrease in thermal strains and increase in concrete shrinkage strains. This shrinkage can be caused by either or both thermal strains and shrinkage strains. As the steel girders restrain the shrinkage of concrete, tensile stresses within the concrete will begin to develop immediately at the end of the temperature rise.

Computational analysis was performed on the full size protype beam to predict the stresses in concrete due to early age shrinkage strains. Fig 68 illustrates theoretical calculations of stresses imposed in the full-size prototype bridge. Measured 3 day modulus of elasticity of *Ec* = 2520 ksi and 3 day unrestrained shrinkage strains of 146 x 10 -6 µ strains that were measured using VWSGs embedded in test cylinders were used for computation purposes.

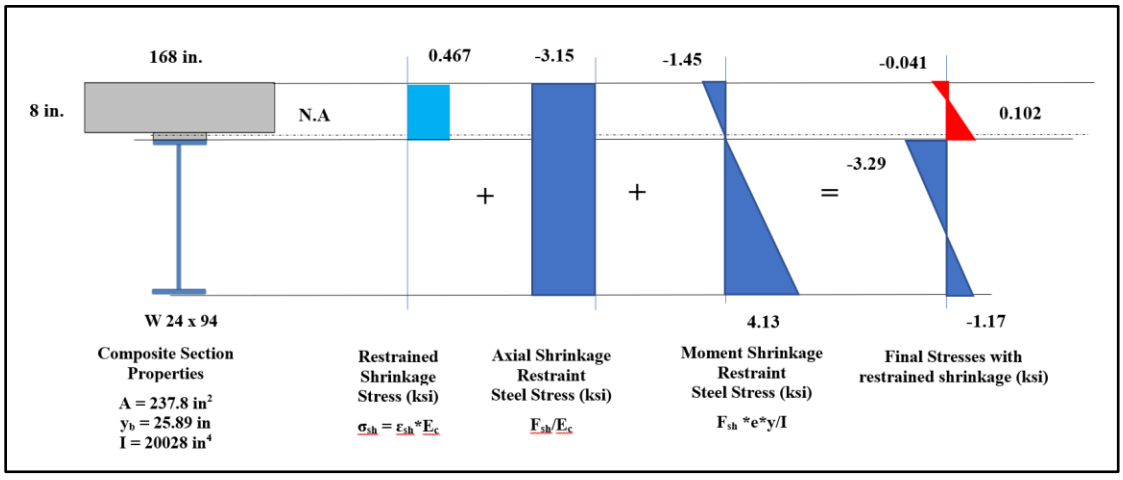

Figure 68. Computational Analysis of Early age Shrinkage strains in laboratory prototype bridge deck

The shrinkage of the slab imposes net compressive strains and stresses into the composite cross section. As the slab shrinkage is restrained by the girder, the slab experiences tensile stresses. The maximum tensile stresses induced in the concrete deck of the laboratory prototype beam due to restrained shrinkage was calculated to be about 102 psi. These stresses were not high enough to cause cracking in the laboratory bridge deck. However, in field conditions where the temperatures are higher, or where shrinkage of concrete is higher, the tensile stresses within the deck could be sufficient enough to cause bridge deck cracking. Despite the compression stresses developed in concrete due to peak hydration temperatures, the stresses are quickly transformed to tensile stresses during the cooling cycle. This agrees with the statement by William et al. (2005) that the stresses developed due to volumetric changes in concrete due to shrinkage is much higher than the effect due to temperature variations. The early age cracking in bridge decks due to high shrinkage stresses in concrete can be reduced by using concrete mixes with low shrinkage and high tensile strength. In addition to the variation in ambient temperatures and concrete material properties other factors that attribute to bridge deck cracking include 1) improper curing of concrete decks; 2) construction loads; 3) vibration due to adjacent traffic during phase construction of bridge decks.

Concrete Creep in Tension

Creep and shrinkage of concrete are interdepended and cause time depended deformations due to the gradual changes in stresses and strains over time. These stresses and strains sometime become too excessive affecting the durability of the concrete resulting in cracking of bridge decks and unexpected deformations in bridge girders. The majority of shrinkage occurs during the hydration process. Concrete is prone to volumetric changes due to thermal and moisture related shrinkage at early ages. When concrete is restrained and prevented from shrinking freely, tensile stresses develop in the restrained concrete.

Concrete creep is the increase in deformation under a constant or sustained load. In other words it is an increase in strain over time when subjected to a constant stress. According to ACI 209-R92 (1992), "Creep is defined as the time dependent increase in strain in hardened concrete subjected to sustained stress". Under a constant stress concrete undergoes two types of strain, Elastic strain or initial strain (ε_i) and Creep Strain (ε_{cr}). Elastic strain is the instantaneous deformation due to the applied load as per Hooke's law. Creep strain is the time depended deformation or additional increase in concrete strain over time under a constant stress. Creep coefficient C_{cr} is defined as the ratio of creep strain to the initial strain. The age adjusted effective modulus E_{eff} accounts for this additional creep strain where $E_{eff} = Ec/(1+Ccr)$. This phenomenon as shown in Figure 69 is better understood when concrete is in compression and not so much in tension. Although it is fair to assume that the same phenomenon occurs in tension; experimental tests by researchers have proven that the actual tensile creep is not equal to compressive creep and is about 2 to 3 times larger than compressive creep (Forth 2015). Creep in tension was found to be more pounced in early ages and is significantly larger than the creep in compression (Rossi et al. 2013). Also experimental tests by Yoshitake et al. (2012) have proved that the tension moduli of concrete is approximately 1.0 to 1.3 times larger than the compression moduli f concrete in early ages.

When the shrinkage of concrete is restrained, tensile stresses develop in the restrained concrete. The risk of early age cracking of concrete due to shrinkage is increased by increasing the degree of restraint. Khan et al. (2015) and (2017) found that the development of the tensile stresses in the deck slab due to restrained shrinkage of concrete is slowed by tensile creep in concrete. In their research they measured the tensile creep coefficients from dog bone specimens subjected to sustained axial loads. Restrained shrinkage ring tests were also performed to monitor the development of cracking in concrete specimens and also to validate the tensile creep coefficients measured from the dog-bone specimens. Their research concluded that the tensile creep

developed in the early ages relaxes the shrinkage induced tensile stresses and delays cracking in concrete structures.

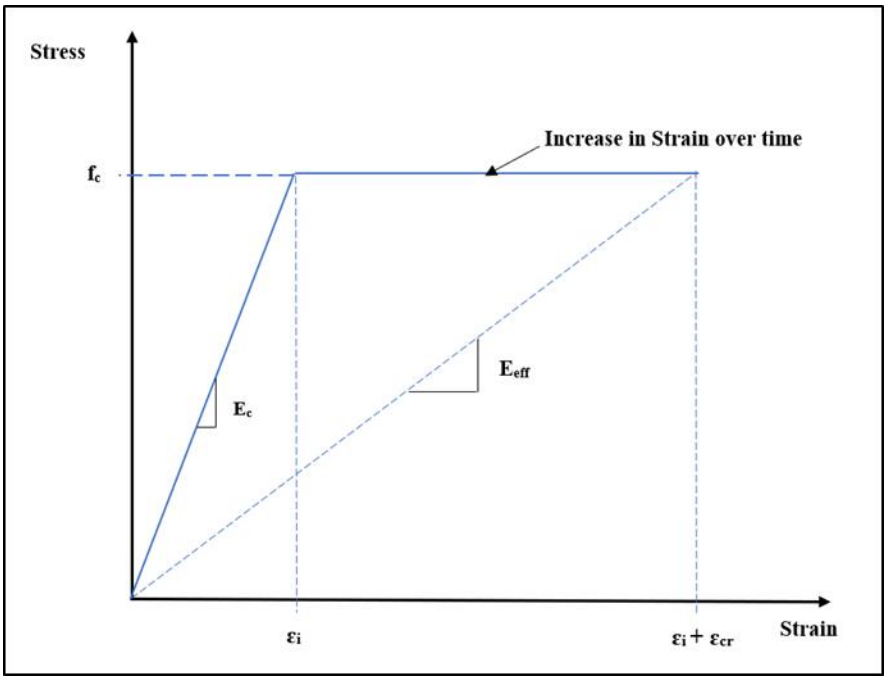

Figure 69. Mechanism of Creep Phenomenon in Concrete

At early ages as the cement hydration continues, initial set of concrete is generally characterized by the onset of rapidly increasing temperatures. Figure 55 shows the full heating and cooling cycle during concrete hydration at early ages. At the end of the heating cycle, concrete begins to cool and shrink which is indicated by the decrease in thermal strains and increase in compressive concrete shrinkage strains. As the steel girders restrain the shrinkage of the concrete, tensile stresses develop within the concrete deck. As the concrete is sustained under this tensile stress over time tensile creep starts to develop. This tensile creep is found to have the opposite effect of concrete shrinkage strains (Ranaivomanana et al. 2013). The tensile creep causes stress relaxation in concrete reducing the tensile stresses due to shrinkage, thereby reducing the risk of cracking in bridge decks. It should also be noted that as the concrete gains strength over time the modulus of elasticity of the concrete is also affected by this tensile creep.

Conclusions

1. Heating of the concrete deck occurred in the first 14 hours from deck placement. Maximum temperature achieved was 114 ^{o}F at 14 hrs. Concrete temperatures returned to ambient temperatures approximately 96 hrs. after concrete placement began.
2. Data show heating of the concrete deck placement at early ages causes upward deflection of the steel girder-composite concrete bridges. Likewise, the data show that the bridge deflected downward as the concrete cooled. Data also show that differential shrinkage through the depth of the deck cause permanent variations in normal strain through the depth of the concrete deck.
3. Midspan deflection caused by the weight of fresh concrete was measured at 0.38 in. on one girder and 0.40 in. on the other. This deflection closely matched the beam theory computation of 0.42 in.
4. Upward deflection caused by the elevated curing temperature of the concrete deck was approximately 0.071 in. Maximum upward deflection occurred at approximately 12.0 hrs. after concrete placement started whereas concrete temperatures occurred at approximately 14.0 hrs.
5. Concrete reached its ambient temperature at approximately 96 hrs. after deck placement. The overall midspan deflection at 96 hrs. was 0.48 in. downward on one girder and 0.50 in. on the other. In approximate terms, the total deflection is caused by two factors: 0.38 in. of downward deflection can be attributed to self-weight with slab cooling and shrinkage accounting for the remaining an additional 0.1 in.
6. Concrete shrinkage and measured deflections of the full-size prototype beam indicate that shrinkage of concrete contributes to permanent downward deflections in composite bridge girders. The amount of measured permanent deflection attributed to shrinkage is

approximately 0.1 in. at 28 days. However, it is noted that shrinkage beyond 28 days is not reported in this article.

7. Early age temperatures in concrete correlates with the strains and deflections in the prototype beam. The increase in concrete temperature due to heat of hydration of cement has a significant effect on concrete strains. Concrete thermal strains increase with increasing temperatures causing the beam to deflect upward slightly.
8. The research indicated that wet curing time of bridge deck significantly reduced the rate of shrinkage of concrete, thereby reducing excessive deflections and helping to mitigate the formation of cracks in the bridge deck. It was observed that shrinkage strains and related downward bridge deformations accelerated after wet curing was removed at 14 days.
9. Poorly braced or inadequate overhang bracing systems cause excessive deformations in bridge overhangs and can affect the overall ride quality of bridge girders.
10. High temperatures developed in concrete due to heat of hydration induces compressive stresses in the deck slab.
11. The addition of flyash to concrete mix is found to reduce concrete temperatures during hydration thereby causing the reduction in shrinkage strains in concrete.
12. Despite the compression stresses developed in concrete due to peak hydration temperatures, the stresses are quickly transformed to tensile stresses during the cooling cycle.
13. In field conditions where the temperatures are higher, or where shrinkage of concrete is higher, the tensile stresses within the deck could be enough to cause bridge deck cracking.
14. Simple computational approach can be used to calculate thermal and shrinkage induced stresses in composite bridge girders.

15. Early age cracking in bridge decks due to high shrinkage stresses in concrete can be reduced by using concrete mixes with low shrinkage and high tensile strength.

CHAPTER VI

IMPACT OF THERMAL STRESSES ON THE PERFORMANCE OF STEEL GIRDER BRIDGES MADE COMPOSITE WITH CONCRETE SLABS

This research focuses on determining the impact of thermal loading on durability and serviceability of steel girder bridges made composite with concrete slabs. Concrete bridge decks are subject to repeated temperature changes that cause temperature gradients through the depth of the slab and through the depth of the cross section. These temperature gradients produce internal thermal strains and stresses that directly result in bridge deformations. Generally, restraint from the composite girders cause compression in the slabs during heating and tension in the slabs during cooling. This phenomenon can adversely affect the ride quality, cause deck cracking and excessive deflections, decrease durability, and reduce long-term performance of bridges.

Introduction

Bridges are subjected to repeated cycles of heating and cooling from solar radiation from temperature differentials from the surrounding air, variations in humidity and wind. For concrete-steel composite bridges, this exposure produces thermal movements and stresses in bridges due to external restraints, temperature gradients and dissimilar material properties. The volumetric changes in concrete due to these temperature gradients cause upward and downward bridge deflections, differential strains, and internal stresses within the concrete deck. These temperature induced stresses depend on the end conditions of the bridge structure and the temperature distribution.

The current *AASHTO LRFD Bridge Design Specifications* (American Association of State and Transportation 2014) provide temperature ranges to account for the overall expansion and contraction due to the presence of thermal changes through the depth of the structure.

.A full-scale prototype bridge was built and instrumented at the Bert Cooper Engineering Laboratory on the campus of Oklahoma State University in Stillwater, OK USA. The bridge was constructed to replicate the Eagle Chief Creek Bridge "A" on SH 14 in Woods Co., Oklahoma. A full-scale model of the bridge allows to capture the absolute values of the original time dependent properties of concrete deck that cannot be completely captured using a small-scale model. A large array of sensors and instruments were installed on the prototype bridge to measure strains, deflections and temperatures in both concrete and steel. Overall bridge deflections were measured with Linear Voltage Displacement Transducers (LVDT's) at midspan and at other points along the length of the steel girders. Concrete temperature gradients throughout the depth of the slab were monitored using thermocouples. Concrete strains were measured with vibrating wire strain gages (VWSG's) embedded in the concrete deck. Steel Strains were measured using Electrical Resistance Bonded Foil (ERBF) gages installed on the webs of the steel girders. Measurements and monitoring are continued through 56 days of heat loading and testing.

This chapter focuses on determining the impact of thermal loading on durability and serviceability of steel girder bridges made composite with concrete slabs. This chapter illustrates the application of thermal loading to the bridge deck of a full-size prototype bridge built in laboratory conditions. This chapter displays that how the uniform heating of the deck can cause a temperature gradient within the bridge deck resulting in differential strains and stresses at various location of the bridge deck. The chapter demonstrations the development of a detailed computational analytical models that can predict and validate the stresses and strains developed in the composite cross-section of the prototype bridge.

The following are the primary objectives for this chapter

1. Measure and quantify the effects of thermal gradient and resulting thermal stresses on the performance of steel-concrete bridges.

2. To compare and correlate the measured and AASHTO positive vertical temperature gradient developed in steel-concrete composite bridge girders.

3. To validate the deformations and thermal stresses and strains developed in the composite section with the use of analytical computational models.

Background

Thermal loads differ from other types of loads in that stresses that occur are caused by restraint from other parts of the composite section. The behavior of bridges under thermal loads is typically observed as two superimposed effects: uniform change in temperature and varying temperature gradient. Varying temperature distributions through bridges result in flexural deformations while uniform temperature changes cause axial deformations (Reynolds 1972). When the thermal expansion or contraction of concrete is restrained, daily temperature variations and solar radiation will result in thermal stresses and a temperature differential throughout the section (Imbsen, Vandershaf et al. 1985, Hadidi, Saadeghvaziri et al. 2003, El-Tayeb, El-Metwally et al. 2017, Krkoska and Moravcik 2017). There are many factors affecting temperature variations such as the difference between the construction temperature and the maximum or minimum temperatures in the summer and winter and the geometry and dimensions of the bridge (Rodriguez, Barr et al. 2014, El-Tayeb, El-Metwally et al. 2017).

In simply supported steel girder bridges, uniform temperature variations do not produce, at least theoretically, temperature related stresses. There is the likelihood that connecting elements, or other continuous elements across joints may produce localized stresses. However, those are not

the point of this paper. On the other hand, temperature gradients can cause differential strain in concrete and steel even in simply supported bridge spans. As a result, temperature gradients produce stresses in both steel and concrete. These internal stresses may cause cracking in concrete and can cause concerns for serviceability. Even so, in simply supported bridge spans, temperature variations and temperature gradients do not affect generally the strength of the bridge whether flexural strength or shear strength. In continuous spans, however, temperature variations and temperature gradients produce secondary reactions, moments and shears. Accordingly, the effects of temperature must be considered in design of continuous span bridges, and those design concerns extend to strength calculations. *Current AASHTO LRFD Bridge Design Specifications 3.12.3* (American Association of State and Transportation 2014) provide design criteria for temperature ranges to account for temperature related strains caused by both extreme temperature and temperature gradients through the depth of a cross section. AASHTO provides both the maximum design temperature and a minimum design temperature. In the majority of Oklahoma, those design temperatures range from the maximum of 120 °F to a minimum of 0 °F.

Temperature gradients have more influence perhaps than overall temperature variation. Temperature gradients produce both internal flexural and shearing stresses within the composite cross section. Figure 70 shows the positive vertical temperature gradient provided by AASHTO. For the design temperature gradients, the United States is divided in to four regions. For each region, a temperature T_1 and T_2 value is provided which defines the design positive temperature gradient. Oklahoma falls under zone 2 where the reference temperatures T_1 and T_2 are given to be 46 ºF and 12 ºF respectively. The absolute values of these temperatures are not as important as the difference as it is the temperature differences that produce bending and shear deformations. For AASHTO designs, a temperature differential of 34 °F must be applied through the depth, ***t*** as indicated in Fig. 70. AASHTO specifies that the distance ***t*** is taken as the depth of the concrete slab. In our case, *t = 8 in.* Additionally, the dimension A is specified as 12 in. So, a linear

interpolation is conducted to find the design temperature for the steel girder. In our case, the steel girder temperature is 6.5 °F and the temperature at t is 8 °F.

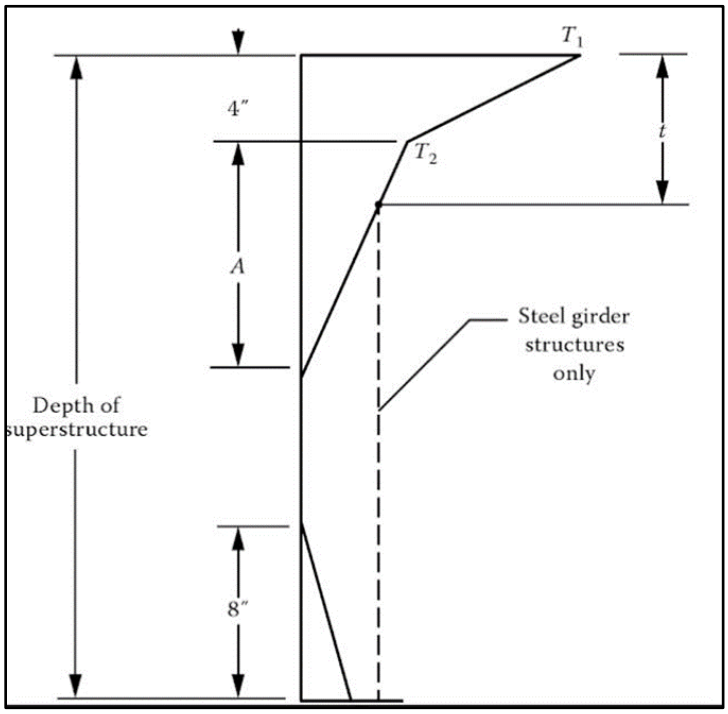

Figure 70. AASHTO Positive Vertical Temperature Gradient (*AASHTO LRFD Bridge Specifications 3.12.3-2)*

Thermal strains induced in field bridges can cause tensile stresses in concrete and cause cracking in bridge decks. In some instances, these thermal strains were found to be much larger than the maximum static strains measured due to live loads on field bridges (Johnson 2005). Other researchers (Rojas 2014, Krkoska and Moravcik 2017) found that the maximum average bridge temperature gradients monitored on field bridges exceeded the service limit state provided in the *AASHTO LRFD Bridge Design Specifications*. In addition, severe cracking and deterioration have been the result of imprecise thermal analysis of bridges (Rodriguez, Barr et al. 2014). Non-linear thermal stresses are developed due to temperature gradient along the vertical axis of the composite section. This causes the development of self-equilibrated thermal stresses within the cross section composite beams. These thermal stresses have to be added to the stresses due to

shrinkage of concrete slab and stresses due to dead and live loads for the design of composite steel-concrete beams (Giussani 2009).

(Krkoska and Moravcik 2017) also found that underestimating the vertical temperature gradient in bridge cross sections can cause significant stress distributions in bridge decks resulting in cracking. In addition, (Fu, Ng et al. 1990) found that the slab overhang depth ratio can also be an influential factor on the thermal stress distributions in various composite bridge girders. The differential heating and cooling of the bridge deck during the course of the day causes cyclic sweeping deflection changes due to differential thermal expansion and contraction. Higher temperatures during the day produced upward deflections, while cooler night time temperature produced downward deflections in the bridge (Pavelchak and Williams 2013).

Experimentation Program

Our experimental program provides heat loading to a full-sized prototype bridge built at the Bert Cooper Engineering Laboratory (BCEL) on the campus of Oklahoma State University. The heat loading replicates a typical summer-time heat loading pattern where concrete surface temperatures approach 120 °F, while ambient temperatures within the laboratory ensure a significant temperature differential through the depth of the composite steel-concrete cross section. The prototype bridge replicates the Eagle Chief Creek Bridge "A" on SH 14 in Woods Co., Oklahoma. Figure 71 shows the photograph of the full-sized prototype bridge at the BCEL. The prototype bridge at the Cooper Lab has a deck 14 ft- 0 in. wide supported by two W24x94 Gr 50 steel girders with 4'-0 cantilevered overhangs. Composite action and shear transfer is achieved by pairs of headed shear studs 7/8 in. diameter x 5 in. long welded to the top flanges at 6 in. centers. The steel girders are spaced at 6 ft. with C12x20.7 steel diaphragms at each end and mid-span locations.

Figure 71. Full-sized prototype at the Bert Cooper Engineering Laboratory at Oklahoma State University.

Concrete Materials

The concrete mix design conformed to the Class AA Concrete specifications contained in the Construction Specifications of the Oklahoma Department of Transportation (ODOT). ODOT concrete mix design proportions are shown in Table 15 Cement conforming to ASTM C150, Type I/II was used for the concrete. Fly Ash conforms to Type C specifications. Locally available aggregates were used. The coarse aggregate is a crushed limestone from a quarry near Drumright, Oklahoma that conforms to ASTM C33, #57 gradation. The fine aggregate also conforms to ASTM C33 and is known locally as "Guthrie sand" used in commercial concrete. The concrete was batched locally and delivered to the Cooper Lab for placement. The concrete mix targeted 5% air content and was achieved using an air entrainment agent. To ensure workability and ease of placement and finishing, a concrete slump of 7 to 8 in. was specified and achieved using both normal range and high range water reducing agents. The minimum 28-day specified compressive strength (f'_c) for the ODOT Class AA concrete is 4000 psi. It is noted that the ODOT AA specification for concrete provides a range of proportions for mixture constituents.

In our mixture design, 20% of the required cement content was replaced with fly ash. It would be reasonable to expect that ODOT AA concrete mixtures with different mixture proportions and constituents would exhibit different time dependent properties and differing hardened properties.

Table 15. Class AA ODOT Mix Proportions

Ingredient	**PCY**	**Volume (ft^3)**
Cement	451	2.29
Flyash	113	0.68
Coarse Aggregate	1845	10.56
Fine Aggregate	1362	8.30
Water	238	3.81
WRA (lq. oz.)	22.6	-
HRWRA (lq. oz.)	15.8	-
AEA (lq. oz.)	6.5	-
Air	5%	1.35
TOTAL	**4009**	**27.00**
	Yield (PCF) =	**148.4**

Notes:
Source of Coarse Aggregate is Quapaw # 57 from Drumright, Oklahoma with a Maximum Agggregate Size of ¾ in.
Source of Fine Aggregate is Gutherie, Natural Sand with a Finess Modulus of 1.60

Bridge Instrumentation and Data Acquisition

Instrumentation and Data Acquisition systems for this project were built in a laboratory environment with the intention to transfer the technology and expertise to the field for structural health monitoring. The instrumentation is robust, as are the data acquisition hardware that should allow the transfer of systems to a more rugged environment. Altogether 100 electronic gages and sensors were employed to measure and monitor concrete and steel strains, concrete and steel temperatures, overall bridge deflections at several locations, and inclination of the steel girders. Instrumentation was installed prior to casting the concrete deck. The instrumentation included the following:

(1) Thermocouples (TC) to measure the temperature within the concrete and ambient temperatures near the bridge deck;

(2) Vibrating wire strain gauges (VWSG) embedded within the concrete deck prior to casting to measure the concrete strains and concrete temperatures within the hardening deck;

(3) Electrical resistance bonded foil strain gages (ERSGs) to measured strains in the steel girders;

(4) Linear Variable Differential Transducers (LVDTs) to measured deflections of the bridge girders at various locations; and,

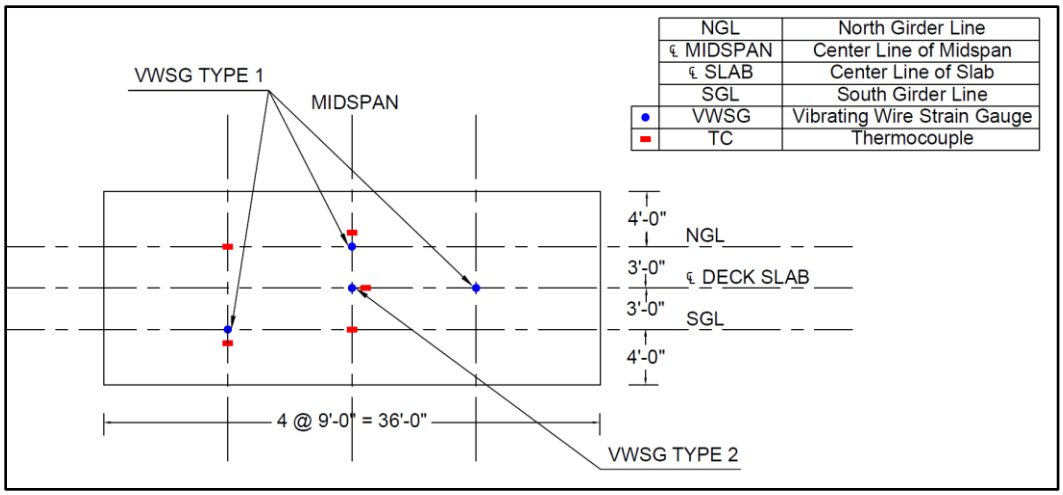

Figure 72. Plan View of Prototype bridge deck showing the location of Sensors

Figure 72 shows the location of the VWSGs and TCs on a plan view of the prototype bridge deck. Geokon 4200 vibrating wire sensors were embedded within the concrete to capture the strains within the concrete deck. All sensors are wired into a datalogger through various multiplexers required for each type of sensor. The sensors were programmed to record data continuously throughout casting, during and testing of the concrete deck. The datalogger was programmed to collect data at 5-minute time intervals during the time of casting, curing and heat

load testing. Figure 73 shows the sensor locations along the mid-span cross section of the prototype bridge. Note that thermocouples (TC) are distributed through the depth of the concrete

slab to capture the temperature gradient through heat loading. As shown in Fig. 73 TCs were installed at numerous locations in the bridge deck to capture the temperature gradient within the deck. TCs are designated by a rectangular symbol whereas VWSGs are designated by a round symbol.

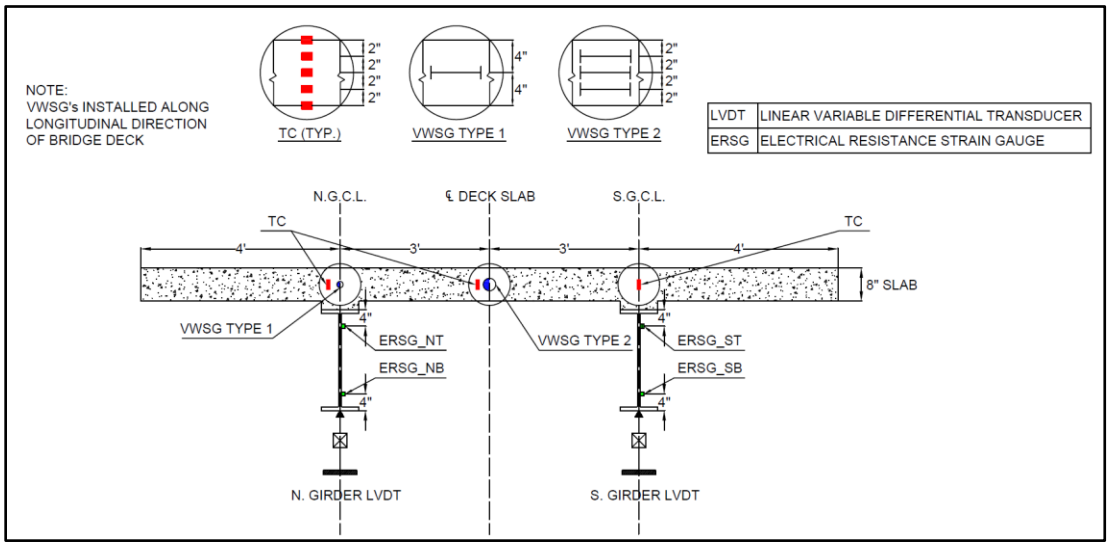

Figure 73. Prototype Bridge Cross Section at Mid-span (View Looking East) showing location of sensors

Figure 74 shows the installation of thermocouples at mid span location of the bridge deck. Five TCs were aligned vertically and spaced at 2 in. through the slab depth to capture the temperature gradient over the full depth of the concrete deck.. The TC sensors were situated away for the rebar to prevent the interaction of the rebar temperature with that of the concrete. Figure 75.a) shows a single vibrating wire sensor installed at the mid-height of the concrete slab. This is referred to as a "Type 1" installation. The "Type 2" installation for VWSGs are shown in Fig. 75.b). "Type 2" refers to locations where three vibrating wire strain gages are installed vertically at 2 in. c/c spacing along the centerline of the deck to capture the strain gradient throughout the depth of the concrete slab. The vibrating wire sensors were placed in the longitudinal direction of the bridge deck and fixed in position by tying two short pieces of rebar to the main reinforcing steel using nylon tie-wraps.

Figure 74. Installation of Thermocouples in concrete deck at mid-span

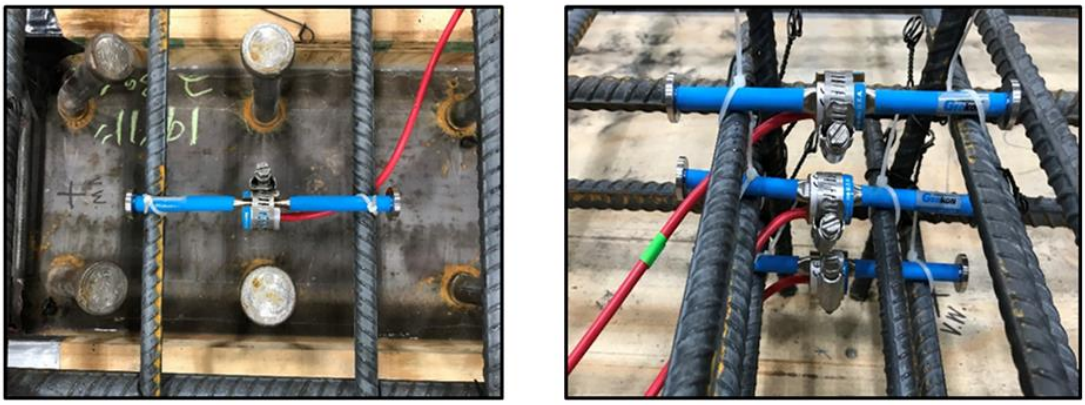

a) VWSG Type 1 Aligned with NGCL b) VWSG Type 2 at CL of Deck Slab

Figure 75. Installation of Vibrating Wire Strain gages in concrete deck at mid-span

The thermistor within the VWSGs also measured concrete temperatures alongside strain measurements. These temperature variations during the heat loading also affect the strain gage. The increase in concrete temperatures cause the vibrating wire inside the gage to elongate and thus go slack, indicating what would appear to be compressive strains in concrete. In addition, the coefficient of expansion of steel is different from the coefficient of expansion of concrete. This is

corrected by the use of a temperature correction. The load related strain in concrete caused due to heat loading is given by,

$$\mu\varepsilon_{load} = (R_1 - R_0)B + (T_1 - T_0)(C_1 - C_2) \quad \text{Eq (5)}$$

where,

R_0 = initial reading

R_1 = current output reading taken in a position

B = batch factor supplied with each gauge, which is 3.304

T_0 = initial temperature

T_1 = current output temperature reading taken in a position

C_1 = coefficient of expansion of steel, taken as 12.2 microstrain/ºC

C_2 = coefficient of expansion of concrete, measured from experimental testing

LVDT sensors were installed at various strategic locations to measure the deflections in the steel girders and bridge overhang. LVDTs installed along the girder center lines, recorded the deflections of the North and South Girders respectively. Electrical resistance bonded foil strain gages were attached to the top and bottom of the webs of the North and South girders to capture the steel girder strains. As shown in Fig.73 NT & NB, and ST & SB represents the Electrical Resistance Strain Gages (ERSG) bonded to the top and bottom webs of the North and South girders respectively. The gages were about 16 in. apart and bonded at 4.0 in from the top and bottom of the flanges of the steel girder.

Casting and Curing of the Composite Concrete Bridge Deck

The concrete deck was cast on July 13, 2017. A total of 14.0 CY was required to cast the prototype bridge deck at the Cooper Lab. Each of two ready-mix trucks delivered 7.0 CY to the Cooper Lab for concrete placement. Concrete was placed via a ¾ CY bucket supported by an overhead crane. Concrete sampling was performed from materials obtained from both trucks. Sampling was performed near the beginning of the pour from each truck and near the middle of each truck. Table 16 reports the fresh concrete properties measured from the two trucks during the time of pour.

Table 16. Fresh Concrete properties

Measured Properties	**Truck 1**	**Truck 2**
Slump (inches)	9.5	8.25
Unit Weight (lb/ft^3)	144.2	141.8
Concrete Temperature (º F)	91.5	91.3
Air Content (%)	8	9

Notes:
The fresh cooncrete properties were measured in accordance to following ASTM.
Slump measured in accordance to ASTM C143
Air Content and Unit Weight measured in accordance to ASTM C138

A total of 118, 4 x 8 in. concrete cylinder specimens were prepared in accordance to ASTM C192. The cylinder specimens were demolded after 24 hrs. and cured in accordance with ASTM C157. Concrete cylinder specimens were used to measured hardened concrete properties at 1, 3, 7, 28, 56, 90, 180 and 365 days respectively. Table 17 reports the hardened concrete properties which included compressive strength, elastic modulus and splitting tensile strength in accordance to ASTM C39, C469 and C496 respectively.

Table 17. Hardened Concrete properties

Age (Days)	Compressive Strength (psi)	Elastic Modulus (ksi)	Splitting Tensile Strength (psi)
1	1790	2512	339
3	3655	3207	429
7	4330	3576	550
28	5425	3935	571
56	5720	-	-
90	6315	4240	603
180	6520	5257	753
365	6810	-	672

Notes:
The hardended concrete properties were measured in accordance to following ASTMs. ASTM C39 for Concrete Compressive Strength, ASTM C469 for Elastic Modulus and ASTM C496 for Splitting Tensile Strength.

The ODOT specifies a curing regimen that requires wet curing regimen for a minimum of 10 days. Specifications allowed wet curing by ponding or by covering with wet burlap. In the prototype bridge, the concrete deck was covered by wettened burlap overlaid by plastic sheeting for 14 days after casting. Formwork at the bottom and sides of the concrete deck remained in place for the same period of time. After removing curing materials and formwork, the concrete deck was inspected for cracking. No cracks were found. The bridge deck was continued to cure within the laboratory at ambient conditions. The bridge and bridge deck remains in place today as additional testing is being performed. External loads were not applied to the prototype bridge during the time of curing and through the heat load testing.

Coefficient of Thermal Expansion of Concrete

The Coefficient of Thermal Expansion (CTE) of hardened concrete is an important parameter when investigating thermal effects on bridge decks due to environmental temperature changes. Accurate prediction of CTE of bridge deck concrete is imperative for determining the internal stresses and strains developed due to thermal loading. The CTE is developed from empirical data

which measures the strain of unrestrained concrete caused by changes in temperature. Concrete, like many other materials, expands when heated. The CTE of concrete varies with differences in mortar and paste, aggregate type, w/cm, and other variations of the concrete mixture. Additionally, the age of concrete and variations in ambient conditions can affect the CTE of hardened concrete (Johnson 2005). The CTE of concrete is influenced predominantly by the type, size and texture of coarse aggregate. Coarse aggregates account for approximately 60% of the total volume of the concrete mixture.

AASHTO T336-09 (T336) "Standard Test Method for the Coefficient of Thermal Expansion of Hydraulic Cement Concrete" is the most widely used method for determining the CTE of concrete. The T336 method, approved as a standard test method in 2009 and used by all state DOTs was based on AASHTO TP 60-00, "Provisional Test Method for the Coefficient of Thermal Expansion of Hydraulic Cement Concrete" (Tanesi, Crawford et al. 2012). The CTE of concrete was determined subjecting the concrete specimen to varying temperature cycles and the change in length of the specimen was measured.

Researchers from Auburn University (Sakyi-Bekoe 2008) further modified the T 336 method to minimize the temperature change of the LVDT during the time of testing. Researchers at OSU (Ebisch 2013) made additional slight modifications to the Auburn University's T 336 method and created a setup that can continuously measure the change length of the concrete specimens during the CTE testing. Laboratory testing was performed at the BCEL to determine the coefficient of thermal expansion of concrete on the concrete cylinder specimens prepared from Class AA ODOT bridge deck cast mix. The test methodology was based on that of Ebisch (2013). The average CTE value from concrete cylinder samples was found to be about 5.69 E-6/°F (9.1×10^{-6} /ºC). This value was used in Eq (5) for the computation of temperature related strains in concrete.

Heat Loading on the Prototype Bridge

As noted, the bridge deck was cast July 13, 2017. Heat loads were first applied 56 days after slab casting. Heat load testing continued for approximately eight weeks thereafter. Radiant heat from radiant heat lamps was applied directly to the surface of the concrete bridge deck to simulate the radiation from summer sun in Oklahoma. An array of 54 infrared heat lamps with 250 W of power each applied the heat loading. Figure 76 shows the plan view layout of the heat lamps. The heating lamps covered the entire 14 ft. width of the bridge deck with length of 22 ft. centered on the midspan of the bridge. A photograph of the heat lamps is shown in Fig. 77. Twelve rows of lamps were placed at 2 ℄ c/c spacing covering the center sections of the bridge span.

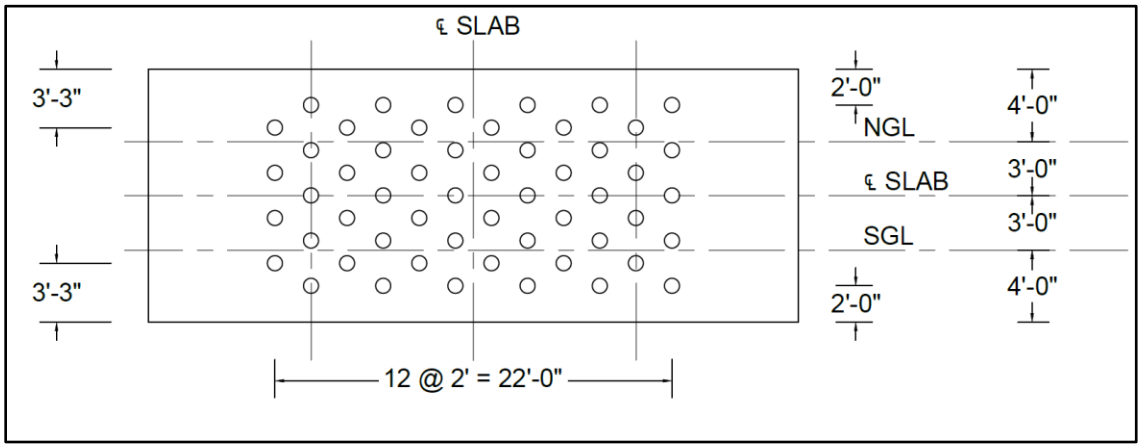

Figure 76. Plan view showing the layout of heating lamps on the prototype bridge deck

The heat lamps produced concrete surface temperatures between 100°F and 120°F. Heating temperatures were sustained at steady state for 6 hrs. followed by a cooling period of 18 hrs. when the lamps were shut off. The heating cycle was repeated every 24 hrs. period for five days per week for approximately eight weeks. There was a total of 40 heating and cooling cycles. Concrete temperature gradients throughout the depth of the slab, concrete and steel strains, and deflections were recorded and continuously monitored. The bridge deck surface was inspected for cracks at the end of every heating cycle and no cracking was reported.

Figure 77. Photograph showing the setup of Heat lamps atop the prototype bridge deck

Results and Discussion

Measured Temperatures and Bridge Deflections from Thermal Loading

Figure 78 shows the typical heating cycle where heat was applied to the concrete deck surface for six hours in every 24 hour period, and that heating was applied for five days in a longer one week cycle that included two days of "cooling." Within Fig. 78, concrete surface temperatures are recorded along with the deflections measured on the two steel girders over the typical 5 day loading cycle within the seven day week. Two days of "cooling" are included in each 7 day period. Concrete temperatures displayed in Fig. 78 were recorded by the thermocouples embedded just under the surface of the concrete deck at the midspan locations of bridge deck. These thermocouples may not be located directly under heating lamps. The data show that the average temperature at these thermocouples reached a maximum of about 100 ^{o}F at the end of each 6 hr. loading cycle. The recorded temperatures also indicate the concrete retained residual heat at the end of each 24 hour heating/cooling cycle, but that temperatures return to ambient

temperatures at the end of each 7-day cycle. The ambient temperature within the Cooper Laboratory was maintained at or near 73°F.

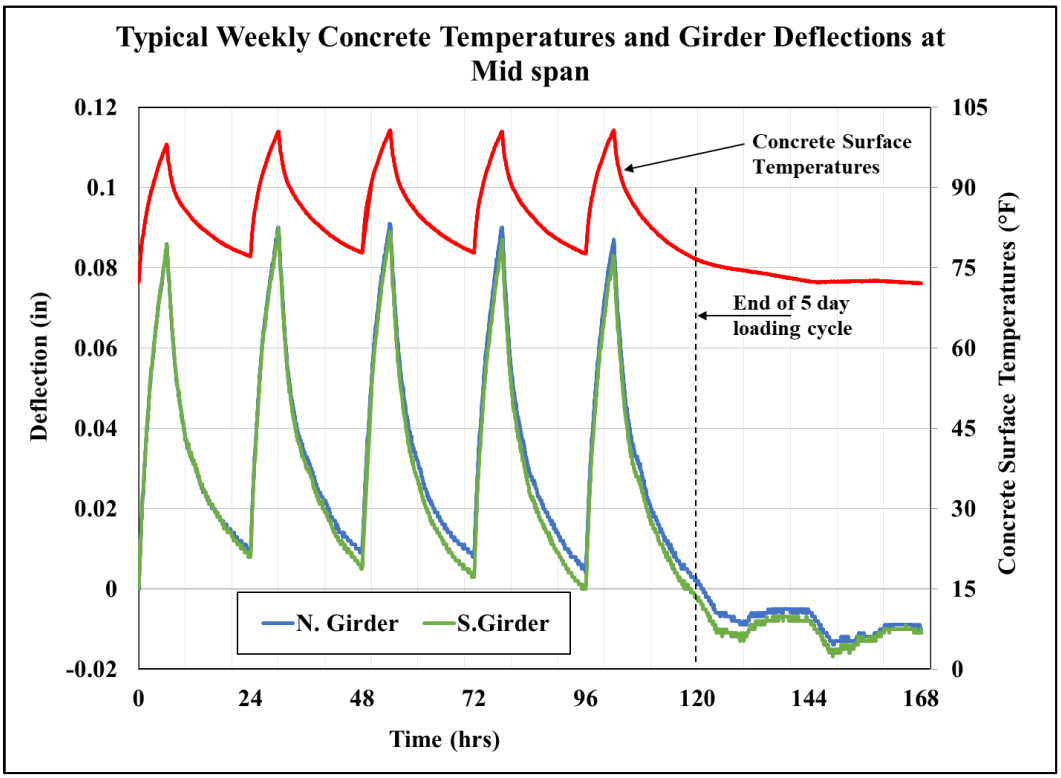

Figure 78. Concrete deck surface temperatures and Steel Girder mid-span deflections typical for a 5-day loading cycle

Figure 78 also shows that upward deflection exceeded 0.80 in. and approached 0.90 in. with each heating cycle. These data provide direct qualitative and quantitative evidence that upward deflections are caused by heating of the concrete deck slabs and that subsequent cooling of the concrete decks cause the bridge deflections to return downward to a neutral position.

Temperature data and midspan deflections are also reported in Table 18. In the tabulation, each temperature shown is the average temperature computed from the thermocouples at the respective location and also averaged recorded temperatures over 40 days of heat loading. Note that even

though slight variations in temperature and deflection are apparent from day 1 to day 5 of each 7 day weekly cycle, these data were averaged together to build Table 18.

Table 18. Measured Deflections, Temperatures and Thermal strains from LVDTs and Thermocouples set at the Bridge Midspan

Average Temperatures (°F) and upward deflections (in.) measured at Bridge Midspan during the heating cycle						
		0.0 hours	2.0 hours	4.0 hours	6.0 hours	12.0 hours
Midspan Deflections (in.)↑	N. Girder LVDT	0.00	0.043	0.066	0.081	0.025
	S. Girder LVDT	0.00	0.044	0.066	0.082	0.025
8 in. Concrete Deck Slab (°F)	T.O. Concrete Deck	75.7	89.1	95.0	99.4	84.5
	2 in. Depth	75.8	84.3	90.3	95.0	85.0
	Mid-Height	75.9	80.4	86.1	90.7	85.1
	6 in. Depth	75.7	78.0	83.2	87.6	84.6
	B.O. Deck	75.5	77.1	81.7	85.9	84.0
Steel W24x94 (°F)	T.O. Steel	75.4	75.6	77.3	79.7	78.4
	Mid-Ht +4 in.	74.0	74.5	75.5	77.1	76.4
	Mid-Height	73.4	74.1	74.7	76.2	75.6
	Mid-Ht – 4 in.	73.3	73.9	74.4	75.8	75.2
	B.O. Steel	73.4	73.5	73.5	74.6	74.5

Notes:
The reported temperatures are the average temperatures recorded for each of three thermocouples located at midspan (locations are shown in Figs 72 and 73), for each of the 40 days that heating was applied. All data were treated equally.

Thermal Strains in Concrete and Steel Girders

Figure 79 shows the concrete surface temperatures, and the steel strains from gages located near the top (NT/ST) and near the bottom (NB/SB) of the steel girders. The temperatures and strains plotted in Fig. 79 are taken from an average of values computed over the 8-week heating period. The NT/ST strain data are the averages of strain readings from gages located near the top on both the North (NT) and South (ST) girders. The NB/SB strain data are the averages from strain readings from gages located near the bottom on both the North (NB) and South (SB) girders.

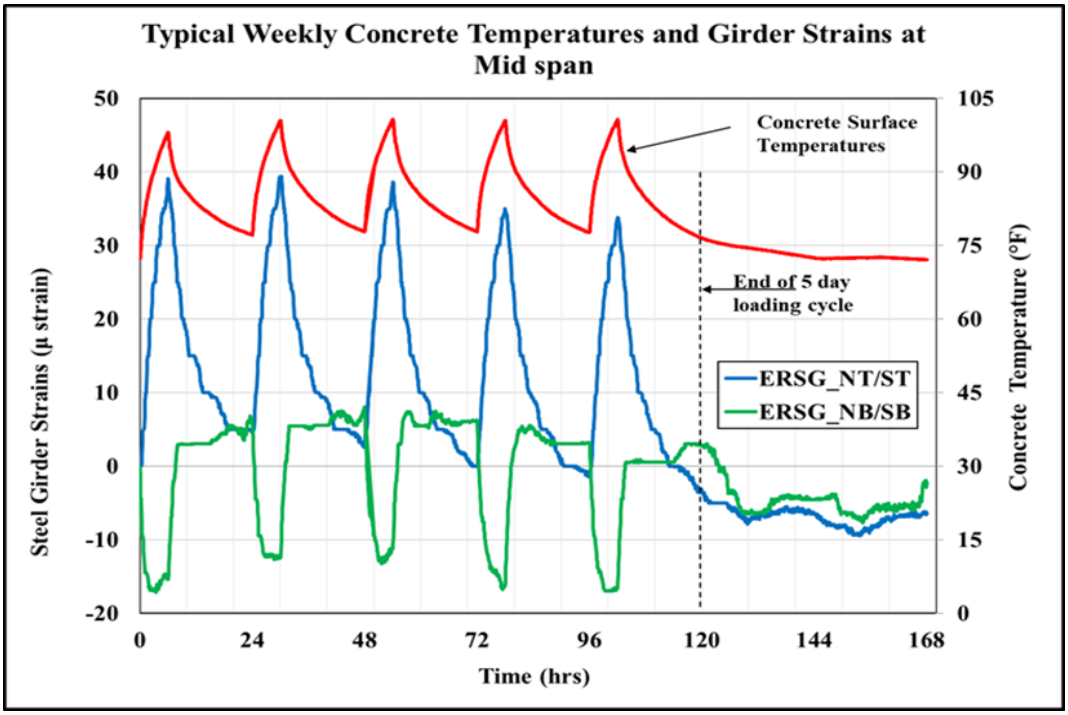

Figure 79. Concrete deck surface temperatures and Steel Girder strains typical for a 5-day loading cycle

It is observed from Fig 79, that with the increase in concrete temperatures at the deck surface, the top of the steel girders experienced tensile strains and the bottom of the steel girders experienced compressive strains. This strain pattern matches that for upward deformations. Averaging the peak strains over the 5 days of heating, the maximum tensile strain is approximately 34 $\mu\varepsilon$. Similarly, the average maximum compressive strain near the bottom of the girder is approximately 15 $\mu\varepsilon$. These strains infer a curvature of

$$\kappa = \frac{\big(34 - (-15)\big)x\ 10^{-6}}{16\ in.} = 3.06\ x\ 10^{-6}\frac{rad}{in}$$

The curvature, if applied over the 22 ft. of heat loading will result in an upward deflection of 0.066 in. which is within 17% of the measured deflections.

It is also seen that at the end of each loading cycle during the cooling phase of the 24 hrs. loading cycle, the strains in the steel girders returned to approximately zero. Small residual strains in the

steel girders are captured from the cyclic loading. During the weekend, after the end of 5 day loading cycle a slight variation in the steel strains can be observed. This corresponds well with the slight variations in the girder deflections from Fig. 78.

Measured and AASHTO Positive Vertical Temperature gradient

Figure 80 shows the average maximum temperatures measured at regular time intervals throughout the depth of the superstructure mid span. Temperatures were recorded at 5-minute intervals, but Fig. 80 charts the average temperature at 2 hr. intervals during the 6 hour. heating cycle. A total of 10 thermocouples were used to measure the temperature gradient throughout the depth of the cross section. Temperatures within the slab were measured using thermocouples embedded at 2 in. c/c spacing along the depth of the slab as shown in Fig. 74. The thermocouples and the data acquisition system allow us to build the temperature gradients at 2.0 hr. intervals. Figure 80 also displays steel girder temperatures that were measured from thermocouples placed at regular intervals through the depth of the girder. The data graphically shown in Fig. 80. are also reported Table 18. Figure 80 shows that slab temperatures increase over the 6-hour heating cycle, and that the maximum average concrete temperature (just under the surface) is approaching 100°F. Figure 80 also illustrates the 20°F temperature gradient that occurs with the 8 in. concrete deck after 6 hrs. of heating. Note also that temperature within the entire cross section increases, but that the steel temperatures are considerably smaller than concrete temperatures. The measured temperature gradient clearly exhibits non-linear temperature changes throughout the depth of the superstructure.

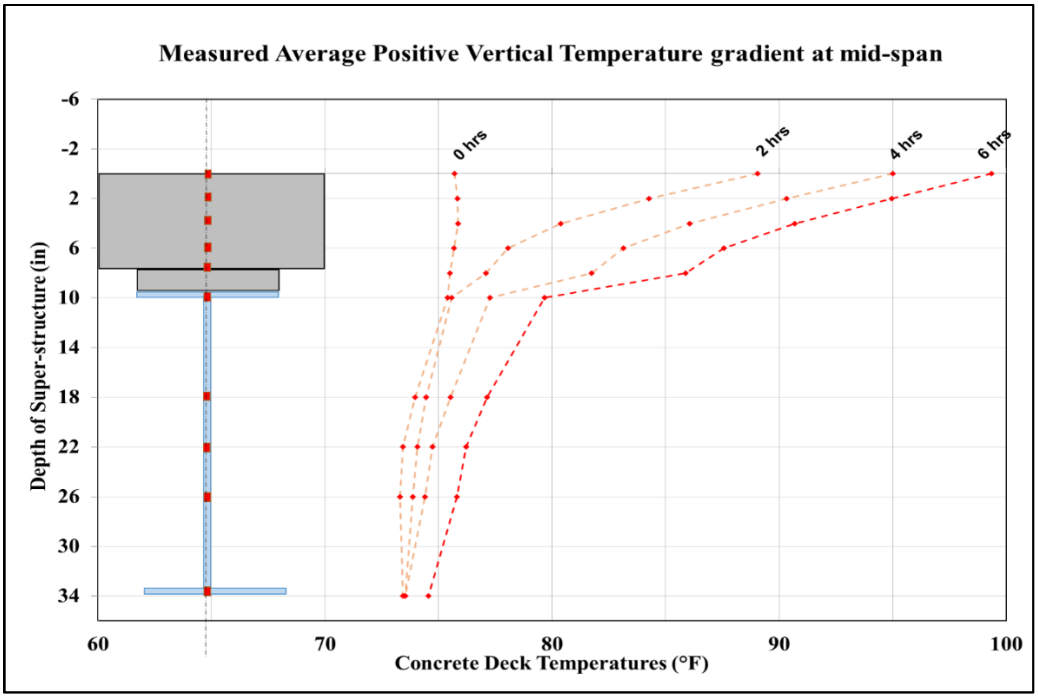

Figure 80. Measured Average Positive Vertical Temperature gradient at mid-span

A comparison between the measured and the AASHTO positive vertical temperature gradient is shown in Fig. 81. Bridges in Oklahoma are located in Region 2 of the AASHTO specification on temperature gradients. AASHTO defines the temperatures as T_1 = 46 ºF and T_2 = 12 ºF respectively. T_3 = 6.5 ºF was calculated to the top of the steel girder assuming a 1.5 in. haunch from interpolation of values shown in the AASHTO standards. These temperatures are not intended as absolute temperatures, but they are used as the basis for calculating the temperature gradient through the depth of the cross section.

In Fig. 81 the measured temperature gradient is "normalized" and overlaid with the AASHTO specified temperature gradient. For comparison purposes, both gradients have a temperature of 6.5°F at the T.O. Steel. From that temperature and at that location, the measured temperature gradient corresponds to a T_1 value of about 20 ºF, T_2 = 15 ºF and T_3 = 6 ºF. Although the measured T1 values are lower than the AASHTO standards the T2 and T3 values closely match that from the AASHTO specifications. The significant differences are that the design gradient

prescribes a larger temperature differential in the top four inches of the slab, but with a more modest temperature differential in the lower portions of the slab. In addition, it can be noted that AASHTO standards specify a constant temperature through the depth of the steel girder, whereas the measured temperatures in the steel girder has a slight variation of about 3 ºF between the top and bottom flanges.

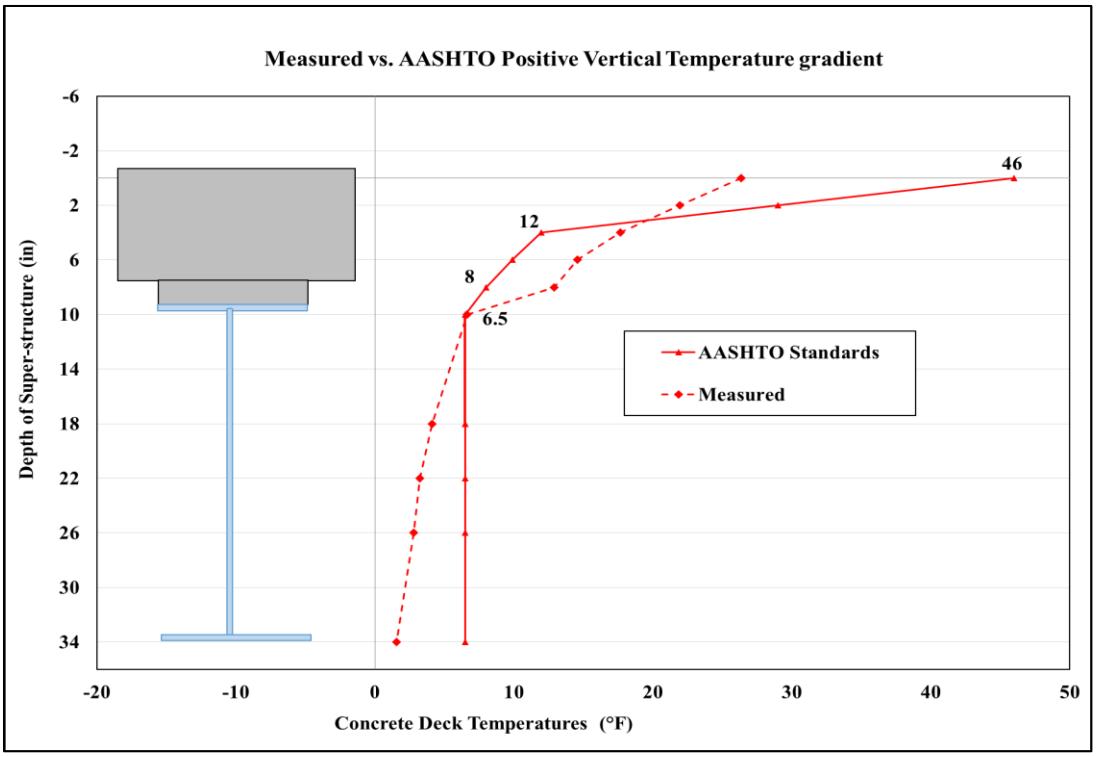

Figure 81. Comparison between the measured and AASHTO standard temperature gradient

Furthermore, please note that the concrete surface temperatures presented in Figs. 78 through 81 were taken from thermocouples located in near the surfaces but with a small layer of concrete between the thermocouple and air. These thermocouples were also located between heat lamps. A different thermocouple was exposed and laid on the surface of the concrete directly under a heat lamp. The maximum recorded temperature for this thermocouple was approximately 20 ºF greater than that recorded for other surface thermocouples. This would indicate that surface temperatures of 120 ºF are possible, but that the temperature gradient within the concrete would

be very steep. These additional readings seem to corroborate to some degree the design curves within the AASHTO specifications.

Thermal strains and stresses from Positive Vertical Temperature Gradient

Uniform changes in temperatures on bridges would lead to the development of only axial strains, where as a non-linear temperature gradient would result in flexural deformations, stresses, and moments throughout the depth of the cross section (Rojas 2014). In addition to this a large temperature difference between the concrete deck and the steel girder at the end of heating cycle may lead to larger magnitude of tensile stresses in the concrete deck (Subramaniam, Kunin et al. 2010).

Thermal strains and stresses imposed on the composite cross section can be computed from the measured thermal gradient using beam mechanics. Table 19 shows peak temperatures during the heating cycle, and the computed thermal strains and stresses throughout the depth of the cross section. Temperatures were measured directly from embedded or attached thermocouples. Heating of the bridge deck results in a temperature gradient on the composite cross section. As the slab expands it is restrained by the steel girder resulting in restrained compressive thermal strains and stresses across the depth of the cross section.

The restrained thermal strains ε and corresponding thermal stresses σ are determined from equations 6 and 7,

$$\varepsilon = \alpha\,(\Delta T) \qquad \text{Eq (6)}$$

$$\sigma_c = \varepsilon E_c \; or \; \sigma_s = \varepsilon E_s \qquad \text{Eq (7)}$$

where,

α = measured coefficient of thermal expansion of concrete, 5.69 10^{-6} / ºF

ΔT = change in temperature

E_c = 4240 ksi, the measured modulus of elasticity of concrete at 90 days, and

E_s = 29,000 ksi

The restrained thermal stresses are integrated over the depth of the cross section and are used to compute the equivalent restraining force $\boldsymbol{F_T}$, and its eccentricity $\boldsymbol{e_T}$. The analysis then removes the restraining force and computes the effective strains and stresses that are caused by the removal of the restraint. In turn, both axial strains and stresses plus bending strains and stresses are produced within the cross section. The final stress distribution on the composite cross section are calculated by superimposing the restrained temperature strains and stresses to the strains and stresses produced from the eccentric axial restraint. Our analysis used the concrete modulus measured at 90 days, 4240 ksi.

The restrained thermal stresses are calculated using the modulus of elasticity of concrete and steel respectively. The axial strain and bending strains are calculated using Eq. 8 and 9

$$\varepsilon_{axial} = \frac{F_T}{A_{tr} * E_c} \qquad \text{Eq (8)}$$

$$\varepsilon_{bending} = \frac{F_T * e_T * y}{A_{tr} * E_c} \qquad \text{Eq (9)}$$

where,

F_T = equivalent axil force from temperature restraint

A_{tr} = Area of the transformed cross section

E_c = measured modulus of elasticity of concrete at 90 days, 4240 ksi

e_T = Eccentricity of the force F_T

y = distance from the neutral axis of the composite cross section

The equivalent axial tensile force from temperature restraint was calculated to be 321.1 kips and the equivalent moment was 1145 kip-in.

As an example, consider the stresses and strains at the top of the concrete deck, which in Table 19 shows a measured temperature of 99.4°F at a vertical distance of 33.81 in. from the bottom of the steel. 99.4°F is a net temperature change of 26.4°F from the baseline temperature of 73°F. When multiplied by the measured coefficient of thermal expansion of 5.69E-6/°F, the 26.4°F temperature change produces a temperature strain of ***150.22 με***. When restrained and multiplying times the measured elastic modulus of 4240 ksi, a temperature stress (compressive) of -0.637 ksi is produced for concrete at the top of the cross section. In order to constrain the whole cross section, the temperature stresses are integrated over the depth of the cross section. From this calculation the restraining axial force is computed along with the restraining bending moment. As shown in Table 19, the equivalent axial force from temperature restraint was calculated to be 321.1 kips and the equivalent moment was 1145 kip-in. In other words, a restraining axial compression of 321.1 kips is required at an eccentricity of 3.566 in. from the composite cross section's center of gravity. These values are shown in Table 19 and displayed in the charts found in Fig. 82.

To produce equilibrium in the cross section, an opposite force is applied to the cross section with equal magnitude to the restraining force but at the same eccentricity. This produces both axial strains and stresses and bending strains and stresses as shown in Table 19 and illustrated in Fig. 82. At the top of the concrete deck, the application of the eccentric axial force produces a net tensile strain of 86.55 με and a bending strain of 31.29 με. These strains are superimposed on the compressive strains caused when the cross section is restrained, and the concrete strain at the top

of the cross section is computed to be -32.38 με or 32.38 με compression. Multiplying the strain times the elastic modulus of concrete gives a net compressive stress of 137 psi, or -0.137 ksi.

In summary as the concrete heats, it expands, and that expansion is resisted by the composite cross section. As a result, the concrete "sees" a net compressive strain of about 32 $\mu\varepsilon$ at the top of the slab. Toward the bottom of the deck slab, the concrete temperatures are lower during the heating cycle than at the top of the concrete, but the whole cross section participates in resisting temperature strains. As a consequence, the bottom of the slab and the top of the steel girder are subjected to tensile strains. The process of calculation is followed for every layer and interpolated between thermocouples. It is evident that the nonlinear temperature gradient from heat loading creates a multilinear strain and stress gradient across the depth of the cross section. The final residual strains and stresses on the composite cross section at maximum temperatures are calculated and shown in Table 19 and Figure 82. One can see that during the heating cycle, compressive stresses are produced at both the top of the concrete deck and at the bottom of the steel girder. Tensile stresses are produced toward the neutral axis. For the average recorded concrete maximum surface temperatures of 99.4 ºF, the maximum concrete compressive stress was 0.137 ksi at the top of the cross section and the maximum concrete tensile stress was 0.178 ksi at the bottom of the slab. It is evident that when this maximum tensile stress exceeds the tensile strength of the slab cracks can develop within the deck slab. From these computations, the stresses reported would be insufficient to cause cracking of the bridge deck under normal conditions.

Additionally, the calculated final strains produce a theoretical curvature of -3.96 x 10^{-6} rad/in. through the cross section over the heated length of the bridge. Using this curvature over the interior 22 ft. of the span where heat loading occurred, an upward deflection of 0.087 in. is computed. This value compares favorably to the measured average girder deflections of 0.082in. Since the two values for deflections are very close to one another, this indicates that the analysis

technique is reliable for computing strains and stresses in the cross-section subject to heat loading and significant temperature gradients. It is noted that hardened concrete material properties evolve daily, and the change in strength, elastic modulus and creep coefficient may produce small effects on results from computational models. However, these effects will remain small during out testing period, and our analysis did not include effects of creep nor time-dependent changes in elastic modulus. Shrinkage is also not considered in the analysis.

Additionally, the same analysis using the prescribed AASHTO Temperature Gradient found in AASHTO 3.12.3 was performed. The AASHTO temperature gradient prescribes a significantly larger temperature gradient, than that measured in this experimental program, with approximately 34 ºF change in temperature prescribed in the top 4 in. of the slab. By applying these thermal strains to the cross section, higher strains and stresses are imposed on the cross section. These are reported in Table 20 and in Figure 83. Notably, the AASHTO temperature gradient causes the concrete stresses to increase significantly, and the maximum tensile stress in the concrete deck is increased by 30% over that found in the experimental work. One can conclude that steeper thermal gradients with higher maximum temperatures will produce larger stresses within the cross section and greater tension in the concrete deck slabs, which turn, could increase the likelihood of cracking. The computed upward deflections using AASHTO temperature gradient was about 0.089 in which is comparable to the measured average upward deflection of 0.082 in.

Table 19. Computations for Average Thermal Stresses and Strains in the Cross Section due to Heating Loads

	Vertical Distance from the Bottom of Steel	Average Peak Temperatures at 6.0 hr. Heating	Temperature Strain (Restrained)	Axial Strain to Relieve Restraint	Bending Strain to Relieve Restraint	Axial + Bending Strains	Residual Strains on Composite Bridge Cross Section at Max.Temperatures	Residual Stresses on Composite Bridge Cross Section at Max.Temperatures
	y (in)	°F	in/in. 10^{-6}	in/in. 10^{-6}	in/in. 10^{-6}	in/in. 10^{-6}	in/in. 10^{-6}	ksi
T.O. Deck	33.81	99.40	-150.22	86.55	31.29	117.84	-32.38	-0.137
2 in.	31.81	95.00	-125.18	86.55	23.36	109.91	-15.27	-0.065
Mid-Height Deck	29.81	90.70	-100.71	86.55	15.44	101.99	1.27	0.005
6 in.	27.81	87.60	-83.07	86.55	7.51	94.06	10.99	0.047
B.O. Deck	25.81	85.90	-73.40	86.55	-0.41	86.14	12.74	0.054
B.O. Haunch	24.31	79.70	-38.12	86.55	-6.35	80.19	42.07	0.178
T.O. Steel	24.31	79.70	-43.55	86.55	-6.35	80.19	36.64	1.063
T.O. Web	23.44	79.42	-41.74	86.55	-9.82	76.73	34.99	1.015
Mid-Height + 4 in.	16.16	77.10	-26.65	86.55	-38.67	47.88	21.23	0.616
Mid-height Steel	12.16	76.20	-20.80	86.55	-54.52	32.03	11.23	0.326
Mid-Height - 4 in.	8.16	75.80	-18.20	86.55	-70.37	16.18	-2.02	-0.059
B.O. Web	0.88	74.73	-11.24	86.55	-99.22	-12.67	-23.90	-0.693
B.O. Steel	0.00	74.60	-10.40	86.55	-102.68	-16.13	-26.53	-0.770

Equivalent Axial Force from Temperature Restraint, F_T = 321.1 kips
Equivalent Moment from Temperature Restraint, $F_T * e_T$ = 1145 k-in.
Notes:
Stresses and Strains are computed fromm the following measured values or commonly used values:

1. Temperatures through the depth of the cross seciton were measured using embedded and external thermocouples.
2. The Coefficient of Thermal Expansion (CTE) for concrete was measured to be 5.69x10-6/°F ; for Steel, CTE = 6.50x10-6/°F.
3. The measured elastic modulus of concrete at 90 days was $E_{c,90}$ = 4240 ksi; for steel, E_s = 29,000 ksi.

Table 20. Computations for average thermal Stresses and Strains from AASHTO Temperature gradient

	Vertical Distance from the Bottom of Steel	Average Peak Temperatures at 6.0 hr. Heating	Temperature Strain (Restrained)	Axial Strain to Relieve Restraint	Bending Strain to Relieve Restraint	Axial + Bending Strains	Residual Strains on Composite Bridge Cross Section at Maximum Temperatures	Residual Stresses on Composite Bridge Cross Section at Maximum Temperatures
	y (in)	°F	in/in. 10-6	in/in. 10-6	in/in. 10-6	in/in. 10-6	in/in. 10-6	ksi
T.O. Deck	33.81	119.00	-261.74	94.51	32.22	126.73	-135.01	-0.572
2 in.	31.81	102.00	-165.01	94.51	24.06	118.56	-46.45	-0.197
Mid-Height Deck	29.81	85.00	-68.28	94.51	15.90	110.40	42.12	0.179
6 in.	27.81	83.00	-56.90	94.51	7.74	102.24	45.34	0.192
B.O. Deck	25.81	81.00	-45.52	94.51	-0.42	94.08	48.56	0.206
B.O. Haunch	24.31	79.50	-36.99	94.51	-6.54	87.96	50.98	0.216
T.O. Steel	24.31	79.50	-42.25	94.51	-6.54	87.96	45.71	1.326
T.O. Web	23.44	79.50	-42.25	94.51	-10.11	84.39	42.14	1.222
Mid-Height + 4 in.	16.16	79.50	-42.25	94.51	-39.82	54.69	12.44	0.361
Mid-height Steel	12.16	79.50	-42.25	94.51	-56.14	38.37	-3.88	-0.113
Mid-Height - 4 in.	8.16	79.50	-42.25	94.51	-72.46	22.05	-20.20	-0.586
B.O. Web	0.88	79.50	-42.25	94.51	-102.16	-7.66	-49.91	-1.447
B.O. Steel	0.00	79.50	-42.25	94.51	-105.73	-11.23	-53.48	-1.551

Equivalent Axial Force from Temperature Restraint, F_T = 350.6 kips
Equivalent Moment from Temperature Restraint, F_T*e_T = 1179 k-in.
Notes:
Stresses and Strains are computed fromm the following measured values or commonly used values:

1. Temperatures through the depth of the cross seciton were measured using embedded and external thermocouples.
2. The Coefficient of Thermal Expansion (CTE) for concrete was measured to be 5.69x10-6/°F ; for Steel, CTE = 6.50x10-6/°F.
3. The measured elastic modulus of concrete at 90 days was $E_{c,90}$ = 4240 ksi; for steel, E_s = 29,000 ksi.

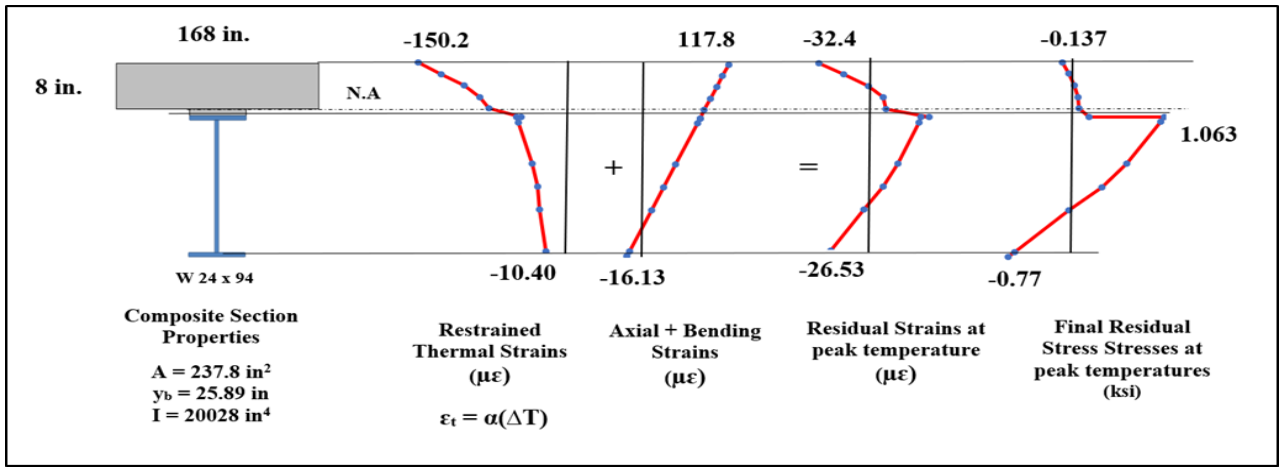

Figure 82. Average Thermal Strain and Stress gradients from measured positive temperature gradient across the depth of the prototype bridge

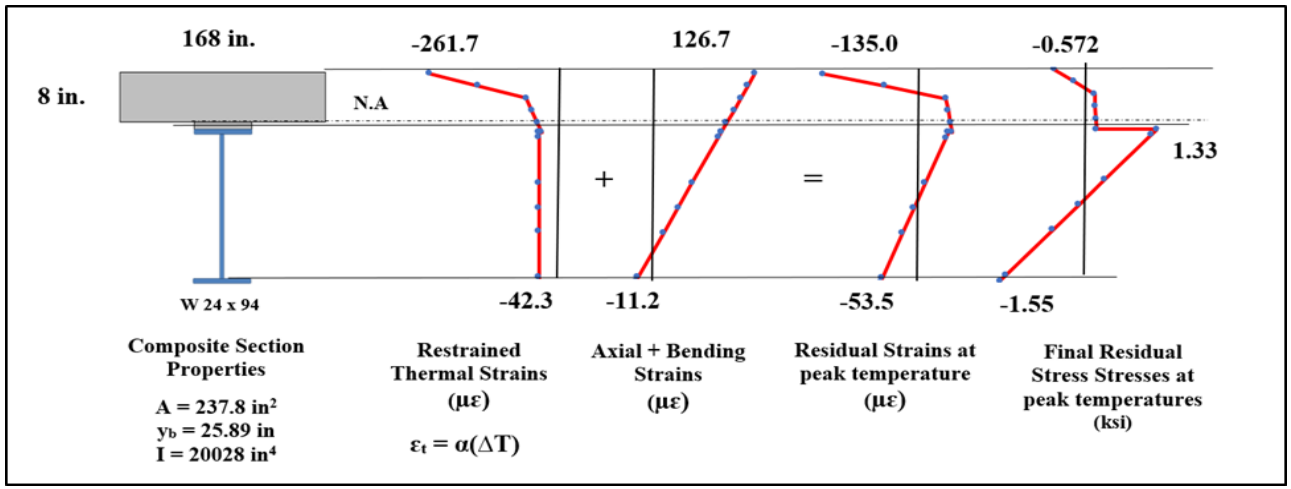

Figure 83. Average Thermal Strain and Stress gradients from AASHTO temperature gradient

Correlation of measured vs. Computed final thermal strains

Figure 84 shows the correlation between the measured and computed residual thermal strains on the composite cross- section from the measured thermal gradient on the laboratory prototype bridge deck. The measured compressive strain of -34.4 με represents the average recorded values from the concrete surface strain gauges located at the mid span location of the bridge deck. This is in very close correlation to the computed concrete strain of -32.4 με calculated at the top of the cross section. It was noted that the concrete surface strains recorded at the West and East sides of the bridge deck were lower due to their position away from the heat lamps and closer to the edge of the heat loading area of the bridge deck.

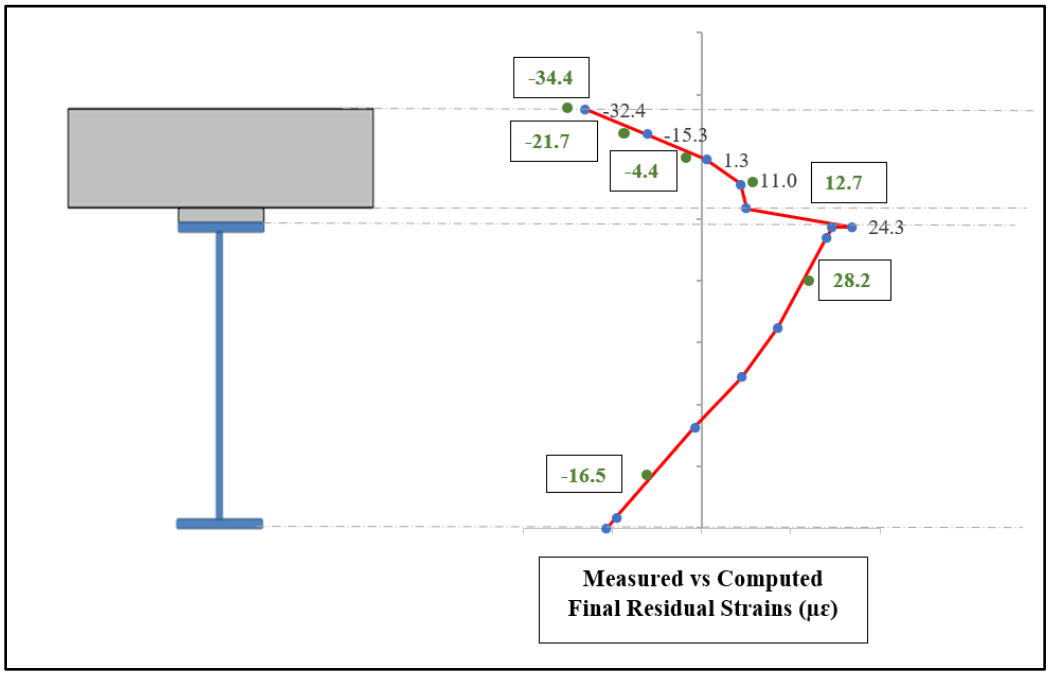

Figure 84. Correlation of Measured vs. Computed final strains

The concrete strains recorded within the concrete deck at 2 in, 4 in, and 6 in from the top of the section were measured using the VWSGs Type 1. We can notice that some of the measured strains are slightly higher than the computed strains. This may be due to the slight variations in concrete material properties of the deck slab. It was noted that the strain recorded at the mid

height of the concrete deck by VWSG Type 2 located along the girder line recorded slightly higher strains. This variation in strains may be due to the shear lag phenomenon caused due to the uneven distribution of the strains in the concrete located away from the girders. From figure we can also see that the maximum average strains measured on the steel girders from the boded foil strain gauges are in very close correlation with the computed strains on the composite cross section.

Conclusions

1. The heating of the bridge deck for 6 hrs. produced maximum concrete surface temperatures of approximately 100ºF and temperature gradient within the concrete decks of approximately 20°F. The cooling period of 18 hrs. allowed the concrete temperatures to return approximately to ambient temperature.

2. The data shows that nonlinear temperature gradient from heat loading causes multilinear stresses across the depth of the cross section, and that final strains and stresses for are not linear but rather are a summation of non-linear strains occurring from temperature effects added to the linear effects from the restraint of the cross section.

3. Data show heating of the concrete deck causes upward deflections of the steel girder-composite concrete bridges. Measured values of upward deflection were 0.082 in. in the 38.83 ft. span. The upward deflection is 0.0176% of the span length. Likewise, the data show that the bridge deflected downward as the concrete cooled.

4. Detailed analysis using measured temperatures during the heating cycle resulted in a computed value for upward deflection of 0.087 in. This compares to the measured value of 0.082 in. The two values are within 6% of one another. This agreement between in computed vs. measured deflections shows that the analysis using measured coefficients of

thermal expansion and measured values for elastic modulus produce reliable results when computing stresses, strains and deformations for composite bridges subjected to thermal gradients. Analysis also shows that the computed value for curvature is -3.965 x 10^{-6} rad/in. Computational analysis using beam mechanics along with measured material properties can be used to evaluate the thermal strains and stresses developed throughout the composite cross-section.

5. Heat loading from radiant sunshine produces a "positive" temperature gradient where higher temperatures exist at the top surface of the deck slab. The temperature gradient from heat loading was approximately 20°F within the 8 in. deck slab plus the 1.5 in. haunch.

6. The radiant heat loading produces compressive stresses at the top of the concrete bridge deck and tensile stresses at the bottom of the concrete deck. Our analysis shows that the maximum concrete compressive stress was 137 psi and the maximum concrete tensile stress was 178 psi when subjected to the heat loading. This compares to measured tensile strength (28d) of the concrete which was 571 psi.

7. The average CTE value from concrete cylinder samples was found to be about 5.69 E-6/°F (9.1x10^{-6} /ºC) and the elastic modulus was found to be 4240 ksi.

8. The measured temperature gradient follows the general trend for the AASHTO standard Temperature gradient. However, our heat loading produced a maximum temperature gradient of 20F through the depth of the slab and haunch whereas the AASHTO temperature gradient will produce 36F through the top four in. of the concrete deck slab. The AASHTO produces a temperature differential of 40 ºF between the top of the slab and the steel girder whereas our measured values are only 25 ºF differential.

9. Despite differences in the design temperature gradient prescribed by AASHTO, the overall beam curvatures and deflections remained nearly the same. This is because the total temperature restraining bending moment for AASHTO closely matched the total restraining bending moment from measured values, despite the fact that AASHTO prescribes a markedly steeper temperature gradient. Evidence for this is found in the computed restraining forces found in Tables 19 and 20. From measured temperatures the required restraining moment was 1145 k-in. whereas the restraining moment required for the AASHTO temperature gradient is 1179 k-in. Because of this, secondary effects produced in multi-span bridges when using the AASHTO temperature gradient will be similar to those produced from temperatures and temperature gradients similar to that applied in our experiments.

10. AASHTO standards specify a constant temperature through the depth of the steel girder, whereas the measured temperatures in the steel girder has a slight variation of about 5 ºF between the top and bottom flanges.

CHAPTER VII

SUMMARY AND CONCLUSIONS

Summary

This dissertation seeks to understand the mechanical properties of concrete, and its interaction with steel bridge girders with the purposes of deepening our understanding of the behavior of steel girder bridges made composite with concrete slabs. This research program identifies and documents several causes for undesirable elevation profiles and recommends design and construction practices to help mitigate problems associated with unwanted deformations and extend the life span of bridges. The research demonstrates that the cumulative effect due to volumetric changes in concrete, temperature effects and poor bracing system can diversely affect the ride quality, cause deck cracking and excessive deflections, decrease durability and reduce long-term performance of steel girder bridges made composite with concrete deck slabs. Forensic investigations were performed on three newly rehabilitated bridges in Oklahoma. The investigations provided evidence that poor elevation control and improper construction practices resulting in unevenness in bridge deck elevations and thin bridge decks. Additional laboratory testing on overhang brackets confirmed that the commercially available brackets used for bridge rehabilitations to support the cantilever portions of the concrete bridge decks are insufficient to provide the elevations control resulting in thin bridge decks and undesired deflections.

A full-scale prototype bridge was built and instrumented at the Bert Cooper Engineering Laboratory on the campus of Oklahoma State University in Stillwater, OK USA. A full-scale model of the bridge allows to capture the absolute values of the original time dependent properties of concrete deck that cannot be completely captured using a small-scale model. Early age deflections of the bridge were measured, as were concrete temperatures, concrete strains, steel girder strains and inclinations of the steel girders at ends. Data were analyzed and their relationship to time dependent concrete properties are established. The results indicated that the concrete strains associated with volume change, including both temperature-related strains and shrinkage strains, are large enough to be considered as one possible cause for adverse ride quality and unwanted deformations in steel girder bridge. Analytical computational models were developed to predict the thermal and shrinkage indices strains, stresses and deformations due to volume changes in the slab at early ages.

Concrete strains and temperatures measured from the VWSGs and thermocouples in the early ages during and immediately after bridge deck cast provided a good understanding of the early age strains developed in the concrete deck. The early age thermal stresses due to heat of hydration were estimated from the measured material properties including the modulus of elasticity and CTE of concrete. The measure unrestrained shrinkage strains and modulus of elasticity of concrete at various ages was used to predict the stresses and overall bridge deformations. The calculated deflections from analytical models found good agreement with measured overall deflections.

Thermal loading was applied to the bridge deck of a full-size prototype bridge built in laboratory conditions. The research principally used the measured concrete temperatures from thermocouples during heat load testing to predict and validate the thermal strains, stresses and deflections in bridge decks. Uniform heating of the deck caused a temperature gradient within the bridge deck resulting in differential strains and stresses at various location of the bridge deck. The

results from the real time thermal loading on the prototype bridge decks showed that the temperature gradients produced internal thermal strains and stresses that directly resulted in bridge deformations. Analytical computational models were developed to estimate the thermal strains and stresses from measured thermal gradient and AASHTO temperature gradient on the prototype bridge deck. The measured material properties including the modulus of elasticity of concrete and CTE of concrete were used to in the models to predict the thermal strains and stresses on the prototype bridge. The measured strains from the VWSGs and bonded foil strain gages were found to have close correlations to the strains computed using the analytical model. The computed deflections using both measured thermal gradient and AASHTO Temperature gradient found good agreement with the measured overall deflections on the prototype bridge

The structural monitoring system used in this research program combines sensors from diverse technologies into a seamless system using a single database and user interface system allowing for real time data acquisition and analysis. The prototype bridge was instrumented and installed with an array of sensors to monitor both the short term and long term performance of the bridge. Synthesis of data collected from the sensors along with analytical computational models that were developed using the measured constitutive properties of concrete validated the methods for structural monitoring. This research program provides a practical means of monitoring bridge performance and offers a good experience for implementation and structural monitoring for both laboratory and field bridges.

Conclusions

The following conclusions are drawn from Chapter III

1. VWSGs are highly recommended for measuring strains within concrete due to their ease of installation, long term stability and maximum resistance to moisture.

2. VWSGS embedded in the concrete are efficient in capturing the early age concrete strains and temperatures in the concrete deck due to heating of the deck during hydration and subsequent cooling and shrinkage of concrete.

3. VWSGs can successfully monitor both static and dynamic responses of structures at one time which makes them the utmost sensors for bridge monitoring systems.

4. The durability and accuracy of thermocouples make them ideal and economic sensors to measure temperatures in both concrete and in steel girders.

5. Thermocouple sensors embedded in the concrete and attached to the steel girders are efficient in capturing the thermal gradient developed across the composite cross section of the prototype bridge. Measured thermal gradient from the thermocouples can be used to predict the thermal strains, stresses and deflections in the prototype bridge.

6. The ease of installation of LVDT sensors makes it ideal for laboratory experimentation where they require a fixed reference point to be mounted from.

7. Inclinometers serve as ideal surrogates for LVDT sensors to measure bridge deformations in field conditions where a fixed reference point is not required.

8. Inclinometers provides an opportunity to measure angles of rotation along any three orthogonal axes at a time which makes the sensor superior to other commercially available deflection measurement technologies.

9. The datalogger and interface systems used in this research are proven to provide reliable data retrieval and monitoring systems for both short term and long-term monitoring of bridges.

10. The reliability and ruggedness of the Campbell Scientific Datalogger along with its capability to accommodate a variety of sensors from different manufacturers makes it an ideal both laboratory and remote applications.

11. Continuous monitoring of remote bridge structures is made possible through interfacing with local network and remote cellular modem.

12. A photovoltaic solar panel was successfully installed in the field bridge to provide a continuous and uninterrupted power supply for the instrumentation systems.

The following conclusions are drawn from Chapter IV

1. **Forensic investigations were performed on three newly rehabilitated bridges in Oklahoma provided evidence that poor elevation control and improper construction practices resulted in poor ride quality in bridges.**

2. Measured roadway elevations showed measurable and significant "dips" in elevation profiles for two of the three bridges examined. Elevation profiles indicate a pattern where driving surfaces are significantly lower at the mid-spans of recently rehabilitated steel girder bridges. Bridge deck elevations "dipped" about 1.0 in. and as much as 1.75 in. in some bridge profiles.

3. Measured roadway elevations confirm that the top surfaces of the bridge decks were screeded and finished in accordance with the 1 percent super-elevation required in construction documents.

4. Under-slab elevations reflect the same 1 percent super-elevations measured on the bottom sides of the bridge decks from CL to the exterior girder; however, from the exterior girder outward and including cantilevered formwork, the under-slab elevations indicate a

significantly steeper slope on the bottom surfaces of the slab. In the case of the SH 86 bridge, slopes exceeding 4.0 percent were measured on the bottom side of the deck slab.

5. Bridge Deck thicknesses for SH 14 Woods Co. Bridge and SH 86 Payne Co. Bridge were significantly thinner than the 8 in. thickness required by contract documents. On the SH 14 Bridge, deck thickness as little as 7.25 in. was measured. On the SH 86 Bridge, a slab thickness of 0.57 ft. or 6-7/8 in. was measured at midspan of the northern-most span.

6. In the case of SH 14, Eagle Chief Creek Bridge and of SH 86, Stillwater Creek Bridge, the formwork that was cantilevered outside of the exterior girder, and braced against the exterior girder, was not properly supported nor braced during construction activities. Significant "dips" in driving surface elevations measured on both bridge decks. Significantly severe slopes measured on the bottom sides of bridge decks, in areas that were supported by cantilevered formwork, which was in turn supported bracing.

7. For SH86 Bridge, the top side super-elevation from CL to Guardrail was 0.16 ft (2.0 in. on the northbound side, and 0.11 ft (1.375 in. on the southbound side. This compares to the under-slab elevation change from CL to Slab Edge of 0.32 ft. (3.8 in., northbound) and 0.29 ft. (3.5 in., southbound). These elevation differences directly correspond to "dips" in roadway elevations in excess of 1 in. and in thin bridge decks.

8. **Laboratory testing showed that poorly braced or inadequate overhang bracing systems cause excessive deformations in bridge overhangs and can affect the overall ride quality of bridge girders.**

The following conclusions are drawn from Chapter V

1. **Concrete strains and temperatures measured from the VWSGs and thermocouples in the early ages during and immediately after bridge deck cast provided a good understanding of the early age strains developed in the concrete deck.**
2. Data show heating of the concrete deck placement at early ages causes upward deflection of the steel girder-composite concrete bridges. Likewise, the data show that the bridge deflected downward as the concrete cooled. Data also show that differential shrinkage through the depth of the deck cause permanent variations in normal strain through the depth of the concrete deck.
3. Midspan deflection caused by the weight of fresh concrete was measured at 0.38 in. on one girder and 0.40 in. on the other. This deflection closely matched the beam theory computation of 0.42 in.
4. Upward deflection caused by the elevated curing temperature of the concrete deck was approximately 0.071 in. Maximum upward deflection occurred at approximately 12.0 hrs. after concrete placement started where as concrete temperatures occurred at approximately 14.0 hrs.
5. Concrete reached its ambient temperature at approximately 96 hrs. after deck placement. The overall midspan deflection at 96 hrs. was 0.48 in. downward on one girder and 0.50 in. on the other. In approximate terms, the total deflection is caused by two factors: 0.38 in. of downward deflection can be attributed to self-weight with slab cooling and shrinkage accounting for the remaining an additional 0.1 in.
6. Concrete shrinkage and measured deflections of the full-size prototype beam indicate that shrinkage of concrete contributes to permanent downward deflections in composite bridge girders. The amount of measured permanent deflection attributed to shrinkage is approximately 0.1 in. at 28 days.

7. Early age temperatures in concrete correlates with the strains and deflections in the prototype beam. The increase in concrete temperature due to heat of hydration of cement has a significant effect on concrete strains. Concrete thermal strains increase with increasing temperatures causing the beam to deflect upward slightly.
8. The research indicated that wet curing time of bridge deck significantly reduced the rate of shrinkage of concrete, thereby reducing excessive deflections and helping to mitigate the formation of cracks in the bridge deck. It was observed that shrinkage strains and related downward bridge deformations accelerated after wet curing was removed at 14 days.
9. Despite the compression stresses developed in concrete due to peak hydration temperatures, the stresses are quickly transformed to tensile stresses during the cooling cycle.
10. Simple computational approach can be used to calculate thermal and shrinkage induced stresses in composite bridge girders.

The following conclusions are drawn from Chapter VI

1. The heating of the bridge deck for 6 hrs. produced maximum concrete surface temperatures of approximately 100ºF and temperature gradient within the concrete decks of approximately 20°F. The cooling period of 18 hrs. allowed the concrete temperatures to return approximately to ambient temperature.

2. The data shows that nonlinear temperature gradient from heat loading causes multilinear stresses across the depth of the cross section, and that final strains and stresses for are not linear but rather are a summation of non-linear strains occurring from temperature effects added to the linear effects from the restraint of the cross section.

3. Data show heating of the concrete deck causes upward deflections of the steel girder-composite concrete bridges. Measured values of upward deflection were 0.082 in. in the 38.83 ft. span. The upward deflection is 0.0176% of the span length. Likewise, the data show that the bridge deflected downward as the concrete cooled.

4. **The measured material properties including the modulus of elasticity of concrete and CTE of concrete were used to in computational models to predict the thermal strains and stresses on the prototype bridge**

5. Detailed analysis using measured temperatures during the heating cycle resulted in a computed value for upward deflection of 0.087 in. This compares to the measured value of 0.082 in. The two values are within 6% of one another. This agreement between in computed vs. measured deflections shows that the analysis using measured coefficients of thermal expansion and measured values for elastic modulus produce reliable results when computing stresses, strains and deformations for composite bridges subjected to thermal gradients. Analysis also shows that the computed value for curvature is -3.965×10^{-6} rad/in. Computational analysis using beam mechanics along with measured material properties can be used to evaluate the thermal strains and stresses developed throughout the composite cross-section.

6. The radiant heat loading produces compressive stresses at the top of the concrete bridge deck and tensile stresses at the bottom of the concrete deck. Analysis shows that the maximum concrete compressive stress was 137 psi and the maximum concrete tensile stress was 178 psi when subjected to the heat loading. This compares to measured tensile strength (28d) of the concrete which was 571 psi.

7. The average CTE value from concrete cylinder samples was found to be about 5.69 E-6/°F (9.1×10^{-6} /ºC) and the elastic modulus was found to be 4240 ksi.

8. The measured temperature gradient follows the general trend for the AASHTO standard Temperature gradient. However, the heat loading produced a maximum temperature gradient of 20 ºF through the depth of the slab and haunch whereas the AASHTO temperature gradient will produce 36 ºF through the top four in. of the concrete deck slab. The AASHTO produces a temperature differential of 40 ºF between the top of the slab and the steel girder whereas the measured values are only 25 ºF differential.

9. Despite differences in the design temperature gradient prescribed by AASHTO, the overall beam curvatures and deflections remained nearly the same. From measured temperatures the required restraining moment was 1145 k-in. whereas the restraining moment required for the AASHTO temperature gradient is 1179 k-in. Because of this, secondary effects produced in multi-span bridges when using the AASHTO temperature gradient will be similar to those produced from temperatures and temperature gradients similar to that applied in our experiments.

10. AASHTO standards specify a constant temperature through the depth of the steel girder, whereas the measured temperatures in the steel girder has a slight variation of about 5 ºF between the top and bottom flanges.

11. The computed deflections using both measured thermal gradient and AASHTO Temperature gradient found good agreement with the measured overall deflections on the prototype bridge

12. The measured strains from the VWSGs and bonded foil strain gages were found to have close correlations to the strains computed using the analytical model.

Recommendations

1. The contract documents should specify that the contractor is responsible for means and methods of supporting bridge decks during construction.

2. The contract documents should specify that the contractor is responsible for maintaining limits on formwork and bracing deflections during construction.

3. The contract documents should specify that the contractor is responsible for roadway elevation profiles and deck slab thicknesses.

4. The Transportation Official's drawings and specifications should remove all references to prescriptive information regarding means and methods for deflection controls.

5. It is recommended that the Transportation Official establish a tolerance limit on roadway elevation profiles, and that these elevation profile requirements should be enforced through bonus/penalty contract language.

6. It is recommended that the Transportation Official establish tolerance limits and performance criteria for bridge deck thicknesses, and that these bridge deck thickness requirements should be enforced or promoted through bonus/penalty contract language.

7. Bridge overhang lengths should not exceed the limits stated in the overhang bracket manufacture's manual respective to the type and depth of girders used.

8. For shallow girders. the slab overhang length beyond the centerline of the exterior girders should not exceed the length stated in the bracket manufacturer's manual.

9. Field engineers should be assigned to verify that the brackets conform to the girder configurations and any faulty brackets should be replaced.

REFERENCES

209R-92, A. (1992). ""Prediction of Creep, Shrinkage, ans Temperature Effects in Concrete Structures." *ACI 209R-92*, Reported by ACI Committe 209.

Abdelmeguid, I. (2015). "Shrinkage induced deformations in composite steel and concrete bridges." B. W. Russell, J. Hartell, and T. Ley, eds., ProQuest Dissertations Publishing.

Abdelmeguid, I. S. (2016). "Shrinkage Induced Deformations in Composite Steel and Concrete Bridges." B. W. Russell, T. M. Ley, and J. Hartell, eds.

Adams, J. S., Ramirez, G., and Browning, J. (2005). "Field Instrumentation and Monitoring of Kansas Department of Transportation Fiber Composite Bridge for Long-Term Behavior Assessment."

Alexander, S. (2003). "Concrete shrinkage affects composite steel beams." *New steel construction*, 11(3), 22-23.

American Association of State, H., and Transportation, O. (2010). *AASHTO LRFD bridge design specifications*, Washington, D.C. : American Association of State Highway and Transportation Officials, Washington, D.C.

American Association of State, H., and Transportation, O. (2014). *AASHTO LRFD bridge design specifications, Seventh Edition.*, Washington, D.C. : American Association of State Highway and Transportation Officials, Washington, D.C.

ASCE (2017). "ASCE analysis of U.S Department of Transportation." *National Bridge Inventory ASCII files*.

ASCE (2017). " Infrastructure Report Card, Federal Highway Administration " *Defecient Bridges*.

Association, P. C. (2002). "Design and control of concrete mixtures." *Design and control of concrete mixtures.*

Bao, Y., Hoehler, M., Choe, L., Klegseth, M. A., and Chen, G. (2017). "Monitoring Early-age Strain and Temperature Distributions in Full-scale Steel-concrete Composite Beams with Distributed Fiber Optic Sensors." *Structural Health Monitoring 2017*.

Belcher, K. (2017). "Laboratory and Field Investigations for Causes of Unwanted Deformations in Existing Steel Girder Bridges Rehabilitated with Concrete Decks." B. W. Russell, R. Emerson, and T. Ley, eds., ProQuest Dissertations Publishing.

Byard, B. (2010). "Summary of Modifications to AASHTO T 336 (2009)." *Auburn: Auburn University*.

Clifton, S. P. (2008). "Bridge deck overhang construction." University of Texas at Austin.

Ebisch, T. (2013). "Temperature effects on concrete pavements in Oklahoma." M. T. Ley, R. Emerson, and B. Russell, eds., ProQuest Dissertations Publishing.

El-Tayeb, E. H., El-Metwally, S. E., Askar, H. S., and Yousef, A. M. (2017). "Thermal analysis of reinforced concrete beams and frames." *HBRC Journal*, 13(1), 8-24.

Farhey, D. N. (2005). "Bridge Instrumentation and Monitoring for Structural Diagnostics." *Structural Health Monitoring*, 4(4), 301-318.

Farrar, C. R., and Worden, K. (2007). "An introduction to structural health monitoring." *Philosophical Transactions of the Royal Society London, Series A (Mathematical, Physical and Engineering Sciences)*, 365(1851), 303-315.

Forth, J. P. (2015). "Predicting the tensile creep of concrete." *Cement and Concrete Composites*, 55, 70-80.

Fu, H. C., Ng, S. F., and Cheung, M. S. (1990). "Thermal behavior of composite bridges." *Journal of Structural Engineering (United States)*, 116(12), 3302-3323.

Gilbert, R. (2012). "Creep and shrinkage induced deflections in RC beams and slabs." *Special Publication*, 284, 1-16.

Giussani, F. (2009). "The effects of temperature variations on the long-term behaviour of composite steel–concrete beams." *Engineering Structures*, 31(10), 2392-2406.

Hadidi, R., Saadeghvaziri, M. A., and Hsu, C. T. T. (2003). "Practical tool to accurately estimate tensile stresses in concrete bridge decks to control transverse cracking." *Practice Periodical on Structural Design and Construction*, 8(2), 74-82.

Hou, X., Yang, X., and Huang, Q. (2005). "Using inclinometers to measure bridge deflection." *Journal of Bridge Engineering*, 10(5), 564-569.

Imbsen, R. A., Vandershaf, D. E., Schamber, R. A., and Nutt, R. V. (1985). "THERMAL EFFECTS IN CONCRETE BRIDGE SUPERSTRUCTURES." *National Cooperative Highway Research Program Report*.

James, E. D., and Yarnold, M. T. (2017). "Rapid evaluation of a steel girder bridge: case study." *Journal of Bridge Engineering*, 22(12), 05017013.

Johnson, J. K. (2005). "Concrete bridge deck behavior under thermal loads." Montana State University-Bozeman, College of Engineering.

Khan, I., Castel, A., and Gilbert, R. I. (2017). "Tensile creep and early-age concrete cracking due to restrained shrinkage." *Construction and Building Materials*, 149, 705-715.

Khan, I., Murray, A., Castel, A., and Gilbert, R. I. (2015). "Experimental and Analytical Study of Creep and Shrinkage in Early-Age Concrete." *10th International Conference on Mechanics and Physics of Creep, Shrinkage, and Durability of Concrete and Concrete Structures*, C. Hellmich, B. Pichler, and J. Kollegger, eds., Reston, VA: American Society of Civil Engineers, Reston, VA, 1066-1075.

Kim, Y. H., Hueste, M. B. D., and Trejo, D. (2015). "Flexural behavior of high-early-strength self-consolidating concrete pretensioned bridge girders: Experimental evaluation." *Journal of Bridge Engineering*, 20(2), <xocs:firstpage xmlns:xocs=""/>.

Krauss, P. D., and Rogalla, E. A. (1996). *Transverse cracking in newly constructed bridge decks*.

Krkoska, L., and Moravcik, M. "Monitoring of temperature gradient development of highway concrete bridge." *Proc., MATEC Web of Conferences*, EDP Sciences, 00091.

Ley, T., Browne, R., Abrams, J., Gonzalez, R., Bussell, L., Padron, M., and Valles, F. "The development and implementation of a precast bridge deck overhang system." *Proc., 3rd International fib Congress and Exhibition, Incorporating the PCI Annual Convention and Bridge Conference 2010, May 29, 2010 - June 2, 2010*, Precast Prestressed Concrete Institute, B.S. Italia - Styl-Comp Group; BASF; Bentley; bsf; et al.; Hamilton Form Company, Ltd (hf).

Li, X., and Glisic, B. (2017). "Evaluating early-age shrinkage effects in steel concrete composite beam-like structures." *Steel Construction*, 10(1), 47-53.

Liu, Y. (2007). "Strength, modulus of elasticity, shrinkage and creep of concrete." M. Tia, and R. Roque, eds., ProQuest Dissertations Publishing.

Naik, T. R., Kraus, R. N., and Kumar, R. (2011). "Influence of types of coarse aggregates on the coefficient of thermal expansion of concrete." *Journal of Materials in Civil Engineering*, 23(4), 467-472.

ODOT (2017). "Deficient Bridges: Replacement and Rehabilitation Progress."

Oehlers, D. J., and Bradford, M. A. (2013). *Composite Steel and Concrete Structures: Fundamental Behaviour: Fundamental Behaviour*, Elsevier.

Patil, S. (2009). "Development of precast bridge deck overhang system." T. M. Ley, R. Emerson, and B. Russell, eds., ProQuest Dissertations Publishing.

Pavelchak, M. A., and Williams, M. E. (2013). "Structural Health Monitoring for Damage Detection Under Heavy Construction Loading."

Pesek, P., Riding, K., Schindler, A., Folliard, K., Drimalas, T., and Byard, B. (2017). "Development of Predictive Model for bridge deck cracking."

Peyton, S. W., Sanders, C. L., John, E. E., and Micah Hale, W. (2012). "Bridge deck cracking: A field study on concrete placement, curing, and performance." *Construction and Building Materials*, 34, 70-76.

Portland Cement Association, P. (2016). *Design and Control of Concrete Mixtures*, Skokie, Ill. etc. Portland Cement Association., Skokie, Ill. [etc.

Ranaivomanana, N., Multon, S., and Turatsinze, A. (2013). "Basic creep of concrete under compression, tension and bending." *Construction and Building Materials*, 38, 173-180.

Reynolds, J. C. (1972). "Thermal Stresses and Movements in Bridges."Masters Theses, Missouri University of Science and Technology.

Riding, K. A., Poole, J. L., Schindler, A. K., Juenger, M. C., and Folliard, K. J. (2009). "Effects of construction time and coarse aggregate on bridge deck cracking." *ACI Materials Journal*, 106(5), 448-454.

Robertson, I. N., Johnson, G. P., and Wang, S. (2005). *Instrumentation performance during long-term bridge monitoring*.

Rodriguez, L. E., Barr, P. J., and Halling, M. W. (2014). "Temperature effects on a box-girder integral-abutment bridge." *Journal of Performance of Constructed Facilities*, 28(3), 583-591.

Rojas, E. (2014). "Uniform temperature predictions and temperature gradient effects on I-girder and box girder concrete bridges." P. J. Barr, J. Bay, and M. Halling, eds., ProQuest Dissertations Publishing.

Rossi, P., Tailhan, J.-L., and Le Maou, F. (2013). "Comparison of concrete creep in tension and in compression: Influence of concrete age at loading and drying conditions." *Cement and Concrete Research*, 51, 78-84.

Russell, B. W. (1992). "Design guidelines for transfer, development and debonding of large diameter seven wire strands in pretensioned concrete girders." University of Texas at Austin.

Russell, B. W., Belcher,K., Abdelmeguid, I.S., Ley, M.T (October 2014). "Shrinkage Induced Deformations in Steel Bridges Made Composite Wiith Concrete Deck Slabs." Oklahoma Department of Transportation (ODOT). Final Report ~ FHWA-OK-14-09. ODOT SP&R Item Number 2260.

Russell, B. W., Yang, X., Li, J., Mosier, R. Wang, K., Volz, J., Pittenger, D., Daily, J. (August 2017). "Comparative Assessment of the Current Gross and Axle Truck Weight and Truck Permitting Laws in the United States." Final Report, ODOT SP&R Item No. 2271, 126 pp.

Sakyi-Bekoe, K. (2008). "Assessment of the coefficient of thermal expansion of alabama concrete."

Smolenski, P. J. (2004). "Field instrumentation and live load testing to evaluate behaviors of three reinforced concrete bridge decks." Montana State University-Bozeman, College of Engineering.

Subramaniam, K., Kunin, J., Curtis, R., and Streeter, D. (2010). "Influence of Early Temperature Rise on Movements and Stress Development in Concrete Decks." *Journal of Bridge Engineering*(1), 108-116.

Superior, D. (2017). "Dayton Superior, Bridge Deck Handbook."Miamisburg, OH.

Tanesi, J., Crawford, G., Gudimettia, J., and Ardani, A. (2012). "Coefficient of Thermal Expansion of Concrete: Changes to test method will enhance pavement designs." *Concrete International*, 55-60.

TRB (April 2019). "Structural Monitoring." *Transportation Research Circular E-C246*, Transportation Research Board, Washington, D.C.

Walter, P. L. (2009). "Metal Strain Gages Remain Key Despite Initial Rejection." *Sound and Vibration*, 43(2), 4.

Wei, Y., Liang, S., and Guo, W. (2017). "Decoupling of autogenous shrinkage and tensile creep strain in high strength concrete at early ages." *Experimental Mechanics*, 57(3), 475-485.

William, G. W., Shoukry, S. N., and Riad, M. Y. (2005). "Early age cracking of reinforced concrete bridge decks." *Bridge Structures*, 1(4), 379-396.

William, G. W., Shoukry, S. N., and Riad, M. Y. (2008). "Development of early age shrinkage stresses in reinforced concrete bridge decks." *Mechanics of Time-Dependent Materials*, 12(4), 343-356.

Yang, S. (2009). "Impact of overhang construction on girder design." T. A. Helwig, M. Engelhardt, R. Klingner, M. Mear, and J. Tassoulas, eds., ProQuest Dissertations Publishing.

Yoshitake, I., Rajabipour, F., Mimura, Y., and Scanlon, A. (2012). "A prediction method of tensile Young's modulus of concrete at early age." *Advances in Civil Engineering*, 2012.

Zheng, Y., Taylor, S., Robinson, D., and Cleland, D. (2010). "Investigation of Ultimate Strength of Deck Slabs in Steel-Concrete Bridges." *ACI Structural Journal*, 107(1), 82-91.

ASTM C150/C150M-18 Standard Specification for Portland Cement, West Conshohocken, PA, 2018.

ASTM C33/C33M-18 Standard Specification for Concrete Aggregates, West Conshohocken, PA, 2018.

ASTM C192/C192M-16a Standard Practice for Making and Curing Concrete Test Specimens in the Laboratory, ASTM International, West Conshohocken, PA, 2016.

ASTM C39/C39M-15 Standard Test Method for Compressive Strength of Cylindrical Concrete Specimens, ASTM International, West Conshohocken, PA, 2015.

ASTM C496/C496M-17 Standard Test Method for Splitting Tensile Strength of Cylindrical Concrete Specimens, ASTM International, West Conshohocken, PA, 2017.

ASTM C469/C469M-14 Standard Test Method for Static Modulus of Elasticity and Poisson's Ratio of Concrete in Compression, ASTM International, West Conshohocken, PA, 2014.

ASTM C157/C157M-17 Standard Test Method for Length Change of Hardened Hydraulic-Cement Mortar and Concrete, ASTM International, West Conshohocken, PA, 2017.

www.infrastructurereportcard.org/cat-item/bridges/
https://www.campbellsci.com/
vishaypg.com
www.micro-measurements.com
https://www.txdot.gov/business/resources/engineering-software.html#

VITA

Hema Jayaseelan

Candidate for the Degree of

Doctor of Philosophy

Dissertation: INFLUENCE OF TIME DEPENDENT PROPERTIES AND TEMPERATURE EFFECTS ON THE PERFORMANCE OF COMPOSITE BRIDGE GIRDERS.

Major Field: Civil Engineering

Biographical:

Education:

Completed the requirements for the Doctor of Philosophy in Civil Engineering at Oklahoma State University, Stillwater, Oklahoma in December, 2019.

Completed the requirements for the Master of Science in Civil Engineering at Oklahoma State University, Stillwater, Oklahoma in 2007.

Completed the requirements for the Bachelor of Science in Civil Engineering at Government College of Technology, Coimbatore, Tamil Nadu, India in 2000.

Experience:

Worked as a Graduate research Assistant in the Civil Engineering Department at Oklahoma State University, Spring 2015 – Fall 2019.

Worked as a Structural Design Engineer at Black and Veatch Ltd., United Kingdom, September 2007 – September 2014.

Professional Memberships:

- Precast Concrete Institute Diversity Committee Member, 2018.
- Active member of American Society of Civil Engineers (ASCE).
- Student Member of American Concrete Institute (ACI).
- Society of Women Engineers, Executive Officer, OSU Student Chapter.